FLORIDA INTERNATIONAL UNIVERSITY

Miami, Florida

INTERROGATION OF ION-NEUTRAL COMPLEXES BY TRAPPED ION MOBILITY-MASS SPECTROMETRY AND THEORETICAL CALCULATIONS

A dissertation submitted in partial fulfillment of

the requirements for the degree of

DOCTOR OF PHILOSOPHY

in

CHEMISTRY

by

Alan Alexander McKenzie-Coe

2019

To: Dean Michael R. Heithaus
College of Arts, Sciences and Education

This dissertation, written by Alan Alexander McKenzie-Coe, and entitled Interrogation of Ion-Neutral Complexes by Trapped Ion Mobility-Mass Spectrometry and Theoretical Calculations, having been approved in respect to style and intellectual content, is referred to you for judgment.

We have read this dissertation and recommend that it be approved.

_____
José R. Almirall

_____
Hebin Li

_____
Alexander M. Mebel

_____
James Martin E. Quirke

_____
Francisco Alberto Fernandez-Lima, Major Professor

Date of Defense: March 22, 2019

The dissertation of Alan Alexander McKenzie-Coe is approved.

_____
Dean Michael R. Heithaus
College of Arts, Sciences and Education

_____
Andrés G. Gil
Vice President for Research and Economic Development
and Dean of the University Graduate School

Florida International University, 2019

DEDICATION

This work is dedicated to the Most High God for His Love, Wisdom, and Grace. I also dedicate this to my parents, my family, and friends for all their love and support. I dedicate this to all my mentors, teachers, and professors that pushed and believed in me even when I did not. To my niece Zoë and my unborn children I pray you put God first ad know that all things are possible through Him.

ACKNOWLEDGMENTS

I would like to acknowledge Dr. Francisco Fernandez-Lima who welcomed me in his lab and advocating for me to be accepted into the PhD program. I would also like to acknowledge Dr. Lima for introducing me to the scientific community outside of FIU.

To my Lima Lab family from the past and present thanks for all the support and good times I treasure each of you and hope that we will never grow apart. To my McKnight Fellows thank you for the support and inspiration.

Thank you to my committee: Dr. José R. Almirall, Dr. Hebin Li, Dr. Alexander M. Mebel, Dr. James Martin E. Quirke for the time and insight that you have provided me with throughout this process. I would like to acknowledge Dr. Quirke for taking a special interest in me and encouraging me to seek my PhD. I remember attending his Organic Chemistry class as an undergraduate and being impressed by his mastery of the class and his sincere desire for us to learn. Also, to Dr. Mebel for always being patience with me all the times I crashed into your office with a calculation that didn't terminate normally. Thank you to Jackie, Maggie, and Dr. Lees for the kindness in which you helped me when I inevitably messed something up.

Thank you to Dr. Gary Eiceman and Dr. Suzanne Bell for being more than collaborators and taking a special interest in me.

I would also like to thank and acknowledge professional mentors at FIU. Thank you to Dr. Sonja Montas-Hunter for all of your guidance and energy in getting to this point and to Christina Dome Dr. Simms and the staff of both the McNair and McKnight fellowships for all of the countless hours that you guys invest in us. Thank you to Dr. Kalai Mathee for

checking in on me and for the positive energy that you fill the entire floor with. Thank you to Dr. Jeremy Chambers for the laughs and always being yourself. Thank you, Mayra and Dr. D, for taking me in like family and for whipping me into shape and not letting me get away with being lazy. Thank you Dr. Kabir for encouraging me and advocating me to become a McNair fellow as undergraduate and for you constant for words of encouragement. Thank you to Dr. Ramon de la Vega for taking interest in my progress and always being willing to write a letter of recommendation. Thank you to Dr. Furton and Jessica Brown for taking me in as undergraduate researcher. Sorry again for the broken syringes. Thank you to Professor Julian Edward for letting me know the potential I had.

In closing, thank you to the people most essential people on this journey, my parents, Rochelle and Thomas, for fostering the curiosity that led me to this point, for demanding excellence, and for making me believe that I could truly be whatever I wanted to be. Thank you to my maternal grandmother Lilia Coe and paternal grandmother Alicia McKenzie for being matriarchs that provided love, support, and discipline to all their children and most importantly instilled in all of us faith in God. Thank you to all my aunts, uncles, and cousins. Thank you to all my family, church family, and friends for believing in me and being there for me. To Genel Christian, thank you for all of your love and support.

ABSTRACT OF THE DISSERTATION

INTERROGATION OF ION-NEUTRAL COMPLEXES BY TRAPPED ION MOBILITY-MASS SPECTROMETRY AND THEORETICAL CALCULATIONS

by

Alan Alexander McKenzie-Coe

Florida International University, 2019

Miami, Florida

Professor Francisco Alberto Fernandez-Lima, Major Professor

In the present study, the fundamentals of molecular ion trapping and the application of trapped ion mobility spectrometry coupled to mass spectrometry (TIMS-MS) to the separation and identification of molecular components in complex mixtures are shown. In particular, ion-neutral complexes lifetimes, relative stability, binding energies and candidate structures are described for common explosives during TIMS-MS, as well as the effect of the micro-environment, during complex sample analysis. A novel TIMS-MS workflow was developed for the detection of both inorganic residues (IGSR; inorganic gunshot residues) and organic residues (OGSR) of firearm discharge residue from skin swabs, capable of high specificity and short analysis time (few min) from a small sample size (<10 μL). The TIMS-MS workflow provided fast, post-ionization, high resolution mobility (R_{IMS} ~ 150–250) and mass separations (R_{MS} ~ 20–40k) with isotopic pattern recognition. In addition, for the first time, liquid chromatography, trapped ion mobility spectrometry and mass spectrometry are combined for fast separation, identification and quantitation of labile juvenile hormones (JHs) with increased sensitivity and confidence levels. In particular, the use of the parent ion and in-source diagnostic fragment ions in a

LC-TIMS-MS workflow was developed, complemented with novel extraction and labeled standards for the detection and quantitation of JHs in biological samples.

TABLE OF CONTENTS

LIST OF TABLES

LIST OF FIGURES

ABBREVIATIONS AND ACRONYMS

μ-PIXE	microbeam ion beam analysis
2D	2-Dimensional
ATR-FTIR	attenuated total reflectance Fourier transform infrared spectroscopy
B3LYP	Becke, three-parameter, Lee-Yang-Parr
Ba	barium
BR-CA-CC	brain corpora allata-corpora cardiaca
CA-CC	corpora allata-corpora cardiaca
CCS	collision cross-section
CE	crown ether
CEl	capillary electrophoresis
Cu	copper
CV	compensation voltage
DART-MS	direct analysis in real time-mass spectrometry
DC	direct current
DFT	density function theory
DHSS	diffuse hard sphere scattering
DMA	differential mobility analyzer
DMS	differential mobility spectrometry
DNT	2,4 dinitrotoluene
DPA	diphenylamine
DTIMS	drift tube ion mobility spectrometry

EC	ethyl centralite
EHSS	elastic hard spheres surfaces
EI	electron ionization
ESI	electrospray ionization
ETD	explosive Trace Detector
eV	electron volt
FAIMS	high-field asymmetric-waveform ion-mobility spectrometry
FDR	firearms discharge residue
FFL	Francisco Fernandez-Lima
FGN	Fernando G. Noriega
FT-ICR	Fourier transform- ion cyclotron resonance
GC	gas chromatography
GC/μ-ECD	GC-micro electron capture detection
HMX	octahydro-1,3,5,7-tetranitro-1,3,5,7-tetrazocine
HPLC-FD	HPLC with fluorescence detection
IBA	ion beam analysis
ICP-MS	Inductively coupled plasma
IGSR	inorganic gunshot residues
IMS	ion mobility spectrometry
IMS-MS	ion mobility spectrometry-mass spectrometry
JH	juvenile hormone
K	potassium

LC	liquid chromatography
LIBS/ICP-OES	laser-induced breakdown spectroscopy/inductively coupled plasma optical emission spectroscopy
m/z	mass-to-charge
MA	Massachusetts
MALDI	matrix-assisted laser desorption/ionization
mbar	millibar
Me	metal
MS	mass spectrometry
MS/MS	tandem mass spectrometry
nESI	nano- electrospray ionization
NIST	National Institute of Standards and Technology
OGSR	organic gunshot residues
PA	projection approximation
Pb	Lead
PETN	3-nitrooxy-2,2-bis-(nitrooxymethyl) propyl nitrate
ppm	parts per million
ppt	part per trillion
Q-TOF	quadrupole time-of-flight
RDX	1,3,5-trinitroperhydro-1,3,5-triazine
RF	radio frequency
S/N	signal-to-noise ratio

SEM/EDS	scanning electron microscopy electron dispersive X-ray spectroscopy
SIMS	Secondary ion mass spectrometry
SLIM	Structures for lossless ion manipulations
SRIG	stacked-ring ion guide
SUPER	serpentine ultralong path with extended routing
Td	Townsend
TIMS	trapped ion mobility spectrometry
TM	trajectory method
TNT	2-methyl-1,3,5-trinitrobenzene
ToF	Time-of-Flight
TWIMS	traveling wave Ion mobility spectrometry
VHA	volatile halogenated anesthetic
VOC	volatile organic compound
WVU IRB	West Virginia University Institutional Review Boards

Chapter One:

INTRODUCTORY CHAPTER

1.1. Mass spectrometry

From its earliest days mass spectrometry (MS) has focused on the formation, separation, and detection of ions.[1] Initially this nameless technique was primarily used by physicists to interrogate the structure of the atom.[2] As instrumentation became commercially available mass spectrometry found a niche in academia.[2] Eventually, research groups dedicated solely to mass spectrometry development emerged and further developed and enhanced every aspect of instrumentation.[3]

The first step of almost every MS workflow is the production of ions by an ionization source. Initial experiments focused on generating charge particles by bombarding the neutral analyte with high-energy electrons (70 eV). These ionization sources referred to as electron impact or electron ionization (EI) work well for small volatile organic molecules ($\leq$ 600 *m/z*) but have the caveat of raising the internal energy. They cannot be used to generate the intact or molecular ion of large molecules, as these larger species would undergo fragmentation if they could be volatilized intact. John B. Fenn and Koichi Tanaka received the 2002 Nobel Prize in Chemistry for the invention of electrospray ionization (ESI) and matrix-assisted laser desorption/ionization (MALDI) source, respectively, both of which ionized large intact biomolecular ions.[3]

The second element of the mass spectrometry triad, the mass analyzer, is where the analytical separation takes places. Ions produced in the source are introduced into the mass analyzer and separated according to their *mass-to-charge* (*m/z*) ratio. The principle of separation varies between mass analyzers and includes separations according to kinetic energy, momentum, trajectory stability, velocity, and resonance frequency.[4] The

performance of a mass analyzer is governed by the mass range limit, the analysis speed, mass accuracy, and mass resolution.[4] The last component of a mass spectrometer is the detector which records the charge induced or current produced by a mass analyzed ion.[1] Although not analytical elements of the mass spectrometer, ion optics and the vacuum system are also vital to optimal working conditions and ion survival.[5] Ion optics are used to transfer ions by electrostatic potential; for example, to transmit a positive ion, the electric potential must become increasingly negative. The reverse is done in the case of negative ions.[1, 4, 5] The low pressure ($< 1x10^{-7}\ mbar$) afforded by high vacuum is necessary to remove gaseous molecules.[5] Collisions with residual gas molecules can neutralize the ion of interest, reducing the signal-to-noise ratio (S/N) or causing undesired reactions, and resulting in products that convolute the analysis.[4, 5] Mass spectrometrists design instruments to have a large mean free path, L, to determine how long an ion can travel before experiencing a collision. The mean free path is measured in meters and is expressed as the following:

$$L = \frac{kT}{\sqrt{2}p\sigma} \qquad (1.1)$$

where k is the Boltzmann constant, T is temperature, p is pressure, and σ is the collision cross-section defined as $\sigma = \pi d^2$ where d is the sum of the radii of the stationary molecule and the colliding ion.[4]

In addition to the development and usage of standalone mass spectrometers came various *coupled* or *hyphenated* mass spectrometers which combine the chemical separation capabilities of chromatography to the mass resolving abilities of the mass spectrometer.

Common chromatography techniques paired with mass spectrometry include gas chromatography (GC), liquid chromatography (LC), and capillary electrophoresis (CEl).[4] These hyphenated setups result in powerful mass spectrometers. For example, gas chromatography-mass spectrometry has become the gold standard for the forensic detection of substances because of its superior sensitivity (femtogram) and selectivity.[6, 7] Similarly, liquid chromatography-mass spectrometry has found a foothold in proteomics, metabolomics, and the pharmaceutical industry.[1]

1.2. Ion mobility

Developed by Earl W. McDaniel and originally referred to as plasma chromatography, ion mobility spectrometry (IMS), is an analytical tool that focuses on the generation, separation, and detection of ions akin to mass spectrometry.[8, 9] The instrumentation of IMS is also similar to that of the mass spectrometer, consisting of an ionization source, a drift region, and a detector.[10, 11] Where the mass spectrometer acts as a molecular scale that "weighs" ions separating according to molecular weight the ion mobility spectrometer differentiates ions based on size.[11] Another key difference is that IMS separation is performed at atmospheric pressure (101.325 kPa) and do not require the same rigorous vacuum systems of MS, making it ideal for miniaturization and field instruments.[11]

The theory of ion mobility spectrometry focuses on the methodology and instrumentation used to characterize the gas-phase ions of chemical substances according to their velocity in an electric field.[11] In drift tube or traditional IMS experiments ions produced from the ionization source are introduced as discrete collections referred to as "ion packets" or "ion swarms" into the drift region where the analytical separation takes place.[8, 11] The drift

region is held under a voltage gradient and is filled with an inert gas, usually helium or nitrogen, referred to as the buffer gas or drift gas.[8, 10-12] Ions are transferred to the drift region and are accelerated by the electric field, E, towards the detector, which records the current flow caused by the arriving ion pulse as ion current versus time.[8, 11]. As the ions travel deeper into the analysis region, they undergo collisions with the drift gas.[1, 11] The ions reach a constant velocity (v_d) that is proportional to the electric field and is calculated by the equation [1, 11, 12]:

$$v_d = KE \qquad (1.2)$$

The proportionality coefficient, K, given in units $\frac{cm^2}{Vs}$ is referred to as the ion mobility and is the physical quantity measured in an IMS experiment.[8, 9, 11-13] The ion mobility coefficient is typically normalized to 273 K and 760 Torr and is reported as the reduced mobility, K_o.[9, 11] The ion mobility of a species is dependent on the size of the ion as larger ions will experience more collisions and be impeded more than smaller ions, giving them a slower drift velocity.[10, 11, 14] The mobility measurement also depends on the drift gas as different gases have different chemical properties. For example, chirality or polarizability may influence additional interactions; polarizable gases have been shown to have long-range effects.[11, 15, 16]

The relationship between ion mobility, drift velocity, and the electric field described by Equation 1.2 is only valid under low-field conditions ($E/N < 45$ Td).[8-11, 13, 17] The parameter E/N is expressed in units of Townsend (Td), where $1\ \text{Td} = 10^{-17} V cm^2$, and is

used to evaluate field strength and is the ratio of the electric field, E, to the number of drift gas molecules, N.[11, 13]

Another important consideration of low-field ion mobility spectrometry is the ability to determine K using the zero-field mobility or Mason-Schamp equation:

$$K = \frac{3q}{16N}\sqrt{\frac{2\pi}{kT}}\sqrt{\left(\frac{m+M}{mM}\right)}\left(\frac{1}{\Omega_{avg}^{(1,1)}}\right) \qquad (1.3)$$

where q is the ionic charge, N the number density of the drift gas, k is Boltzmann's constant, T is the absolute temperature, m is the mass of the drift gas, M is the mass of the analyte ion, and $\Omega_{avg}^{(1,1)}$ is the orientationally averaged collision cross-section.[1, 9, 11, 12]

The resolution of an IMS experiment can be expressed by the resolving power, R_p, which is determined by the equation:

$$R_p = \frac{t_d}{w_h} \qquad (1.4)$$

where t_d is the drift time, and w_h is the ion pulse duration measured at full width at half maximum at the time of detection.[18] Experimentally this means that the larger the pulse duration the lower the resolution will be.

Revercomb and Mason presented four aspects that affect the attributes of the ion pulse: **(1)** the initial phase width and shape as introduced into the drift region, which was classified as an instrumental effect, **(2)** peak broadening caused by Coulombic repulsion, **(3)** broadening by diffusion as the pulse drifts down the electric field, and **(4)** ion-molecule reactions with the drift gas or impurities although this can be advantageous in studying ion-

molecule reactions.[8] Revercomb and Mason also proposed that broadening caused by diffusion could be understood using the Einstein relation and diffusion theory.[8] In the same work they showed that when only the initial pulse width and broadening because of diffusion are significant, the measured peak width can be expressed as the following:

$$w_h^2 = t_g^2 + \left(\frac{16kT \ln 2}{Vez}\right) t_d^2 \qquad (1.5)$$

where w_h is the ion pulse duration, t_g is the initial ion pulse width, k is Boltzman's constant, T is the temperature of the drift gas in degrees Kelvin, V is the potential across the drift length, e is the elementary charge, z is the number of charges on the ion, t_d and is the drift time of the ion.[8, 18]

Early on, researchers were stymied by the experimental resolution of IMS as it consistently underachieved from what was expected theoretically.[19] Several studies propose that the underwhelming resolving power was the result of peak broadening caused by electric field inhomogeneity and Coulombic repulsion.[8, 19] The work of Revercomb and Mason Hill et al. showed that mobility resolution can be divided into two regimes.[20] Ideally, the initial pulse width is significantly smaller than the diffusion broadened pulse width that is measured at the detector.[8, 19, 20] When the initial pulse width is significantly smaller then diffusion becomes the major factor contributing to peak broadening and resolution is defined as

$$R = \sqrt{\left(\frac{qEL}{44.2kT}\right)} \qquad (1.6)$$

where L is the length of the drift tube, E is the applied electric field, k is Boltzman's constant, and T is the temperature of the drift gas in degrees Kelvin.[20]

In the reverse situation when the initial pulse width is larger than the diffusion broadened pulse width then resolution is defined as[20]

$$R = \frac{L}{t_g KE} \qquad (1.7)$$

In the first regime resolution can be improved by increasing the electric field and the length of the drift tube, and resolution is independent of the ion's mobility.[20] Hill was able to observe the two-regime resolution experimentally by monitoring the resolution as function of various instrumental parameters and the initial ion pulse width.[19, 20]

From Formula 1.7 it is possible to increase resolution by decreasing the ion pulse duration, which can be achieved by by increasing the potential V that is applied to the drift tube.[8, 9, 17, 18] Clemmer and Jarrold took advantage of this concept by producing a 63 cm drift tube with an applied potential of 14,000 V and a pressure of 500 torr in order to remain in the low-field regime.[17] Other means of improving resolution include more precise electronics that can generate a more homogenous electric field.[21]

With the advances of instrumentation, ion mobility spectrometry now has a wide range of applications in various realms. The bulk of IMS operation is rooted in security, forensics, and military use where the high sensitivity of the technique allows it to detect trace amounts of compounds of interest within complex mixtures.[11, 22, 23] Ion mobility spectrometry is the most widely used technology for the detection of explosives in airport security and its miniaturization has allowed it to be deployed during military field operations.[24-26] In

forensic investigations ion mobility has been used to screen for legal and illegal drugs and has shown potential to detect drugs in human hair.[27-31] In the medical arena, two independent studies using IMS to analyze human breath have demonstrated the ability to detect volatile halogenated anesthetics (VHAs) and volatile organic compounds (VOCs) both of which are indicative of lung disease.[32, 33]

1.3. Ion mobility spectrometry-mass spectrometry

For a time after the introduction of the ion mobility spectrometer, the scientific community was underwhelmed with the technique. This was largely because of comparisons with mass spectrometry which offers mass information and higher peak resolution.[12, 34] While operating at atmospheric pressure does not require the rigorous vacuum system of MS and allows for field deployable instruments, early on it presented challenges for understanding the underlying chemistry that took place during ion formation.[12]

A significant innovation has been the union of ion mobility spectrometry to the MS workflow. Ion mobility spectrometry-mass spectrometry (IMS-MS), like other hyphenated techniques results in a whole that is greater than the sum of its parts. Specifically with IMS-MS, the complementary information gained from mass spectrometry (*mass-to-charge*) and ion mobility (ion size) along with the similar instrumental requirements allows the nearly seamless merging of the two techniques.[14] The union of ion mobility spectrometry-mass spectrometry also benefits from the timescale of the individual techniques. Ion mobility spectrometry separations occur on a millisecond timescale whereas MS analysis can be done in microseconds this allows for the identification by MS of ions that have been characterized according to their drift times via IMS.[14, 35] The IMS-MS instruments offer

improved characterization of ion and ion-neutral ion mobilities by simultaneous acquisition of MS data and provide a better understanding of ionization and fragmentation pathways by providing insight into the gas-phase ion structures.[35]

Over the last few years several IMS-MS devices have been developed in addition to the traditional drift tube IMS-MS outlined below.

1.3.1. Drift Tube

Earl McDaniel, the pioneer of modern ion mobility, is also credited with developing the first IMS-MS by coupling a drift tube to a magnetic sector mass spectrometer.[14, 36] The primary use of McDaniel's IMS-MS instrument was to explore ion-molecule reactions specifically those related to the terminal ion species produced in hydrogen and was also able to identify ions from the preceding mobility spectrometer.[14, 36] Research by McAfee and Edelson at Bell Telephone Laboratories resulted in the first IMS coupled to a time-of-flight mass spectrometer.[37-41]

The first commercial IMS-MS instrument, the Alpha II, was produced by the Franklin GNO Corporation in 1971 by combining traditional drift tube ion mobility with a quadrupole mass spectrometer and an electron multiplier detector.[12] The Alpha II was used to separate trace amounts of 1-octanol and 1-nonanol more importantly it helped to resolve some of the mystery of ion formation that occurs at ambient pressure and helped in establishing a correlation between mass and mobility.[12, 42] A later version of the Alpha II was used to structurally characterize ions with the same *mass-to-charge* values as legal and illegal drugs and to detect explosives.[12, 14, 43-46] Guevremont and coworkers modified the Alpha II by replacing the quadrupole mass spectrometer with a contemporary time-of-flight

mass spectrometer.[12, 14, 47] At this point time-of-flight mass spectrometry had improved tremendously from when it was first coupled to drift tube IMS.[12, 14, 48, 49] Time-of-flight MS benefited from technological advancements such as the reflectron, which increased resolution by collating ions with different kinetic energy and high-speed electronics that allow all ions to be detected thus increasing the mass range, sensitivity, and duty cycle.[14, 50]

Clemmer et al. further innovated IMS-MS technology and extended the class of molecules studied by IMS-MS by pursuing biologically relevant molecules.[12, 17, 51-53] One such innovation used to characterize intact and fragmented oligosaccharides and proteins was a drift tube quadrupole IMS-MS that produced fragments by varying the injection energy used to introduce the ions into the drift region.[52, 54, 55] Clemmer also developed nested ion mobility-mass spectrometry using a homebuilt ESI-ion trap-IMS-ToF mass spectrometer.[52, 56, 57] Nested ion mobility-mass spectrometry takes advantage of the difference in analysis time between IMS (milliseconds) and MS (microseconds) and allows for simultaneous measurements of mobilities and *mass-to-charge* ratios.[12, 52, 56, 57] Data acquired using this setup made it possible to produce 3D plots and contour plots as function of drift time, *mass-to-charge* and intensity.[52, 56-58] Using nested ion mobility-mass spectrometry together with synthetic combinatorial peptide libraries, Clemmer et al. were able to survey scores of generated peptides concurrently.[59-62]

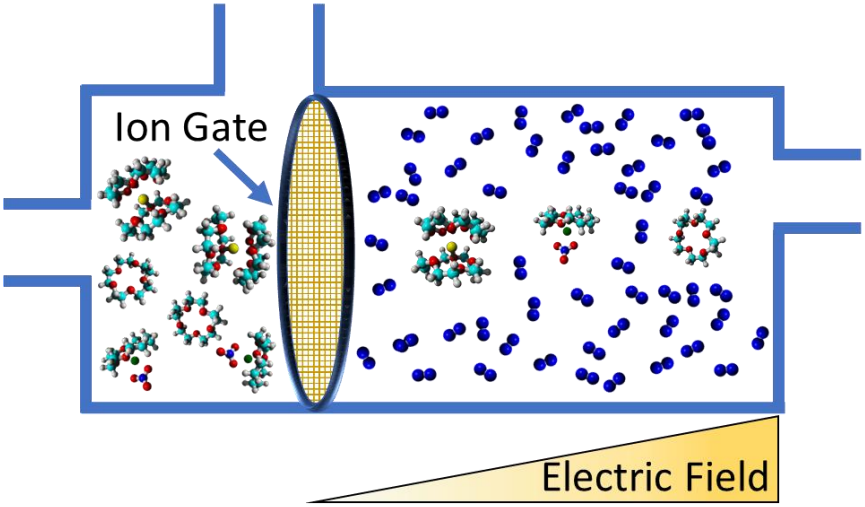

Figure 1.1. Schematic of a drift tube IMS. Ions are pulsed into the instrument by an ion gate and experience an increasing electric field along with collisions with a drift gas. Larger ions undergo more collisions and require more time to exit the drift region.

1.3.2. High-field asymmetric-waveform ion-mobility spectrometry (FAIMS)

High-field asymmetric-waveform ion-mobility spectrometry or differential mobility spectrometry (DMS) is an ion mobility separation technique that takes advantage of the nonlinear behavior of the ion mobility coefficient, K, under high-field conditions.[11, 63, 64] In practice a FAIMS device consists of two parallel plates, the lower plate is held at ground and an asymmetric waveform is applied to the upper plate.[11, 13, 65] The waveform is composed of a high-field region generated by voltage $(E)_h$ and a relatively lower field region of opposite polarity generated by voltage $(E)_l$ so that,

$$(E)_h t_h + (E)_l t_l = 0 \qquad (1.8)$$

where t_h is the time that the high-field voltage is applied and t_l is the time that the low-field voltage is applied.[65] Under working conditions an ion that experiences the high-field region will travel a distance, d_h, in the high field regime, defined by:

$$d_h = K_h(E)_h t_h$$

and travel a distance, d_l, under the lower field environment.[64, 65]

$$d_l = K_l(E)_l t_l$$

If the ions have the same ion mobility under high-field conditions and low-field exposure then the distances, namely, d_h and d_l, will be equal and the ion will experience no net displacement.[63-65] If, however, the behavior of the ion differs during high-field exposure in comparison to low-field exposure then the ion will experience a net displacement. Eventually the ion will eventually collide with the upper plate or the lower plate if no other voltage is applied.[13, 65] To prevent a neutralization event a constant direct current (DC) voltage of appropriate polarity and magnitude is applied so that the ion will traverse the alternating currents of the analysis region and arrive at the detector.[65] The applied DC voltage referred to as the compensation voltage (CV), is the key parameter in a FAIMS experiment.[10] In general, the more that the compensation voltage deviates from zero the greater the sensitivity.[65]

Research into instrumental design has resulted in several variations (e.g., planar or coaxial) of the electrodes used to generate the fields in a FAIMS experiment.[11, 65, 66] In general, planar electrodes have a shorter ion residence time, making them ideal for coupling to high-throughput pre-separation techniques such as GC.[65] Planar electrodes also function independently of the type of ion produced and have been used for the simultaneous separation and detection of positive and negative ions; from a practical aspect planar components are also easier and cheaper to manufacture.[65, 67] The ion focusing effect of

coaxial electrodes give them greater field dependence and longer ion residence times, attributes that enhance ion intensity and selectivity.[67]

Dome-type electrodes have been shown to be well-suited for resolving protein conformers and are used for systems with low flow rates.[65, 68, 69]

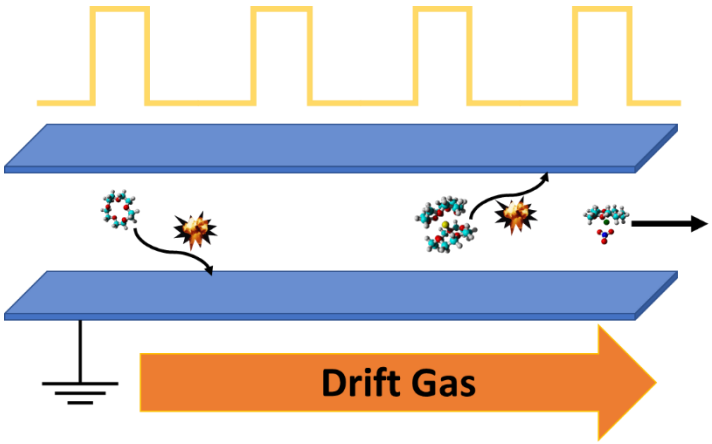

Figure 1.2. Schematic of a FAIMS instrument. FAIMS separates ions based on differences of an ion's mobility in a low electric field and a high electric field.

1.3.3. Differential Mobility Analyzer (DMA)

There have been extensive developments of the differential mobility analyzer, and after many refinements, the first successful commercial instrument, the TSI Model 3030 Electrical Aerosol Analyzer (EAA), was introduced in the mid-1970s.[70] The differential mobility analyzer consists of two electrodes. One electrode is held at ground with an inlet to introduce ions from the ionization source and the other is biased at a voltage of 1V to 10 kV with an outlet located distally from the inlet.[71-73] As ions enter from the inlet aperture there is an electrostatic attraction towards the other electrode. At the same time a pure sheath gas flows perpendicular to the ion motion and only ions of a specific mobility reach the outlet orifice.[13, 70, 71, 74] Ions that survive are detected by an electrometer or a mass

spectrometer. Differential mobility analyzers are mainly used to characterize nanoparticle aerosols with environmental implications.[70-72, 75, 76]

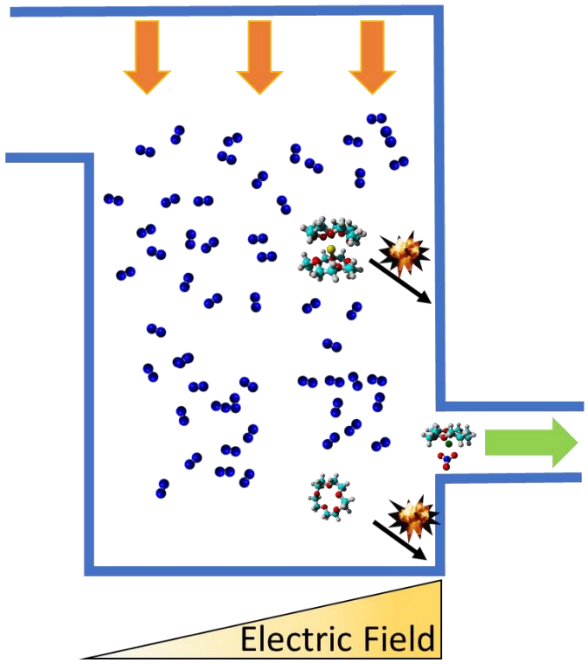

Figure 1.3. In a differential mobility analyzer, ions traverse between two electrodes and undergo collisions with a drift gas traveling orthogonal to direction of the electric field. Only ions of a specific trajectory, governed by the ion's mobility, arrive at the detector.

1.3.4. Traveling Wave Ion Mobility Spectrometry (TWIMS)

Traveling wave IMS instruments are composed of a gas filled stacked-ring ion guide (SRIG). Adjacent rings are given RF (radio frequency) opposite potentials which serves to radially confine ions improving ion transmission.[77-79] A pulsed DC voltage is superimposed onto the ring electrodes in a stepwise fashion and repeated. Ions undergo a shift in the axial direction which is parallel to the DC pulse; as the pulse is repeated the ions are iteratively displaced further from their initial position.[13, 74, 80] As the ions "surf" the wave they experience collisions with the drift gas resulting in dispersion based on the ions' mobilities.[13, 74, 80]

Structures for lossless ion manipulations (SLIM) have also been used to perform TWIMS experiments.[74, 81] Structures for lossless ion manipulations technology is constructed using printed circuit boards and has the ability to trap ions and perform ion reactions.[81, 82] Structures for lossless ion manipulations can also be used to conduct multiple passes to increase mobility resolution. This approach is referred to as serpentine ultralong path with extended routing (SUPER).[83]

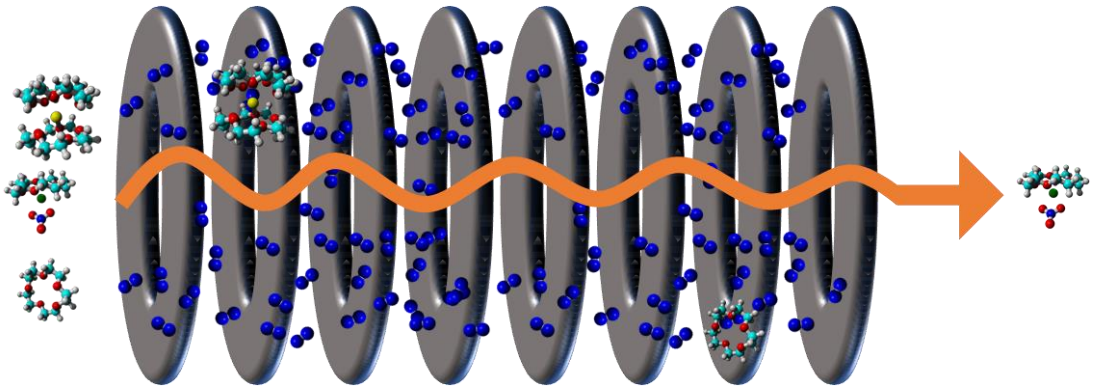

Figure 1.4. In a TWIMS mobility instrument a DC voltage is pulsed onto a stacked-ring ion guide. Ions accelerate axially during each DC pulse and are radially confined by an RF potential placed on the ring electrodes.

1.3.5. Trapped Ion Mobility Spectrometry (TIMS)

An alternative approach to IMS is the TIMS platform which uses an electric field to counteract the drift force imparted by a moving gas to trap ions at a point in space where the two forces negate each other.[84-86] The TIMS device consists of an entrance funnel, an analyzer tunnel, and an exit funnel.[13, 74, 84] The entrance and exit funnel are ion funnels, which serve to increase ion transmission, and are made up of stacked ring electrodes with decreasing diameters where each ring is segmented into four electrically isolated panels.[86, 87] Within the entrance and exit funnels adjacent ring electrodes are 180° out of phase resulting in a dipole electric field that guide ions axially and offers radial confinement.[86-89] In the analyzer tunnel the segmented ring electrodes have the same diameter and adjacent panels are out of phase, producing a quadrupolar field that radially confines ions but has negligible effect in the axial direction.[84-89]

A routine TIMS analysis consists of a fill time, trap time, and a ramp time.[86] Throughout the fill time ions are pushed into the analyzer region by a deflector of opposite polarity.[84-86, 89] During the trapping time ions entering the analyzer tunnel experience collisions with the drift gas and are pushed axially into the cell.[85-87] Ions traversing the cell encounter an increasing electric field and become "trapped" at a position where the two forces cancel each other out.[13, 85, 86] The electric field is determined by the voltage difference between the entrance and exit electrodes with all intermediate electrodes being electrically connected through resistive dividers.[85, 86, 88, 90] To elute ions the electric field is weakened stepwise to retain analytical separation, by ramping the entrance electrode voltage to the voltage of the exit electrode.[86-88, 90] The time it takes to complete the process of ramping the voltage of the entrance funnel is referred to as the ramp time.[84, 85, 89] By decreasing the

rate at which the voltages are ramped higher experimental resolution can be acheived.[23, 91] Eluted ions are detected using a mass analyzer as a result the mass spectra can be correlated to the voltage (referred to elution voltage) of the ramp and therefore to a specific ion mobility.[87-90]

Particularly noteworthy is the ability of the TIMS-MS device to produce high resolution (>300) mobility profiles, operate at or near the low field limit ($E/N \approx 45\,\mathrm{Td}$), and perform duty cycle free.[23, 92, 93]

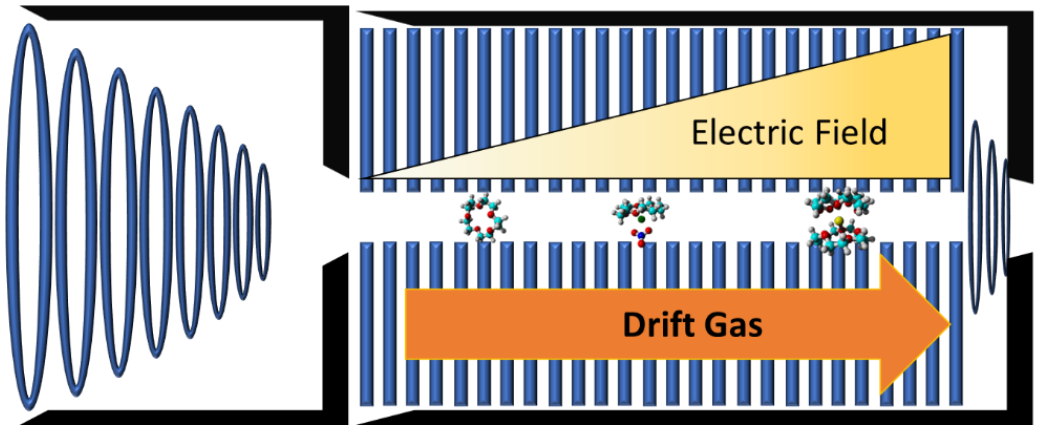

Figure 1.5. In a TIMS device a drift gas pushes the ions deeper into the cell, larger ions undergo more collisions and travel further. At the same time the ions encounter an increasing electric field acting in the opposite direction. Ions are trapped where the two forces cancel and are eluted by weakening the electric field.

1.4. Structural insights from IMS and computational chemistry

An important consequence of operating an IMS-MS setup at the low field limit is the ability to measure collision cross-section (CCS) which give information about size and shape either by analysis within a series of compounds or by comparison with computational modeling.

Nearly a century ago researchers proposed structures by comparing the average cross-section obtained experimentally from the diffusion of liquids or solids through a headspace to the cross-section calculated using a model constructed from X-ray crystallography and chemical properties.[10, 94] Likewise, pioneers of IMS research realized the potential of ion mobility experiments to give insight into structure.[11, 14] Initial work by Bowers et al. and Jarrold et al., using carbon clusters and silicon clusters respectively, demonstrated that IMS could provide experimental data to support the structural findings of computational chemists.[95-97] Computational chemists use mathematical algorithms, statistics, and large databases to integrate theories and models with experimental observations.[98] In particular computational chemistry is used to explore the structure, potential energy surface, and chemical properties of single molecules or a group of molecules.[99] Both Bowers and Jarrold would go on to use Equation (1.3), which defines the mobility of an ion under a low-field IMS experiment, to calculate a theoretical ion mobility in addition to the ion mobility measured experimentally.[95, 97, 100] The experimental ion mobility is then compared to the theoretical ion mobility. If the two are in close agreement then the geometry of the two are also in close agreement.[10] A prerequisite to calculating the theoretical ion mobility using Equation (2) is determining $\Omega_{avg}^{(1,1)}$, the orientationally averaged collision cross-section. Once input geometry that has been found from structural calculations via computational chemistry, computational modeling is used to determine analytically the orientationally averaged collision cross-section. Several models have been developed to calculate the orientationally averaged collision cross-section some of which are outlined below.

1.4.1. Projection approximation

The projection approximation (PA) developed by Bowers et al. treats the atoms of the molecule as rigid spheres and calculates the orientationally averaged collision numerically using a Monte Carlo approach.[95] In the PA method an input geometry is randomly rotated and projected onto a plane and random points are cast onto the projection. If a point is closer to an atomic center than the sum of the van der Waals radii of carbon and helium, it is counted as a collision.[10, 95, 101] The workflow is repeated several hundred times until an average collisional cross-section is obtained.

1.4.2. Elastic hard spheres scattering

The elastic hard spheres scattering (EHSS) method developed by Jarrold and Shvartsburg also treats the atoms of the input geometry as hard spheres. Unlike the projection approximation the EHSS model considers the possibility of multiple collisions between the drift gas and ion, a factor that becomes pronounced when working with concave polyatomic molecules.[10, 97, 100-102] To account for the additional collisions the EHSS follows the trajectory of the drift gas both throughout collision events until it is no longer in the range of collisions.[100] Comparison of the two methods show that the PA approach deviates over 20% when performed on structures with concave features.

1.4.3. Trajectory method

A further improvement of the orientationally averaged collision cross-section computational models is the trajectory method (TM). The EHSS method, while rigorously describing the collisional events lacks, the means to account for long-range interactions between the drift gas and ion swarm.[97] To account for long-rang interactions, the trajectory

method includes a 12-6 potential in combination with an ion-induced dipole interaction potential.

$$\Phi(\theta,\phi,\gamma,b,r) = 4\epsilon\sum_i^n\left[\left(\frac{\sigma}{r_i}\right)^{12} - \left(\frac{\sigma}{r_i}\right)^{6}\right] - \frac{\alpha}{2}\left(\frac{ze^2}{n}\right)\left[\left(\sum_i^n \frac{x_i}{r_i^3}\right)^2 + \left(\sum_i^n \frac{y_i}{r_i^3}\right)^2 + \left(\sum_i^n \frac{z_i}{r_i^3}\right)^2\right] \quad (3)$$

The first term encompasses the repulsive forces that arise from the overlap of electron clouds at short ranges and the attractive forces that occur at long ranges, whereas the second term, represents ion-induced dipole interaction.[11, 97] Results from this work show that about 10% deviation can occur between the trajectory method and models that do not address the long-range potential. This difference is significant because this error can propagate to structural assignment.

Currently, efforts have been made to refine the accuracy of the projection approximation by incorporating superposition techniques.[10] Regarding the EHSS and TM methods focus has been directed on "relaxing" the impact of the calculated collisions to reflect the real-life probability of elastic versus inelastic collisions occurring.[103] As improvements are made the "best" model varies from experiment to experiment.

1.5. MS and IMS as *in-vacuo* laboratories

The modern mass spectrometer and ion mobility spectrometers in all their various forms are essential tools to answer a plethora of analytical questions because of their unparalleled sensitivity, detection limits, speed, and diversity of applications.[4] Today the mass spectrometer can be regarded as a kind of chemical laboratory designed to study ions in the gas phase.[1, 104] Indeed, in the computer age the use of tools to explore gas-phase ion chemistry has increased along with the synergy between them (see **Figure 1.6**).

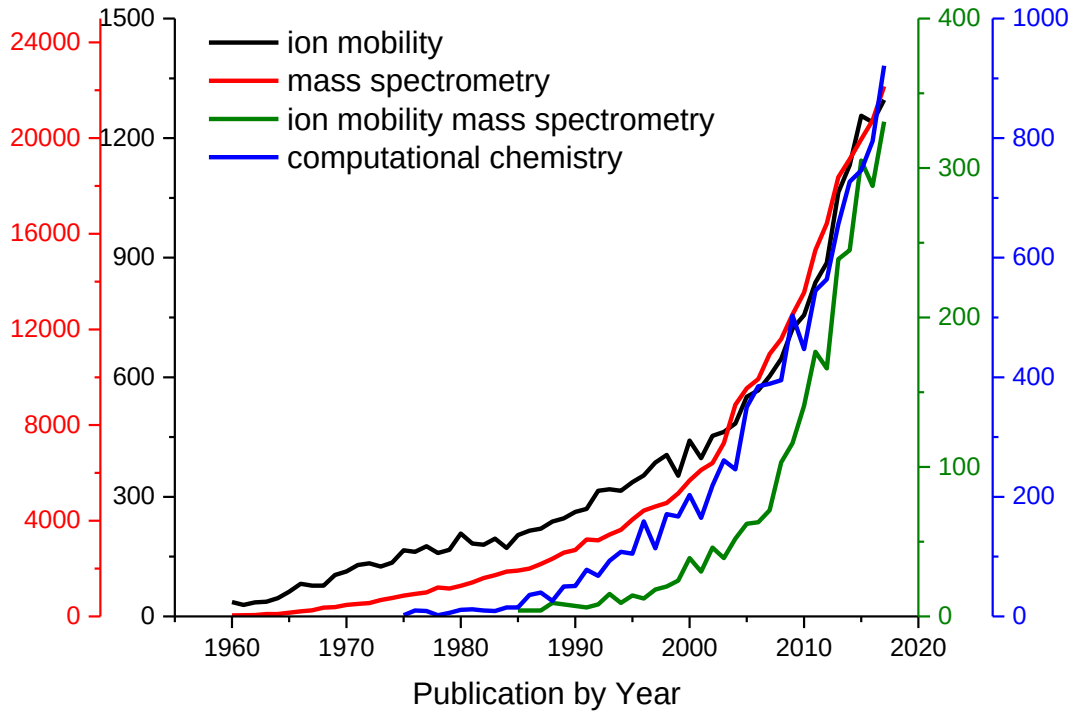

Figure 1.6. Publications by year showing the upward trend in the topics discussed in this manuscript.

Herein we present our findings on the chemical environment of the TIMS-MS device during various applications. In chapter two, *Lifetimes and stabilities of familiar explosive molecular adduct complexes during ion mobility measurements*, published in *The Analyst* we look at the ion stability of ion neutral complexes formed during the analysis of explosives. In chapter 3, I*nfluence of gas modifiers on the TIMS analysis of familiar explosives*, published in *International Journal for Ion Mobility Spectrometry* we continue the exploration of the ion kinetics by introducing dopant gases to the TIMS-MS procedure. Chapter four, *Detection of firearm discharge residue from skin swabs using trapped ion mobility spectrometry coupled to mass spectrometry*, featured on the cover of *Analytical*

Methods follows with the study of organometallics during the analysis of gunshot residue. Chapter five, *Rapid screening of labile juvenile hormone III using liquid chromatography - trapped ion mobility spectrometry - mass spectrometry*, which has been submitted to *Journal of Pharmaceutical and Biomedical Analysis* focuses on implementing liquid chromatography in front of the TIMS-MS device for the detection of juvenile hormones relevant to mosquito population control along with the resulting fragment ions that occur.

List of References

1. Gross, J.H., *Mass Spectrometry A Textbook Second Edition*. 2011, Berlin Heidelberg: Springer-Verlag.

2. Griffiths, J., *A brief history of mass spectrometry.* Anal Chem, 2008. **80**(15): p. 5678-5683.

3. Russell, H. and G. Siuzdak, *A Mass Spec Timeline.* Today'S Chemist AT Work, 2003.

4. De Hoffmann, E., *Mass spectrometry.* Kirk-Othmer Encyclopedia of Chemical Technology, 2000.

5. Dass, C., *Fundamentals of contemporary mass spectrometry*. Vol. 16. 2007: John Wiley & Sons.

6. Lynch, K., *Toxicology: liquid chromatography mass spectrometry*, in *Mass Spectrometry for the Clinical Laboratory*. 2017, Elsevier. p. 109-130.

7. Fialkov, A.B., et al., *Sensitivity and noise in GC–MS: Achieving low limits of detection for difficult analytes.* International Journal of Mass Spectrometry, 2007. **260**(1): p. 31-48.

8. Revercomb, H. and E.A. Mason, *Theory of plasma chromatography/gaseous electrophoresis. Review.* Analytical Chemistry, 1975. **47**(7): p. 970-983.

9. Ellis, H., et al., *Transport properties of gaseous ions over a wide energy range.* Atomic Data and Nuclear Data Tables, 1976. **17**(3): p. 177-210.

10. Gabelica, V. and E. Marklund, *Fundamentals of ion mobility spectrometry.* Current opinion in chemical biology, 2018. **42**: p. 51-59.

11. Eiceman, G.A., Z. Karpas, and H.H. Hill Jr, *Ion mobility spectrometry*. 2013: CRC press.

12. Collins, D. and M. Lee, *Developments in ion mobility spectrometry–mass spectrometry.* Analytical and bioanalytical chemistry, 2002. **372**(1): p. 66-73.

13. Cumeras, R., et al., *Review on ion mobility spectrometry. Part 1: current instrumentation.* Analyst, 2015. **140**(5): p. 1376-1390.

14. B., K.A., et al., *Ion mobility–mass spectrometry.* Journal of Mass Spectrometry, 2008. **43**(1): p. 1-22.

15. Enders, J.R. and J.A. Mclean, *Chiral and structural analysis of biomolecules using mass spectrometry and ion mobility-mass spectrometry.* Chirality: The Pharmacological, Biological, and Chemical Consequences of Molecular Asymmetry, 2009. **21**(1E): p. E253-E264.

16. Dwivedi, P., et al., *Gas-phase chiral separations by ion mobility spectrometry.* Analytical chemistry, 2006. **78**(24): p. 8200-8206.

17. Dugourd, P., et al., *High-resolution ion mobility measurements.* Review of Scientific Instruments, 1997. **68**(2): p. 1122-1129.

18. Asbury, G.R. and H.H. Hill Jr, *Evaluation of ultrahigh resolution ion mobility spectrometry as an analytical separation device in chromatographic terms.* Journal of Microcolumn Separations, 2000. **12**(3): p. 172-178.

19. Siems, W.F., et al., *Measuring the resolving power of ion mobility spectrometers.* Analytical Chemistry, 1994. **66**(23): p. 4195-4201.

20. Rokushika, S., et al., *Resolution measurement for ion mobility spectrometry.* Analytical Chemistry, 1985. **57**(9): p. 1902-1907.

21. May, J.C., et al., *Conformational ordering of biomolecules in the gas phase: nitrogen collision cross sections measured on a prototype high resolution drift tube ion mobility-mass spectrometer.* Analytical chemistry, 2014. **86**(4): p. 2107-2116.

22. Karasek, F. and D. Denney, *Detection of 2, 4, 6-trinitrotoluene vapours in air by plasma chromatography.* Journal of Chromatography A, 1974. **93**(1): p. 141-147.

23. McKenzie-Coe, A., et al., *Lifetimes and stabilities of familiar explosive molecular adduct complexes during ion mobility measurements.* Analyst, 2015. **140**(16): p. 5692-5699.

24. Ewing, R.G., et al., *A critical review of ion mobility spectrometry for the detection of explosives and explosive related compounds.* Talanta, 2001. **54**(3): p. 515-529.

25. Wu, C., et al., *Construction and characterization of a high-flow, high-resolution ion mobility spectrometer for detection of explosives after personnel portal sampling.* Talanta, 2002. **57**(1): p. 123-134.

26. Karpas, Z., *Forensic Science Applications of Ion Mobility Spectrometry.* Forensic science review, 1989. **1**(2): p. 103-119.

27. Miki, A., et al., *Application of ion mobility spectrometry to the rapid screening of methamphetamine incorporated in hair.* Journal of Chromatography B: Biomedical Sciences and Applications, 1997. **692**(2): p. 319-328.

28. Miki, A., et al., *Detection of internal and external methamphetamine in human hair by ion mobility spectrometry.* Eisei kagaku, 1997. **43**(1): p. 15-24.

29. Keller, T., et al., *Detection of designer drugs in human hair by ion mobility spectrometry (IMS).* Forensic science international, 1998. **94**(1-2): p. 55-63.

30. Eiceman, G.A., et al., *Screening of solid commercial pharmaceuticals using ion mobility spectrometry.* Analytical chemistry, 1990. **62**(14): p. 1374-1379.

31. Keller, T., et al., *Analysis of psilocybin and psilocin in Psilocybe subcubensis GUZMAN by ion mobility spectrometry and gas chromatography–mass spectrometry.* Forensic science international, 1999. **99**(2): p. 93-105.

32. Ruzsanyi, V., S. Sielemann, and J. Baumbach, *Determination of VOCs in human breath using IMS.* Int. J. Ion Mobility Spectrom, 2002. **5**: p. 45-48.

33. Eiceman, G., et al., *Ion mobility spectrometry of halothane, enflurane, and isoflurane anesthetics in air and respired gases.* Analytical chemistry, 1989. **61**(10): p. 1093-1099.

34. Eiceman, G.A., *Advances in ion mobility spectrometry: 1980–1990.* Critical Reviews in Analytical Chemistry, 1991. **22**(1-2): p. 471-490.

35. Lapthorn, C., F. Pullen, and B.Z. Chowdhry, *Ion mobility spectrometry-mass spectrometry (IMS-MS) of small molecules: Separating and assigning structures to ions.* Mass spectrometry reviews, 2013. **32**(1): p. 43-71.

36. McDaniel, E., D. Martin, and W. Barnes, *Drift tube-mass spectrometer for studies of low-energy ion-molecule reactions.* Review of Scientific Instruments, 1962. **33**(1): p. 2-7.

37. McAfee Jr, K. and D. Edelson, *Identification and mobility of ions in a Townsend discharge by time-resolved mass spectrometry.* Proceedings of the Physical Society, 1963. **81**(2): p. 382.

38. Edelson, D., et al., *Interpretation of ion-mobility experiments in reacting systems.* Physical Review, 1967. **164**(1): p. 71.

39. McAfee Jr, K.B., D. Sipler, and D. Edelson, *Mobilities and reactions of ions in argon.* Physical Review, 1967. **160**(1): p. 130.

40. McKnight, L., K. McAfee, and D. Sipler, *Low-field drift velocities and reactions of nitrogen ions in nitrogen.* Physical Review, 1967. **164**(1): p. 62.

41. Young, C., D. Edelson, and W. Falconer, *Water cluster ions: rates of formation and decomposition of hydrates of the hydronium ion.* The Journal of Chemical Physics, 1970. **53**(11): p. 4295-4302.

42. Karasek, F.W., M.J. Cohen, and D.I. Carroll, *Trace studies of alcohols in the plasma chromatograph—mass spectrometer.* Journal of Chromatographic science, 1971. **9**(7): p. 390-392.

43. Kolaitis, L. and D.M. Lubman, *Atmospheric pressure ionization mass spectrometry with laser-produced ions.* Analytical Chemistry, 1986. **58**(9): p. 1993-2001.

44. Huang, S.D., L. Kolaitis, and D.M. Lubman, *Detection of explosives using laser desorption in ion mobility spectrometry/mass spectrometry.* Applied spectroscopy, 1987. **41**(8): p. 1371-1376.

45. Kim, S. and G. Spangler, *Ion Mobility Spectrometry/Mass Spectromentry of Two Structurally Different Ions Having Identical Ion Mass.* Analytical Chemistry, 1985. **57**(2): p. 567-569.

46. Karasek, F., S. Kim, and H. Hill, *Mass identified mobility spectra of p-nitrophenol and reactant ions in plasma chromatography.* Analytical Chemistry, 1976. **48**(8): p. 1133-1137.

47. Guevremont, R., et al., *Combined ion mobility/time-of-flight mass spectrometry study of electrospray-generated ions.* Analytical chemistry, 1997. **69**(19): p. 3959-3965.

48. Wollnik, H., *History of mass measurements in time-of-flight mass analyzers.* International Journal of Mass Spectrometry, 2013. **349**: p. 38-46.

49. Campana, J.E., *Time-of-flight mass spectrometry: a historical overview*. 1987.

50. Cotter, R.J., *Time-of-flight mass spectrometry: An increasing role in the life sciences.* Biomedical & environmental mass spectrometry, 1989. **18**(8): p. 513-532.

51. Shelimov, K.B., et al., *Protein structure in vacuo: gas-phase conformations of BPTI and cytochrome c.* Journal of the American Chemical Society, 1997. **119**(9): p. 2240-2248.

52. Hoaglund, C.S., S.J. Valentine, and D.E. Clemmer, *An Ion trap interface for ESI–ion mobility experiments.* Analytical chemistry, 1997. **69**(20): p. 4156-4161.

53. Valentine, S., et al., *Gas-phase separations of protease digests.* Journal of the American Society for Mass Spectrometry, 1998. **9**(11): p. 1213-1216.

54. Liu, Y. and D.E. Clemmer, *Characterizing oligosaccharides using injected-ion mobility/mass spectrometry.* Analytical Chemistry, 1997. **69**(13): p. 2504-2509.

55. Hoaglund-Hyzer, C.S., J. Li, and D.E. Clemmer, *Mobility labeling for parallel CID of ion mixtures.* Analytical chemistry, 2000. **72**(13): p. 2737-2740.

56. Hoaglund, C.S., et al., *Three-dimensional ion mobility/TOFMS analysis of electrosprayed biomolecules.* Analytical chemistry, 1998. **70**(11): p. 2236-2242.

57. Henderson, S.C., et al., *ESI/ion trap/ion mobility/time-of-flight mass spectrometry for rapid and sensitive analysis of biomolecular mixtures.* Analytical chemistry, 1999. **71**(2): p. 291-301.

58. Hoaglund-Hyzer, C.S. and D.E. Clemmer, *Ion trap/ion mobility/quadrupole/time-of-flight mass spectrometry for peptide mixture analysis.* Analytical chemistry, 2001. **73**(2): p. 177-184.

59. Srebalus Barnes, C.A. and D.E. Clemmer, *Assessment of purity and screening of peptide libraries by nested ion mobility-TOFMS: identification of RNase S-protein binders.* Analytical chemistry, 2001. **73**(3): p. 424-433.

60. Srebalus, C.A., et al., *Determining synthetic failures in.* Journal of the American Society for Mass Spectrometry, 2000. **11**(4): p. 352-355.

61. Valentine, S.J., A.E. Counterman, and D.E. Clemmer, *A database of 660 peptide ion cross sections: use of intrinsic size parameters for bona fide predictions of cross sections.* Journal of the American Society for Mass Spectrometry, 1999. **10**(11): p. 1188-1211.

62. Srebalus, C.A., et al., *Gas-phase separations of electrosprayed peptide libraries.* Analytical chemistry, 1999. **71**(18): p. 3918-3927.

63. Buryakov, I., et al., *A new method of separation of multi-atomic ions by mobility at atmospheric pressure using a high-frequency amplitude-asymmetric strong electric field.* International Journal of Mass Spectrometry and Ion Processes, 1993. **128**(3): p. 143-148.

64. Buryakov, I., et al., *Separation of ions according to mobility in a strong AC electric field.* Sov. Tech. Phs. Lett, 1991: p. 446-447.

65. Kolakowski, B.M. and Z. Mester, *Review of applications of high-field asymmetric waveform ion mobility spectrometry (FAIMS) and differential mobility spectrometry (DMS).* Analyst, 2007. **132**(9): p. 842-864.

66. Shvartsburg, A.A., et al., *High-resolution field asymmetric waveform ion mobility spectrometry using new planar geometry analyzers.* Analytical chemistry, 2006. **78**(11): p. 3706-3714.

67. Krylov, E., *Comparison of the planar and coaxial field asymmetrical waveform ion mobility spectrometer (FAIMS).* International Journal of Mass Spectrometry, 2003. **225**(1): p. 39-51.

68. Guevremont, R., et al., *Analysis of a tryptic digest of pig hemoglobin using ESI-FAIMS-MS.* Analytical chemistry, 2000. **72**(19): p. 4577-4584.

69. Shvartsburg, A.A., G.A. Anderson, and R.D. Smith, *Pushing the frontier of high-definition ion mobility spectrometry using FAIMS.* Mass Spectrometry, 2013. **2**(Special_Issue): p. S0011-S0011.

70. Flagan, R.C., *History of electrical aerosol measurements.* Aerosol Science and Technology, 1998. **28**(4): p. 301-380.

71. Intra, P. and N. Tippayawong, *An overview of differential mobility analyzers for size classification of nanometer-sized aerosol particles.* 2008.

72. Salm, J. and U. Horrak, *Diffusion distortions in a differential mobility analyzer with inclined electric field.* Aerosol Science and Technology, 2009. **43**(3): p. 227-231.

73. Tammet, H., *The aspiration method for the determination of atmospheric-ion spectra*. 1970.

74. Gabelica, V., et al., *Recommendations for Reporting Ion Mobility Mass Spectrometry Measurements.* 2018.

75. Alonso, M., et al., *First differential mobility analysis (DMA) measurements of air ions produced by radioactive source and corona.* Aerosol Air Qual. Res, 2009. **9**: p. 453-457.

76. Reischl, G.P., *Measurement of ambient aerosols by the differential mobility analyzer method: Concepts and realization criteria for the size range between 2 and 500 nm.* Aerosol Science and Technology, 1991. **14**(1): p. 5-24.

77. Pringle, S.D., et al., *An investigation of the mobility separation of some peptide and protein ions using a new hybrid quadrupole/travelling wave IMS/oa-ToF instrument.* International Journal of Mass Spectrometry, 2007. **261**(1): p. 1-12.

78. Giles, K., et al., *Applications of a travelling wave-based radio-frequency-only stacked ring ion guide.* Rapid Communications in Mass Spectrometry, 2004. **18**(20): p. 2401-2414.

79. Giles, K., J.P. Williams, and I. Campuzano, *Enhancements in travelling wave ion mobility resolution.* Rapid Communications in Mass Spectrometry, 2011. **25**(11): p. 1559-1566.

80. Shvartsburg, A.A. and R.D. Smith, *Fundamentals of traveling wave ion mobility spectrometry.* Analytical chemistry, 2008. **80**(24): p. 9689-9699.

81. Webb, I.K., et al., *Experimental evaluation and optimization of structures for lossless ion manipulations for ion mobility spectrometry with time-of-flight mass spectrometry.* Analytical chemistry, 2014. **86**(18): p. 9169-9176.

82. Hamid, A.M., et al., *Characterization of traveling wave ion mobility separations in structures for lossless ion manipulations.* Analytical chemistry, 2015. **87**(22): p. 11301-11308.

83. Deng, L., et al., *Serpentine ultralong path with extended routing (SUPER) high resolution traveling wave ion mobility-MS using structures for lossless ion manipulations.* Analytical chemistry, 2017. **89**(8): p. 4628-4634.

84. Park, M.A., *Apparatus and method for parallel flow ion mobility spectrometry combined with mass spectrometry*. 2010, Google Patents.

85. Hernandez, D.R., et al., *Ion dynamics in a trapped ion mobility spectrometer.* Analyst, 2014. **139**(8): p. 1913-1921.

86. Fernandez-Lima, F.A., et al., *Gas-phase separation using a Trapped Ion Mobility Spectrometer.* Int. J. Ion Mobil. Spectrom., 2011. **14**(2-3): p. 93-98.

87. Michelmann, K., et al., *Fundamentals of trapped ion mobility spectrometry.* Journal of the American Society for Mass Spectrometry, 2015. **26**(1): p. 14-24.

88. Ridgeway, M.E., et al., *Trapped ion mobility spectrometry: A short review.* International Journal of Mass Spectrometry, 2018.

89. Fernandez-Lima, F.A., D.A. Kaplan, and M.A. Park, *Note: Integration of trapped ion mobility spectrometry with mass spectrometry.* Rev. Sci. Instr., 2011. **82**(12): p. 126106.

90. Silveira, J.A., et al., *Fundamentals of trapped ion mobility spectrometry part II: fluid dynamics.* Journal of The American Society for Mass Spectrometry, 2016. **27**(4): p. 585-595.

91. Silveira, J.A., M.E. Ridgeway, and M.A. Park, *High resolution trapped ion mobility spectrometery of peptides.* Analytical chemistry, 2014. **86**(12): p. 5624-5627.

92. Adams, K.J., et al., *Analysis of isomeric opioids in urine using LC-TIMS-TOF MS.* Talanta, 2018. **183**: p. 177-183.

93. Benigni, P., et al., *Increasing Analytical Separation and Duty Cycle with Nonlinear Analytical Mobility Scan Functions in TIMS-FT-ICR MS.* Analytical chemistry, 2018. **90**(4): p. 2446-2450.

94. Mack Jr, E., *Average cross-sectional areas of molecules by gaseous diffusion methods.* Journal of the American Chemical Society, 1925. **47**(10): p. 2468-2482.

95. von Helden, G., et al., *Carbon cluster cations with up to 84 atoms: structures, formation mechanism, and reactivity.* The Journal of Physical Chemistry, 1993. **97**(31): p. 8182-8192.

96. Jarrold, M.F. and V.A. Constant, *Silicon cluster ions: evidence for a structural transition.* Physical review letters, 1991. **67**(21): p. 2994.

97. Mesleh, M., et al., *Structural information from ion mobility measurements: effects of the long-range potential.* The Journal of Physical Chemistry, 1996. **100**(40): p. 16082-16086.

98. ACS. *Computational Chemistry-Overview*. Available from: https://www.acs.org/content/acs/en/careers/college-to-career/chemistry-careers/computational-chemistry.html.

99. Cramer, C.J., *Essentials of computational chemistry: theories and models*. 2013: John Wiley & Sons.

100. Shvartsburg, A.A. and M.F. Jarrold, *An exact hard-spheres scattering model for the mobilities of polyatomic ions.* Chemical physics letters, 1996. **261**(1-2): p. 86-91.

101. D'Atri, V., et al., *Linking molecular models with ion mobility experiments. Illustration with a rigid nucleic acid structure.* Journal of Mass Spectrometry, 2015. **50**(5): p. 711-726.

102. Paizs, B., *A divide-and-conquer approach to compute collision cross sections in the projection approximation method.* International Journal of Mass Spectrometry, 2015. **378**: p. 360-363.

103. Larriba, C. and C.J. Hogan Jr, *Free molecular collision cross section calculation methods for nanoparticles and complex ions with energy accommodation.* Journal of Computational Physics, 2013. **251**: p. 344-363.

104. J., P.C., B.J. H., and A. T., *The modern mass spectrometer—a complete chemical laboratory.* Organic Mass Spectrometry, 1981. **16**(3): p. 101-114.

Chapter Two:

LIFETIMES AND STABILITIES OF FAMILIAR EXPLOSIVE MOLECULAR ADDUCT COMPLEXES DURING ION MOBILITY MEASUREMENTS

This chapter was published in *Analyst* and reproduced with permission.

McKenzie-Coe, A., et al., *Lifetimes and stabilities of familiar explosive molecular adduct complexes during ion mobility measurements.* Analyst, 2015. **140**(16): p. 5692-5699.

2.1. Abstract

Trapped ion mobility spectrometry coupled to mass spectrometry (TIMS-MS) was utilized for the separation and identification of familiar explosives in complex mixtures. For the first time, molecular adduct complex lifetimes, relative stability, binding energies and candidate structures are reported for familiar explosives. Experimental and theoretical results showed that the adduct size and reactivity, complex binding energy and the explosive structure tailor the stability of the molecular adduct complex. The flexibility of TIMS to adapt the mobility separation as a function of the molecular adduct complex stability (i.e., short or long IMS experiments/low or high IMS resolution) permits targeted measurements of explosives in complex mixtures with high confidence levels.

2.2. Introduction

Methods for the determination of trace levels of explosives and explosive related materials were developed rapidly and placed into service following several incidents in the 1980s involving catastrophic attacks with bombs on large civilian aircrafts.[1,2] The method chosen and distributed widely was ion mobility spectrometry (IMS) which was still in nascent stages of discovery concerning principles of ionization chemistry and best practices for measurements of ion mobility.[3–7] Nonetheless, embodiments of IMS were able to operate economically for on-site screening of hand-luggage at security check points of passengers and were distributed in airports worldwide. Measurements by the Explosive Trace Detectors (ETDs) with IMS depend upon the collection and vaporization of explosive residue, formation of molecular ions through chemical reactions in the gas phase, and their separation in a weak electric field as they drift in a bath gas.[8] A necessary requirement for an IMS measurement is that molecular ions formed from a substance should be distinctive

and should have lifetimes sufficient to pass through the drift region with a characteristic mobility. This can be challenging with explosive molecular ions which may exhibit brief lifetimes and undergo reactions or decompositions either in the reaction region or in the drift region.[9,10] While sufficient understanding existed on the ionization chemistry and stability of ions in air at ambient pressure to justify the development of ETDs based on IMS, precise knowledge of the kinetics of ion decompositions and even the means to measure ion lifetimes in air at ambient pressure were developed only recently.

Explosive ions are formed in IMS based ETDs through chemical reactions where an explosive molecule, M, is electrostatically associated with a reactant or reagent ion, commonly Cl^-, through ion-dipole or ion-induced dipole interactions.[6,11,12] The ions have thermal energies in the ion source of an IMS analyzer and ion and molecule associations are favorable without an energy barrier. Excess energy from the association can be lost by collisions, by reactions, and by dissociation of the explosives from the ions by the high collision frequency and abundance of small polar neutrals in the purified air of the IMS drift tube. Common reactions with explosives include hydrogen abstraction of protons that are acidic enough to be lost as HCl from an adduct $[M+Cl]^-$ and loss of NO_3^- which appears to arise as a Cl^- displacement reaction with a fracture in a weak carbon–oxygen bond.[8] In other instances, the original adduct $[M+Cl]^-$ has sufficient lifetime to pass through the drift region and reach the detector as an intact ion. In other instances, the ion may survive in the reaction region (~3 ms) and undergo reactions or dissociation in the drift region, appearing as a distortion in the baseline of the mobility spectrum.[13] Methods were described to extract kinetic information from baseline distortions and refined methods developed recently as a kinetic IMS instrument to obtain rate data for specific ions over a

range of temperatures without interferences from unwanted ion neutral interactions.[14] Reactions including loss of NO_3^- and Cl^- from thermalized ions require energy which has been measured with the kinetic IMS method as 60 to 89 kJ/mol and match favorably with ab initio calculations.[9, 10] These reactions are dependent not only on temperature and moisture but also on the precursor ion. While commercial ETDs produce Cl^- by dissociative electron capture in a beta emitter source, electrospray ionization (ESI) sources affords flexibility and convenience to form adducts from other anions by spiking the ESI starting solution with various salts.[15, 16] For example, measurement of multiple adduct forms of a targeted compound increases the identification confidence while reducing the probability of having interferences from the sample matrix.

With the recent development of trapped ion mobility spectrometry (TIMS), higher mobility resolution and the capability to interrogate and simultaneously measure the molecular ion neutral collision cross section (CCS) as a function of time after the molecular ion formation has permitted kinetic studies of molecular ion–neutral bath gas interactions at the millisecond to second time scale.[17–22] In the current study, the unique potential of TIMS to hold ions while interacting with bath gas molecules ("TIMS" thermostat) is utilized to study the stability and dissociation kinetics of familiar explosives with different adduct forms at the level of individual molecules. In particular, ion-neutral collision cross sections (CCS) are measured using TIMS for a series of familiar explosive standards in nitrogen as a bath gas and compared with traditional drift tube IMS measurements and theoretical calculations. TIMS-MS capability to separate and identify explosives from complex samples is also demonstrated. In addition, for the first time, molecular ion stability and lifetimes are reported for a series of familiar explosive molecular adducts.

2.3. Experimental Section

2.3.1. Chemicals

Individual standards of 2-methyl-1,3,5-trinitrobenzene (TNT), 1,3,5-trinitroperhydro-1,3,5-triazine (RDX), 3-nitrooxy-2,2-bis-(nitrooxymethyl) propyl nitrate (PETN) and octahydro-1,3,5,7-tetranitro-1,3,5,7-tetrazocine (HMX) were obtained from AccuStandard (New Haven, CT) and used as received. Ammonium chloride, ammonium formate, ammonium acetate and ammonium nitrate salts and chromatography grade water, methanol and acetonitrile solvents were obtained from Fisher Scientific (Suwanee, GA) and used as received. TNT, RDX and HMX were dissolved in 1: 1 water: methanol v/v ratio, and PETN was dissolved in 1: 1: 1 water: methanol: acetonitrile v/v ratio to a final concentration of 1 μM. Each ammonium salt containing solution was prepared separately and added to each explosive solution to a final concentration of 10 mM of ammonium salt. An electrospray ionization source (ESI, Bruker Daltonics Inc., MA) was used for all analyses in negative ion mode. The sample purity was confirmed with sub ppm mass accuracy for each standard using ultra-high-resolution mass spectrometry with a Solarix 7 T FT-ICR MS mass spectrometer (Bruker Daltonics Inc., Billerica, MA). A complex mixture of TNT + cappuccino was prepared by doping a standard cappuccino coffee solution with the TNT standard (1 μM) to 100: 1 v/v ratio; the complex mixture sample was diluted in 1: 1: 1 water: methanol: acetonitrile v/v ratio to a final concentration of 10 nM of the TNT standard.

2.3.2. TIMS-MS operation

Details regarding the TIMS operation and specifics compared to traditional IMS can be found elsewhere.[17,19,21,23,24] Briefly, mobility separation in TIMS is based on holding the ions stationary using an electric field against a moving gas. The separation in a TIMS device can be described by the center of the mass frame using the same principles as in a conventional IMS drift tube.[25] In traditional drift tube cells, mobility separation is related to the number of ion-neutral collisions (or drift time); analogously, the mobility separation in a TIMS device is related to the bath gas drift velocity, ion confinement and ion elution parameters. The mobility, K, of an ion in a TIMS cell is described by:

$$K = \frac{v_g}{E} = \frac{A}{(V_{elution} - V_{base})} \qquad (1)$$

where v_g, E, $V_{elution}$ and V_{base} are the velocity of the gas, applied electric field, elution and base voltages, respectively. The constant A was determined using the reported mobilities of explosives.[8,26] In TIMS operation, multiple geometric isomers/conformers can be trapped simultaneously at different E values resulting from a voltage gradient applied across the IMS tunnel. After thermalization, trapped species are eluted by decreasing the electric field in stepwise decrements (referred to as the "ramp"). Each mobility-separated isomer/conformer eluting from the TIMS cell can be described by a characteristic voltage difference (i.e., $V_{elution} - V_{base}$). Eluted ions are then mass analyzed and detected by using a maXis impact Q-ToF mass spectrometer (Bruker Daltonics Inc., Billerica, MA). In a TIMS device, the total analysis time can be described as:

$$\text{Total IMS time} = T_{trap} + (V_{elution}/V_{base}) \times T_{trap} + \text{ToF}$$

$$= T_o + \left(V_{elution}/V_{ramp}\right) \times T_{ramp} \qquad (2)$$

where T_{trap} is the thermalization/trapping time, ToF is the time after the mobility separation, and V_{ramp} and T_{ramp} are the voltage range and time required to vary the electric field, respectively. The elution voltage can be experimentally determined by varying the ramp time for a constant ramp voltage. This procedure also determines the time ions spend outside the separation region T_o (e.g., ion trapping and time-of-flight).

The TIMS funnel is controlled using in-house software, written in National Instruments Lab VIEW, and synchronized with the maXis Impact Q-ToF acquisition program.[17,23] TIMS separation was performed using nitrogen as a bath gas at *ca.* 300 K and typical pressures at the entrance and back regions of the TIMS analyzer were P_1 = 2.6 and P_2 = 1.0 mbar, respectively (see more details in ref. 19). The same RF (2040 kHz and 200–350 V_{pp}) was applied to all electrodes including the entrance funnel, the mobility separating section, and the exit funnel. At all times, the axial electric field was kept under the low field limit (E/p < 10 V cm^{-1} torr^{-1}) throughout the TIMS and no significant ion heating is produced by the RF confinement.

Mobility values (K) were correlated with CCS (Ω) using the equation:

$$\Omega = \frac{(18\pi)^{1/2}}{16}\frac{ze}{(k_B T)^{1/2}}\left(\frac{1}{m_i}+\frac{1}{m_b}\right)^{1/2}\frac{1}{K}\times\frac{760}{P}\frac{T}{273.15}\frac{1}{N^*} \qquad (3)$$

where ze is the charge of the ion, k_B is the Boltzmann constant, N^* is the number density under standard temperature and pressure conditions, and m_i and m_b refer to the masses of the ion and bath gas, respectively.[25]

The analysis of the molecular adduct decomposition was considered as a first order reaction. The molecular adduct abundance at a given time is defined by the equation:

$$I = I_o e^{(-kt)} \qquad (4)$$

where k is the decomposition rate (k = 1/td), td is the lifetime of the molecular adduct complex, and Io is the initial abundance.

2.3.3. Theoretical calculations

Geometries and binding energies of candidate structures were optimized at the DFT/B3LYP/6-31+g(d) level using Gaussian 09 software.[27] Vibrational frequencies were calculated to guarantee that the optimized structures correspond to a real minima in the energy space, and zero-point energy corrections were applied to calculate the relative stability. Partial atomic charges were calculated using the Merz–Singh–Kollman scheme constrained to the molecular dipole moment.[28,29] Theoretical ion-neutral collision cross sections were calculated using the trajectory method (TM) in MOBCAL version for nitrogen30,31 with a bath gas at *ca.* 300 K. It should be noted that the MOBCAL version for nitrogen was used assuming the similarity of the molecules to those used to develop the Lennard-Jones potential at 300 K in ref. 30 and 31; for other molecules, alternative methods may be more accurate (see ref. 32). All optimized geometries and MOBCAL input files can be found in the ESI. †

2.4. Results and Discussion

A prerequisite for good analytical IMS performance is the ability to separate and identify molecular species with high reproducibility. The IMS resolution of handheld IMS instruments (*e.g.*, ETDs) is commonly $R_{IMS} = 20$ or below; however, laboratory research IMS instruments using drift tube IMS designs can routinely reach $R_{IMS} = 80 - 100$.[33–37] Recently, we have reported the advantages of TIMS technology to achieve higher mobility resolution ($R_{IMS} = 120 - 250$).[19,20] Different from other IMS forms (*e.g.*, field asymmetric IMS,38 differential mobility spectrometer,[39–41] segmented quadrupole drift cell,[42] cylindrical drift tubes,[43] and traveling wave ion guide[44]), TIMS mobility resolution varies with the size, mass and charge of the molecule of interest; that is, different trapping conditions are required to compensate for molecular ion diffusion and for coulombic repulsion of molecular ions during the trapping and elution steps. In practice, this translates into a lower mobility resolution for high mobility and low mass-to-charge ratio species when compared to previously reported values during fast TIMS mobility scans (see Fig. 2.1 for common explosives). One alternative to increase the TIMS mobility resolution is to reduce the ramp speed which results in higher IMS resolution. For example, a high mobility resolution of $R_{TIMS} > 120$ can be achieved for the analysis of explosives which results in a 3–5-fold increase in resolution when compared to commercially available ETD instruments.

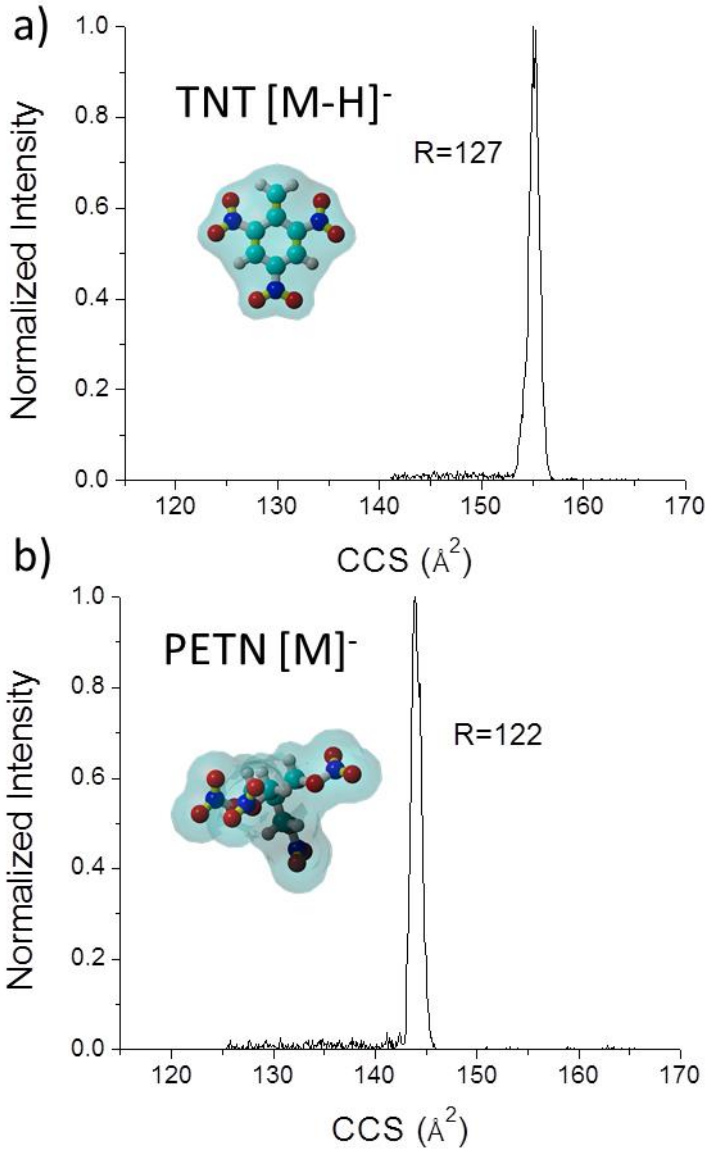

Figure 2.1. Typical IMS spectra for a) TNT and b) PETN.

The high mobility resolution of a TIMS device provides great potential for the analysis of explosives in complex mixtures when coupled to mass spectrometry (see Fig. 2.2). That is, the ability to separate common interferences, to increase peak capacity, and to reduce chemical noise using orthogonal separations permits better identification of explosives using accurate CCS (<5% accuracy using external calibration) and *m/z* measurements (in the example presented, mass resolution was $R_{ToF} = 30-40$k). Thus, when internal calibrants are used for CCS determination in a TIMS device over a narrower CCS range the accuracy is better than a few percent. When compared to other hyphenated MS techniques for the analysis of familiar explosives,[15,28,45–51] TIMS-MS provides higher throughput, dynamic range and reduced analysis time. While an increase in peak capacity is observed during TIMS-MS analysis, the most challenging part involves the identification of compounds from the 2D IMS-MS plots. If standards are available for the *a priori* selected target (see Fig. 2.2c), the identification can be achieved by direct correlation of the IMS and MS data. It should be noted that additional IMS-MS/MS can further increase the identification capabilities. Another alternative is the coupling of TIMS to ultrahigh resolution MS analyzers (see the example in ref. 52); however, it should be noted that TIMS-TOF-MS operates with much shorter acquisition times.

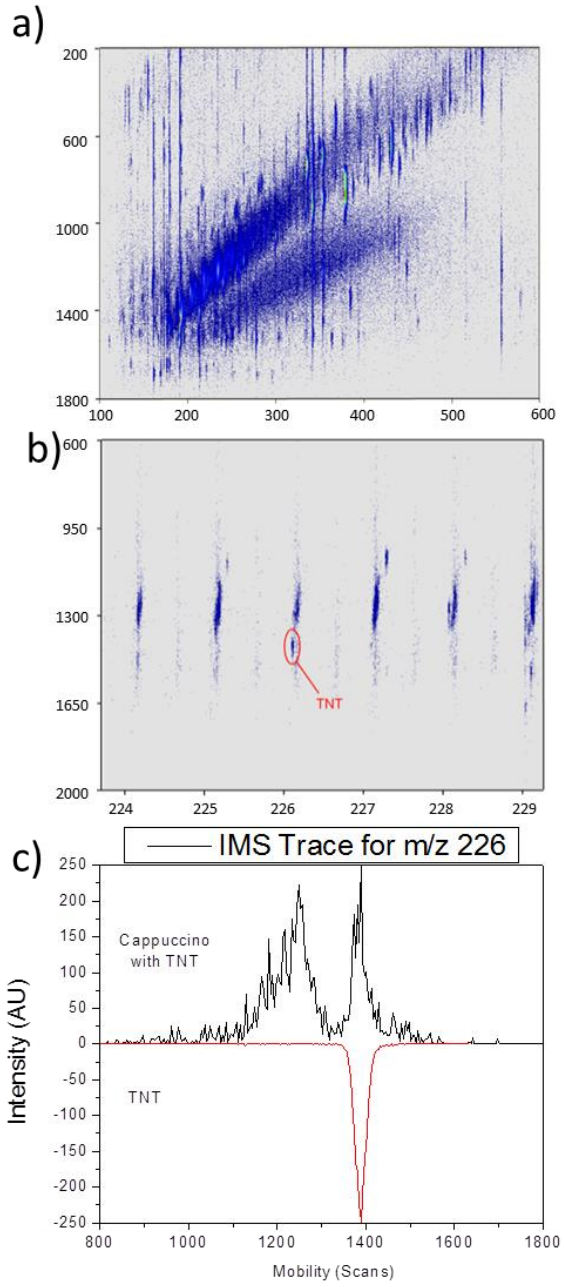

Figure 2.2. a) 2D IMS-MS contour plot of a complex mixture (cappuccino) spiked; b) inset in the *m/z*=224-229 range, and c) trace IMS projection plots of *m/z*=226 for the complex mixture and a TNT standard.

While TIMS-MS provides high confidence for the analysis of common explosives, one way to further improve the confidence level is to simultaneously measure different molecular adducts.[15,16] That is, each measured molecular adduct form provides a two-point identification (i.e., CCS and *m/z*). Multiple molecular adducts can be formed during ESI of explosives by spiking the ESI starting solution with various salts (see the example in Fig. 2.3). In practice, this translates into a CCS and *m/z* shift for each adduct form, thus increasing the confidence level (see more details in Table 2.1). Compound identification from complex mixtures is typically challenged by the existence of molecular interferences in the IMS or MS domain. The use of multiple IMS and MS identification points from multiple adduct forms of a targeted compound increases the identification confidence while reducing the probability of interferences from the sample matrix. In addition, since TIMS permits the measurement of CCS using first principles, the identification can be complemented with theoretical calculations; this approach can be very useful for the case of molecular adduct complexes that can exist as multiple conformations in the gas phase (see the example in ref. 52). Table 2.1 summarizes theoretical and experimental CCS of all the molecular adduct complexes observed (all structures are provided in the ESI, † see Fig. S1†). A K_o absolute error of less than 0.5% was observed in TIMS replicate measurements. Close inspection shows that a good agreement is observed between the theoretical and TIMS experimental values (<5% difference). The largest difference between K_o values measured by using TIMS and literature values can be attributed to the sample introduction (see ref. 8). For example, K_o values of 1.45, 1.48 and 1.54 have been reported for TNT $[M-H]^-$ for sample introduction by desorption, ESI, and vapor (membrane), respectively.

Compound	Ionic Form	*m/z*	TIMS Experimental		Ko (cm^2/Vs) [refs]	Theoretical CCS ($Å^2$)	% Error
			Ko (cm^2/V·s)	CCS ($Å^2$)			
TNT	$[M-H]^-$	226.010	1.483	143.35	1.54	136.33	5.15
RDX+NH_4Cl	$[M+Cl]^-$	257.003	1.437	147.00	1.44*	149.41	1.61
RDX+NH_4NO_3	$[M+NO_3]^-$	284.022	1.361	154.49	1.35*	151.77	1.79
HMX+NH_4Cl	$[M+Cl]^-$	331.015	1.293	161.55	1.25	162.53	0.60
HMX+HCO_2	$[M+HCOOH-H]^-$	341.044	1.280	162.95	-	160.59	1.47
HMX+$NH_4C_2H_3O_2$	$[M+CH_3COOH-H]^-$	355.059	1.227	169.75	-	168.36	0.83
HMX+NH_4NO_3	$[M+NO_3]^-$	358.034	1.234	167.42	-	164.62	1.70
PETN	$[M^*]^-$	316.013	1.368	152.91	-	150.60	1.53
PETN+NH_4Cl	$[M+Cl]^-$	350.982	1.175	177.36	1.20	182.10	2.60
PETN+HCO_2	$[M+HCOOH-H]^-$	361.011	1.140	182.58	-	179.24	1.86
PETN+NH_4NO_3	$[M+NO_3]^-$	378.001	1.105	187.25	1.14	188.79	0.82
*Literature values used to calculate calibration constant, A (rf, vg).							

Table 2.1. Experimental and theoretical ion-neutral collision cross section for familiar explosives molecular complexes ion forms.

The measurement of multiple adduct forms of familiar explosives depends on the probability of forming the molecular adduct complex and its relative stability. During ESI ion formation, changes in the relative salt content can be used to preferentially target the formation of an adduct form as a way to avoid potential CCS and/or *m/z* interference. In addition, the relative stability of the molecular ion complex during the TIMS-MS measurements will provide the best adduct candidate for effective detection. Explosives present different affinities for each molecular adduct complex. For example, TNT presents very low affinity to form a molecular adduct; however, HMX, RDX and PETN form a variety of complexes (*e.g.*, $[M+Cl]^-$, $[M+HCOOH-H]^-$, $[M+CH_3COOH-H]^-$ and $[M+NO_3]^-$). Inspection of the molecular adduct lifetimes shows that the larger the adduct size the lower the complex stability (see Fig. 2.4 and Table 2.2). For example, PETN $[M]^-$ shows the largest lifetime (400 ms) when compared to the other molecular adducts $[M+Cl]^-$ (85 ms), $[M+HCOOH-H]^-$ (92 ms), and $[M+NO3]^-$ (85 ms). Moreover, the explosive structure influences the probability of forming molecular adducts. For example, HMX presents larger binding energy and longer lifetimes (∼3–4×) for the molecular adduct forms when compared with RDX and PETN (see Table 2.2). Inspection of the HMX complex optimized geometries shows that the multiple coordination between the HMX molecule and the adduct favors the stability of the complex. That is, if the charge is protected, TIMS-MS experiments show no ion loss in up to two seconds of trapping (*e.g.*, *m/z* = 301 $C_3N_3(CF_3)_3$ $[M]^-$ from the Agilent tuning mix,[53] Fig. 2.4a). Moreover, if the charge is exposed (e.g., TNT $[M-H]^-$), ions can undergo charge neutralization via charge transfer with the bath gas molecules (e.g., proton transfer). In the case of the molecular adduct, the reactive nature of the adduct ion and the probability to collide with a bath gas molecule

increase the chances for decomposition of the molecular adduct complex by transferring the charge carrying adduct to a bath gas molecule (*e.g*., decomposition by adduct transfer). That is, TIMS-MS experiments suggest that the collision rate and bath gas composition (or impurities) can be the defining factors for the observation of the molecular adduct complex. Although we cannot establish the mechanism for the molecular adduct complex decomposition, preliminary results suggest that the electrostatic nature of the complex can be lost by the interaction with a third partner (bath gas molecule), a short life complex formation, followed by the detachment of the adduct from the molecular complex.

During TIMS analysis, a short analysis time will increase the probability to observe a molecular adduct complex; however, a slower electric field ramp speed will provide higher mobility separations but longer measurement times. That is, high resolution TIMS separation can be limited by the molecular adduct complex lifetime and initial population (or abundance). Moreover, this observation can be extrapolated to the case of traditional drift tube IMS measurements in that long drift times will reduce the probability to observe a molecular complex ion form. In any IMS separation, since the number of collisions defines the mobility resolution, the probability to observe a molecular adduct complex at high IMS resolution is limited by its stability and the composition of the bath gas.

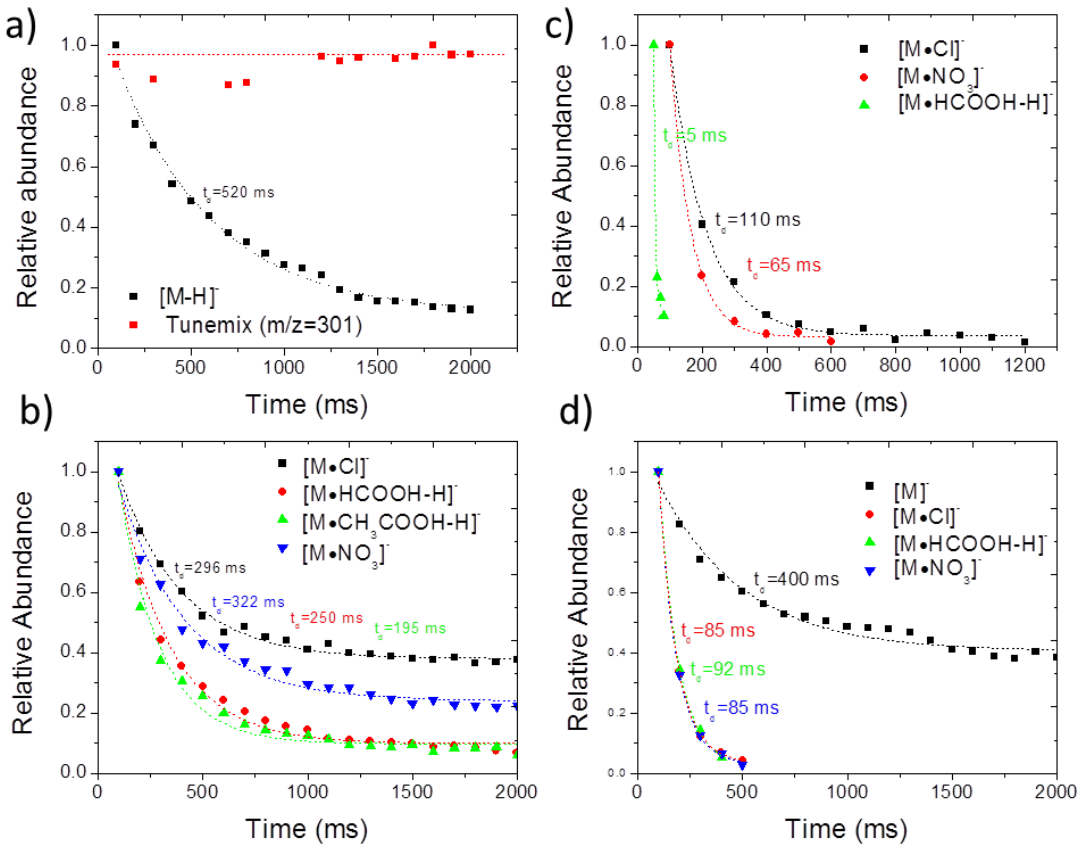

Figure 2.3. Relative abundance of familiar explosive molecular ions as a function of the trapping time: a) TNT, b) HMX, c) RDX and d) PETN

Compound	Ionic Form	Time Decay (ms)	Rate constant k (s^{-1})	Binding Energy (kcal/mol)	Bond Distance (Å)
TNT	$[M-H]^-$	520	1.92	-	
RDX+NH_4Cl	$[M+Cl]^-$	110	9.09	36.93	2.52
RDX+NH_4NO_3	$[M+NO_3]^-$	65	15.38	33.73	1.97
HMX+NH_4Cl	$[M+Cl]^-$	296	3.38	47.47	2.52
HMX+HCO_2	$[M+HCOOH-H]^-$	250	4.00	50.25	2.14
HMX+$NH_4C_2H_3O_2$	$[M+CH_3COOH-H]^-$	195	5.13	52.61	2.08
HMX+NH_4NO_3	$[M+NO_3]^-$	322	3.11	41.06	2.13
PETN	$[M]^-$	400	2.50	-	
PETN+NH_4Cl	$[M+Cl]^-$	85	11.76	30.95	2.39
PETN+HCO_2	$[M+HCOOH-H]^-$	92	10.87	33.57	2.10
PETN+NH_4NO_3	$[M+NO_3]^-$	85	11.76	28.50	2.28

Table 2.2. Relative stabilities of molecular complexes ion forms from familiar explosives

2.5. Conclusions

The analytical capabilities of TIMS-MS for the separation and identification of familiar explosives have been demonstrated. In particular, a three to five-fold increase in mobility resolution was observed for the TIMS analyzer when compared with commercial ETD IMS devices. The use of molecular adduct complexes increases the confidence level and permits the identification of familiar explosives using first principle CCS and *m/z* measurements. For the first time, lifetimes, relative stability, binding energies and candidate structures are reported for molecular adducts of familiar explosives. Inspection of the molecular adduct interaction with the residual bath gas showed three major trends: (i) molecular ions (*e.g.*, $[M-H]^-$) are more stable than their molecular adduct counterparts (e.g., $[M+Cl]^-$, $[M+HCOOH-H]^-$, $[M+CH_3COOH-H]^-$ and $[M+NO_3]^-$), (ii) the stability of the chloride and nitrate adducts is higher than the formate and acetate adducts, and (iii) HMX forms the most stable molecular adduct complexes when compared with RDX and PETN. We interpret this relative stability as a consequence of the probability of decomposition and of charge exchange with the bath gas of the molecular adduct complexes. That is, the adduct size and reactivity, complex binding energy and the explosive structure define the stability of the molecular adduct complex. The TIMS flexibility to modify the mobility separation as a function of the molecular adduct stability (i.e., short or long IMS experiments/low or high IMS resolution) permits targeted measurements of explosives in complex mixtures.

2.6. Acknowledgements

This work was supported by the National Institute of Health (Grant No. R00GM106414). The authors would like to thank Dr. Alexander Mebel and the Instructional & Research Computing Center (Florida International University) for helpful discussions during the

theoretical calculations. AMC acknowledges the McKnight doctoral fellowship. We would like to acknowledge the technical support provided by the Advanced Mass Spectrometry Facility at Florida International University.

List of References

1. D. P. Lucero, J. Test. Eval., 1985, 13, 12.

2. D. D. Fetterolf and T. D. Clark, J. Forensic Sci., 1993, 38, 28–39.

3. W. D. Kilpatrick, Plasma Chromatography (trademark) and Dynamite Vapor Detection, Defense Technical Information Center, 1971.

4. F. W. Karasek, Res./Dev., 1974, 25, 3.

5. F. W. Karasek and D. W. Denney, J. Chromatogr. A, 1974, 93, 141–147.

6. G. E. Spangler and P. A. Lawless, Anal. Chem., 1978, 50, 884–892.

7. G. E. Spangler, J. P. Carrico and S. H. Kim, Presented in part at the Proceedings of the International Symposium on Analysis and Detection of Explosive, Quantico, VA, 1983.

8. R. G. Ewing, A. D. A. Atkinson, G. A. Eiceman and G. J. Ewing, Talanta, 2001, 54, 515–529.

9. M. Y. Rajapakse, J. A. Stone and G. A. Eiceman, J. Phys. Chem. A, 2014, 118, 2683–2692.

10. R. M. M. Y. Rajapakse, J. A. Stone and G. A. Eiceman, Int. J. Mass Spectrom., 2014, 371, 28–35.

11. F. W. Karasek, O. S. Tatone and D. M. Kane, Anal. Chem., 1973, 45, 1210–1214.

12. 12 A. H. Lawrence and P. Neudorfl, Anal. Chem., 1988, 60, 104–109.

13. R. G. Ewing, G. A. Eiceman, C. S. Harden and J. A. Stone, Int. J. Mass Spectrom., 2006, 255–256, 76–85.

14. Y. Valadbeigi, H. Farrokhpour and M. Tabrizchi, J. Phys. Chem. A, 2014, 118, 7663–7671.

15. A. Gapeev, M. Sigman and J. Yinon, Rapid Commun. Mass Spectrom., 2003, 17, 943–948.

16. J. A. Mathis and B. R. McCord, Rapid Commun. Mass Spectrom., 2005, 19, 99–104.

17. F. A. Fernandez-Lima, D. A. Kaplan and M. A. Park, Rev. Sci. Instrum., 2011, 82, 126106.

18. F. Fernandez-Lima, D. Kaplan, J. Suetering and M. Park, Int. J. Ion Mobility Spectrom., 2011, 14, 93–98.

19. D. R. Hernandez, J. D. DeBord, M. E. Ridgeway, D. A. Kaplan, M. A. Park and F. Fernandez-Lima, Analyst, 2014, 139, 1913–1921.

20. J. A. Silveira, M. E. Ridgeway and M. A. Park, Anal. Chem., 2014, 86, 5624–5627.

21. E. R. Schenk, M. E. Ridgeway, M. A. Park, F. Leng and F. Fernandez-Lima, Anal. Chem., 2014, 86, 1210–1214.

22. J. C. Molano-Arevalo, D. R. Hernandez, W. G. Gonzalez, J. Miksovska, M. E. Ridgeway, M. A. Park and F. Fernandez-Lima, Anal. Chem., 2014, 86, 10223–10230.

23. F. A. Fernandez-Lima, D. A. Kaplan, J. Suetering and M. A. Park, Int. J. Ion Mobility Spectrom., 2011, 14, 93–98.

24. E. R. Schenk, V. Mendez, J. T. Landrum, M. E. Ridgeway, M. A. Park and F. Fernandez-Lima, Anal. Chem., 2014, 86, 2019–2024.

25. E. W. McDaniel and E. A. Mason, Mobility and diffusion of ions in gases, John Wiley and Sons, Inc., New York, New York, 1973.

26. M. Tam and H. H. Hill, Anal. Chem., 2004, 76, 2741–2747.

27. M. J. Frisch, G. W. Trucks, H. B. Schlegel, G. E. Scuseria, M. A. Robb, J. R. Cheeseman, J. A. Montgomery, Jr., T. Vreven, K. N. Kudin, J. C. Burant, J. M. Millam, S. S. Iyengar, J. Tomasi, V. Barone, B. Mennucci, M. Cossi, G. Scalmani, N. Rega, G. A. Petersson, H. Nakatsuji, M. Hada, M. Ehara, K. Toyota, R. Fukuda, J. Hasegawa, M. Ishida, T. Nakajima, Y. Honda, O. Kitao, H. Nakai, M. Klene, X. Li, J. E. Knox, H. P. Hratchian, J. B. Cross, V. Bakken, C. Adamo, J. Jaramillo, R. Gomperts, R. E. Stratmann, O. Yazyev, A. J. Austin, R. Cammi, C. Pomelli, J. W. Ochterski, P. Y. Ayala, K. Morokuma, G. A. Voth, P. Salvador, J. J. Dannenberg, V. G. Zakrzewski, S. Dapprich, A. D. Daniels, M. C. Strain, O. Farkas, D. K. Malick, A. D. Rabuck, K. Raghavachari, J. B. Foresman, J. V. Ortiz, Q. Cui, A. G. Baboul, S. Clifford, J. Cioslowski, B. B. Stefanov, G. Liu, A. Liashenko, P. Piskorz, I. Komaromi, R. L. Martin, D. J. Fox, T. Keith, M. A. Al-Laham, C. Y. Peng, A.

Nanayakkara, M. Challacombe, P. M. W. Gill, B. Johnson, W. Chen, M. W. Wong, C. Gonzalez and J. A. Pople, Gaussian 03, revision C.02, Gaussian, Inc., Wallingford, CT, 2004.

28. U. C. Singh and P. A. Kollman, J. Comput. Chem., 1984, 5, 129–145.

29. B. H. Besler, K. M. Merz and P. A. Kollman, J. Comput. Chem., 1990, 11, 431–439.

30. I. Campuzano, M. F. Bush, C. V. Robinson, C. Beaumont, K. Richardson, H. Kim and H. I. Kim, Anal. Chem., 2011, 84, 1026–1033.

31. H. I. Kim, H. Kim, E. S. Pang, E. K. Ryu, L. W. Beegle, J. A. Loo, W. A. Goddard and I. Kanik, Anal. Chem., 2009, 81, 8289.

32. 32 C. Larriba and C. J. Hogan, J. Phys. Chem. A, 2013, 117, 3887–3901.

33. A. B. Kanu, P. Dwivedi, M. Tam, L. Matz and H. H. Hill, J. Mass Spectrom., 2008, 43, 1–22.

34. P. Dugourd, R. R. Hudgins, D. E. Clemmer and M. F. Jarrold, Rev. Sci. Instrum., 1997, 68, 1122–1129.

35. S. I. Merenbloom, R. S. Glaskin, Z. B. Henson and D. E. Clemmer, Anal. Chem., 2009, 81, 1482–1487.

36. P. R. Kemper, N. F. Dupuis and M. T. Bowers, Int. J. Mass Spectrom., 2009, 287, 46–57.

37. R. C. Blase, J. A. Silveira, K. J. Gillig, C. M. Gamage and D. H. Russell, Int. J. Mass Spectrom., 2011, 301, 166–173.

38. B. M. Kolakowski and Z. Mester, Analyst, 2007, 132, 842–864.

39. G. A. Eiceman, E. V. Krylov, N. S. Krylova, E. G. Nazarov and R. A. Miller, Anal. Chem., 2004, 76, 4937–4944.

40. E. V. Krylov, S. L. Coy, J. Vandermey, B. B. Schneider, T. R. Covey and E. G. Nazarov, Rev. Sci. Instrum., 2010, 81, 024101.

41. E. G. Nazarov, R. A. Miller, G. A. Eiceman and J. A. Stone, Anal. Chem., 2006, 78, 4553–4563.

42. Y. Guo, J. Wang, G. Javahery, B. A. Thomson and K. W. M. Siu, Anal. Chem., 2004, 77, 266–275.

43. R. S. Glaskin, M. A. Ewing and D. E. Clemmer, Anal. Chem., 2013, 85, 7003–7008.

44. S. D. Pringle, K. Giles, J. L. Wildgoose, J. P. Williams, S. E. Slade, K. Thalassinos, R. H. Bateman, M. T. Bowers and J. H. Scrivens, Int. J. Mass Spectrom., 2007, 261, 1–12.

45. B. Casetta and F. Garofolo, Org. Mass Spectrom., 1994, 29, 517–525.

46. F. Garofolo, A. Longo, V. Migliozzi and C. Tallarico, Rapid Commun. Mass Spectrom., 1996, 10, 1273–1277.

47. J. Yinon, J. E. McClellan and R. A. Yost, Rapid Commun. Mass Spectrom., 1997, 11, 1961–1970.

48. X. Zhao and J. Yinon, J. Chromatogr. A, 2002, 977, 59–68.

49. Z. Wu, C. L. Hendrickson, R. P. Rodgers and A. G. Marshall, Anal. Chem., 2002, 74, 1879–1883.

50. X. Zhao and J. Yinon, J. Chromatogr. A, 2002, 946, 125–132.

51. C. Sánchez, H. Carlsson, A. Colmsjö, C. Crescenzi and R. Batlle, Anal. Chem., 2003, 75, 4639–4645.

52. P. Benigni, C. J. Thompson, M. E. Ridgeway, M. A. Park and F. Fernandez-Lima, Anal. Chem., 2015, 87, 4321–4325.

53. L. A. Flanagan, Hewlett-Packard Company, U.S. Patent, 5872357, 1999.

Chapter Three:

INFLUENCE OF GAS MODIFIERS ON THE TIMS ANALYSIS OF FAMILIAR EXPLOSIVES

This chapter has been submitted to *International Journal for Ion Mobility Spectrometry*.

Alan McKenzie-Coe,[a] and Francisco Fernandez-Lima[a,b*]

Abstract

In the present work, we study the influence of the bath composition (e.g., organic modifiers) on the mobility resolving power, resolution and lifetime of familiar explosives during trapped ion mobility spectrometry (TIMS). Experimental results showed the dependence of the mobility with the organic modifiers (mass and size) for the case of TIMS-MS. Different from trends observed in drift tube like IMS devices, no correlation between the mobility resolving power and resolution in TIMS was observed with the bath gas composition (e.g., air, air + methanol, air + 2-propanol, and air + acetone). Time decay plots showed that common explosives with adduct complexes signal decrease over time as a function of the trapping time, without any significant improvement with the addition of the organic modifiers. Theoretical calculation of potential clustering and dissociation pathways supported the time decay findings since no major energetic differences between the pathways were observed as a function of the organic modifiers. Our findings suggest that beside the size of the collision partner, there are specific intermolecular dynamics that drive the trapping behavior of familiar explosives.

3.2. Introduction

Ion mobility spectrometry (IMS) depends on the separation of charged species as a result of differences in their mobility under the influence of an electric field in a bath gas. In a conventional drift tube, the separation of chemical species results from numerous, near-thermal collision between analyte ions and a chemically-inert drift gas. The bath gas composition affects the separation efficiency. For example, in high-field asymmetric waveform ion mobility spectrometry (FAIMS) and differential mobility spectrometry (DMS), the carrier gas composition is commonly altered to increase the resolution for closely spaced analytes. For conventional low field IM techniques such as drift tube (DTIMS) this practice is also utilized. Hill and coworkers demonstrated enhanced analyte selectivity on an ambient pressure drift tube when varying the drift gas from low to high polarizability (helium, nitrogen, argon, and carbon dioxide) [11-14]. Yost and coworkers demonstrated increased resolving power for several isobaric steroids, analyzed in a reduced-pressure drift tube instrument, using CO_2 as the drift gas. Fjeldsted and coworkers investigated the separation of isomeric carbohydrates, fluoroalkyl phosphazenes, and various small molecule pesticides under various drift gases (He, N_2, Ar, CO_2, N_2O, SF_6). In addition, gas modifiers have been used to increase the analytical power of IMS by increasing the size of the collision partner or inducing higher order multi-pole interactions,[1-6].

We have recently reported on the effect of bath gas modifiers on the conformational space of peptides and heme proteins during trapped ion mobility spectrometry (TIMS).[7, 8] Different from other IMS separations, in the case of TIMS, ions are held stationary under the influence of an electric field that compensates the drift force induced by a moving gas.

[9-13] In TIMS, the increase in size of the collision partner necessitates a larger electric field to trap the ions and subsequently an increase in the resolution. However, since recent experiments showed, the interaction between charge species and bath gas modifiers can lead to the formation of metastable complexes, that can lead to conformational rearrangement.[7]

In the present study we further investigate the role of bath gas modifiers during TIMS experiments for the case of familiar explosives. In particular, molecular ion species formed by the explosives HMX and PETN are studied as a function of the bath gas composition and trapping time. Previous studies have also shown that in the case of the molecular ion of familiar explosives, the ion abundances decreases with the trapping time.[14] Several clustering and dissociation pathways are discussed theoretically.

3.3. Experimental Methods

3.3.1. Materials and reagents

Individual standards of 3-nitrooxy-2,2-bis-(nitrooxymethyl)propyl nitrate (PETN) and octahydro-1,3,5,7-tetranitro-1,3,5,7-tetrazocine (HMX) were obtained from AccuStandard (New Haven, CT) and used as received. Ammonium chloride, ammonium formate, and ammonium nitrate salts and chromatography grade water, methanol and acetonitrile solvents were obtained from Fisher Scientific (Suwanee, GA) and used as received. HMX was dissolved in 1: 1 water : methanol v/v ratio, and PETN was dissolved in 1 : 1 : 1 water : methanol : acetonitrile v/v ratio to a final concentration of 1 μM. Each ammonium salt containing solution was prepared separately and added to each explosive solution to a final

concentration of 10 mM of ammonium salt. A Tuning Mix calibration standard (G24221A) was obtained from Agilent Technologies (Santa Clara, CA) and used as received.

3.3.2. Trapped Ion Mobility Spectrometry – Mass Spectrometry Analysis (TIMS-MS)

Details regarding the TIMS operation and specifics compared to traditional IMS can be found elsewhere. [9-13] Briefly, mobility separation in TIMS is based on holding the ions stationary against a moving gas using an electric field. The separation in a TIMS device can be described in the center of the mass reference frame using the same principles as in a conventional IMS drift tube.[15] Since mobility separation is related to the number of ion-neutral collisions (or drift time in traditional drift tube cells), the mobility separation in a TIMS device depends on the bath gas drift velocity, ion confinement and ion elution parameters. The reduced mobility, K, of an ion in a TIMS cell is described by:

$$K = \frac{v_g}{E} \approx \frac{A}{(V_{elution} - V_{out})}$$

where v_g and E are the velocity of the gas and the applied electric field across the TIMS analyzer region. The variable $V_{elution}$ is the voltage when the ions elute in the V_{ramp} sweep and V_{out} is the voltage applied at the end of the TIMS analyzer region. A is a constant that relates to the velocity of the bath gas and electric field axial distribution and can be calculated using mobility standards. Notice that, once A is calculated for a given bath gas (e.g., Tuning Mix as calibrants for N_2 bath gas), it will not change when using gas modifiers since the pressure difference between P_1 and P_2 are kept the same (see details in **Figure 3.1**).

A custom-built, pulled capillary nano-ESI source was utilized for all the experiments. Quartz glass capillaries (O.D.: 1.0 mm and I.D.: 0.70 mm) were pulled utilizing a P-2000 micropipette laser puller (Sutter Instruments, Novato, CA) and loaded with 10 μL aliquot of the sample solution. A typical nano-ESI source voltage of +/- 600-1200 V was applied between the pulled capillary tips and the TIMS-MS instrument inlet. Ions were introduced via a stainless-steel tube (1/16 x 0.020'', IDEX Health Science, Oak Harbor, WA) held at room temperature into the TIMS cell. It should be noted that all solvent studies were performed with nitrogen as the bath gas, and that all dopant experiments were conducted with peptides sprayed from 10 mM NH_4AC.

Mobility calibration was performed using the Tuning Mix calibration standard (G24221A, Agilent Technologies, Santa Clara, CA) in negative ion mode (e.g., $m/z = 301, K0 = 1.497\ cm^2/Vs$ and $\frac{m}{z} = 601, K0 = 1.139\ cm^2/Vs$ [13]. The A constant obtained in positive mode was used for negative ion mode mobility calculations. Trapped ion mobility spectrometry operation was controlled using in-house software, written in National Instruments Lab VIEW, and synchronized with the maXis Impact Q-ToF acquisition program.[9, 10] Gas modifiers were introduced at the entrance of the TIMS cell via vaporization of the respective solvents (e.g., methanol, 2-propanol or acetone) at a ratio of 2:1 air:air modified mix (scheme shown in **Appendix 3.2**.); this method was preferred to guarantee reproducibility across the experiments and simplified mobility calibration (i.e., constant gas flow in the TIMS analyzer). Room humidity was kept at 60% during all the experiments. For simplified mobility calibration, the gas velocity was kept constant in all experiments (P_1 and P_2 values). For TIMS, the resolving power (R) and resolution (r) are

defined as $R = K/w$ and $r = 1.18 \times (K_2 - K_1)/(w_1 + w_2)$, where w is the full peak width at half-maximum (w).

3.3.3. Theoretical calculations

Candidate structures were generated, and energy minimized for the parent and in-source characteristic fragments at the DFT/B3LYP/6-31+g(d) level using the Gaussian 09 software [16]. Vibrational frequencies were calculated to guarantee that the optimized structures correspond to real minima in the energy space.

3.4. Results and Discussion

The nESI-TIMS-MS analysis of HMX and PETN in the presence of various salts resulted in the observation of mainly four adducts species: **1.** HMX+Cl^-, **2.** HMX+HCO_2^-, **3.** HMX+NO_3^- and **4.** PETN + NO_3^-. While these species are easily resolved in the 2D IMS-MS space, our discussion focuses on the effect of the bath gas composition on the resolving power, resolution and lifetime as a function of the trapping time. Inspection of **Figure 3.1** shows that in the TIMS trapping experiments, the increase in size of the collision partner leads to an increase of electric field require to hold the ions for a constant bath gas velocity. That is, an effective change in the mobility of the ions as a function of the size of the collision partner (see **Figure 3.1**) is observed. In the case considered, as the bath composition changes from air to air doped with methanol, 2-propanol and acetone, a reduction in mobility (or increase in CCS) is observed for all the familiar explosive complexes (see **Table 3.1**).

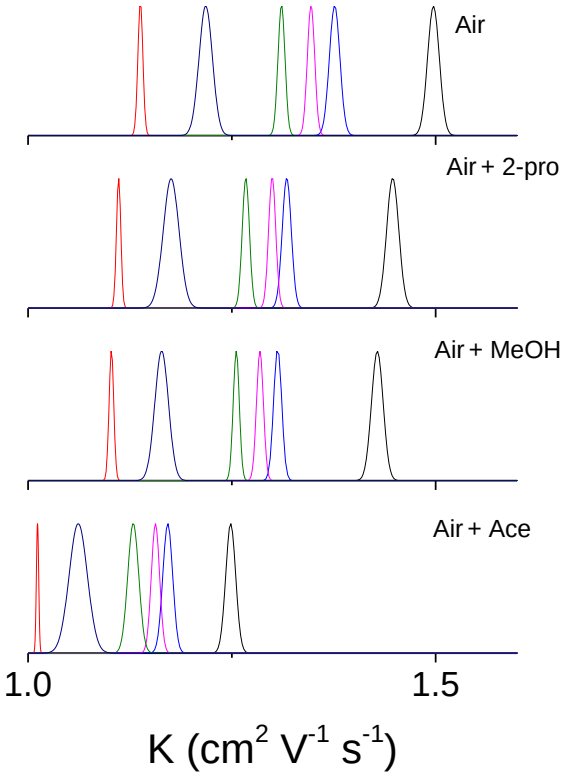

Figure 3.1. Typical mobility profiles as a function of the bath gas composition for Tuning Mix standards (301 and 601 *m/z*) and four familiar explosives molecular ions (HMX+Cl, HMX+HCO_2, HMX+NO_3 and PETN + NO_3).

	Air			Air + MeOH			Air + 2-propanol			Air + Acetone		
	K	**ΔK**	**R**	**K**	**ΔK**	**R**	**K**	**ΔK**	**R**	**K**	**ΔK**	**R**
$[HMX+Cl]^-$	1.376	0.012	107	1.306	0.009	133	1.317	0.011	119	1.171	0.012	97
$[HMX+HCO_2]^-$	1.347	0.008	150	1.284	0.008	152	1.299	0.00869	149	1.156	0.010	114
$[HMX+NO_3]^-$	1.310	0.008	153	1.255	0.007	168	1.267	0.00877	144	1.129	0.013	84
$[PETN+NO_3]^-$	1.217	0.016	74	1.163	0.016	70	1.175	0.01924	61	1.061	0.022	47
301	1.497	0.014	104	1.428	0.014	100	1.447	0.01485	97	1.248	0.012	102
601	1.137	0.006	187	1.102	0.005	194	1.111	0.0067	165	1.011	0.002	354

Table 3.1. Mobility and resolving power for familiar explosives molecular ions as a function of the bath composition.

The dependence of the resolution and resolving power as a function of the bath composition is summarized in **Figure 3.2** and **Table 3.1** and **Table 3.2**. Differences in resolution are observed as a function on the adduct form and of the bath gas composition. We attribute these differences to the flexibility of the different adduct forms in the gas-phase and to the interaction of the molecular complexes with the bath gas dopants. In the case of resolution, a significant decrease (up to 2x fold) in resolution is observed for all the familiar explosives in the presence of the bath gas dopants (see **Figure 3.2**). Under the same conditions, the resolution of the tuning mix ions (301 and 601 *m/z*) only showed minor variations with the bath gas composition (see **Table 3.2**). These effects suggest that there is a strong interaction between the familiar explosive complexes and the residual bath gas molecules.

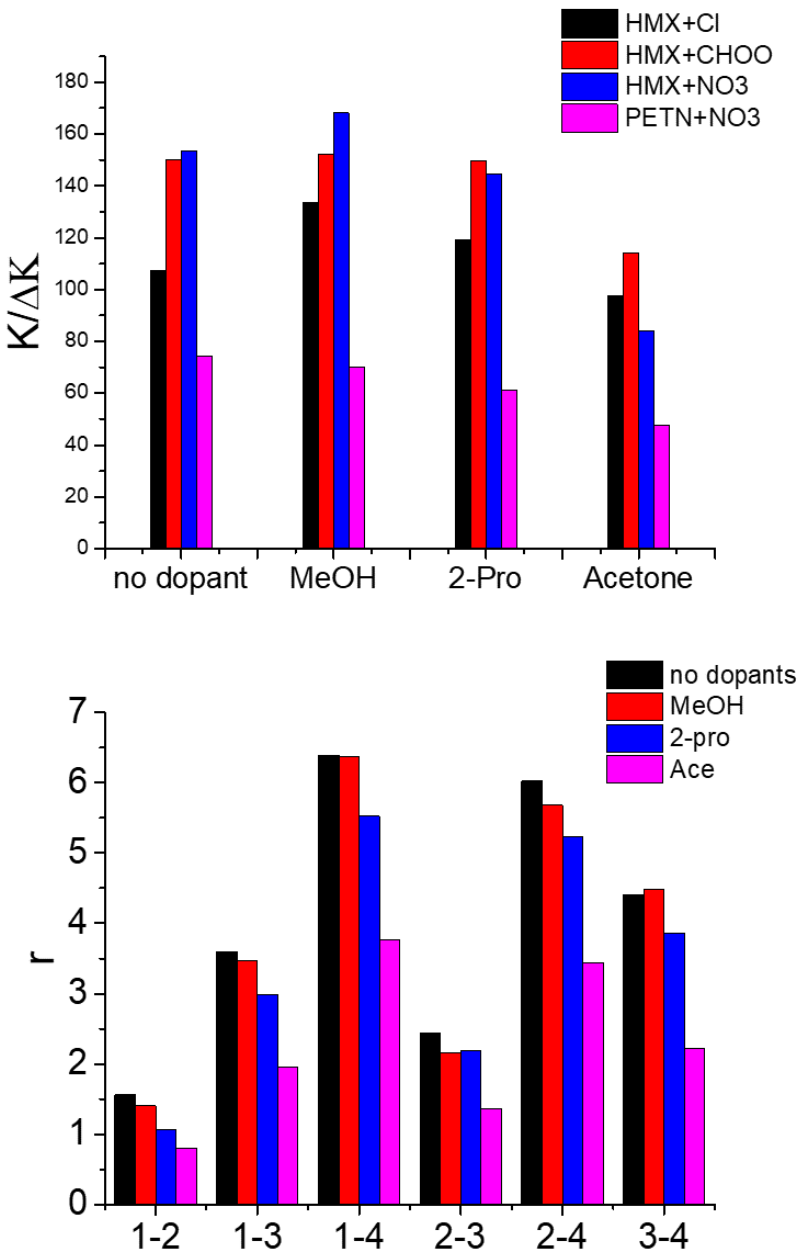

Figure 3.2. Dependence of the mobility resolving power and the mobility resolution as a function of the bath gas composition. For the resolution calculation, the following nomenclature was used **1.** HMX+Cl^-, **2.** HMX+HCO_2^-, **3.** HMX+NO_3^- and **4.** PETN + NO_3^- (more details in **Table 3.2**)

	Bath Gas Modifier			
Molecular species	**Air**	**Air + MeOH**	**Air + 2-propanol**	**Air + Acetone**
1-2	1.56	1.40	1.06	0.80
1-3	3.59	3.47	2.99	1.96
1-4	6.39	6.36	5.52	3.77
2-3	2.44	2.15	2.18	1.36
2-4	6.02	5.68	5.23	3.44
3-4	4.40	4.48	3.85	2.22
301-601	20.7	19.4	18.4	18.5

Table 3.2. Mobility resolution for familiar explosives molecular ions as a function of the bath composition. For the resolution calculation, the following nomenclature was used **1.** HMX+Cl^-, **2.** HMX+HCO_2^-, **3.** HMX+NO_3^- and **4.** PETN + NO_3^-.

The analysis of the relative abundance of the familiar explosives as a function of the trapping time is summarized in **Figure 3.3** and **Table 3.3**. Only small changes in the lifetimes are observed in the stability curves of the familiar explosives in the presence of the dopants. These observations are in good agreement with the theoretical clustering and dissociation reactions presented in **Table 3.4** and **Appendix 3.2**. In our previous report [14], we suggested that the familiar explosive complex stability could be driven by bath gas impurities, where bath gas molecules could act as scavengers of the adducted anions. Inspection of **Figure 3.3** and **Table 3.3** and **Table 3.4** suggest that the presence of water and/or other organic molecules does not changes dramatically the energy for clustering and dissociation of the complexes. However, the larger the number of clustering molecules, the higher the stability of the complex. If the clustering mechanism involves several neutral molecules, a higher stability of the complex can be reached in a clustering / de-clustering dynamic. This proposed mechanism will also explain the trends in resolving power and resolution shown in **Figure 3.1** and **Figure 3.2** for the case of the familiar explosives, where the increase in size of the bath gas dopant did not lead to an increase in resolution. The comparison between the different adducts for the case of HMX in the presence of different bath gas dopants suggested that beside the size, there are specific intermolecular dynamics that drive the trapping behavior.

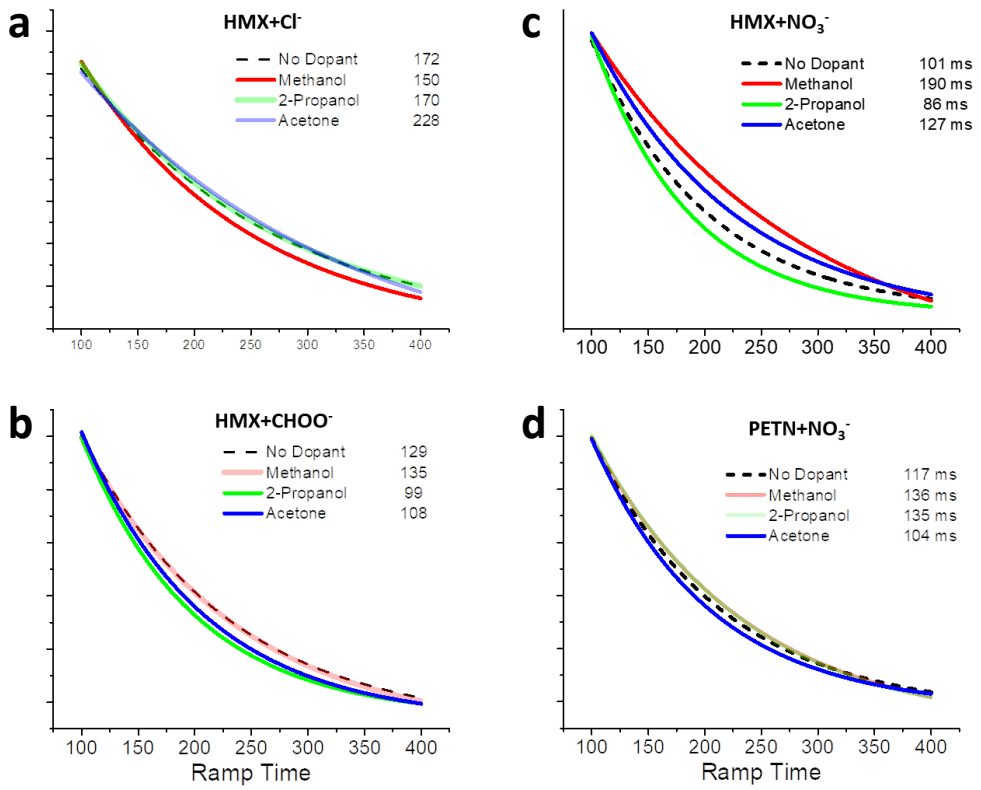

Figure 3.3. Relative abundance of familiar explosive molecular ions as a function of the trapping time and bath gas compositions: **a)** $HMX+Cl^-$, **b)** $HMX+HCO_2^-$, **c)** $HMX+NO_3^-$ and **d)** $PETN + NO_3^-$.

	Air	Air + MeOH	Air + 2-propanol	Air + Acetone
	τ (ms)	**τ (ms)**	**τ (ms)**	**τ (ms)**
$[HMX+Cl]^-$	172	150	170	228
$[HMX+HCO_2]^-$	129	135	99	108
$[HMX+NO_3]^-$	101	190	86	127
$[PETN+NO_3]^-$	117	136	135	104

Table 3.3. Time decays of familiar explosive molecular ions as a function of the trapping time and bath gas composition.

HMX+[X]$^-$+H_2O	→	[HMX+X]$^-$+H_2O	→	[HMX+X+H_2O]$^-$	→	HMX+[X+H_2O]$^-$
		-44/-46/-38 kJ/mol		-53/-56/-46 kJ/mol		-14/-16/-14 kJ/mol
Methanol				[HMX+X+CH_3OH]$^-$		HMX+[X+CH_3OH]$^-$
				-53/-57/-47 kJ/mol		-14/-16/-13 kJ/mol
Acetone				[HMX+X+$(CH_3)_2CO$]$^-$		HMX+[X+$(CH_3)_2CO$]$^-$
				-52/-54/-44 kJ/mol		-14/-15/-14 kJ/mol
2-Propanol				[HMX+X+$(CH_3CHOHCH_3)$]$^-$		HMX+[X+$(CH_3CHOHCH_3)$]$^-$
				-53/-56/-45 kJ/mol		-15/-17/-14 kJ/mol
HMX+[X]$^-$+$(H_2O)_2$	→	[HMX+X]$^-$+$(H_2O)_2$	→	[HMX+X+$(H_2O)_2$]$^-$	→	HMX+[X+$(H_2O)_2$]$^-$
		-44/-46/-38 kJ/mol		-60/-65/-56 kJ/mol		-25/-31/-25 kJ/mol
Methanol				[HMX+X+$(CH_3OH)_2$]$^-$		HMX+[X+$(CH_3OH)_2$]$^-$
				-61/-66/-55 kJ/mol		-27/-30/-25 kJ/mol
Acetone				[HMX+X+$((CH_3)_2CO)_2$]$^-$		HMX+ [X+$((CH_3)_2CO)_2$]$^-$
				-58/-60/-55 kJ/mol		-25/-25/-22 kJ/mol
2-Propanol				[HMX+X+$(CH_3CHOHCH_3)$]$^-$		[HMX+X+$(CH_3CHOHCH_3)$]$^-$
				-60/-65/-54 kJ/mol		-27/-31/-25 kJ/mol
HMX+[X]$^-$+H_2O	→	[HMX+X]$^-$+H_2O	→	[HMX+X+H_2O]$^-$	→	HMX+[X+H_2O]$^-$
		-44/-46/-38 kJ/mol		-53/-56/-46 kJ/mol		-14/-16/-14 kJ/mol
Methanol				[HMX+X+CH_3OH]$^-$		HMX+[X+CH_3OH]$^-$
				-53/-57/-47 kJ/mol		-14/-16/-13 kJ/mol
Acetone				[HMX+X+$(CH_3)_2CO$]$^-$		HMX+[X+$(CH_3)_2CO$]$^-$
				-52/-54/-44 kJ/mol		-14/-15/-14 kJ/mol
2-Propanol				[HMX+X+$(CH_3CHOHCH_3)$]$^-$		HMX+[X+$(CH_3CHOHCH_3)$]$^-$
				-53/-56/-45 kJ/mol		-15/-17/-14 kJ/mol
HMX+[X]$^-$+$(H_2O)_2$	→	[HMX+X]$^-$+$(H_2O)_2$	→	[HMX+X+$(H_2O)_2$]$^-$	→	HMX+[X+$(H_2O)_2$]$^-$
		-44/-46/-38 kJ/mol		-60/-65/-56 kJ/mol		-25/-31/-25 kJ/mol
Methanol				[HMX+X+$(CH_3OH)_2$]$^-$		HMX+[X+$(CH_3OH)_2$]$^-$
				-61/-66/-55 kJ/mol		-27/-30/-25 kJ/mol
Acetone				[HMX+X+$((CH_3)_2CO)_2$]$^-$		HMX+ [X+$((CH_3)_2CO)_2$]$^-$
				-58/-60/-55 kJ/mol		-25/-25/-22 kJ/mol
2-Propanol				[HMX+X+$(CH_3CHOHCH_3)$]$^-$		[HMX+X+$(CH_3CHOHCH_3)$]$^-$
				-60/-65/-54 kJ/mol		-27/-31/-25 kJ/mol

Table 3.4. Energies associated to adduct formation and dissociation in the presence of water, methanol, acetone and 2-propanol molecules for $[HMX+X]^-$ where X = Cl^- / HCO_2^- /NO_3^-.

3.5. Conclusions

A systematic study of the influence of the bath gas composition using organic modifiers on the analytical performance of trapped IMS (TIMS) is described for two familiar explosives: HMX and PETN. In the presence of salts in the starting solution, the nESI process leads to the formation of single charged characteristic molecular complexes of the form: **1.** $HMX+Cl^-$, **2.** $HMX+HCO_2^-$, **3.** $HMX+NO_3^-$ and **4.** $PETN + NO_3^-$. Experimental results show the dependence of the mobility with the organic modifiers (mass and size). Different from trends observed in drift tube like IMS devices with the use of bath gases of varying size, no direct correlation and no significant improvement in mobility resolving power and resolution is observed under the conditions considered (e.g., air, air + methanol, air + 2-propanol, and air + acetone). Time decay plots showed that common explosives with adduct complexes signal decrease over time as a function of the trapping time, without any significant improvement with the addition of the organic modifiers. Theoretical calculation of potential dissociation pathways showed that there are minor energetic differences between the process considered with the organic modifiers in the presence of water contaminants. However, if the clustering mechanism involves several neutral molecules, a higher stability of the complex can be reached in a clustering / de-clustering dynamics. This proposed mechanism will also explain the non-expected trends in resolving power and resolution with the increase in the collision partner.

3.6. Acknowledgements

This work was supported by the National Science Foundation Division of Chemistry, under CAREER award CHE-1654274, with co-funding from the Division of Molecular and Cellular Biosciences to F.F.-L. The authors will also like to acknowledge the helpful

discussions and technical support from Dr. Mark E. Ridgeway and Dr. Melvin A. Park from Bruker Daltonics Inc. during the development and installation of the custom-built TIMS-TOF MS instrument. We will also like to acknowledge Dr Alexander Mebel support for the theoretical calculations.

List of References

[1] B. Schneider, T. Covey, E. Nazarov, DMS-MS separations with different transport gas modifiers, 2013.

[2] A. Kafle, S.L. Coy, B.M. Wong, A.J. Fornace, Jr., J.J. Glick, P. Vouros, Understanding gas phase modifier interactions in rapid analysis by differential mobility-tandem mass spectrometry, J Am Soc Mass Spectrom, 25 (2014) 1098-1113.

[3] D.S. Levin, P. Vouros, R.A. Miller, E.G. Nazarov, J.C. Morris, Characterization of Gas-Phase Molecular Interactions on Differential Mobility Ion Behavior Utilizing an Electrospray Ionization-Differential Mobility-Mass Spectrometer System, Analytical Chemistry, 78 (2006) 96-106.

[4] T. Porta, E. Varesio, G. Hopfgartner, Gas-Phase Separation of Drugs and Metabolites Using Modifier-Assisted Differential Ion Mobility Spectrometry Hyphenated to Liquid Extraction Surface Analysis and Mass Spectrometry, Analytical Chemistry, 85 (2013) 11771-11779.

[5] R. Fernández-Maestre, C. Wu, H.H. Hill, Buffer Gas Modifiers Effect Resolution in Ion Mobility Spectrometry through Selective Ion-Molecule Clustering Reactions, Rapid communications in mass spectrometry : RCM, 26 (2012) 2211-2223.

[6] E. Waraksa, U. Gaik, J. Namieśnik, M. Sillanpää, T. Dymerski, M. Wójtowicz, J. Puton, Dopants and gas modifiers in ion mobility spectrometry, 2016.

[7] D. Butcher, J. Miksovska, M.E. Ridgeway, M.A. Park, F. Fernandez-Lima, The effects of solution additives and gas-phase modifiers on the molecular environment and conformational space of common heme proteins, Rapid Communications in Mass Spectrometry, 0.

[8] A. Garabedian, F. Leng, M.E. Ridgeway, M.A. Park, F. Fernandez-Lima, Tailoring peptide conformational space with organic gas modifiers in TIMS-MS, International Journal for Ion Mobility Spectrometry, 21 (2018) 43-48.

[9] F.A. Fernandez-Lima, D.A. Kaplan, M.A. Park, Note: Integration of trapped ion mobility spectrometry with mass spectrometry, Rev. Sci. Instr., 82 (2011) 126106.

[10] F.A. Fernandez-Lima, D.A. Kaplan, J. Suetering, M.A. Park, Gas-phase separation using a Trapped Ion Mobility Spectrometer, International Journal for Ion Mobility Spectrometry, 14 (2011) 93-98.

[11] E.R. Schenk, M.E. Ridgeway, M.A. Park, F. Leng, F.A. Fernandez-Lima, Isomerization Kinetics of AT Hook Decapeptide Solution Structures, Anal. Chem., 86 (2014) 1210-1214.

[12] E.R. Schenk, V. Mendez, J.T. Landrum, M.E. Ridgeway, M.A. Park, F.A. Fernandez-Lima, Direct Observation of Differences of Carotenoid Polyene Chain cis/trans Isomers Resulting from Structural Topology, Anal. Chem., 86 (2014) 2019-2024.

[13] D.R. Hernandez, J.D. DeBord, M.E. Ridgeway, D.A. Kaplan, M.A. Park, F.A. Fernandez-Lima, Ion dynamics in a trapped ion mobility spectrometer, Analyst, 139 (2014) 1913-1921.

[14] A. McKenzie, J.D. DeBord, M.E. Ridgeway, M.A. Park, G.A. Eiceman, F. Fernandez-Lima, Lifetimes and Stabilities of familiar explosives molecular adduct complexes during ion mobility measurements, Analyst, 140 (2015) 5692-5699.

[15] E.W. McDaniel, E.A. Mason, Mobility and diffusion of ions in gases, John Wiley and Sons, Inc., New York, New York, 1973.

[16] M.J. Frisch, G.W. Trucks, H.B. Schlegel, G.E. Scuseria, M.A. Robb, J.R. Cheeseman, J. Montgomery, J. A., T. Vreven, K.N. Kudin, J.C. Burant, J.M. Millam, S.S. Iyengar, J. Tomasi, V. Barone, B. Mennucci, M. Cossi, G. Scalmani, N. Rega, G.A. Petersson, H. Nakatsuji, M. Hada, M. Ehara, K. Toyota, R. Fukuda, J. Hasegawa, M. Ishida, T. Nakajima, Y. Honda, O. Kitao, H. Nakai, M. Klene, X. Li, J.E. Knox, H.P. Hratchian, J.B. Cross, V. Bakken, C. Adamo, J. Jaramillo, R. Gomperts, R.E. Stratmann, O. Yazyev, A.J. Austin, R. Cammi, C. Pomelli, J.W. Ochterski, P.Y. Ayala, K. Morokuma, G.A. Voth, P. Salvador, J.J. Dannenberg, V.G. Zakrzewski, S. Dapprich, A.D. Daniels, M.C. Strain, O. Farkas, D.K. Malick, A.D. Rabuck, K. Raghavachari, J.B. Foresman, J.V. Ortiz, Q. Cui, A.G. Baboul, S. Clifford, J. Cioslowski, B.B. Stefanov, G. Liu, A. Liashenko, P. Piskorz, I. Komaromi, R.L. Martin, D.J. Fox, T. Keith, M.A. Al-Laham, C.Y. Peng, A. Nanayakkara, M. Challacombe, P.M.W. Gill, B. Johnson, W. Chen, M.W. Wong, C. Gonzalez, J.A. Pople, Gaussian 03, Revision C.02, in: Gaussian, Inc., Wallingford CT, 2004.

Chapter Four:

DETECTION OF FIREARM DISCHARGE RESIDUE FROM SKIN SWABS USING TRAPPED ION MOBILITY SPECTROMETRY COUPLED TO MASS SPECTROMETRY

This chapter was published in *Analytical Methods* and reproduced with permission. McKenzie-Coe, Alan, Suzanne Bell, and Francisco Fernandez-Lima. *Detection of firearm discharge residue from skin swabs using trapped ion mobility spectrometry coupled to mass spectrometry.* Analytical Methods 10.35 (2018): 4219-4224.

4.1. Abstract

In the present work, a novel workflow for the detection of both elemental and organic constituents of the firearm discharge residue from skin swabs was developed using trapped ion mobility spectrometry coupled to mass spectrometry. The small sample size ($< 10\ \mu L$), high specificity and short analysis time (few min) permits the detection of inorganic residues (IGSR; inorganic gunshot residues) and organic residues (OGSR) from one sample and in a single analysis. The analytical method is based on the simultaneous extraction of inorganic and organic species assisted by the formation organometallic complexes (*e.g.*, 15-5 crown ethers for the sequestering of metals and nitrate species), followed by fast, post-ionization, high resolution mobility ($R_{IMS} \sim 150 - 250$) and mass separations ($R_{MS} \sim 20 - 40k$) with isotopic pattern recognition. The analytical performance is illustrated as a proof of concept for the case of the simultaneous detection of Ba^{+2}, Pb^{+2}, Cu^{+}, K^{+}, NO_3^{-}, diphenylamine (DPA), ethyl centralite (EC) and 2,4 dinitrotoluene (DNT) in positive and negative nESI-TIMS-MS modes. Candidate structures are proposed, and collisional cross sections are reported for all organic and organometallic species of interest.

4.2. Introduction

The discharge of a firearm provides a chemically rich and complex assortment of molecules, typically classified into organic and inorganic gunshot residues (O- and IGSRs), collectively referred to as firearms discharge residue (FDR). FDR is not only composed of species and particulates from the starting material (e.g., primer, propellant, cartridge, projectile jacket, gun barrel and lubricants) but also from combustion and transformation

byproducts. [1] The analysis of these species and particulates is pivotal in providing evidence in criminal cases hence much effort has been exerted in developing techniques to collect, identify, and detect them.

Current analytical methods are compartmentalized for the detection of OGSR or GSR. [1, 2] GSR particulates have been traditionally analyzed by scanning electron microscopy electron dispersive X-ray spectroscopy (SEM/EDS). [3] Alternatively, microbeam ion beam analysis (e.g., m-PIXE) can provide elemental quantitative and more sensitive determination of "characteristic" GSR species. [4] OGSR detection typically includes various pre-separation and extraction techniques (e.g., gas chromatography, liquid chromatography, and solid-phase microextraction) followed by their detection (e.g., electron capture detection, ultraviolet and fluorescence detection, thermal energy analysis, ion mobility, and mass spectrometry). When using multiple assays and complementary techniques (e.g., ATR-FTIR [5], micro-Raman combined with laser ablation ICP-MS [6, 7], LIBS/ICP-OES and GC/μ-ECD and GC/MS [8, 9], SEM/EDS and LC-MS/MS [10-12], SEM/EDS and IBA/μPIXE [4, 13] and TOF-SIMS [14-18]), several reports have shown higher confidence and the need for simultaneous detection of GSR and OGSRs. Recently, we reported on the advantages of high resolution, ion beam-based mass spectrometry imaging combining secondary electron and secondary ion images in order to characterize the firearm discharge from skin swabs based on the morphology and composition of the collected species (*e.g.*, particulates and organic compounds) in a single analysis.[19]

In the current work, we propose as a proof of concept an alternative, facile, high throughput method based on the analysis of skin swab samples for both inorganic and organic species

using electrospray trapped ion mobility mass-spectrometry (ESI-TIMS-MS). The proposed method is based on the simultaneous extraction of inorganic and organic species assisted by the formation organometallic complexes (e.g., 15-5 crown ethers for the sequestering of metals and nitrate species), followed by fast, post-ionization, high resolution mobility and mass separations. A key feature is the use of nano-ESI to optimize the transfer of material into the gas phase and utilize small sample volumes (e.g., tens of microliters) for higher sensitivity.

4.3. Experimental Section

4.3.1. Materials and Reagents

All metal stock standards were single element ICP-MS standards purchased from ULTRA Scientific® (N. Kingstown, Rhode Island) with the exception of potassium which was purchased from SPEX CertiPrep® (Metuchen, New Jersey). 15-crown-5 at 98% purity was purchased from Sigma-Aldrich® (St. Louis, Missouri). Antimony, barium, copper, and lead stock standard solutions were at a concentration of 10,000 $\mu g/mL$ in water with dilute nitric acid, while potassium was at 1,000 mg/L in 2% nitric acid. The metal charge state in solution was defined by the salt used. A 12,056 ppm stock solution of 15-crown-5 was prepared in HPLC grade methanol (Fisher Chemical, Fair Lawn, New Jersey). The metal stock standards and methanol were used without further purification. The stock metal and crown ether solutions were diluted to working solutions of 3.0 x 10^{-3} M each in methanol. Any additional dilutions were also prepared in the HPLC grade methanol. Other solvents used were acetonitrile and ethyl acetate, LC/MS grade and certified ACS respectively (Fisher Chemical, Fair Lawn, New Jersey). Stock standard solutions of

diphenylamine (DPA), ethyl centralite (EC), and 2,4-dinitrotolune (DNT) were prepared at approximately 10 mg/mL from analytical grade solids in methanol (0.2 micron filtered) purchased from Fisher Scientific®.

The sampling media used, CapSure® (Boston, Massachusetts) VP (low particulate clean room wipe), was obtained from Berkshire® (Boston, Massachusetts). The media is 100% knitted polyester and originally $23\ cm\ x\ 23\ cm$ in size. To allow for easy handling while sampling the media was cut to approximately $4.0\ cm\ x\ 1.5\ cm$. The swabs were pre-conditioned prior to use by placing and storing them in a glass jar in a laboratory oven at approximately 80 ^{o}C. Collection of control shooting samples was accomplished by firing 3 shots from a Smith and Wesson 0.38 revolver firearm then wiping both the left and right hands of the shooter with a pre-wetted swab (WVU IRB protocol #1209000337). The swabs were pre-wet with ~ 1 mL of isopropyl alcohol prior to thorough wiping of the top and palm of the hand and the crease between the index finger and thumb. Both hands were sampled on the same swab which was then placed in a glass tube, capped, and labeled. Swab samples were expose to CE based extraction for the inorganic content and organic extraction for the organic content.

4.3.2. nESI-TIMS-MS analysis

A custom nESI-TIMS unit coupled to an Impact Q-TOF mass spectrometer (Bruker, Billerica, Massachusetts) was used for all the experiments.[20-22] The TIMS unit is controlled by custom software in LabView (National Instruments) synchronized with the MS platform controls.[20] Sample aliquots (<10 μL) of the extracted material in the low micromolar range (~1-15 μM) were loaded in a pulled-tip capillary biased at 700-1200 V to the MS inlet.

TIMS separation depends on the gas flow velocity (v_g), elution voltage ($V_{elution}$), ramp time (t_{ramp}) and base voltage (V_{out}).[21, 23] The mobility, *K*, is defined by:

$$K = \frac{v_g}{E} \cong \frac{A}{(V_{elution} - V_{out})} \quad (1)$$

The mobility calibration constant *A* was determined using known reduced mobilities of Agilent Tuning Mix (Santa Clara, California) components (K_0 of 1.376, 1.013, and 0.835 $\frac{cm^2}{Vs}$ for respective *m/z* 322, 622, and 922) as described in ref [22]. The buffer gas was N_2 at ambient temperature (*T*) with v_g set by the pressure difference between the funnel entrance (P_1 = 2.6 $mbar$) and exit (P_2 = 1.1 $mbar$). An RF voltage of 230 V_{pp} at 2080 kHz was applied to all electrodes. Ions were softly transferred and injected into the TIMS analyser section injection to avoid collisional induced activation (see TIMS schematics in **Appendix 4.1**). Peak fronting in the CCS profiles (or tailing in the scan domain) was observed at higher masses was due to poor transmission in the collision cells since the instrument was tuned for low mass ions. A typical analysis consisted of 2,000 IMS-MS spectra, divided in 100 accumulations in 20 frames (i.e., ~3-15 min depending on the t_{trap}). The measured mobilities were converted into collision cross sections (CCS, Å²) using the Mason-Schamp equation:

$$\Omega = \frac{(18\pi)^{1/2}}{16} \frac{q}{(k_B T)^{1/2}} \left(\frac{1}{m} + \frac{1}{M}\right)^{1/2} \frac{1}{N} \times \frac{1}{K} \quad (2)$$

where q is the ion charge, k_B is the Boltzmann constant, *N* is the gas number density, *m* is the ion mass, and *M* is the gas molecule mass.[23]

4.3.3. Theoretical Section

Candidate structures were proposed for the organic and organometallic species observed from the skin swabs. Several initial guess structures were proposed for the crown ether (CE) and metal (Me) complexes, but they mostly converged to ones described here; other initial guesses attempts did not converge. The candidate structures were optimized at DFT/B3LYP/6-31+g(d) level of theory using the electrostatic potential (ESP) for all metals of the organometallic complexes except for potassium using the Gaussian 09 package.[24] Partial atomic charges were calculated using the Merz−Singh−Kollman scheme constrained to the molecular dipole moment.[25, 26] Theoretical ion-neutral collision cross-sections (CCS) were calculated using IMoS [27-29] packages with the trajectory method and the diffuse hard sphere scattering (DHSS) method. In the case of DHSS, a temperature of 304 K, a pressure of 101325 Pa, 3 rotations, and 3 million collisions with N_2 gas molecules were considered; an accommodation (percentage of non-elastic collisions) of 0.70 yielded the best results when compared with the experimental CCS. Details on the optimized geometries can be found in the supplemental information.

4.4. Results and Discussion

The analysis of the skin swab extractions using nESI-TIMS-MS resulted in the observation of multiple single and double charged species (see **Figure 4.1**). Closer inspection of **Figure 4.1** permitted the identification of a series of organometallic and organic species simultaneously. In positive ion mode, all the organometallic species were detected, while organic species are detected in positive or negative mode depending on the functional groups of the molecule of interest. The high mass resolution permitted the identification of the metals based on their isotopic pattern and the high mobility separation provided reduced

chemical noise and higher peak capacity (see **Figure 4.2** and **Table 4.1**). That is, from a single analysis, both organic and organometallic species are detected. One of the advantages of gas-phase, post-ionization separations using TIMS-MS is that a single acquisition takes typically 100 ms (up to 500 ms for the highest mobility resolution (R_{IMS}~250), with a total analysis time in the order of few minutes.

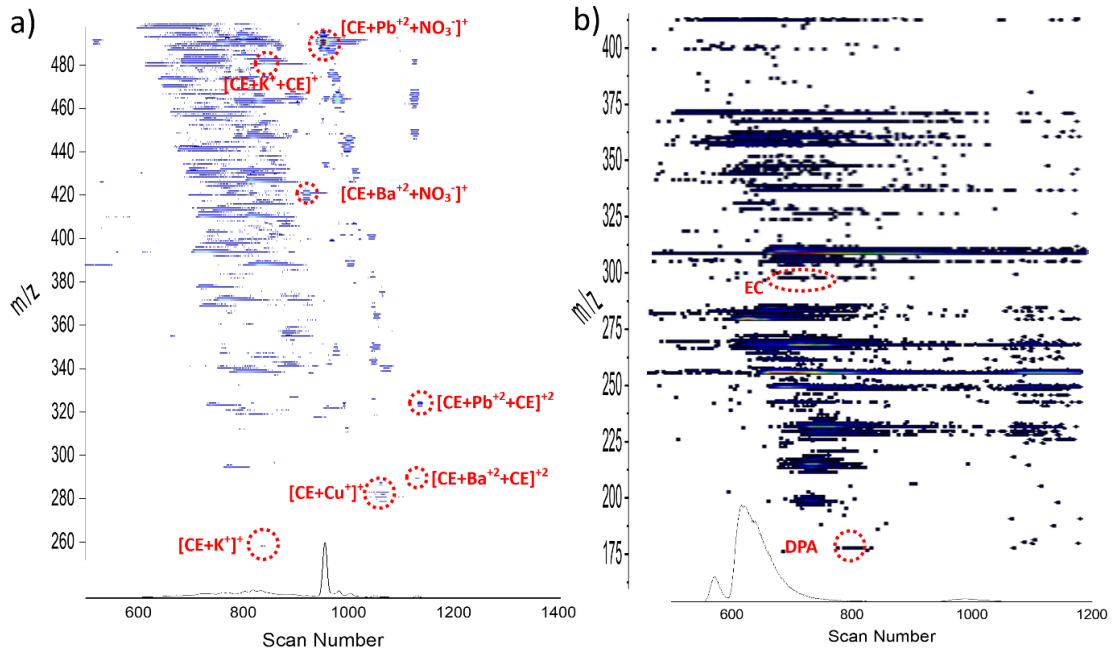

Figure 4.1. Typical 2D-IMS-MS contour plots obtained in positive (a) and negative (b) ion modes.

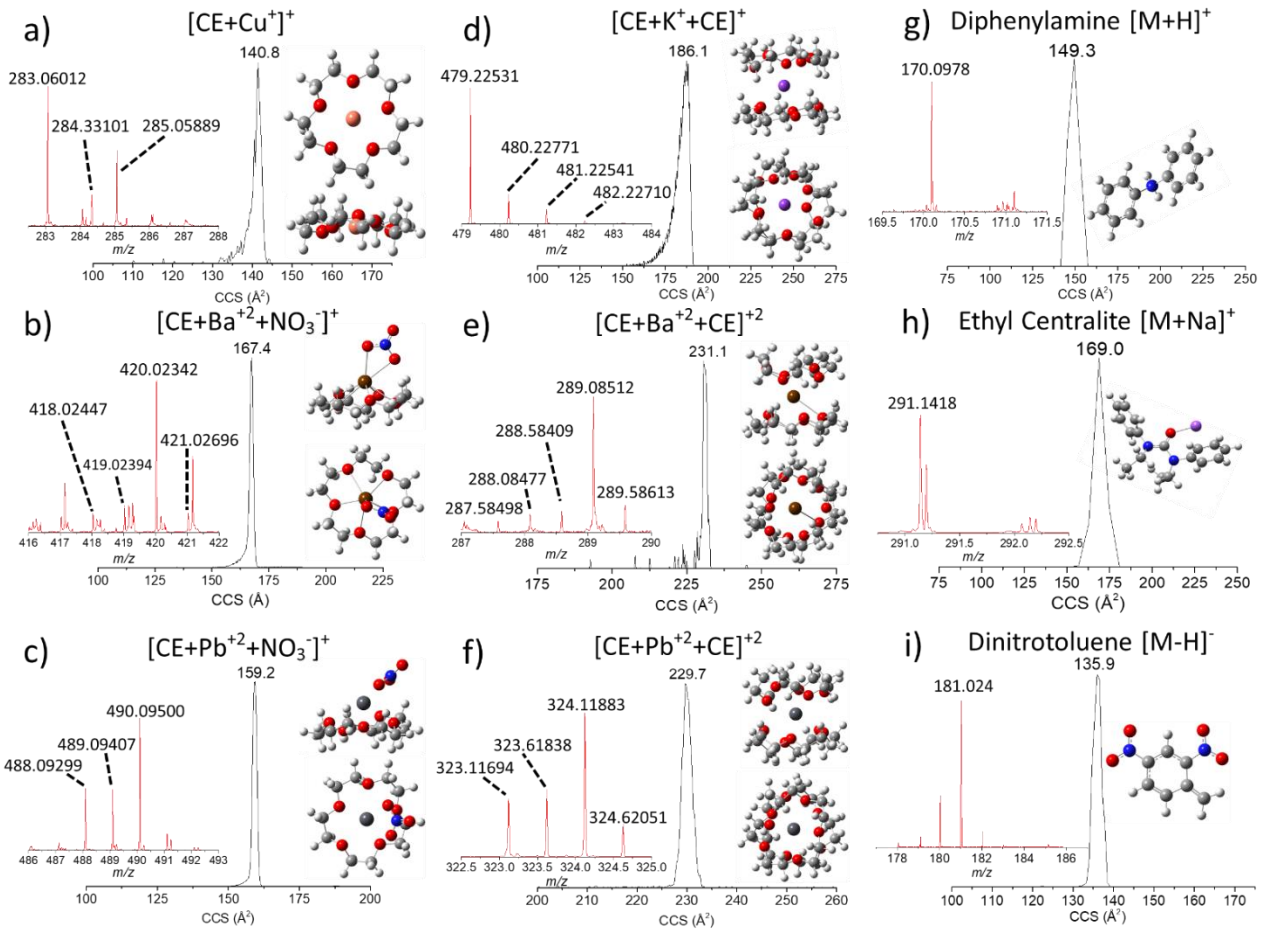

Figure 4.2. TIMS mobility profiles with theoretical structure and mass spectrum as an inset.

Organic Gunshot Residue					
Compound	Molecular Ion	Theoretical *m/z*	Observed *m/z*	Experimental CCS	Theoretical CCS
Diphenylamine	$[M+H]^+$	170.096	170.097	149.9	139.6‡
Ethyl Centralite	$[M+Na]^+$	291.146	291.141	167.3	171.5‡
Dinitrotoluene	$[M-H]^-$	181.025	181.025	140.8	127.4‡
Inorganic Gunshot Residue					
Ion Species	Ionic Radius of Metal (pm)	Theoretical *m/z*	Observed *m/z*	Experimental CCS	Theoretical CCS
$[CE+Ba+NO_3^-]^+$	1.49	420.023	420.023	167.4	163.6†
$[CE+Pb+NO_3^-]^+$	1.33	490.095	490.095	159.2	163.2†
$[CE+Cu]^+$	0.91	283.060	283.060	140.8	147.4†
$[CE+Ba+CE]^{+2}$	1.49	289.083	289.084	231.3	224.5‡
$[CE+Pb+CE]^{+2}$	1.33	324.119	324.118	229.7	222.3‡
$[CE+K+CE]^+$	1.52	479.225	479.225	186.1	180.7‡
†Diffuse Hard Sphere Scattering (DHSS) ‡Trajectory Method (TM)					

Table 4.1. Comparison of theoretical and experimental CCS for organic and inorganic gunshot residue.

The search for organic gunshot residue revealed the presence of diphenylamine and ethyl centralite in positive ion mode as protonated and sodiated species, respectively (**Figure 4.1** and **4.2**). These two compounds are commonly used as stabilizers in smokeless gunpowder. Analysis of the mobility profile showed a single IMS bands for both compounds, which makes them easily identifiable in the IMS-MS domain. In addition, other potential organic components can be observed in negative ion mode as deprotonated species. To illustrate the potential of the proposed nESI-TIMS-MS workflow for their detection a typical IMS and MS profiles of a dinitrotoluene (DNT) standard are shown in **Figure 4.2**. DNT is observed in the $[M-H]^-$ form and is commonly used as a plasticizer and burn rate modifier in smokeless gun powder and propellants. A good agreement is observed between the experimental and theoretical CCS of the proposed candidate structures (**Figure 4.2**).

The organometallic species composed of the 15-5 crown ether (CE) and a metal (Me) had the general form: $[CE+Me]^{+1}$ with Me = Cu; $[CE+Me+NO_3]^{+1}$ with Me = Ba and Pb; $[CE+Me+CE]^{+1}$ with Me = K; $[CE+Me+CE]^{+2}$ with Me = Ba and Pb; and $[CE+Me+(NO_3)_3+Me+CE]^{+1}$ with Me = Ba and Pb. A single mobility band was observed for all organometallic species, which makes them easily identifiable in the IMS-MS domain. Notice that this approach using organometallic complexes provides similar chemical signatures as those obtained using traditional particulate GSR detection with SEM/EDX. [3]

Candidate structures proposed for all the organometallic species provide insights of the coordination of the CE with the Me and with the nitrate group (see **Figure 4.2**). The pocket size of 15-5 and the ionic radius of the metal determines the observation of $[CE+Me]^{+1}$

and $[CE+Me+CE]^{+1}$ species. For example, $[CE+Me+CE]^{+1}$ species were observed for Me = K and not for Cu. This observation does not stem from the oxidation state of the metal, but from their ionic radius. Copper, with a smaller ionic radius, resides deeper within the pocket of the 15-5 CE (**Figure 4.2a**); the copper ion is essentially coplanar with the atoms which make up the CE pocket, thus shielding the copper ion from potential coordination with a second crown ether. The proposed structures are in good agreement with previously reported X-ray structures of $[CE+Me+NO_3]$.[30]

4.5. Conclusions

The analytical power of TIMS-MS for the fast separation and identification of compounds from a complex mixture was used for the detection of organometallic and organic species from skin swabs of firearms gunshot residues. The use of 15-5 crown ether allowed the complexation of a variety of metals and nitrate (Me= Ba^{+2}, Pb^{+2}, Cu^{+}, K^{+}, and NO_3^{-}), that are traditionally used as fingerprints of the gunshot residue. In addition, the observation of organic compounds adds selectivity to the workflow by identification of organic gunshot residues (e.g., diphenylamine, ethyl centralite, and dinitrotoluene). The high mass resolution allowed the clear identification of the compounds based on their mass accuracy and isotopic pattern. Theoretical calculations provided candidate structures for all species observed.

4.6. Acknowledgments

This work was supported by NSF CAREER (CHE-1654274), with co-funding from the Division of Molecular and Cellular Biosciences to FFL. We will like to acknowledge Dr. Mark E. Ridgeway and Dr. Melvin A. Park support during the development and

installation of the custom nESI-TIMS-MS instruments. Work by the WVU researchers was supported by a grant from the US Department of Commerce, National Institute of Standards and Technology (NIST), award number 70NANB16H104.

LIST OF REFERENCES

1. Dalby, O., D. Butler, and J.W. Birkett, *Analysis of gunshot residue and associated materials—a review.* Journal of forensic sciences, 2010. **55**(4): p. 924-943.

2. Taudte, R.V., et al., *Detection of Gunshot Residues Using Mass Spectrometry.* BioMed Research International, 2014. **2014**: p. 965403.

3. International, A., *Standard Guide for Gunshot Residue Analysis by Scanning Electron Microscopy/Energy Dispersive X-ray Spectrometry*. 2010, ASTM International: East Conshohocken, PA.

4. Romolo, F.S., et al., *Integrated Ion Beam Analysis (IBA) in Gunshot Residue (GSR) characterisation.* Forensic Science International, 2013. **231**(1–3): p. 219-228.

5. Bueno, J. and I.K. Lednev, *Attenuated Total Reflectance-FT-IR Imaging for Rapid and Automated Detection of Gunshot Residue.* Analytical Chemistry, 2014. **86**(7): p. 3389-3396.

6. Abrego, Z., et al., *A novel method for the identification of inorganic and organic gunshot residue particles of lead-free ammunitions from the hands of shooters using scanning laser ablation-ICPMS and Raman micro-spectroscopy.* Analyst, 2014. **139**(23): p. 6232-6241.

7. Freitas, J.C.D., et al., *Identification of Gunshot Residues in Fabric Targets Using Sector Field Inductively Coupled Plasma Mass Spectrometry Technique and Ternary Graphs*.* Journal of forensic sciences, 2012. **57**(2): p. 503-508.

8. Tarifa, A. and J.R. Almirall, *Fast detection and characterization of organic and inorganic gunshot residues on the hands of suspects by CMV-GC-MS and LIBS.* Science & justice : journal of the Forensic Science Society, 2015. **55**(3): p. 168-75.

9. Weyermann, C., et al., *Analysis of organic volatile residues in 9 mm spent cartridges.* Forensic Science International, 2009. **186**(1–3): p. 29-35.

10. Thomas, J.L., D. Lincoln, and B.R. McCord, *Separation and Detection of Smokeless Powder Additives by Ultra Performance Liquid Chromatography with Tandem Mass Spectrometry (UPLC/MS/MS).* Journal of forensic sciences, 2013. **58**(3): p. 609-615.

11. Laza, D., et al., *Development of a Quantitative LC-MS/MS Method for the Analysis of Common Propellant Powder Stabilizers in Gunshot Residue**. Journal of forensic sciences, 2007. **52**(4): p. 842-850.

12. Benito, S., et al., *Characterization of organic gunshot residues in lead-free ammunition using a new sample collection device for liquid chromatography–quadrupole time-of-flight mass spectrometry.* Forensic Science International, 2015. **246**: p. 79-85.

13. Christopher, M.E., et al., *A new quantitative method for gunshot residue analysis by ion beam analysis.* Analyst, 2013. **138**(16): p. 4649-4655.

14. Coumbaros, J., et al., *Characterisation of 0.22 caliber rimfire gunshot residues by time-of-flight secondary ion mass spectrometry (TOF-SIMS): a preliminary study.* Forensic Science International, 2001. **119**(1): p. 72-81.

15. Mahoney, C.M., G. Gillen, and A.J. Fahey, *Characterization of gunpowder samples using time-of-flight secondary ion mass spectrometry (TOF-SIMS).* Forensic Science International, 2006. **158**(1): p. 39-51.

16. Szynkowska, M.I., et al., *Examination of gunshot residues transfer using ToF-SIMS.* Surface and Interface Analysis, 2013. **45**(1): p. 596-600.

17. Szynkowska, M.I., et al., *Detection of exogenous contaminants of fingerprints using ToF-SIMS.* Surface and Interface Analysis, 2010. **42**(5): p. 393-397.

18. Szynkowska, M.I., et al., *Preliminary studies using imaging mass spectrometry TOF-SIMS in detection and analysis of fingerprints.* Imaging Science Journal, 2007. **55**(3): p. 180-187.

19. Castellanos, A., S. Bell, and F. Fernandez-Lima, *Characterization of firearm discharge residues recovered from skin swabs using sub-micrometric mass spectrometry imaging.* Analytical Methods, 2016. **8**(21): p. 4300-4305.

20. Fernandez-Lima, F.A., D.A. Kaplan, and M.A. Park, *Note: Integration of trapped ion mobility spectrometry with mass spectrometry.* Rev. Sci. Instr., 2011. **82**(12): p. 126106.

21. Fernandez-Lima, F.A., et al., *Gas-phase separation using a Trapped Ion Mobility Spectrometer.* Int. J. Ion Mobil. Spectrom., 2011. **14**(2-3): p. 93-98.

22. Hernandez, D.R., et al., *Ion dynamics in a trapped ion mobility spectrometer.* Analyst, 2014. **139**(8): p. 1913-1921.

23. McDaniel, E.W. and E.A. Mason, *Mobility and diffusion of ions in gases*. Wiley Series in Plasma Physics. 1973, New York: John Wiley and Sons, Inc., New York. 381.

24. Frisch, M.J., et al., *Gaussian 09*. 2016, Gaussian, Inc.: Wallingford CT.

25. Singh, U.C. and P.A. Kollman, *An approach to computing electrostatic charges for molecules.* Journal of Computational Chemistry, 1984. **5**(2): p. 129-145.

26. Besler, B.H., K.M. Merz, and P.A. Kollman, *Atomic charges derived from semiempirical methods.* Journal of Computational Chemistry, 1990. **11**(4): p. 431-439.

27. Larriba, C. and C.J. Hogan, *Free molecular collision cross section calculation methods for nanoparticles and complex ions with energy accommodation.* Journal of Computational Physics, 2013. **251**: p. 344-363.

28. Larriba, C. and C.J. Hogan, *Ion Mobilities in Diatomic Gases: Measurement versus Prediction with Non-Specular Scattering Models.* The Journal of Physical Chemistry A, 2013. **117**(19): p. 3887-3901.

29. Larriba-Andaluz, C., et al., *Gas molecule scattering & ion mobility measurements for organic macro-ions in He versus N 2 environments.* Physical Chemistry Chemical Physics, 2015. **17**(22): p. 15019-15029.

30. C. Junk, P. and J. W. Steed, *Crown ether chemistry of the alkaline earth nitrates.* Journal of the Chemical Society, Dalton Transactions, 1999(3): p. 407-414.

Chapter Five:

RAPID SCREENING OF LABILE JUVENILE HORMONE III USING LIQUID CHROMATOGRAPHY – TRAPPED ION MOBILITY SPECTROMETRY – MASS SPECTROMETRY

This chapter has been submitted to *Journal of Pharmaceutical and Biomedical Analysis*.

Alan McKenzie-Coe, Cesar E. Ramirez, Marcela Nouzova, Fernando G. Noriega, and Francisco Fernandez-Lima

5.1. Abstract

Juvenile hormones (JH) are key molecules that regulate development and reproductive maturation in insects. The development of new methods to identify and quantify JHs should facilitate the study of different biological aspects of insect pests or vector of diseases. In the present work, we describe a liquid-chromatography–trapped-ion-mobility–mass spectrometry (LC-TIMS–MS) method to identify and quantify JH-III, based on the parent ion ($[M+Na]^+$) and in-source diagnostic fragment ions. The use of in-source diagnostic fragments as confirmation channels was possible by the isolation of ions based on retention time, mobility and accurate *m/z* ($< 1\ ppm$). Theoretical structures are proposed for the JH-III sodiated species and the in-source diagnostic fragment ions. The use of mobility measurements from the parent and the in-source fragments, in addition to the retention time and the accurate mass, permitted higher confidence in the identification and evaluation of interferences. The use of an extraction protocol with an internal deuterated JH-III standard

(JH-III-D_3) allowed for the quantification of JH-III in biological samples at trace levels (LOQ of $75\ ppt$). While this workflow was established for the analysis of JH-III, it can be easily adapted for the detection of other known JHs, or to implement discovery and targeted workflows to identify new sesquiterpenoids.

5.2. Introduction

Juvenile hormones (JHs) play key roles controlling important processes in insect development and reproduction; including inhibition of metamorphosis, caste determination and differentiation, stimulation of flight and migration, stimulation of reproduction, regulation of diapause, stress resistance, and aging [1-6]. Several JHs have been identified and characterized in insects, with JH-III being the most widespread [6-9]. The JHs are acyclic sesquiterpenoids that have a methyl ester head and an epoxide on the opposite end. We have recently developed a high performance liquid chromatography–mass spectrometry (HPLC-ESI-MS/MS) workflow for the detection and quantification of JH-III in *Aedes aegypti* mosquitoes using a multiple reaction monitoring (MRM) scheme and an internal deuterated standard (JH-III-D3).[10] This protocol featured ultra-trace sensitivity (LOD of $8\ pg/mL$ or $0.32\ pg$ on column), high reproducibility, and reduced analysis time ($15\ min$) compared to alternative workflows based on gas chromatography - mass spectrometry (GC-MS), HPLC with fluorescence detection (HPLC-FD) and mass detection (HPLC-MS and MS/MS), and direct analysis in real time-MS (DART-MS). [11-25]. However, despite the use of soft ionization techniques (e.g. ESI), a major limitation for the analysis of labile hormones when using MS-related techniques is the reduced parent protonated ion signal via dissociation events [26].

The use of post-ionization separation techniques based on ion mobility spectrometry resulted in increased peak capacity, reduced chemical noise and the possibility of adding confirmation channel (e.g. collision cross section)[27-30]. We have recently reported the advantages of trapped ion mobility spectrometry in tandem with HPLC-MS approaches (HPLC-TIMS-MS) [31-35], for targeted detections, or projects involving the identification of unknown molecules [36-39]. Different from other IMS-MS approaches, HPLC-TIMS-TOF MS allows for direct detection and quantification of molecular ions based on retention time, accurate collision cross section and mass; with the additional possibility to perform MS/MS on mobility and mass-separated precursor ions [40].

In the present work, we take advantage of the high mobility resolution of TIMS, for the identification and quantification of JH-III, based on retention time, collision cross section (CCS) and accurate mass of the parent ion and in-source diagnostic fragment ions. While this approach is developed for the analysis of JH-III, it can be easily adapted for the detection of other known JHs, or to implement discovery workflows to identify new sesquiterpenoids.

5.3. Experimental Section

5.3.1. Materials and Reagents

Certified standard solutions for JH-III and its deuterated analog (JH-III-D_3) were obtained from Toronto Research Chemicals (Toronto, Canada). Sodium chloride, potassium chloride, hydrochloric acid, sodium hydroxide, ammonium acetate, ammonium formate and ammonium hydroxide salts were analytical grade or better (Fisher Scientific, Pittsburgh, PA). Water, methanol, hexane and acetonitrile were all Optima grade or better

(Fisher Scientific). Chromatographic mobile phases (0.1% formic acid in water, and 0.1% formic acid in acetonitrile) of Optima LC-MS grade were also purchased from Fisher Scientific and used as received. Tissue culture media Gibco M-199, silanized LC vials and silanized LC vials with fused $250\ \mu L$ inserts were also purchased from Fisher Scientific. The tuning mix calibration standard (G24221A) was obtained from Agilent Technologies (Santa Clara, CA).

5.3.2. Sample preparation and storage

Biological samples were prepared following the same protocol as previously described.[10] Briefly, intact *corpora allata-corpora cardiaca* (CA-CC) complexes connected to the brain and head capsule (BR-CA-CC complexes[14]) were dissected from *Aedes aegypti* female adult mosquitoes. The aorta-CA-CC was left connected to the intact head capsule to facilitate the visualization and transfer of the glands. BR-CA-CC were dissected in a drop of saline-buffer containing $138\ mM$ NaCl, $8.4\ mM$ KCl, $4\ mM$ $CaCl_2$, $12\ mM$ NaH_2PO_4 and $42.5\ mM$ sucrose[41]. After dissection, the BR-CA-CC complexes were incubated in $150\ \mu L$ of tissue culture media M-199, containing 2% Ficoll 400 and $50\ \mu M$ methionine. Incubations of BR-CA-CC complexes were carried out in a humid chamber in silanized $2\ mL$ vials for $4\ h$ in the dark at $32°C$, and under continuous gentle agitation. After incubation, $10\ \mu L$ of $6.25\ ppb$ JH-III-D_3 in acetonitrile were added to each sample, followed by $600\ \mu L$ of Hexane. Samples were vortexed for 1 minute and spun for 5 minutes at $4°C$ and $2000\ g$. The organic phase was transferred to a new silanized vial and dried under nitrogen flow. Dried extracts were re-suspended in $100\ \mu l$ of acetonitrile, vortexed

1 minute, transferred to a new silanized vial with a fused $250\ \mu L$ insert and stored at $-20\ ^{\circ} C$.

5.3.3. HPLC-TIMS-MS analysis

The mass spectrometry analyses were carried out in-house using HPLC-TIMS-MS. Slight changes to the previously reported liquid chromatography method were used. [10] Briefly, sample injections ($40\ \mu L$) and LC separations were performed by a Prominence LC-20AD Ultra-Fast Liquid Chromatograph (Shimadzu, Kyoto, Japan), equipped with a Dionex Acclaim 120 C18 Column ($250\ x\ 2.1\ mm,\ 5\ \mu m$) obtained from Thermo Scientific (Sunnyvale, CA). Column temperature was kept at $40°C$. A 15 minutes binary gradient program between 0.1% formic acid dissolved in water (mobile phase A) and 0.1% formic acid dissolved in acetonitrile (mobile phase B) was run according to the following timetable: hold 15% B for $0.5\ min$; ramp to 25% B in $3.5\ min$, ramp to 99% B in $4.0\ min$; hold 99% B for $4\ min$; return to 15% B in $0.5\ min$; hold 15% B for $2.5\ min$ (until end). Total flow rate was changed during the run as follows: hold $0.8\ mL/min$ for $10\ min$, ramp to $1.3\ mL/min$ in $0.2\ min$, hold $1.3\ mL/min$ for $2.3\ min$, return to $0.8\ mL/min$ in $0.1\ min$ and hold for $2.4\ min$ (until end). Detection was performed using a commercial TIMS-TOF instrument (Bruker Daltonics, Bremen, Germany) equipped with an Apollo II ESI source. ESI source parameters were: capillary voltage: $4500\ V$; end plate: $100\ V$; dry gas flow rate: $5.0\ L/min$; dry gas temperature: $200\ °C$; nebulizer: $1.4\ bar$. The TIMS was operated in custom mode over the $0.50 - 1.50\ \frac{cm^2}{Vs}$ 1/Ko range with a $100\ ms$ ramp time, locked 100% duty cycle, $250\ V_{pp}$ RF amplitude, $\Delta 1 = -20\ V$, $\Delta 2 = -150V$, $\Delta 3 = 40V$, $\Delta 4 = 100V$, $\Delta 5 = 0V$ and $\Delta 6 = 100V$. Transfer parameters were: the quadrupole was

operated at 10 eV with a low mass cut-off value of *m/z* 100; collision cell was operated at 4 eV, 1300 V_{pp} RF amplitude, 30% collision gas, and 40 μs transfer time and 10 μs pre-pulse storage time. The TOF analyzer was operated at 10 kHz (*m/z* 100–1250). Mass and mobility calibrations were performed internally using the ESI-L tuning mix calibration standard (G1969-85000, Agilent Technologies, Santa Clara, CA) in positive ion mode (calibration ions: *m/z* 322.0481, K_0= 0.731 $cm^2V^{-1}s^{-1}$; *m/z* 622.0290, K_0= 0.988 $\frac{cm^2}{Vs}$ and *m/z* 922.0098, K0= 1.187 $\frac{cm^2}{Vs}$) using the linear calibration algorithm implemented in Data Analysis 5.2 (Bruker Daltonics Inc, Billerica MA).

5.3.4. Theoretical Section

Candidate structures were generated, and energy minimized for the parent and in-source characteristic fragments at the DFT/B3LYP/6-31+g(d) level using the Gaussian 09 software [42]. Vibrational frequencies were calculated to guarantee that the optimized structures correspond to real minima in the energy space. Partial atomic charges were calculated using the Merz–Singh–Kollman scheme constrained to the molecular dipole moment [43, 44]. Theoretical ion-neutral collision cross sections were calculated using MOBCAL version for helium [45, 46], and nitrogen [47, 48] as a bath gas at ca. 300K. It should be noted that the MOBCAL version for nitrogen was used assuming the similarity of the molecules to those used to develop the Lennard-Jones potential at 300 K as described in refs [47, 48]; for other molecules, alternatives methods may be more accurate (see reference [49]). All optimized geometries and MOBCAL input files can be found in the supporting information.

5.4. Results and Discussion

The ESI process of JH-III is characterized by the observation of the parent ion (e.g., $[M+H]^+$ and $[M+Na]^+$), as well as in-source diagnostic fragment ions (see **scheme 5.1** for JH-III). Depending on the solvent conditions, changes in the ratio of the parent protonated versus the sodiated species can be observed; where the sodiated species is at least an order of magnitude more abundant than the protonated species. This observation led us to consider the use of in-source diagnostic fragment ions as potential identifiers, since all of them share the same retention time of the parent ion, as an alternative to perform MS/MS analysis on the protonated species.

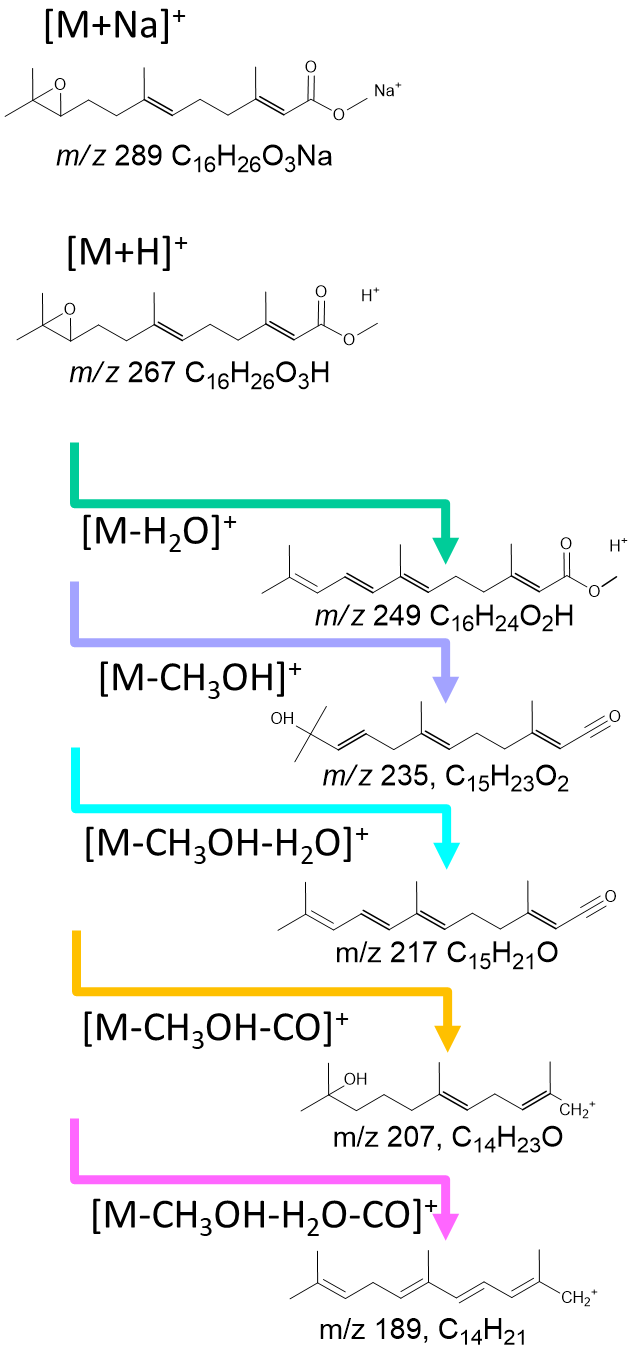

Scheme 5.1. Chemical structure and typical in-source diagnostic fragment ions of JH-III.

Five in-source diagnostic fragment ions were observed during the ESI and nESI process of JH-III (289 *m/z*) and JH-III-D3 (292 *m/z*), corresponding to the neutral loss of H_2O (249 and 252 *m/z*, respectively), CH_3OH (235 *m/z*), CH_3OH-H_2O (217 *m/z*), CH_3OH-CO (207 *m/z*) and CH_3OH-H_2O-CO (189 *m/z*). No major changes in the relative abundances of the parent ion and in-source diagnostic fragment ions were observed between ESI and nESI (see Scheme 5.1 and Table 5.1). Although, the neutral loss of CH_3OH (235 *m/z*) is the most abundant ion, it is a shared fragment between JH-III and JH-III-D3, therefore, for analytical purposes, is better to utilize the neutral loss of H_2O, since it generates two different fragments from JH-III and JH-III-D3 (249 and 252 *m/z*, respectively).

Ion Species	*m/z*	Formula	1/Ko (V s cm^{-2})	CCS (Å^2)	ESI (%)	nESI (%)
$[M+Na]^+$	289.1774	$C_{16}H_{26}O_3Na$	0.804	168.6	73	79
$[M+H]^+$-H_2O	249.1849	$C_{16}H_{25}O_2$	0.734	155.0	3	2
$[M+Na]^+$-CH_3OH	235.1693	$C_{15}H_{23}O_2$	0.722	152.9	17	10
$[M+Na]^+$-CH_3OH-H_2O	217.1587	$C_{15}H_{21}O$	0.707	150.4	4	5
$[M+Na]^+$-CH_3OH-CO	207.1743	$C_{14}H_{23}O$	0.696	148.5	2	1
$[M+Na]^+$-CH_3OH-H_2O-CO	189.1638	$C_{14}H_{21}$	0.665	142.6	2	3
$[D+Na]^+$	292.1962	$C_{16}H_{23}O_3D_3Na$	0.808	169.4	-	-
$[D+H]^+$-H_2O	252.2038	$C_{16}H_{22}O_2D_3$	0.735	155.1	-	-

Table 5.1. Retention times, mobilities and accurate monoisotopic masses of the parent ion and in-source characteristic fragments of JH-III (M) and JH-III-D_3 (D) for n=16. Relative ion abundances are shown for ESI-and nESI sources.

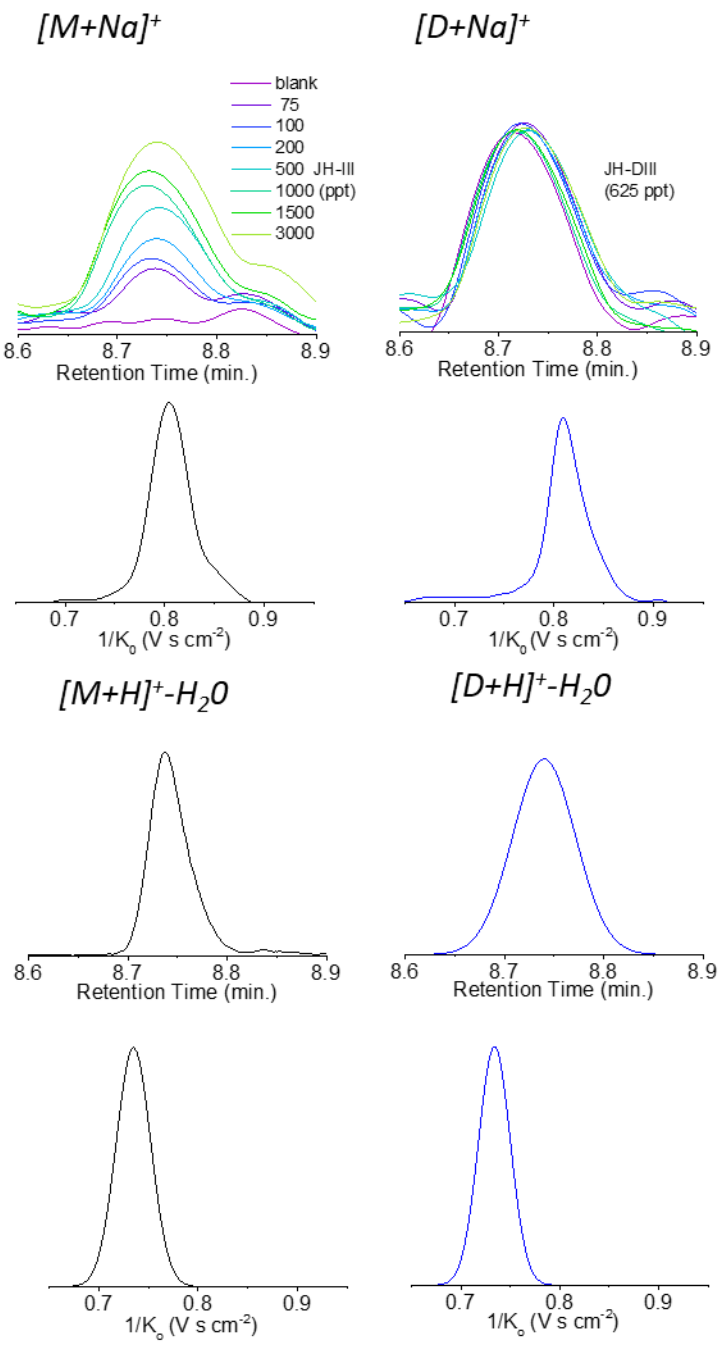

Figure 5.1. Typical chromatography and mobility profiles for JH-III ($75 - 300ppt$) and JH- III-D_3 ($625ppt$) parent ions and in-source characteristic fragments ions.

The mobility profile of the sodiated form of JH-III consists of one single band (see **Figure 5.1**). Several candidate structures were proposed using DFT calculations for the sodiated form of JH-III (see supporting information). Structures with the intramolecular coordination archetype exhibited lower energy (6-19 kcal/mol) and were more compact (smaller CCS 10-37 $Å^2$). The most stable structure revealed that oxygens on both the epoxy end and the carboxyl end of the molecule intra-coordinated to the sodium ion. Theoretical calculations showed that the most stable structures of the protonated species also exhibit intra-coordination with the charge carrying a proton. The mobility profile of the H_2O neutral loss fragments of JH-III showed a single mobility band (see **Figure 5.1**). This fragment results from the epoxide group opening and rearranging. Inspection of the candidate structures proposed using DFT calculations showed two scenarios: **i)** proton driven intramolecular coordination with the carboxyl end, and **ii)** elongation due to changes in the cis-trans orientation along the aliphatic carbon backbone (see supporting information).

During the HPLC-TIMS-MS analysis, the parent and in-source diagnostic fragment ions of JH-III were characterized by their retention time, mobility and high-resolution mass (see **Figure 5.1** and **Table 5.1**). In our current chromatography program, the analysis of JH-III and JH-III-D3 yielded similar retention times and mobility values; but they were easily identified based on accurate *m/z* values (<1 ppm). This allows for a fast and effective quantification of JH-III from biological samples. For example, we changed the concentration of the JH-III standard ($75 - 3000\ ppt$), while keeping the JH-III-D_3 constant ($625\ ppt$). We analyzed the HPLC-TIMS-MS instrument responses for the parent ion $[M+Na]^+$ and the diagnostic H_2O neutral loss fragment ions, as a function of the JH-III

concentration (see **Figure 5.2**). In these experiments, we identified the targeted ions by retention time and mobility domains for each *m/z* of interest. Inspection of **Figure 5.2** shows the increase of the $[M+Na]^+$ and the characteristic H_2O neutral loss signals with the concentration of JH-III standard, while only a small variation was observed for the JH-III-D_3 standard concentration (< 5 %). The parent ions 289/292 yielded a good linear response (R^2 of 0.9994) over the concentration range considered (see **Figure 5.2**).

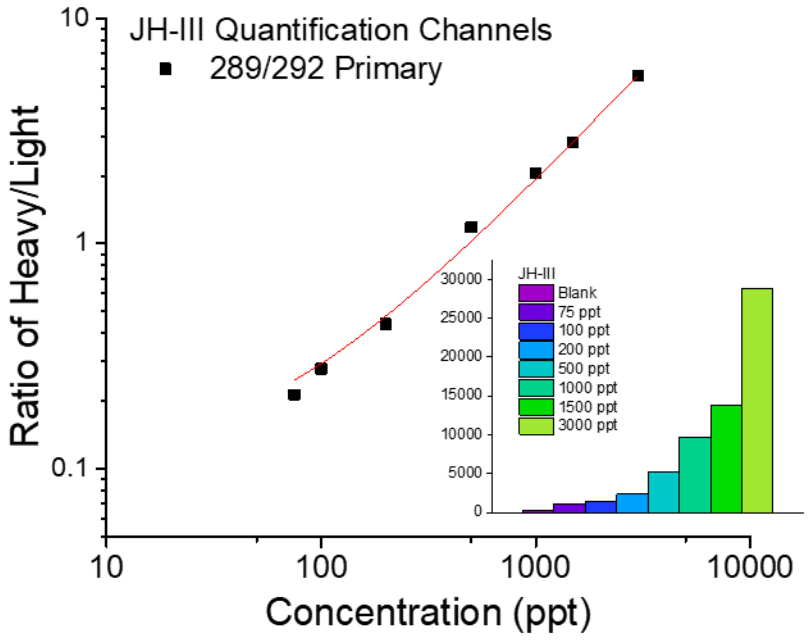

Figure 5.2. Changes in the ratio of JH-III/JH-III-D_3 signals as a function of increases of JH III concentration, while keeping the concentration of JH-III-D_3 fixed at $625\ ppt$. Signals are extracted from the RT $8.7 - 8.8\ min$ and $1/K_0$ 0.75-0.85 $\frac{cm^2}{Vs}$ range with a 0.002 *m/z* window.

This protocol was further evaluated for the analysis of JH-III synthesis by *Aedes aegypti* female mosquitoes. When the results of the analysis of biological samples were compared with those for the standards, we observed that the retention time, mobility and accurate mass of the ions from biological samples were identical to those of the JH-III standards. The method allowed for identifications with high mass accuracy (<1 ppm). The corresponding filtered extracted ion signal in both the chromatography and mobility domain resulted in effective separation from potential interferences (see **Figure 5.3**). We quantified the concentration of JH-III in biological samples using the 289/292 signals (parent ions) and corrected these values for loses and potential sources of errors using the internal standard JH-III-D3 (**Table 5.2**). These measurements corresponded to the production of JH-III by CA of twenty 4-days old sugar-fed *Aedes aegypti* females mosquitoes incubated for 4 hours. The CA glands produced between $18 - 26\ fmol/CA/h$, with a variability of about 30% between the two samples, a difference that is normal in this type of biological experiments.

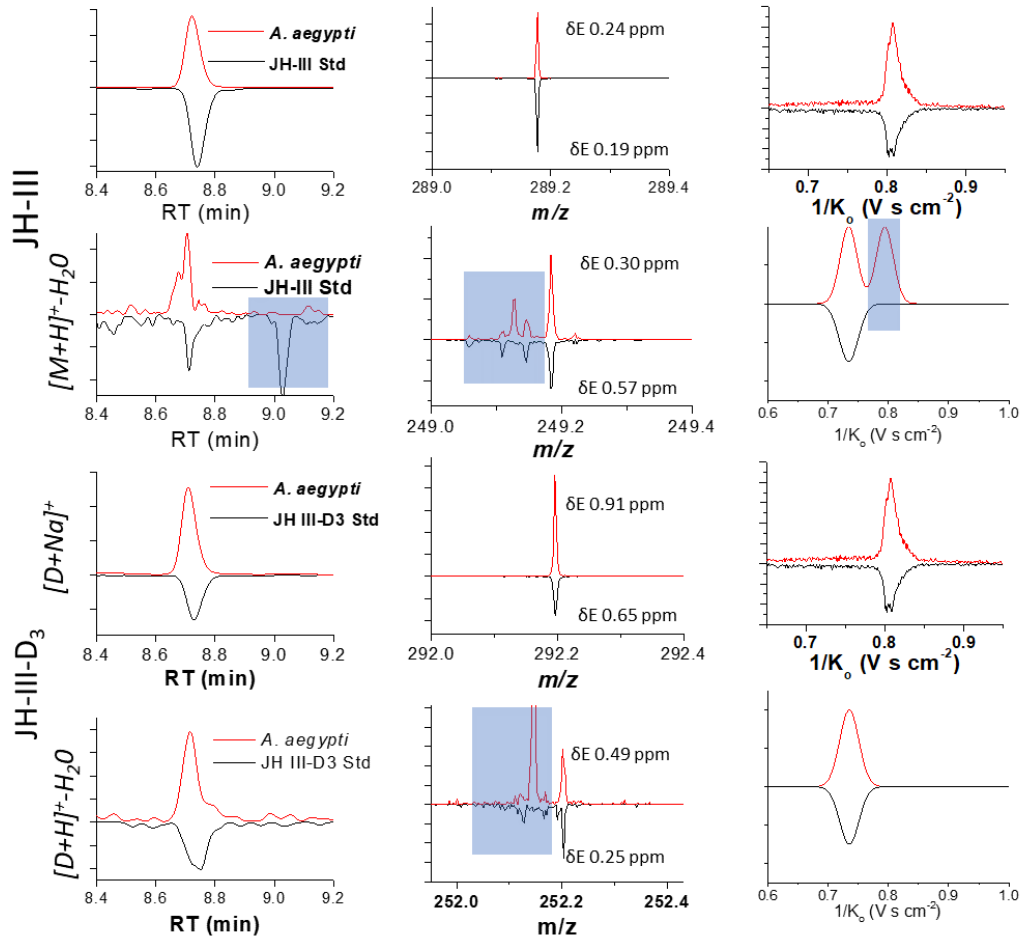

Figure 5.3. HPLC-TIMS-MS detection of JH-III in samples from *Aedes aegypti*. For comparison the signal of JH-III from mosquitoes (red) is compared with that of the JH-III standard (black). Shadow boxes represent potential interferences identified in the biological sample in the retention time (RT), mobility (IMS) and mass (MS) profiles.

JH-III detection		Sample A (fmol)	Sample B (fmol)	
289/292 signal		2059 (1.7%) 2095 (1.6%)	1401 (2.0%) 1407 (2.4%)	

Table 5.2. Amount of JH-III synthesized by CA of *Aedes aegypti* female mosquitoes. We quantified the parent ion signals (289/292) and corrected for loses using the signal of the JH-III-D_3 internal standard. The confirmation ratio (249/289) for the standard was 2.6 ± 1.3 %. A typical value for the JH-III synthesized by a CA, under similar conditions, measured by LC-MS/MS is 2800 ± 1200 ($35\ fmol/CA/h$). Each sample (A and B) corresponds to the synthesis of CA from 20 mosquitoes. There are two 2 analytical replicates for each sample.

5.5. Conclusions

We have established a HPLC-TIMS-MS workflow for the rapid and effective detection of low levels of JH-III, based on the detection of the sodiated parent ion and in-source diagnostic fragment ions. When compared with the HPLC-MS/MS detection of JH-III, HPLC-TIMS-MS showed an increased peak capacity as a result of the combined analysis of retention time, accurate mobility and mass measurements. This allowed the detection of JH-III in *Aedes aegypti* samples with high sensitivity. Candidate structures were proposed for the observed gas-phase species. Low limits of detection were observed. High reproducibility was revealed across multiple measurements. While this workflow was developed for JH-III, we anticipate facile implementation of similar methods for other JHs. The selection of the confirmation ion as the water loss ion (249 *m/z*), is due to the fragmentation of the JH-III-D3 standard. The use of alternative JH-III standards without interferences at the CH_3OH neutral loss (235 *m/z*), could increase the sensitivity by almost a $3 - 5x$ fold.

5.6. Acknowledgements

This work was supported by the NIH grant No. R21AI135469-01A1 to F.F.-L. and No. 2R01AI045545 to F.G.N.

LIST OF REFERENCES

1. Goodman, W.G. and M. Cusson, *The Juvenile Hormones*, in *Insect Endocrinology*, L.I. Gilbert, Editor. 2012, Academic Press: San Diego. p. 310-365.

2. Gilbert, L.I., N. A. Granger, and R.M. Roe, *The juvenile hormones: historical facts and speculations on future research directions.* Insect Biochemistry and Molecular Biology, 2000. **30**(8–9): p. 617-644.

3. Jindra, M., S.R. Palli, and L.M. Riddiford, *The juvenile hormone signaling pathway in insect development.* Annual review of entomology, 2013. 58: p. 181-204.

4. Wyatt, G. and K. Davey, *Cellular and Molecular Actions of Juvenile Hormone. ll. Roles of Juvenile Hormone in Adult Insects*. Advances in insect physiology, 1996. 26(1).

5. Watanabe, D. and K. Maekawa, *Relationships between frontal-gland formation and mandibular modification during JH III-induced presoldier differentiation in the termite Reticulitermes speratus (Isoptera: Rhinotermitidae).* Entomological Science, 2012. **15**(1): p. 56-62.

6. Engel, K.C., et al., *A hormone-related female anti-aphrodisiac signals temporary infertility and causes sexual abstinence to synchronize parental care*. Nat Commun, 2016. 7.

7. Noriega, F.G., *Juvenile hormone biosynthesis in insects: what is new, what do we know, and what questions remain?* International scholarly research notices, 2014. 2014.

8. Riddiford, L.M., *Cellular and Molecular Actions of Juvenile Hormone I. General Considerations and Premetamorphic Actions*, in *Advances in Insect Physiology*, P.D. Evans, Editor. 1994, Academic Press. p. 213-274.

9. Schooley, D.A., et al., *Biosynthesis of the juvenile hormones of Manduca sexta: labeling pattern from mevalonate, propionate, and acetate. Proceedings of the National Academy of Sciences, 1973. 70(10): p. 2921-2925.*

10. Ramirez, C.E., et al., *Fast, ultra-trace detection of juvenile hormone III from mosquitoes using mass spectrometry. Talanta, 2016. 159: p. 371-378.*

11. Gomez-Simuta, P.E.T.Y., *Juvenile hormone: action in regulation of sexual maturity in Caribbean fruit flies and potential use in improving efficacy of sterile insect control technique for tephritid fruit flies. IOBC wprs Bulletin, 2002. 25.*

12. Teal, P., A. Proveaux, and R. Heath, *Analysis and quantitation of insect juvenile hormones using chemical ionization ion-trap mass spectrometry. Analytical Biochemistry, 2000. 277(2): p. 206-213.*

13. Rembold, H. and B. Llackner, *Convenient method for the determination of picomole amounts of juvenile hormone.* Journal of Chromatography A, 1985. **323**(2): p. 355-361.

14. Li, Y., et al., *Stimulation of JH biosynthesis by the corpora allata of adult female Aedes aegypti in vitro: effect of farnesoic acid and Aedes allatotropin. Journal of Experimental Biology, 2003. 206(11): p. 1825-1832.*

15. Sperling, S., et al., *Size Exclusion High Performance Liquid Chromatography: Re-Discovery of a Rapid and Versatile Method for Clean-Up and Fractionation in Chemical Ecology. Journal of Chemical Ecology, 2015. 41(6): p. 574-583.*

16. Ichikawa, A., et al., *Enantioselective separation of racemic juvenile hormone III by normal-phase high-performance liquid chromatography and preparation of [2H3]juvenile hormone III as an internal standard for liquid chromatography–mass spectrometry quantification. Journal of Chromatography A, 2007. 1161(1–2): p. 252-260.*

17. Chen, Z., et al., *Comparison of radioimmunoassay and liquid chromatography tandem mass spectrometry for determination of juvenile hormone titers. Insect biochemistry and molecular biology, 2007. 37(8): p. 799-807.*

18. Zhou, J., et al., *Quantitative determination of juvenile hormone III and 20-hydroxyecdysone in queen larvae and drone pupae of Apis mellifera by ultrasonic-assisted extraction and liquid chromatography with electrospray ionization tandem mass spectrometry. Journal of Chromatography B, 20II. 879(25): p. 2533-2541.*

19. Navare, A.T., et al., *Rapid direct analysis in real time (DART) mass spectrometric detection of juvenile hormone III and its terpene precursors.* Analytical and bioanalytical chemistry, 2010. **398**(7-8): p. 3005-3013.

20. Ares, A., et al., *Liquid chromatography coupled to ion trap-tandem mass spectrometry to evaluate juvenile hormone III levels in bee hemolymph from Nosema spp. infected colonies. Journal of Chromatography B, 2012. 899: p. 146-*153.

21. Westerlund, S.A. and K.H. Hoffmann, *Rapid quantification of juvenile hormones and their metabolites in insect haemolymph by liquid chromatography–mass spectrometry (LC-MS). Analytical and bioanalytical chemistry, 2004. 379(3): p. 540-543.*

22. Furuta, K., et al., *Determination by LC-MS of juvenile hormone titers in hemolymph of the silkworm, Bombyx mori. Bioscience, biotechnology, and biochemistry, 2013. 77(5): p. 988-991.*

23. Rivera-Perez, C., M. Nouzova, and F.G. Noriega, *A quantitative assay for the juvenile hormones and their precursors using fluorescent tags.* Plos One, 2012. *7(8): p. e43784.*

24. Miyazaki, M., et al., *Liquid chromatography–electrospray ionization-mass spectrometric quantitation of juvenile hormone III in whole body extracts of the Formosan subterranean termite. Journal of Chromatography B, 2009. 877(27): p. 3175-3180.*

25. Watanabe, D., et al., *Soldier presence suppresses presoldier differentiation through a rapid decrease of JH in the termite Reticulitermes speratus. Journal of Insect Physiology, 2011. 57(6): p. 791-795.*

26. Vilaró, F., et al., *UHPLC–MS Analysis of Juvenile Hormone II in Mediterranean Corn Borer (Sesamia nonagrioides) Hemolymph Using Various Ionization Techniques. Journal of agricultural and food chemistry, 2012. 60(12): p. 3020-3025.*

27. Cumeras, R., et al., *Review on Ion Mobility Spectrometry. Part 1: current instrumentation.* Analyst, 2015. **140**(5): p. 1376-1390.

28. Lapthorn, C., F. Pullen, and B.Z. Chowdhry, *Ion mobility spectrometry-mass spectrometry (IMS-MS) of small molecules: Separating and assigning structures to ions.* Mass Spectrometry Reviews, 2013. **32**(1): p. 43-71.

29. Borsdorf, H., et al., *Recent Developments in Ion Mobility Spectrometry.* Applied Spectroscopy Reviews, 2011. **46**(6): p. 472-521.

30. Kanu, A.B., et al., *Ion mobility–mass spectrometry.* Journal of Mass Spectrometry, 2008. **43**(1): p. 1-22.

31. Hernandez, D.R., et al., *Ion dynamics in a trapped ion mobility spectrometer.* Analyst, 2014. **139**(8): p. 1913-1921.

32. Fernandez-Lima, F.A., et al., *Gas-phase separation using a Trapped Ion Mobility Spectrometer.* International Journal for Ion Mobility Spectrometry, 2011. **14**(2-3): p. 93-98.

33. Fernandez-Lima, F.A., D.A. Kaplan, and M.A. Park, *Note: Integration of trapped ion mobility spectrometry with mass spectrometry.* Rev. Sci. Instr., 2011. **82**(12): p. 126106.

34. Fernandez-Lima, F., *Trapped Ion Mobility Spectrometry: past, present and future trends.* International Journal for Ion Mobility Spectrometry, 2016. **19**(2): p. 65-67.

35. Ridgeway, M.E., et al., *Trapped ion mobility spectrometry: A short review.* International Journal of Mass Spectrometry, 2018. **425**: p. 22-35.

36. Garabedian, A., et al., *Towards Discovery and Targeted Peptide Biomarker Detection Using nanoESI-TIMS-TOF MS.* Journal of The American Society for Mass Spectrometry, 2018. **29**(5): p. 817-826.

37. Adams, K.J., et al., *Analysis of isomeric opioids in urine using LC-TIMS-TOF MS.* Talanta, 2018. **183**: p. 177-183.

38. Adams, K.J., et al., *Discovery and targeted monitoring of polychlorinated biphenyl metabolites in blood plasma using LC-TIMS-TOF MS.* International Journal of Mass Spectrometry, 2018. **427**: p. 133-140.

39. Baglai, A., et al., *Comprehensive lipidomic analysis of human plasma using multidimensional liquid- and gas-phase separations: Two-dimensional liquid chromatography–mass spectrometry vs. liquid chromatography–trapped-ion-mobility–mass spectrometry.* Journal of Chromatography A, 2017. **1530**: p. 90-103.

40. Meier, F., et al., *Parallel Accumulation–Serial Fragmentation (PASEF): Multiplying Sequencing Speed and Sensitivity by Synchronized Scans in a Trapped Ion Mobility Device.* Journal of Proteome Research, 2015. **14**(12): p. 5378-5387.

41. Li, Y., et al., *Activity of the corpora allata of adult female Aedes aegypti: effects of mating and feeding.* Insect biochemistry and molecular biology, 2003. **33**(12): p. 1307-1315.

42. Frisch, M.J., et al., *Gaussian 03, Revision C.02*, in *Gaussian, Inc.* 2004: Wallingford CT.

43. Singh, U.C. and P.A. Kollman, *An approach to computing electrostatic charges for molecules.* Journal of Computational Chemistry, 1984. **5**(2): p. 129-145.

44. Besler, B.H., K.M. Merz, and P.A. Kollman, *Atomic charges derived from semiempirical methods.* Journal of Computational Chemistry, 1990. **11**(4): p. 431-439.

45. Mesleh, M.F., et al., *Structural Information from Ion Mobility Measurements: Effects of the Long-Range Potential.* J. Phys. Chem., 1996. **100**(40): p. 16082-16086.

46. Shvartsburg, A.A. and M.F. Jarrold, *An exact hard-spheres scattering model for the mobilities of polyatomic ions.* Chemical Physics Letters, 1996. **261**(1-2): p. 86-91.

47. Campuzano, I., et al., *Structural Characterization of Drug-like Compounds by Ion Mobility Mass Spectrometry: Comparison of Theoretical and Experimentally Derived Nitrogen Collision Cross Sections.* Analytical Chemistry, 2011. **84**(2): p. 1026-1033.

48. Kim, H.I., et al., Anal. Chem., 2009. **81**: p. 8289.

49. Larriba, C. and C.J. Hogan, *Ion Mobilities in Diatomic Gases: Measurement versus Prediction with Non-Specular Scattering Models.* The Journal of Physical Chemistry A, 2013. **117**(19): p. 3887-3901.

CLOSING REMARKS

The findings from Chapter 2 show it is possible to use the TIMS-MS device to monitor the stability of gas-phase ion-neutral complexes. Here stability was investigated by monitoring the intensity as a function of the trapping time. Furthermore, insights from computational calculations reveal that the binding energy between the neutral compound and charge carrying partner along with the CCS play a role in the overall stability. From this work three major trends were observed: **(1)** molecular ions are more stable than ion-neutral complexes **(2)** adduct complexes containing chlorine or nitrate are significantly more stable than analogous formate and acetate complexes **(3)** HMX complexes are more stable than corresponding RDX and PETN complexes.

Chapter 3 continues the lifetime studies of Chapter 2. In this follow-up chapter the chemical environment within the TIMS device is modified by introducing various organic solvents. The results of this work show that there is no significant improvement to lifetime stability, resolving power, or resolution. Theoretical calculation of possible dissociation reactions supports these findings as there were only minimal energetic differences between the pathways considered.

Chapter 4 details another forensic application of TIMS-MS in conjunction with theoretical calculations for the fast separation and identification of both organic and inorganic gunshot residue. 15–5 crown ethers were used to form complexes with metals indicative of gunshot residue. The high mass resolution allowed the metals to be identified by their unique isotopic pattern. Theoretical calculations reveal that the ionic radius of the metal determines the amount of crown ethers that can bind to the metal (e.g. one or two).

In Chapter 5 high performance liquid chromatography was interfaced to the TIMS-MS device resulting in an increase in peak capacity this along with the use of an internal deuterated JH-III standard allow for the detection and quantification of juvenile hormone III extracted from *Aedes aegypti*. Confirmation using in-source fragments was possible by isolating ions based on retention time, mobility and accurate *mass-to-charge*.

In closing, the concerted approach of the versatile TIMS-MS platform and theoretical calculations allows for a plethora of analytical queries to be investigated. In particular, the workflow demonstrates the ability to interrogate the stability of gas-phase ions and identify and quantify compounds from complex mixtures. Finally, insight from theoretical calculations reveal the role that chemical nature and structure play within the context of the TIMS device.

APPENDICES

Appendix 2.1 Optimized structures of the molecular adduct complexes of TNT, RDX, PETN and HMX.

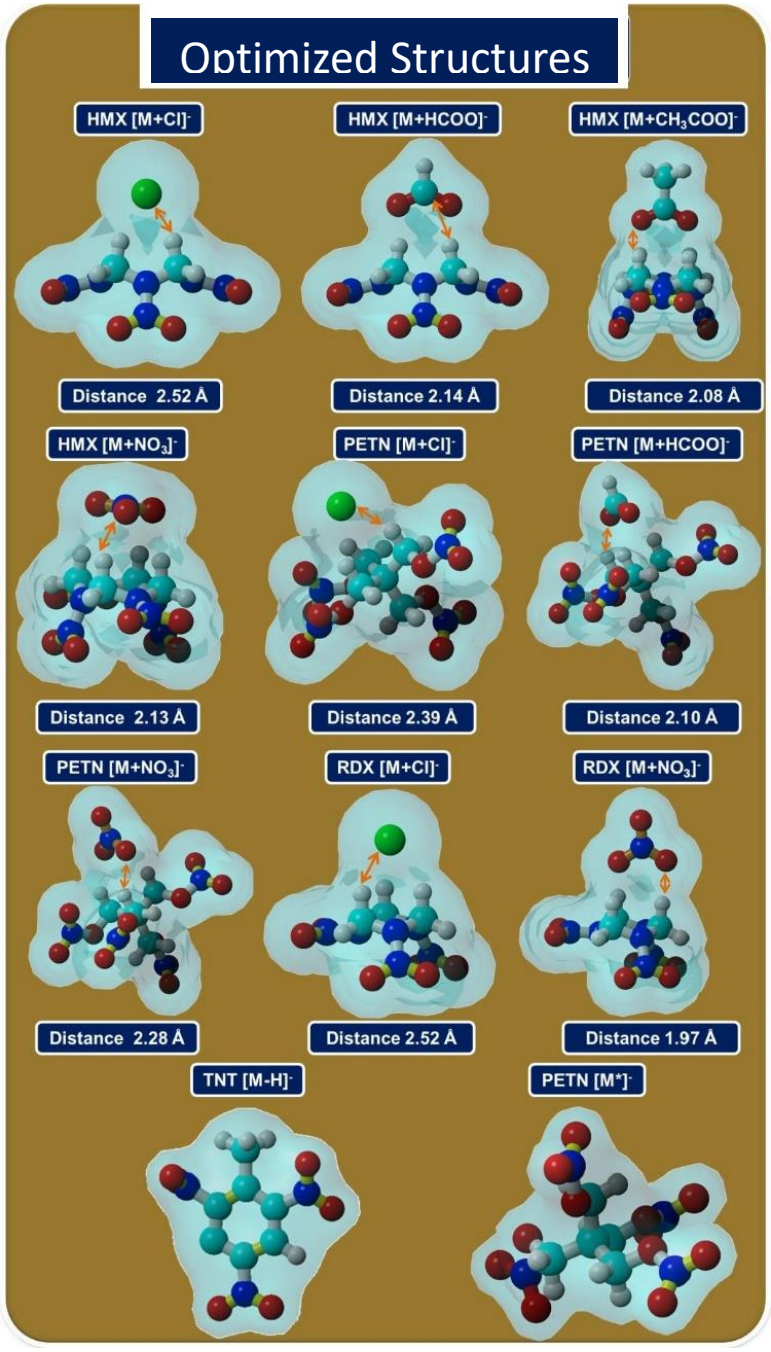

Appendix Table 2.2 Optimized geometry files, charges and structures utilized to calculate the CCS in MOBCAL.

TNT
$[M-H]^-$
1
20
ang
calc
1

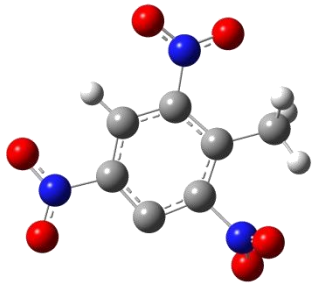

X	Y	Z	Atom #	ESP Charges
2.750958	0.001056	0	12	-0.669564
1.403681	0.000544	0	12	0.025134
0.569041	-1.231409	0	12	0.145063
-0.806829	-1.214515	0	12	-0.423731
-1.510661	-0.000584	0	12	0.249954
-0.807779	1.213893	0	12	-0.423704
0.568081	1.231861	0	12	0.145039
1.144085	2.561020	0	14	0.671619
0.400576	3.548814	0	16	-0.514657
2.357861	2.691424	0	16	-0.480116
-2.935022	-0.001138	0	14	0.602739
-3.534707	1.094430	0	16	-0.492816
-3.533853	-1.097178	0	16	-0.492818

1.146090	-2.560135	0	14	0.671627
2.359979	-2.689581	0	16	-0.480112
0.403334	-3.548510	0	16	-0.51466
3.296371	-0.926327	0	1	0.246534
3.295656	0.928867	0	1	0.246533
-1.350450	-2.148101	0	1	0.243972
-1.352119	2.147059	0	1	0.243964

RDX
$[M+Cl]^-$
1
22
ang
calc
1

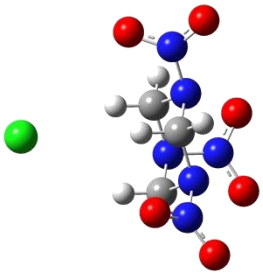

X	Y	Z	Atom #	ESP Charges
-0.713117	-0.016687	1.243280	12	-0.127403
0.619782	0.566343	1.201934	14	-0.197300
0.910031	1.343218	-0.011003	12	-0.130355
0.617745	0.549083	-1.212368	14	-0.201476
-0.715507	-0.033988	-1.243061	12	-0.127207
-0.899125	-0.811955	0.005695	14	-0.000726
-1.894963	-1.762041	0.013296	14	0.669666
-2.290512	-2.177815	-1.079877	16	-0.446854
-2.287502	-2.163428	1.112897	16	-0.446630
1.660379	-0.176823	-1.800776	14	0.723680
2.804102	0.226112	-1.598055	16	-0.415474
1.353722	-1.110668	-2.542383	16	-0.437511
1.663566	-0.148554	1.801307	14	0.719455
1.358562	-1.072245	2.556241	16	-0.436646

2.806508	0.253817	1.593173	16	-0.414519
-1.422181	0.824994	1.246455	1	0.184649
-0.823003	-0.658809	2.108460	1	0.183495
1.941960	1.673930	-0.014281	1	0.199214
0.195156	2.177577	-0.016474	1	0.179116
-0.827308	-0.687995	-2.099040	1	0.183703
-1.424307	0.807813	-1.256862	1	0.185191
-2.168205	2.879334	-0.017832	28	-0.846069

RDX
$[M+NO_3]^-$
1
25
ang
calc
1

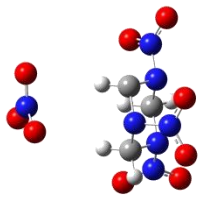

X	Y	Z	Atom #	ESP Charges
0.03258	0.641167	1.242867	12	-0.166948
-0.468995	-0.723678	1.205694	14	-0.220514
-0.115485	-1.477992	-0.005767	12	-0.257471
-0.475011	-0.716824	-1.211301	14	-0.225139
0.025891	0.648492	-1.24324	12	-0.160871
-0.408752	1.324192	0.002945	14	0.013967
-0.381243	2.703634	0.006797	14	0.680895
-0.396326	3.272373	-1.087548	16	-0.444198
-0.39073	3.266147	1.10439	16	-0.444151
-1.725521	-0.95777	-1.80095	14	0.762461
-2.235039	-2.056302	-1.595706	16	-0.417753
-2.178725	-0.087199	-2.543972	16	-0.445293
-1.716304	-0.967894	1.800497	14	0.760397
-2.165514	-0.101447	2.550749	16	-0.444888

-2.22704	-2.065194	1.591677	16	-0.417464
1.127983	0.581989	1.25124	1	0.216803
-0.358221	1.167563	2.105014	1	0.191861
-0.61223	-2.441391	-0.007271	1	0.23686
0.97879	-1.587643	-0.008425	1	0.291573
-0.369972	1.179566	-2.100184	1	0.190476
1.12119	0.589879	-1.258397	1	0.214791
2.997374	-1.786698	0.006186	16	-0.655485
3.608052	-0.67423	-0.004122	14	0.986512
2.922515	0.403481	-0.007499	16	-0.664811
4.852105	-0.629157	-0.011032	16	-0.581608

HMX
$[M+Cl]^-$
1
29
ang
calc
1

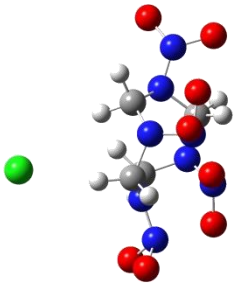

X	Y	Z	Atom #	ESP Charges
-1.280590	0.636044	1.265014	12	-0.363223
-0.000016	0.000149	1.537468	14	0.115953
1.280499	0.636218	1.265060	12	-0.360283
1.877347	0.186910	0.000012	14	0.238469
1.280511	0.635944	-1.265129	12	-0.360285
0.000013	-0.000204	-1.537450	14	0.115972
-1.280546	0.635784	-1.265121	12	-0.363187
-1.877342	0.186465	-0.000021	14	0.218278
-3.217196	-0.170829	0.000007	14	0.630980
-3.768397	-0.319063	1.092173	16	-0.439021
-3.768403	-0.319315	-1.092122	16	-0.439017
0.000071	-1.290322	-2.040773	14	0.534527
1.097690	-1.808244	-2.248100	16	-0.392940
-1.097500	-1.808293	-2.248249	16	-0.390763

3.217054	-0.170857	0.000034	14	0.613797
3.768248	-0.319260	1.092185	16	-0.435060
3.768183	-0.319507	-1.092115	16	-0.435060
0.000034	-1.289889	2.041029	14	0.534547
-1.097540	-1.807833	2.248544	16	-0.390762
1.097648	-1.807786	2.248435	16	-0.392943
-1.078510	1.712935	1.194856	1	0.191220
-1.984776	0.411115	2.060108	1	0.205810
1.984700	0.411298	2.060146	1	0.204645
1.078269	1.713093	1.195046	1	0.186312
1.984740	0.410909	-2.060159	1	0.204653
1.078224	1.712816	-1.195306	1	0.186301
-1.984729	0.410784	-2.060198	1	0.205793
-1.078381	1.712665	-1.195110	1	0.191209
0.000120	3.656170	-0.000380	28	-0.815922

HMX
$[M+CH_3COOH-H]^-$
1
35
ang
calc
1.0000

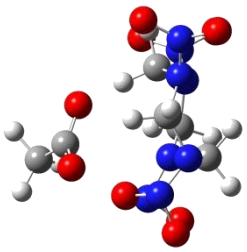

X	Y	Z	Atom #	ESP Charges
-1.256969	0.355496	1.268469	12	-0.595280
-0.036181	-0.398945	1.514136	14	0.359245
1.290653	0.148889	1.268003	12	-0.622339
1.866985	-0.316121	0.000024	14	0.319646
1.290605	0.148486	-1.268061	12	-0.622135
-0.036024	-0.399862	-1.514281	14	0.359092
-1.257100	0.354333	-1.269470	12	-0.595410
-1.901106	-0.010740	-0.000286	14	0.275302
-3.261611	-0.256689	-0.000129	14	0.620637
-3.825917	-0.355017	1.092297	16	-0.436176
-3.825900	-0.356240	-1.092460	16	-0.436190
-0.140597	-1.692730	-1.993879	14	0.462673
0.911628	-2.301906	-2.191492	16	-0.382661
-1.276932	-2.125713	-2.190609	16	-0.381439

3.162585	-0.798420	0.000097	14	0.626215
3.700689	-0.994014	1.092591	16	-0.443151
3.700833	-0.994089	-1.092312	16	-0.443138
-0.141297	-1.691415	1.994645	14	0.462633
-1.277839	-2.123827	2.191457	16	-0.381419
0.910659	-2.300854	2.192906	16	-0.382691
-0.950158	1.410644	1.237537	1	0.300891
-1.974184	0.174274	2.063303	1	0.230014
1.968631	-0.144450	2.063795	1	0.238066
1.156960	1.239550	1.235077	1	0.297998
1.968793	-0.144660	-2.063750	1	0.237992
1.156454	1.239092	-1.235265	1	0.297896
-1.974227	0.171846	-2.064089	1	0.230061
-0.950853	1.409666	-1.239618	1	0.300954
1.556955	5.446514	-0.004656	1	0.091316
0.483040	5.214906	-0.001065	12	-0.442257
0.307047	3.688081	-0.000230	12	0.975277
0.047361	5.659254	0.899601	1	0.086128
0.041712	5.658747	-0.899246	1	0.086167
0.255940	3.112050	1.127833	16	-0.846886
0.254290	3.111214	-1.127817	16	-0.847029

HMX
$[M+NO_3]^-$
1
32
ang
calc
1

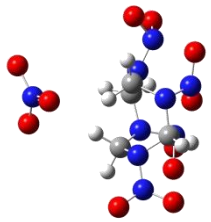

X	Y	Z	Atom #	ESP Charges
1.285739	0.376327	-1.280849	12	-0.189881
0.026455	-0.309189	-1.531470	14	-0.142322
-1.284264	0.273035	-1.280705	12	0.014395
-1.863430	-0.157011	-0.003823	14	0.099583
-1.285166	0.311965	1.259884	12	-0.167862
0.024492	-0.267296	1.526700	14	0.113122
1.283734	0.414019	1.261350	12	-0.234359
1.898518	-0.005706	-0.003416	14	0.128115
3.251579	-0.320952	0.001941	14	0.624758
3.805773	-0.470362	-1.087443	16	-0.428573
3.806053	-0.431718	1.095731	16	-0.429318
0.075098	-1.559268	2.026318	14	0.483787
-1.001112	-2.120401	2.230874	16	-0.380974
1.191909	-2.035061	2.229832	16	-0.374731

-3.185182	-0.586281	0.001982	14	0.620406
-3.724412	-0.783096	-1.087124	16	-0.427641
-3.727641	-0.743298	1.095869	16	-0.428025
0.078332	-1.614322	-1.998882	14	0.618244
1.195457	-2.094285	-2.188781	16	-0.399743
-0.997205	-2.180394	-2.191518	16	-0.410982
1.074972	1.452926	-1.279446	1	0.159732
1.997346	0.135570	-2.065084	1	0.193332
-1.973640	-0.024363	-2.065317	1	0.143560
-1.166197	1.362599	-1.278004	1	0.067653
-1.975172	0.039033	2.052765	1	0.171936
-1.150499	1.398906	1.236171	1	0.089801
1.993502	0.195795	2.053793	1	0.188121
1.060787	1.487698	1.238804	1	0.122826
0.788575	3.512218	-0.793544	16	-0.590839
-0.207442	3.446332	-0.019958	14	0.909188
-1.376827	3.397796	-0.491810	16	-0.573864
-0.029357	3.363054	1.231976	16	-0.569446

PETN	
$[M^*]^-$	
1	
29	
ang	
calc	
1	

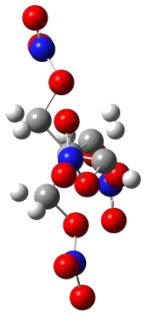

X	Y	Z	Atom #	ESP Charges
0.687075	-1.248249	0.170054	12	0.064415
-0.181022	-0.125539	-0.440166	12	-0.189551
-1.435950	-0.792734	-1.052582	12	-0.074121
-2.145811	-1.427387	0.031183	16	-0.314517
-3.374501	-2.049077	-0.361118	14	0.845912
-3.950403	-2.553061	0.567730	16	-0.365996
-3.668258	-1.995465	-1.536456	16	-0.384242
0.507790	0.589464	-1.632509	12	0.136217
1.610596	1.421791	-1.235376	16	-0.312479
2.919887	0.852080	-1.396063	14	0.724347
3.781643	1.592832	-1.007776	16	-0.312007
3.001803	-0.250498	-1.897271	16	-0.348838
-0.557918	0.881428	0.666742	12	0.387326
-1.489633	1.806863	0.060723	16	-0.357593

-1.921452	2.855443	0.927776	14	0.811406
-1.487957	2.850645	2.059604	16	-0.381509
-2.684053	3.615239	0.385767	16	-0.364884
1.795080	-0.618961	0.848584	16	-0.337221
2.671790	-1.546475	1.502612	14	0.814449
2.393732	-2.723260	1.412155	16	-0.385258
3.584383	-0.998185	2.062901	16	-0.345229
1.066114	-1.910439	-0.614123	1	0.118227
0.111027	-1.835572	0.888696	1	0.104091
-1.155424	-1.546327	-1.796025	1	0.128234
-2.080691	-0.048046	-1.523387	1	0.129816
-0.186791	1.295998	-2.093514	1	0.080991
0.841553	-0.129568	-2.383565	1	0.083990
0.322778	1.421210	1.016318	1	0.018640
-1.037457	0.378303	1.509769	1	0.025383

PETN	
$[M+Cl]^-$	
1	
30	
ang	
calc	
1	

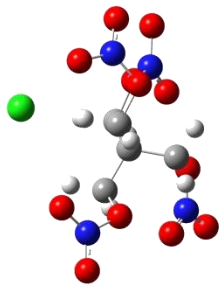

X	Y	Z	Atom #	ESP Charges
0.563563	-0.964377	0.785729	12	0.172219
-0.230054	-0.051086	-0.172515	12	-0.392951
-1.492050	-0.826356	-0.616348	12	0.311580
-2.266007	-1.069333	0.598339	16	-0.366140
-3.535056	-1.624931	0.385449	14	0.864343
-4.121839	-1.868897	1.419947	16	-0.427488
-3.906332	-1.781471	-0.760358	16	-0.420999
0.562017	0.220982	-1.483053	12	0.118964
1.464270	1.345506	-1.324947	16	-0.286649
2.858137	1.057520	-1.315189	14	0.707488
3.518608	2.056076	-1.126194	16	-0.381517
3.218937	-0.079854	-1.504283	16	-0.320947
-0.595159	1.252701	0.562524	12	0.172809
-1.416057	2.030201	-0.354582	16	-0.294759

-1.800732	3.288415	0.129742	14	0.827592
-1.447446	3.599680	1.252065	16	-0.407256
-2.464444	3.919721	-0.663366	16	-0.411283
1.728107	-0.195539	1.215128	16	-0.274024
2.539755	-0.844984	2.160320	14	0.815431
2.174944	-1.926713	2.575658	16	-0.410372
3.524669	-0.202754	2.456536	16	-0.410883
0.877109	-1.869299	0.249864	1	0.146215
-0.025319	-1.227270	1.666943	1	0.055739
-1.204415	-1.780358	-1.081224	1	0.071452
-2.094796	-0.225216	-1.299313	1	0.042369
-0.113781	0.543075	-2.279205	1	0.073036
1.085006	-0.684568	-1.806701	1	0.136377
0.294223	1.828440	0.815440	1	0.068963
-1.174180	1.045607	1.465375	1	0.076086
0.530132	-3.245101	-1.881353	28	-0.855393

PETN
[M+HCOOH-H]$^-$
1
33
ang
calc
1

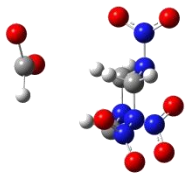

X	Y	Z	Atom #	ESP Charges
0.664108	-0.588581	0.972726	12	0.291904
-0.206842	0.050524	-0.130732	12	-0.401483
-1.369220	-0.936344	-0.396658	12	0.096443
-2.193972	-0.915612	0.811006	16	-0.344014
-3.357466	-1.690244	0.739094	14	0.853621
-3.984227	-1.697971	1.779606	16	-0.427554
-3.617716	-2.236721	-0.313812	16	-0.415266
0.534647	0.173225	-1.487125	12	0.089189
1.484868	1.272570	-1.491141	16	-0.351482
2.854499	0.932257	-1.355837	14	0.771120
3.569821	1.910386	-1.398844	16	-0.393132
3.155079	-0.232674	-1.228236	16	-0.370137
-0.708639	1.421997	0.363057	12	0.375098
-1.654866	1.903445	-0.633824	16	-0.327763

-2.200040	3.164427	-0.358524	14	0.831139
-1.858876	3.722333	0.668210	16	-0.423907
-2.972324	3.544918	-1.211585	16	-0.408788
1.697529	0.385697	1.315632	16	-0.362068
2.528479	0.002800	2.379839	14	0.800723
2.291135	-1.049876	2.938311	16	-0.415011
3.398841	0.814355	2.615317	16	-0.396090
1.104283	-1.522771	0.609636	1	0.181328
0.071242	-0.789112	1.868048	1	0.035447
-0.970770	-1.944845	-0.556520	1	0.213281
-1.979029	-0.613243	-1.241677	1	0.078308
-0.169042	0.467979	-2.269241	1	0.084733
0.988983	-0.779349	-1.784108	1	0.254448
0.111264	2.135281	0.444892	1	0.039880
-1.222370	1.335301	1.322423	1	0.017252
0.661092	-2.716344	-2.530845	16	-0.857534
0.764845	-3.577729	-1.618348	12	0.860255
0.538648	-3.430969	-0.383045	16	-0.861746
1.093485	-4.600771	-1.936973	1	-0.118194

PETN
$[M+NO_3]^-$
1
33
ang
calc
1

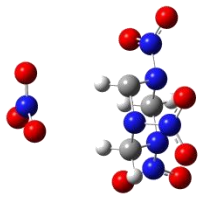

X	Y	Z	Atom #	ESP Charges
-0.668410	-0.031337	1.100097	12	0.349655
0.312602	-0.124288	-0.089343	12	-0.370339
0.981876	1.264550	-0.227630	12	0.160322
1.800541	1.432355	0.969724	16	-0.349897
2.577494	2.601769	0.988934	14	0.839424
3.201815	2.733377	2.020997	16	-0.417886
2.554808	3.317286	0.008879	16	-0.401504
-0.410052	-0.364075	-1.440397	12	0.089751
-0.832182	-1.742946	-1.597890	16	-0.350964
-2.212039	-2.013698	-1.391847	14	0.756401
-2.469904	-3.185986	-1.550353	16	-0.375241
-2.947245	-1.095522	-1.107405	16	-0.361948
1.343325	-1.233172	0.202695	12	0.293716
2.332199	-1.171249	-0.863062	16	-0.330996

3.347876	-2.135970	-0.771987	14	0.845417
3.323576	-2.900176	0.174558	16	-0.422432
4.144863	-2.071977	-1.681716	16	-0.408770
-1.196860	-1.373528	1.317423	16	-0.379422
-2.047991	-1.491460	2.432869	14	0.800579
-2.225792	-0.504544	3.117616	16	-0.406767
-2.494478	-2.609906	2.566872	16	-0.388113
-1.474911	0.671078	0.872911	1	0.136316
-0.151054	0.288372	2.007340	1	0.023753
0.221431	2.049462	-0.271427	1	0.162130
1.629607	1.303703	-1.104596	1	0.065497
0.290394	-0.231052	-2.268105	1	0.101815
-1.238335	0.335091	-1.576071	1	0.212662
0.876665	-2.217907	0.195413	1	0.059118
1.842993	-1.067094	1.159114	1	0.035136
-1.771549	2.829599	0.159662	16	-0.715352
-2.091940	3.121052	-1.039526	14	1.075163
-2.896864	4.041792	-1.274740	16	-0.598235
-1.568758	2.454728	-1.987593	16	-0.728987

Appendix 3.1 Scheme utilized for the nESI-TIMS-MS experiments with organic gas modifiers. Notice that the gas velocity in the TIMS analyzer is kept constant.

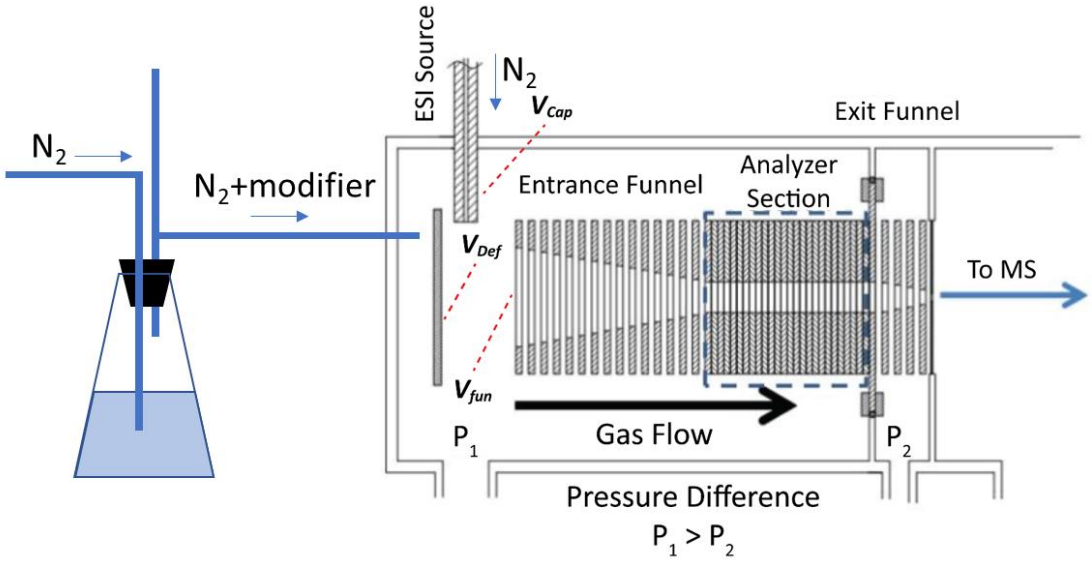

Appendix 3.2. Energies associated to adduct formation and dissociation in the presence of water, methanol, acetone and 2-propanol molecules for PETN + NO_3

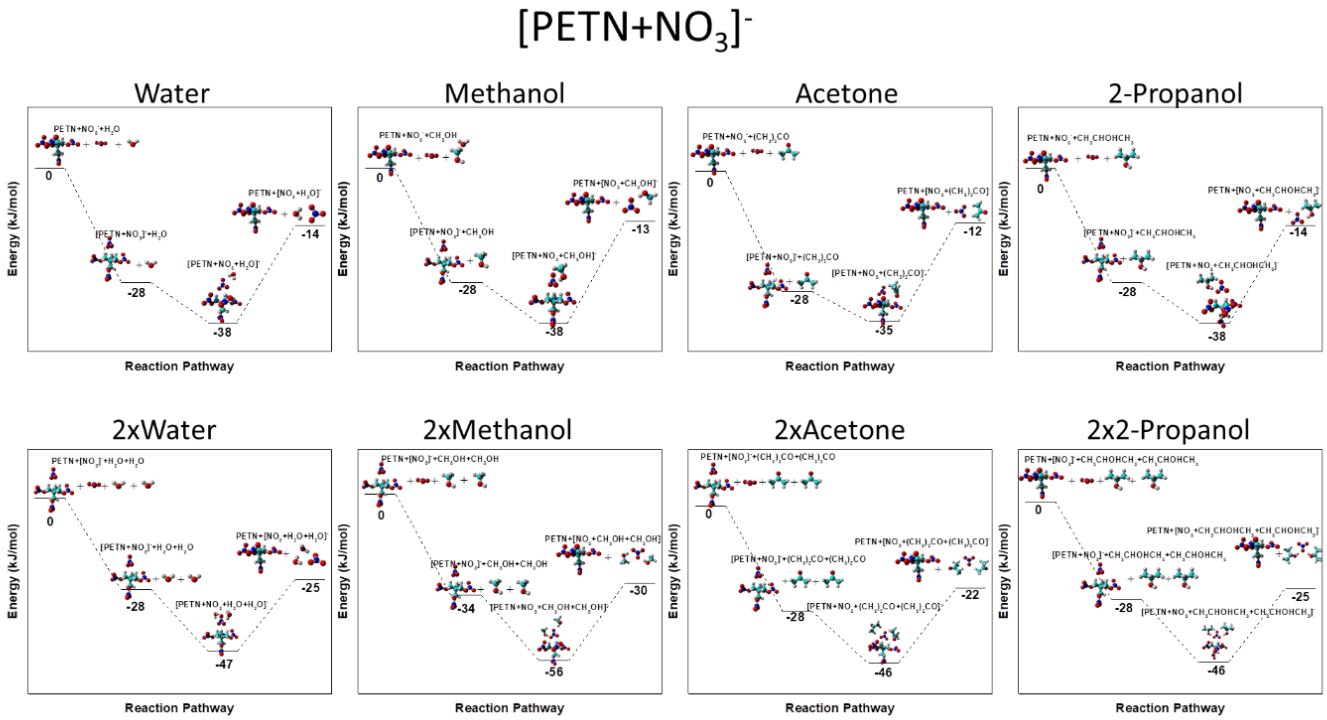

Appendix 4.1 Scheme of the TIMS cell.

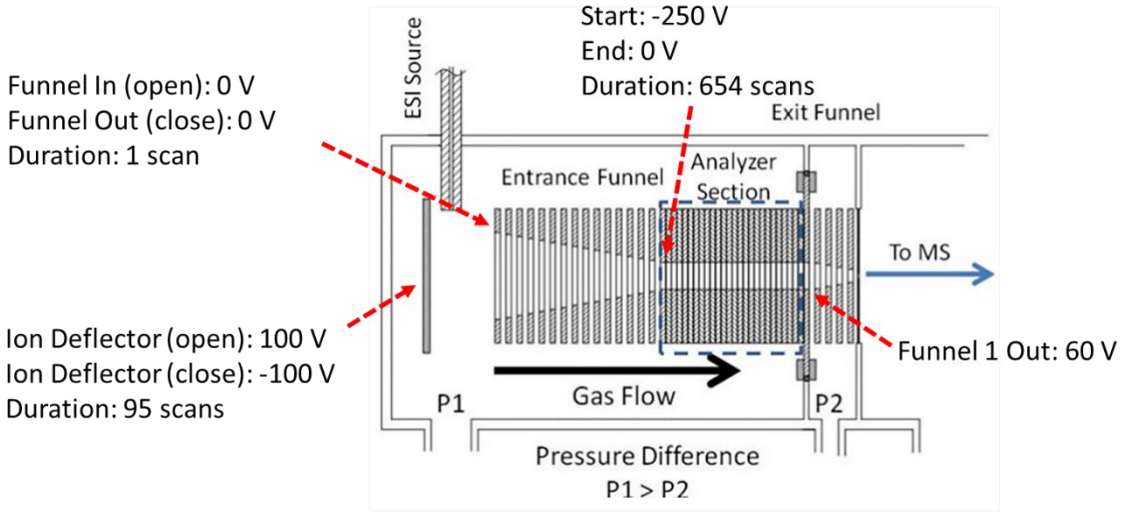

Appendix 4.2. Geometry coordinates of 15-5 Crown Ether and Copper optimized structure

Element	(X, Y, and Z coordinates)		
O	-0.363222	2.149494	0.410556
O	-2.238633	0.406092	-0.545466
O	2.026119	1.055537	-0.324598
O	-1.012784	-1.984866	-0.112281
O	1.631153	-1.566010	0.273230
C	-1.691006	2.606300	0.119546
C	0.677642	3.006118	-0.076736
C	-2.641909	1.448604	0.349619
C	2.004392	2.360136	0.266211
C	-3.017522	-0.797764	-0.532114
C	3.139948	0.247480	0.075722
C	-2.365725	-1.864943	0.337669
C	2.859702	-1.180331	-0.349581
C	-0.234267	-3.006144	0.520676
C	1.175885	-2.888228	-0.026312
H	-1.746218	2.931366	-0.927943
H	-1.948273	3.449580	0.773903
H	0.613110	3.992302	0.402132
H	0.571395	3.128127	-1.163435
H	-2.593568	1.106494	1.392781
H	-3.669064	1.764827	0.124710
H	2.828198	2.969887	-0.128549
H	2.116143	2.270758	1.355529
H	-3.055110	-1.139032	-1.570634
H	-4.040058	-0.596899	-0.190080
H	3.254473	0.298760	1.166965

H	4.060687	0.610950	-0.399578
H	-2.377445	-1.594361	1.403731
H	-2.895578	-2.819295	0.212027
H	2.762098	-1.255647	-1.441733
H	3.679363	-1.832279	-0.018587
H	-0.648007	-3.995993	0.287278
H	-0.242769	-2.860779	1.609868
H	1.829349	-3.632955	0.447508
H	1.180084	-3.047352	-1.113575
Cu	0.018527	0.006283	-0.135932

Appendix 4.3. Geometry coordinates of 15-5 Crown Ether and Potassium optimized structure

Element	(X, Y, and Z coordinates)		
O	0.068157	-2.071720	-0.371500
O	-2.351370	-0.876620	0.443570
O	2.421956	-0.704988	0.207586
O	-1.494283	1.846721	0.046693
O	1.269991	1.757224	-0.298354
C	-1.144963	-2.818096	-0.284232
C	1.270821	-2.799544	-0.127861
C	-2.295464	-1.873100	-0.583179
C	2.443284	-1.924787	-0.539724
C	-3.253803	0.210551	0.205863
C	3.186229	0.355841	-0.374632
C	-2.643878	1.331231	-0.628316
C	2.638167	1.694204	0.094974
C	-0.795818	2.857487	-0.687145
C	0.607274	3.006681	-0.123416
H	-1.258338	-3.257281	0.719236
H	-1.146783	-3.635027	-1.020518
H	1.295288	-3.722584	-0.725267
H	1.337885	-3.082850	0.935110
H	-2.137499	-1.408361	-1.565491
H	-3.238514	-2.437565	-0.606385
H	3.384022	-2.467159	-0.366201
H	2.361368	-1.697383	-1.611031
H	-3.526550	0.590948	1.195429
H	-4.169704	-0.149599	-0.282449

H	3.108206	0.305185	-1.468580
H	4.245037	0.266866	-0.092780
H	-2.349973	0.971290	-1.625352
H	-3.398373	2.121621	-0.761224
H	2.731139	1.802401	1.188724
H	3.219792	2.502111	-0.372548
H	-1.330155	3.815700	-0.617303
H	-0.729682	2.567345	-1.744831
H	1.131790	3.806270	-0.666650
H	0.575482	3.284528	0.943031
K	0.026782	-0.001275	1.400376

Appendix 4.4. Geometry coordinates of 15-5 Crown Ether, Potassium, and 15-5 Crown Ether optimized structure

Element	Element	(X, Y, and Z coordinates)		
O		1.697400	-1.136800	-2.248700
O		1.538100	-2.517300	0.292900
O		2.067800	1.547700	-1.560400
O		2.442600	-0.321400	1.815700
O		1.836400	2.304400	1.095700
C		2.398000	-2.355200	-2.015200
C		2.412600	-0.232100	-3.087100
C		1.657000	-3.175400	-0.968200
C		1.861100	1.170000	-2.911300
C		2.688900	-2.581900	1.130500
C		1.752600	2.897900	-1.240400
C		2.477700	-1.653800	2.310900
C		2.363700	3.199400	0.116600
C		2.367400	0.690900	2.807900
C		2.733200	2.016300	2.165400
H		3.424000	-2.129900	-1.688100
H		2.465800	-2.946800	-2.942900
H		2.328400	-0.537200	-4.141700
H		3.476600	-0.231800	-2.810100
H		0.629500	-3.355600	-1.294600
H		2.162100	-4.146500	-0.850900
H		2.395100	1.849600	-3.594600
H		0.790800	1.207000	-3.167400
H		3.590600	-2.269900	0.586500
H		2.836400	-3.612300	1.490200

H	0.663100	3.045800	-1.238700
H	2.192700	3.586800	-1.979200
H	1.538700	-1.899600	2.830900
H	3.310400	-1.778100	3.020900
H	3.452100	3.070700	0.048900
H	2.156200	4.244200	0.395400
H	3.082200	0.494500	3.622600
H	1.358500	0.723100	3.247900
H	2.704000	2.813500	2.924900
H	3.758500	1.946200	1.777100
K	-0.000800	-0.066700	0.000400
O	-2.447100	-0.286200	-1.817100
O	-1.574900	-2.496200	-0.296300
O	-1.804000	2.328100	-1.092200
O	-1.712200	-1.118400	2.248300
O	-2.044600	1.571300	1.563300
C	-2.502000	-1.617300	-2.313600
C	-2.354800	0.725600	-2.808300
C	-2.726400	-2.543600	-1.134200
C	-2.701700	2.055900	-2.165400
C	-1.703400	-3.154700	0.963600
C	-2.321400	3.227800	-0.112200
C	-2.431600	-2.325300	2.012200
C	-1.713600	2.918000	1.244400
C	-2.413200	-0.204500	3.088800
C	-1.841900	1.189700	2.913800
H	-1.567000	-1.876400	-2.834400

H	-3.336800	-1.728600	-3.023400
H	-3.071000	0.540600	-3.624600
H	-1.344700	0.742800	-3.246500
H	-3.623700	-2.219600	-0.589900
H	-2.888400	-3.571400	-1.495100
H	-2.657000	2.853600	-2.923700
H	-3.729300	2.002000	-1.780900
H	-0.678700	-3.351100	1.289600
H	-2.223200	-4.117800	0.844800
H	-3.411100	3.110900	-0.044600
H	-2.102400	4.270600	-0.389700
H	-3.454000	-2.083200	1.685500
H	-2.508700	-2.917600	2.938700
H	-0.622400	3.053300	1.242700
H	-2.145600	3.611200	1.983800
H	-2.331800	-0.512200	4.143000
H	-3.477500	-0.188600	2.813500
H	-2.365700	1.876200	3.598000
H	-0.771000	1.211500	3.169000

Appendix 4.5. Geometry coordinates of 15-5 Crown Ether, Barium, and Nitrate optimized structure

Element	(X, Y, and Z coordinates)		
O	0.498710	2.444829	0.346501
O	2.407321	0.858152	-1.140559
O	-0.890977	0.657103	1.973853
O	2.019017	-1.606939	0.015291
O	-0.375139	-1.964382	1.259420
C	1.917142	2.467986	0.602132
C	-0.327340	2.882057	1.449914
C	2.618387	2.196782	-0.669072
C	-1.451449	1.947458	1.651787
C	3.495584	-0.048198	-0.875126
C	-1.883751	-0.375084	2.173128
C	2.997155	-1.426425	-1.021232
C	-1.163596	-1.637487	2.421066
C	1.511918	-2.932950	0.253816
C	0.733785	-2.840962	1.502208
H	2.101027	1.725985	1.365939
H	2.133483	3.487576	0.878765
H	-0.726770	3.828934	1.132979
H	0.286457	2.892626	2.335192
H	2.179576	2.828258	-1.427432
H	3.672546	2.371745	-0.548610
H	-1.952810	2.273089	2.545506
H	-2.146668	1.840544	0.808689
H	3.818907	0.106994	0.139489
H	4.205240	0.148445	-1.661553

H	-2.565061	-0.382047	1.310526
H	-2.373920	-0.122190	3.096163
H	2.529225	-1.553577	-1.987172
H	3.814045	-2.094988	-0.825221
H	-0.486508	-1.498412	3.246825
H	-1.888307	-2.425077	2.516978
H	2.353909	-3.573238	0.441703
H	0.876331	-3.240029	-0.564719
H	0.330431	-3.800285	1.770431
H	1.357404	-2.347829	2.231188
Ba	-0.082254	0.001057	-0.503341
N	-3.027298	-0.168336	-1.739530
O	-2.006943	-0.660832	-2.327976
O	-4.150380	-0.234346	-2.200832
O	-2.802638	0.413108	-0.597394

Appendix 4.6. Geometry coordinates of 15-5 Crown Ether, Barium, and 15-5 Crown Ether optimized structure

Element	(X, Y, and Z coordinates)		
O	-2.051510	-2.137849	0.479903
O	-1.439204	-1.290299	-2.175914
O	-1.850529	0.019578	2.118204
O	-1.906771	1.382239	-1.688447
O	-1.688792	2.399636	0.856937
C	-2.728500	-2.722875	-0.640780
C	-2.874203	-2.074052	1.654756
C	-1.820058	-2.642778	-1.858029
C	-2.165808	-1.246217	2.713018
C	-2.395883	-0.565201	-2.968199
C	-1.791952	1.193440	2.939839
C	-1.974731	0.890787	-3.033583
C	-2.362805	2.341600	2.123306
C	-1.894495	2.809028	-1.518102
C	-2.438601	3.117494	-0.135369
H	-3.677149	-2.193718	-0.808486
H	-2.960702	-3.777943	-0.436061
H	-3.066451	-3.085901	2.037850
H	-3.834322	-1.606188	1.397802
H	-0.884375	-3.171869	-1.660208
H	-2.310669	-3.110804	-2.720759
H	-2.835958	-1.113519	3.571288
H	-1.244607	-1.735549	3.053326
H	-3.392849	-0.638616	-2.517028
H	-2.432531	-0.987633	-3.981154

H	-0.752066	1.384161	3.238831
H	-2.393162	1.064383	3.847856
H	-1.000525	1.001393	-3.531413
H	-2.723352	1.452277	-3.607436
H	-3.432864	2.165816	1.952963
H	-2.245000	3.290145	2.665408
H	-2.543997	3.286231	-2.262950
H	-0.874044	3.191074	-1.643494
H	-2.382666	4.199008	0.050947
H	-3.490582	2.807863	-0.081631
Ba	-0.086228	0.004943	-0.027553
O	1.224231	-1.658205	1.908551
O	1.471168	-2.324724	-0.814225
O	2.051950	1.011242	1.799478
O	2.221479	0.147009	-1.972156
O	1.374016	2.420419	-0.569469
C	1.556152	-2.989789	1.476818
C	1.974536	-1.072627	2.984891
C	2.303489	-2.978917	0.154358
C	2.862928	0.059136	2.499662
C	2.026494	-2.233757	-2.136813
C	2.766947	2.204821	1.452205
C	2.955566	-1.042351	-2.289970
C	1.858882	3.084684	0.608629
C	3.032764	1.325051	-2.024717
C	2.146812	2.534159	-1.775029
H	0.606851	-3.522760	1.361445

H	2.152467	-3.504712	2.238683
H	2.587051	-1.830293	3.487047
H	1.247088	-0.689879	3.709556
H	3.265344	-2.457104	0.249972
H	2.499849	-4.012994	-0.162521
H	3.341453	0.534897	3.367658
H	3.653597	-0.310178	1.830269
H	1.170751	-2.126966	-2.809539
H	2.557226	-3.159758	-2.392506
H	3.686525	1.938975	0.912794
H	3.053055	2.749456	2.363483
H	3.829489	-1.121469	-1.627224
H	3.319602	-0.997227	-3.326179
H	0.964185	3.354053	1.178002
H	2.385026	4.008156	0.336882
H	3.495616	1.423759	-3.017420
H	3.838567	1.248151	-1.281222
H	2.757203	3.445166	-1.755431
H	1.422186	2.631086	-2.590673

Appendix 4.7. Geometry coordinates of 15-5 Crown Ether, Lead, and Nitrate optimized structure.

Element	(X, Y, and Z coordinates)		
O	-1.740927	0.362579	1.030866
O	-0.506503	2.417277	-0.437231
O	-0.304171	-1.903387	0.644663
O	1.974784	1.067106	-0.630733
O	1.849713	-1.709853	-0.993388
C	-1.754671	1.704244	1.549764
C	-1.733569	-0.652172	2.054151
C	-1.657072	2.682893	0.387555
C	-1.516165	-2.009634	1.410558
C	0.734722	3.001905	-0.000928
C	0.256246	-3.120583	0.119293
C	1.859332	2.471185	-0.869725
C	1.729977	-2.854959	-0.144454
C	2.954034	0.390109	-1.425269
C	3.102863	-1.024933	-0.896060
H	-0.919098	1.820853	2.253645
H	-2.694332	1.877235	2.090764
H	-2.693373	-0.639436	2.585718
H	-0.923605	-0.433672	2.762408
H	-2.520434	2.581254	-0.274212
H	-1.620709	3.710721	0.768209
H	-1.393912	-2.762171	2.199844
H	-2.350595	-2.291810	0.759577
H	0.926948	2.750739	1.049611
H	0.669386	4.092494	-0.104437

H	-0.282739	-3.418994	-0.789879
H	0.160537	-3.925509	0.858307
H	1.650984	2.667468	-1.932272
H	2.794613	2.981713	-0.600183
H	2.237439	-2.657085	0.808959
H	2.190491	-3.735062	-0.614398
H	3.924768	0.899428	-1.347983
H	2.649642	0.390928	-2.482994
H	3.872303	-1.552930	-1.476542
H	3.418568	-0.986564	0.155096
N	-3.473836	-0.522741	-1.805649
O	-4.654112	-0.704187	-1.988944
O	-2.925166	0.640793	-1.908323
O	-2.672325	-1.492759	-1.483111
Pb	-0.620027	-0.112469	-1.282288

Appendix 4.8. Geometry coordinates of 15-5 Crown Ether, Lead, and 15-5 Crown Ether optimized structure

Element	(X, Y, and Z coordinates)		
O	-2.346863	0.137746	1.855981
O	-1.701538	-2.220601	0.450292
O	-1.333020	2.421410	0.598369
O	-0.902348	-1.526949	-2.174737
O	-1.834595	1.127711	-1.896931
C	-3.211482	-0.996776	1.955801
C	-3.014971	1.383018	2.065381
C	-2.377114	-2.242699	1.718744
C	-2.000273	2.496734	1.865764
C	-2.477192	-2.668953	-0.667706
C	-1.928920	3.095610	-0.520960
C	-1.547586	-2.776376	-1.864059
C	-2.710312	2.165197	-1.435328
C	-1.402755	-0.768257	-3.288544
C	-2.432654	0.269386	-2.875337
H	-4.028653	-0.904304	1.224927
H	-3.659234	-1.048653	2.958809
H	-3.412946	1.434548	3.089235
H	-3.860389	1.473942	1.368546
H	-1.585246	-2.303266	2.468878
H	-3.005784	-3.138817	1.794822
H	-2.485509	3.473566	1.984734
H	-1.207652	2.414139	2.615820
H	-3.307530	-1.977174	-0.863290
H	-2.897229	-3.661801	-0.453817

H	-1.099199	3.539355	-1.077968
H	-2.587046	3.901040	-0.172478
H	-0.745309	-3.484979	-1.637649
H	-2.102171	-3.141600	-2.736330
H	-3.573296	1.715162	-0.925327
H	-3.081708	2.745065	-2.292210
H	-1.830079	-1.439209	-4.043056
H	-0.530665	-0.272903	-3.726335
H	-2.727394	0.855727	-3.757416
H	-3.336171	-0.198277	-2.458196
Pb	0.008779	-0.009602	-0.014542
O	0.884506	-1.340308	2.262698
O	1.695215	-2.271681	-0.268069
O	1.794974	1.293675	1.800880
O	2.385655	-0.026947	-1.822828
O	1.346881	2.365555	-0.804526
C	1.513653	-2.623458	2.082084
C	1.355736	-0.495162	3.325631
C	2.453969	-2.640180	0.889750
C	2.383738	0.517665	2.851684
C	2.384696	-2.392989	-1.523271
C	2.666451	2.308610	1.283141
C	3.237223	-1.176300	-1.836242
C	1.899792	3.143021	0.269461
C	3.072559	1.193169	-2.111486
C	2.062175	2.325932	-2.047527
H	0.703947	-3.340585	1.916730

H	2.055678	-2.910181	2.990475
H	1.774982	-1.102115	4.136650
H	0.471174	0.023434	3.708357
H	3.298789	-1.953386	1.033986
H	2.852486	-3.656730	0.763895
H	2.658473	1.172136	3.691153
H	3.297533	0.028474	2.484970
H	1.600507	-2.497626	-2.276932
H	3.003087	-3.299373	-1.527706
H	3.555171	1.836691	0.841939
H	2.996987	2.964566	2.101013
H	4.048516	-1.043620	-1.105318
H	3.692969	-1.300895	-2.828973
H	1.046314	3.618718	0.760198
H	2.556328	3.926694	-0.128132
H	3.508690	1.154157	-3.120245
H	3.892028	1.336514	-1.392840
H	2.560768	3.285390	-2.231968
H	1.297571	2.183479	-2.817450

Appendix Table 5.2 Summary of Optimized Energies and CCS for [M+Na]+ JH-III *m/z* 289.

JH-III $[M+Na]^+$ *m/z* 289			
Closed Epoxy			
Configuration	Starting Charge location	Energy (kcal/mol)	CCS (Å2)
2Z-6E-10R	Carbo	-635515.2695	197.87
2Z-6E-10S	Carbo	-635514.5874	198.49
2Z-6Z-10R	Carbo	-635516.239	185.40
2Z-6Z-10S	Carbo	-635514.1118	195.77
2E-6E-10R	Carbo	-635515.2921	205.99
2E-6E-10S	Carbo	-635514.8497	204.66
2E-6Z-10R	Carbo	-635516.6513	193.22
2E-6Z-10S	Carbo	-635514.2555	200.91
Opened Epoxy			
2E-6E-9E	Carbo	-635519.2523	198.71
2E-6E-9Z	Carbo	-635514.221	197.37
2E-6Z-9E	Carbo	-635521.5665	191.05
2E-6Z-9Z	Carbo	-635514.4306	184.63
2Z-6E-9E	Carbo	-635519.3791	199.20
2Z-6E-9Z	Carbo	-635513.7635	191.02
2Z-6Z-9E	Carbo	-635521.2459	182.44
2Z-6Z-9Z	Carbo	-635514.2040	185.63
Closed Epoxy			
Configuration	Starting Charge location	Energy (kcal/mol)	CCS (Å2)
2Z-6E-10R	Epoxy	-635532.5158	169.00
2Z-6E-10S	Epoxy	-635505.4127	195.12
2Z-6Z-10R	Epoxy	-635535.1237	173.45
2Z-6Z-10S	Epoxy	-635532.8277	170.65
2E-6E-10R	Epoxy	-635501.2856	200.10
2E-6E-10S	Epoxy	-635501.6339	204.99
2E-6Z-10R	Epoxy	-635529.7655	168.63
2E-6Z-10S	Epoxy	-635501.3791	203.47
Opened Epoxy			
2E-6E-9E	Epoxy	-635514.9721	183.08
2E-6E-9Z	Epoxy	-635512.4514	181.99
2E-6Z-9E	Epoxy	-635527.7374	171.40
2E-6Z-9Z	Epoxy	-635503.7116	194.51
2Z-6E-9E	Epoxy	-635514.3528	186.67

2Z-6E-9Z	Epoxy	-635510.9636	181.34
2Z-6Z-9E	Epoxy	-635540.162	172.01
2Z-6Z-9Z	Epoxy	-635510.8883	187.82

Appendix Table 5.2 Summary of Optimized Energies and CCS for [M+H]+ JH-III *m/z* 267.

JH-III $[M+H]^+$ *m/z* 267			
Closed Epoxy			
Configuration	Starting Charge location	Energy (kcal/mol)	CCS (Å2)
2Z-6E-10R	Carbo	-533978.0283	182.79
2Z-6E-10S	Carbo	-533977.4636	184.52
2Z-6Z-10R	Carbo	-533980.5114	168.51
2Z-6Z-10S	Carbo	-533976.9955	179.61
2E-6E-10R	Carbo	-533978.2555	187.39
2E-6E-10S	Carbo	-533977.8225	188.97
2E-6Z-10R	Carbo	-533981.0215	176.1
2E-6Z-10S	Carbo	-533977.1975	183.97
Opened Epoxy			
Configuration	Starting Charge location	Energy (kcal/mol)	CCS (Å2)
2E-6E-9E	Carbo	-533982.6995	185.36
2E-6E-9Z	Carbo	-533977.0639	177.44
2E-6Z-9E	Carbo	-533983.9388	173.43
2E-6Z-9Z	Carbo	-533982.9379	163.08
2Z-6E-9E	Carbo	-533982.3487	183.97
2Z-6E-9Z	Carbo	-533976.5123	177.01
2Z-6Z-9E	Carbo	-534000.6053	163.76
2Z-6Z-9Z	Carbo	-533995.0167	163.45
Closed Epoxy			
Configuration	Starting Charge location	Energy (kcal/mol)	CCS (Å2)
2Z-6E-10R	Epoxy	-533990.4391	160.55
2Z-6E-10S	Epoxy	-533965.0892	186.62
2Z-6Z-10R	Epoxy	-533992.4383	163.1
2Z-6Z-10S	Epoxy	-533989.7237	157.8
2E-6E-10R	Epoxy	-533961.5551	190.19
2E-6E-10S	Epoxy	-533961.3223	189.24
2E-6Z-10R	Epoxy	-533961.4039	182.6
2E-6Z-10S	Epoxy	-533961.1303	186.49
Opened Epoxy			
2E-6E-9E	Epoxy	-533982.6995	185.36
2E-6E-9Z	Epoxy	-533977.0639	177.44
2E-6Z-9E	Epoxy	-533983.9388	173.43

2E-6Z-9Z	Epoxy	-533982.9379	163.08
2Z-6E-9E	Epoxy	-533982.3487	183.97
2Z-6E-9Z	Epoxy	-533976.5123	177.01
2Z-6Z-9E	Epoxy	-534000.6053	163.76
2Z-6Z-9Z	Epoxy	-533995.0167	163.45

Appendix Table 5.3 Summary of Optimized Energies and CCS for $[M\text{-}H_2O+H]^+$ JH-III *m/z* 249.

JH-III $[M\text{-}H_2O+H]^+$ *m/z* 249		
Configuration	Energy (kcal/mol)	CCS (Å2)
2E-6E-8E	-486043.1011	167.51
2E-6E-8Z	-486035.7179	163.21
2E-6Z-8E	-486042.7836	175.60
2E-6Z-8Z	-486037.7209	174.34
2Z-6E-8E	-486042.9411	166.56
2Z-6E-8Z	-486037.6475	160.14
2Z-6Z-8E	-486042.7391	164.78
2Z-6Z-8Z	-486037.6839	172.02

Appendix Table 5.4. Geometry coordinates of JH-III $[M+Na]^+$ *m/z* 289 structures and optimized structures.

JH-III 2Z-6E-10R and sodium $[M+Na]^+$ located on carboxyl end

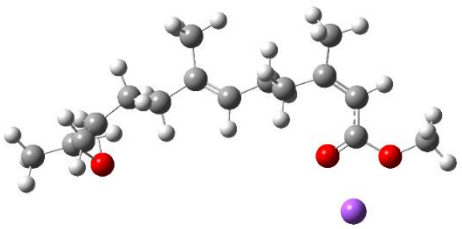

1 1

6	-1.600195	2.832768	-1.227975
6	-1.442216	1.332770	-1.153049
6	-0.276895	0.691629	-0.947405
6	1.097051	1.272494	-0.751137
6	1.625782	1.000024	0.696031
6	3.047888	1.452963	0.866642
6	4.157050	0.702274	0.590171
6	4.137494	-0.663028	0.120180
8	3.147724	-1.333816	-0.197835
8	5.326889	-1.351086	-0.015050
6	6.613941	-0.777075	0.330350
6	3.232837	2.858768	1.360273
6	-2.714060	0.527808	-1.341605
6	-3.756346	0.706522	-0.213649
6	-4.927334	-0.229414	-0.416739
6	-5.687598	-0.932216	0.640281
8	-4.695346	-1.630603	-0.157046
6	-7.116739	-1.349500	0.351185
6	-5.355928	-0.793056	2.112338
1	-2.100226	3.118323	-2.163431
1	-0.651934	3.374337	-1.180447
1	-2.233137	3.203433	-0.410973
1	-0.305509	-0.399083	-0.913115
1	1.115878	2.348986	-0.948106

1	1.792051	0.806090	-1.461409
1	1.528908	-0.068365	0.899680
1	0.988001	1.544132	1.401366
1	5.127571	1.158404	0.744265
1	7.340042	-1.570981	0.156887
1	6.629819	-0.484984	1.382723
1	6.835625	0.073800	-0.317750
1	4.277117	3.182553	1.357642
1	2.842098	2.944639	2.383301
1	2.645279	3.556931	0.749819
1	-2.468246	-0.537563	-1.412320
1	-3.179709	0.810223	-2.298328
1	-4.133305	1.738353	-0.196367
1	-3.277348	0.516168	0.752263
1	-5.463212	-0.057869	-1.355954
1	-7.336474	-2.311609	0.830097
1	-7.285085	-1.458203	-0.724614
1	-7.825405	-0.609050	0.742478
1	-5.571330	-1.735010	2.631407
1	-5.970527	-0.010142	2.573562
1	-4.303656	-0.552198	2.279501
11	4.049109	-3.259968	-0.785280

JH-III 2Z-6E-10S and sodium $[M+Na]^+$ located on carboxyl end

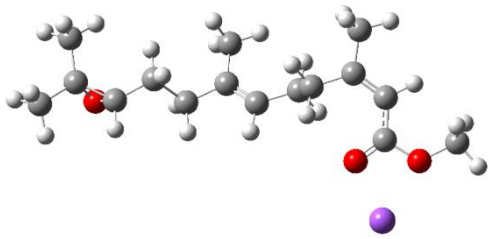

1 1

C	-1.068275	-2.324314	2.055207
C	0.050715	-1.538152	2.628830
C	1.328822	-1.737902	2.268750
C	1.751918	-2.762617	1.285347
C	3.154960	-2.495709	0.769737
C	3.624712	-3.553417	-0.168262
C	4.812197	-4.175427	-0.064178
C	5.790041	-3.962232	1.004911
O	5.590366	-3.797981	2.210602
O	7.136213	-3.961037	0.709919
C	7.516837	-4.083508	-0.653498
C	2.707592	-3.879243	-1.291128
C	-0.314324	-0.515094	3.649855
C	-1.095871	0.631995	3.035950
C	-1.541926	1.608627	4.082645
C	-2.224867	2.892057	3.725043
O	-2.961951	1.764096	4.243787
C	-2.510346	3.244973	2.299325
C	-2.129370	4.064851	4.650993
H	-2.013696	-2.165263	2.629459
H	-0.826691	-3.416942	2.068095
H	-1.247681	-2.021539	0.992425
H	2.138485	-1.140458	2.719538
H	1.028982	-2.788680	0.424348
H	1.718900	-3.775448	1.773976

H	3.856307	-2.407113	1.644525
H	3.169158	-1.511522	0.225430
H	5.108120	-4.937003	-0.806398
H	8.614224	-3.860743	-0.647346
H	6.970028	-3.348391	-1.291833
H	7.333006	-5.126037	-1.011558
H	3.225157	-4.453340	-2.098021
H	2.286879	-2.942247	-1.733578
H	1.857019	-4.499376	-0.908502
H	0.608203	-0.111931	4.147444
H	-0.936261	-1.003209	4.448878
H	-1.988982	0.227900	2.487685
H	-0.454276	1.169854	2.288632
H	-0.992556	1.545844	5.045212
H	-3.415804	3.896785	2.241047
H	-2.695534	2.326173	1.691597
H	-1.639508	3.796230	1.869295
H	-3.080096	4.651043	4.624917
H	-1.287898	4.725858	4.332014
H	-1.951543	3.728796	5.701105
Na	7.900050	-4.201476	3.078197

JH-III 2Z-6Z-10R and sodium $[M+Na]^+$ located on carboxyl end

1 1

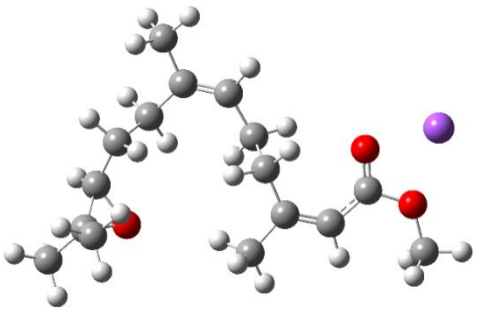

C	-2.077378	4.013020	0.246277
C	-1.517221	2.701625	-0.252335
C	-0.212854	2.405011	-0.094816
C	0.500057	1.150355	-0.527428
C	0.825737	0.215892	0.685733
C	1.367411	-1.104553	0.216960
C	2.677346	-1.370634	-0.077591
C	3.767572	-0.439398	0.068957
O	3.708769	0.748585	0.410938
O	5.059120	-0.864808	-0.189601
C	5.377072	-2.222354	-0.589249
C	0.350460	-2.193758	0.042344
C	-2.515400	1.768872	-0.906106
C	-3.443926	1.049534	0.108888
C	-4.064568	-0.177442	-0.519021
C	-4.410892	-1.438490	0.171097
O	-3.204082	-1.337822	-0.638066
C	-5.482522	-2.325297	-0.431998
C	-4.184737	-1.641199	1.655481
H	-2.514818	4.589450	-0.580546
H	-1.310305	4.631481	0.723428
H	-2.882949	3.852237	0.975501
H	0.415906	3.136910	0.415690
H	1.447196	1.410886	-1.015128
H	-0.091172	0.589356	-1.257043

H	-0.101691	0.037432	1.239314
H	1.531112	0.728916	1.343471
H	2.919860	-2.364395	-0.434505
H	C.461482	-2.245284	-0.697064
H	4.906246	-2.456479	-1.546792
H	5.067290	-2.928628	0.184339
H	0.748350	-3.074273	-0.469537
H	-0.534263	-1.827398	-0.494252
H	-0.016309	-2.503308	1.031800
H	-1.999945	1.004219	-1.494087
H	-3.135799	2.335710	-1.614428
H	-4.238598	1.726754	0.449522
H	-2.865345	0.761173	0.991939
H	-4.618762	0.029368	-1.439512
H	-5.234321	-3.382722	-0.278730
H	-5.579925	-2.149498	-1.507622
H	-C.453624	-2.135895	0.041552
H	-3.937794	-2.691284	1.855182
H	-5.095991	-1.402511	2.217396
H	-3.371043	-1.022053	2.040246
Na	5.839802	1.330463	0.351867

JH-III 2Z-6Z-10S and sodium [M+Na]$^+$ located on carboxyl end

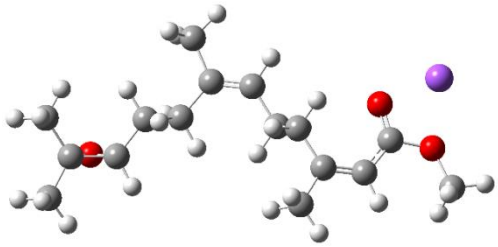

1 1

C	-1.940681	3.162318	0.373660
C	-1.356875	1.830354	-0.043874
C	-0.035118	1.607952	0.087915
C	0.755697	0.382734	-0.285783
C	1.472412	-0.232042	0.960492
C	2.285262	-1.440790	0.593387
C	3.579481	-1.427017	0.152540
C	4.394663	-0.244292	0.004954
O	4.048457	0.932983	0.159913
O	5.721757	-0.378401	-0.353779
C	6.359285	-1.666163	-0.556328
C	1.578254	-2.760789	0.708586
C	-2.345867	0.842032	-0.627270
C	-3.424804	0.361439	0.371920
C	-4.356423	-0.638140	-0.277506
C	-5.825257	-0.715704	-0.103750
O	-5.240711	-0.138467	-1.299643
C	-6.595468	0.251751	0.772010
C	-6.513979	-2.047369	-0.333277
H	-2.488603	3.625548	-0.457988
H	-1.164585	3.860889	0.702583
H	-2.658197	3.049835	1.196597
H	0.569761	2.413573	0.509747
H	1.527370	0.653035	-1.018902
H	0.124416	-0.378428	-0.754158

H	0.707610	-0.524081	1.688554
H	2.099100	0.540383	1.412079
H	4.037971	-2.376868	-0.095305
H	7.401093	-1.439776	-0.782629
H	5.903043	-2.186390	-1.401675
H	6.300371	-2.266389	0.354340
H	2.162181	-3.598041	0.317194
H	0.615672	-2.723345	0.182332
H	1.341778	-2.960874	1.762799
H	-1.832702	-0.033925	-1.039364
H	-2.863390	1.317741	-1.472147
H	-3.991969	1.216470	0.748617
H	-2.942865	-0.115064	1.238389
H	-3.860713	-1.570418	-0.569741
H	-7.595005	0.415193	0.351370
H	-6.104047	1.224397	0.846599
H	-6.721229	-0.156938	1.782438
H	-7.494146	-1.892816	-0.800335
H	-6.673281	-2.572194	0.617015
H	-5.921051	-2.689548	-0.992050
Na	5.918354	2.021953	-0.287667

JH-III 2E-6E-10R and sodium $[M+Na]^+$ located on carboxyl end

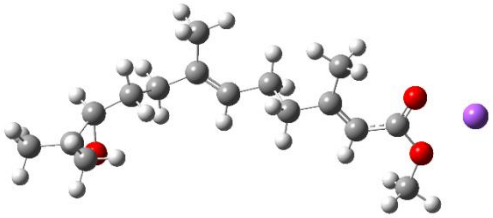

1 1

C	-1.918962	2.830971	-0.166418
C	-1.936262	1.443597	-0.763918
C	-0.842701	0.700446	-1.015756
C	0.602459	1.046135	-0.770913
C	1.235314	0.102624	0.301100
C	2.698852	0.372541	0.507770
C	3.608249	-0.530933	0.031439
C	5.037754	-0.379437	0.139040
O	5.651194	0.564825	0.652691
O	5.868321	-1.363352	-0.361644
C	5.367078	-2.560076	-1.011574
C	3.060162	1.651273	1.210627
C	-3.308295	0.895928	-1.107031
C	-4.224537	0.661039	0.116216
C	-5.527184	0.018507	-0.305720
C	-6.286709	-1.007529	0.443131
O	-5.473744	-1.367572	-0.703638
C	-7.779869	-1.123715	0.203465
C	-5.814881	-1.563637	1.771601
H	-2.476711	3.528377	-0.805819
H	-0.912951	3.237172	-0.033259
H	-2.413473	2.844268	0.813640
H	-0.998685	-0.285264	-1.458064
H	0.722529	2.087970	-0.459461
H	1.170217	0.927213	-1.704999

H	1.071672	-0.938156	0.000134
H	0.704519	0.259452	1.249339
H	3.230957	-1.423066	-0.453760
H	6.253284	-3.129953	-1.290303
H	4.800815	-2.296177	-1.907692
H	4.756756	-3.142062	-0.317274
H	3.643466	2.311408	0.557812
H	3.696100	1.454984	2.080870
H	2.164607	2.183698	1.539263
H	-3.202408	-0.053474	-1.643802
H	-3.811519	1.594109	-1.793654
H	-4.452421	1.613203	0.615269
H	-3.702065	0.028182	0.841066
H	-6.111027	0.633628	-0.998089
H	-8.092292	-2.174175	0.249486
H	-8.051915	-0.730015	-0.780722
H	-8.340817	-0.571512	0.967781
H	-6.116059	-2.614615	1.860753
H	-6.271535	-1.014138	2.604363
H	-4.728446	-1.517554	1.876843
Na	7.752585	-0.075556	0.381149

JH-III 2E-6E-10S and sodium $[M+Na]^+$ located on carboxyl end

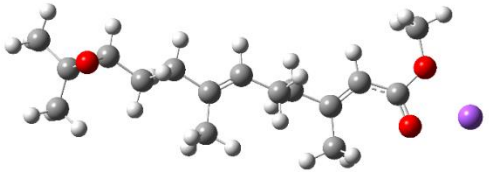

1 1

C	-1.960674	-2.025451	0.879278
C	-1.870457	-0.518114	0.942834
C	-0.719687	0.180217	0.962470
C	0.691320	-0.344585	0.923004
C	1.423446	0.084866	-0.388658
C	2.845319	-0.398964	-0.428199
C	3.855578	0.504828	-0.246857
C	5.256263	0.164001	-0.227772
O	5.750702	-0.963326	-0.355701
O	6.199582	1.157845	-0.052630
C	5.847379	2.555469	0.114127
C	3.053408	-1.873021	-0.638025
C	-3.198076	0.210930	1.017798
C	-4.094502	0.040115	-0.229889
C	-5.388102	0.808906	-0.074056
C	-6.731657	0.369699	-0.514876
O	-6.340732	0.298350	0.880137
C	-6.973306	-0.966154	-1.188539
C	-7.779923	1.425420	-0.810133
H	-2.630566	-2.400150	1.664067
H	-0.996237	-2.525600	1.000053
H	-2.386211	-2.356878	-0.077010
H	-0.792393	1.268064	1.020244
H	0.718427	-1.434307	1.015943
H	1.258040	0.060030	1.773925

H	1.380918	1.176013	-0.479867
H	0.876177	-0.340526	-1.239844
H	3.588012	1.546086	-0.112435
H	6.795712	3.081324	0.223412
H	5.244560	2.689834	1.015166
H	5.321198	2.922388	-0.770065
H	3.720316	-2.058705	-1.486961
H	2.102799	-2.381099	-0.815971
H	3.541317	-2.331690	0.230251
H	-3.019060	1.280676	1.185937
H	-3.761145	-0.155010	1.888093
H	-4.305809	-1.019523	-0.398764
H	-3.564933	0.414748	-1.118303
H	-5.243346	1.890873	0.012542
H	-7.967607	-1.341940	-0.918327
H	-6.240911	-1.719146	-0.888682
H	-6.941789	-0.860129	-2.280246
H	-8.771395	1.074471	-0.499006
H	-7.821815	1.643066	-1.884763
H	-7.564457	2.354896	-0.274074
Na	7.913254	-0.520882	-0.192255

JH-III 2E-6Z-10R and sodium [M+Na]$^+$ located on carboxyl end

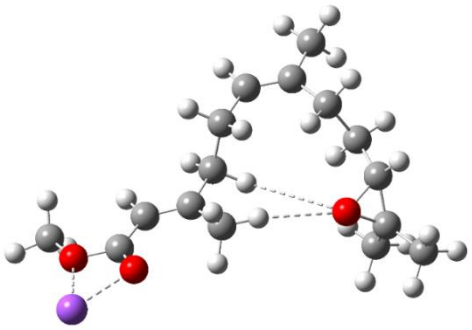

1 1

C	-3.690092	3.600396	0.140367
C	-2.649345	2.620141	-0.346649
C	-1.335515	2.891949	-0.230325
C	-0.182878	2.020024	-0.663467
C	0.388344	1.172055	0.519825
C	1.482438	0.246317	0.067953
C	2.775077	0.538705	0.410417
C	3.920356	-0.233257	0.001539
O	3.930683	-1.220621	-0.744483
O	5.179599	0.119063	0.455224
C	5.404894	1.229899	1.359248
C	1.062675	-0.931466	-0.765285
C	-3.182706	1.333993	-0.940695
C	-3.767347	0.362321	0.120971
C	-3.788121	-1.053152	-0.407610
C	-3.590615	-2.287727	0.382121
O	-2.512952	-1.743851	-0.433553
C	-4.166222	-3.586669	-0.147249
C	-3.349490	-2.267481	1.877746
H	-4.352599	3.905331	-0.681469
H	-3.236584	4.502185	0.563790
H	-4.332572	3.152339	0.910568
H	-1.051129	3.835130	0.238477
H	0.626663	2.650097	-1.054741
H	-0.476017	1.346248	-1.474454

H	-0.431634	0.572208	0.931975
H	0.741176	1.847409	1.307487
H	2.951220	1.409960	1.030184
H	6.477732	1.233576	1.551906
H	4.861868	1.075135	2.294402
H	5.112149	2.170195	0.886166
H	1.358705	-0.782954	-1.812784
H	-0.019760	-1.080025	-0.726960
H	1.565320	-1.848222	-0.443615
H	-2.392553	0.807558	-1.483660
H	-3.964030	1.566746	-1.677840
H	-4.786879	0.663248	0.396149
H	-3.162140	0.408059	1.031759
H	-4.345946	-1.169559	-1.341469
H	-3.502756	-4.426022	0.094880
H	-4.288372	-3.549430	-1.233979
H	-5.144009	-3.789675	0.306499
H	-2.688506	-3.096404	2.159691
H	-4.294676	-2.397630	2.418785
H	-2.886528	-1.336568	2.212909
Na	6.081317	-1.712905	-0.808690

JH-III 2E-6Z-10S and sodium [M+Na]$^+$ located on carboxyl end

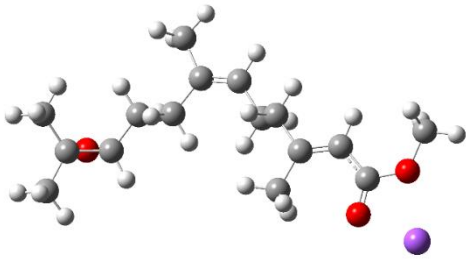

1 1

C	-2.905505	3.416889	-0.078541
C	-2.027684	2.224776	-0.388934
C	-0.689135	2.332395	-0.289954
C	0.356859	1.286930	-0.575073
C	1.199579	0.962944	0.699219
C	2.281816	-0.042136	0.423604
C	3.581261	0.381936	0.384908
C	4.705977	-0.471621	0.092265
O	4.673429	-1.678693	-0.179216
O	5.983078	0.053523	0.098688
C	6.257668	1.446112	0.400590
C	1.844292	-1.459203	0.177947
C	-2.764677	0.975223	-0.827436
C	-3.539566	0.272445	0.313053
C	-4.258985	-0.957090	-0.196589
C	-5.616584	-1.408248	0.187013
O	-5.377131	-0.742076	-1.079077
C	-6.484423	-0.644578	1.166530
C	-5.956347	-2.880603	0.054918
H	-3.511775	3.689569	-0.952918
H	-2.316827	4.291921	0.214510
H	-3.610235	3.198978	0.734141
H	-0.283938	3.296016	0.025309
H	1.045457	1.656248	-1.349273
H	-0.089649	0.366645	-0.962692

H	0.522537	0.560375	1.463990
H	1.624848	1.893391	1.091668
H	3.781071	1.427163	0.588268
H	7.340927	1.547324	0.336933
H	5.922371	1.688115	1.411636
H	5.781805	2.095186	-0.338084
H	2.085841	-1.776049	-0.843790
H	0.768547	-1.569097	0.333584
H	2.372640	-2.154988	0.838435
H	-2.081193	0.252388	-1.287389
H	-3.490620	1.246633	-1.605673
H	-4.251167	0.969352	0.763714
H	-2.839329	-0.030693	1.105420
H	-3.581740	-1.738273	-0.559581
H	-7.539427	-0.752574	0.887145
H	-6.252748	0.422740	1.180880
H	-6.365367	-1.043778	2.181600
H	-6.997850	-3.002935	-0.266219
H	-5.838530	-3.395518	1.016655
H	-5.313433	-3.368718	-0.684297
Na	6.815953	-2.131679	-0.482568

JH-III 2E-6E-9E and sodium $[M+Na]^+$ located on carboxyl end

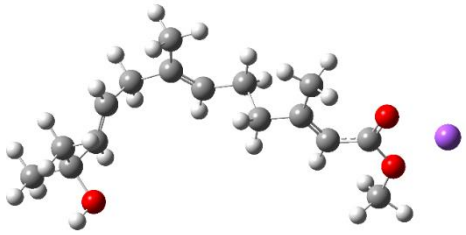

1 1

C	-2.062203	3.001199	0.304695
C	-2.047581	1.935276	-0.763743
C	-0.945875	1.320607	-1.228754
C	0.481289	1.508126	-0.785993
C	0.973320	0.275655	0.039953
C	2.417435	0.387671	0.437268
C	3.329208	-0.443807	-0.152683
C	4.745440	-0.420010	0.114241
O	5.352042	0.362132	0.857482
O	5.570914	-1.344362	-0.496818
C	5.071826	-2.372508	-1.390796
C	2.761908	1.439951	1.453814
C	-3.412650	1.555882	-1.324811
C	-4.263333	0.783356	-0.339100
C	-4.619480	-0.493141	-0.509338
C	-5.473714	-1.343860	0.407736
O	-4.692711	-2.552220	0.581777
C	-6.796029	-1.690868	-0.302997
C	-5.743475	-0.710007	1.778103
H	-2.641278	2.672715	1.177817
H	-2.550719	3.910846	-0.070099
H	-1.065810	3.281050	0.656813
H	-1.080999	0.564317	-2.003892
H	0.604482	2.419932	-0.193982
H	1.130062	1.612072	-1.666812

H	0.799907	-0.635848	-0.542436
H	0.356668	0.207855	0.945792
H	2.963329	-1.175038	-0.863390
H	5.947543	-2.952612	-1.681422
H	4.619397	-1.918781	-2.275599
H	4.358521	-3.014856	-0.869548
H	3.378372	1.029937	2.259784
H	1.858398	1.880627	1.881876
H	3.357896	2.241259	0.998998
H	-3.283880	0.960155	-2.235354
H	-3.942990	2.476197	-1.616001
H	-4.585836	1.323544	0.550088
H	-4.290540	-1.025024	-1.403825
H	-5.249889	-3.215935	1.020669
H	-7.391388	-2.383750	0.307340
H	-6.600072	-2.167416	-1.269481
H	-7.398104	-0.791660	-0.473652
H	-6.320463	-1.403054	2.402581
H	-6.326445	0.213879	1.690736
H	-4.803329	-0.490480	2.293979
Na	7.438064	-0.340500	0.637630

JH-III 2E-6E-9Z and sodium $[M+Na]^+$ located on carboxyl end

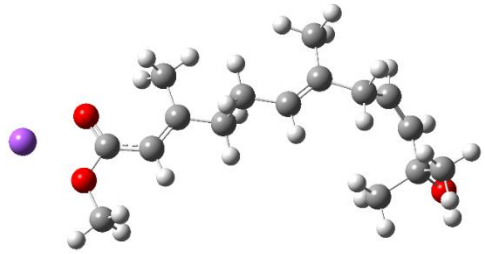

1 1

C	2.022062	3.109143	0.080810
C	2.176827	1.722480	0.658524
C	1.156093	0.915570	0.999764
C	-0.320965	1.180122	0.865246
C	-0.947064	0.319215	-0.278773
C	-2.426877	0.538205	-0.417756
C	-3.281124	-0.462372	-0.044169
C	-4.718488	-0.365867	-0.101894
O	-5.390916	0.611948	-0.451079
O	-5.487508	-1.457028	0.259787
C	-4.911297	-2.718192	0.686984
C	-2.867137	1.875348	-0.945289
C	3.613406	1.259145	0.871961
C	4.402912	1.130037	-0.413910
C	5.098915	0.086950	-0.887585
C	5.332361	-1.299962	-0.304061
O	6.155205	-1.940874	-1.304880
C	4.028763	-2.108012	-0.159173
C	6.115299	-1.244320	1.020459
H	2.617640	3.831596	0.654499
H	0.988156	3.463564	0.075062
H	2.390301	3.150528	-0.952348
H	1.401243	-0.065066	1.411005
H	-0.524109	2.238652	0.678252
H	-0.828809	0.921281	1.804787

H	-0.726065	-0.737713	-0.093158
H	-0.455663	0.598363	-1.220084
H	-2.851846	-1.390593	0.313233
H	-5.760657	-3.372084	0.884180
H	-4.331924	-2.579613	1.602663
H	-4.294823	-3.142513	-0.108707
H	-3.566042	1.761576	-1.780298
H	-2.010477	2.467816	-1.275052
H	-3.408709	2.441151	-0.177190
H	3.613827	0.321869	1.432842
H	4.118873	2.003849	1.509379
H	4.424307	2.031740	-1.025654
H	5.614598	0.221300	-1.837031
H	6.420974	-2.815000	-0.976844
H	4.252872	-3.129027	0.177893
H	3.517514	-2.167245	-1.125152
H	3.346648	-1.658673	0.569741
H	7.058783	-0.708940	0.876745
H	6.342392	-2.260223	1.371923
H	5.548666	-0.739488	1.809565
Na	-7.450367	-0.184039	-0.219791

JH-III 2E-6Z-9E and sodium $[M+Na]^+$ located on carboxyl end

1 1

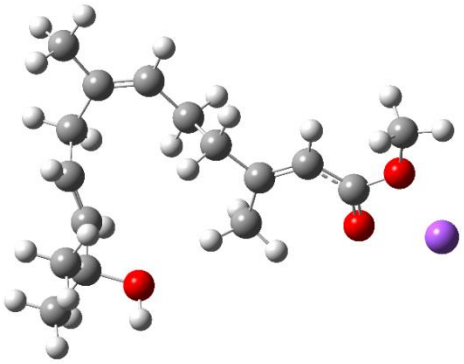

C	-3.782058	3.674045	0.259893
C	-2.863886	2.632440	-0.331759
C	-1.528275	2.742530	-0.225022
C	-0.488166	1.783651	-0.741313
C	0.239664	1.058423	0.433214
C	1.388911	0.199960	-0.023819
C	2.655350	0.565411	0.346221
C	3.872535	-0.110987	-0.028349
O	4.009723	-1.059467	-0.810641
O	5.073953	0.317934	0.513292
C	5.162768	1.384867	1.490985
C	1.035509	-0.989462	-0.863553
C	-3.558805	1.462325	-1.024228
C	-3.635580	0.239387	-0.138171
C	-3.171527	-0.966116	-0.481048
C	-3.193887	-2.233476	0.345454
O	-1.792072	-2.632080	0.405013
C	-3.992097	-3.319910	-0.396676
C	-3.722423	-2.046568	1.771727
H	-4.385182	4.152761	-0.524016
H	-3.230145	4.455867	0.791303
H	-4.492966	3.219901	0.964699
H	-1.130555	3.612693	0.300717
H	0.260916	2.336425	-1.326884
H	-0.931557	1.037377	-1.405867

H	-0.495944	0.421229	0.939935
H	0.585770	1.807903	1.154170
H	2.757235	1.440201	0.977299
H	6.217657	1.444181	1.759339
H	4.569226	1.141298	2.375024
H	4.841084	2.331774	1.050999
H	1.832418	-1.730389	-0.908466
H	0.841686	-0.656996	-1.894718
H	0.108835	-1.448245	-0.499180
H	-3.055320	1.201815	-1.962725
H	-4.575949	1.775743	-1.298029
H	-4.092095	0.392358	0.839470
H	-2.718741	-1.100361	-1.465644
H	-1.748158	-3.528820	0.776695
H	-3.947261	-4.273648	0.146460
H	-3.587644	-3.477568	-1.402320
H	-5.046122	-3.036159	-0.487877
H	-3.656404	-2.993690	2.320918
H	-4.773839	-1.738534	1.774733
H	-3.133221	-1.299498	2.312796
Na	6.195023	-1.359804	-0.775590

JH-III 2E-6Z-9Z and sodium $[M+Na]^+$ located on carboxyl end

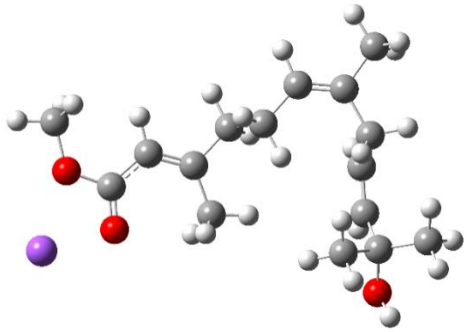

1 1

C	3.562340	3.779645	0.019033
C	2.695356	2.563234	0.235167
C	1.360688	2.677493	0.345568
C	0.367484	1.564751	0.552711
C	-0.614488	1.460063	-0.656584
C	-1.630484	0.366563	-0.485350
C	-2.933009	0.708421	-0.244884
C	-3.998226	-0.242404	-0.049412
O	-3.905785	-1.476510	-0.050747
O	-5.287331	0.208532	0.164104
C	-5.629718	1.617688	0.200459
C	-1.125061	-1.045290	-0.581432
C	3.440957	1.232774	0.309751
C	3.192771	0.331304	-0.886080
C	3.285522	-1.003933	-0.976923
C	3.678471	-2.039417	0.069869
O	3.644052	-3.280747	-0.670197
C	2.667855	-2.141491	1.228260
C	5.104968	-1.802542	0.595638
H	4.283676	3.896608	0.839764
H	2.973594	4.699780	-0.051014
H	4.153420	3.679713	-0.902251
H	0.926256	3.676256	0.274233
H	-0.226062	1.758033	1.458314
H	0.873889	0.606146	0.696098

H	-0.020363	1.250114	-1.555411
H	-1.106893	2.428167	-0.802468
H	-3.183849	1.761776	-0.207633
H	-6.704813	1.649550	0.376714
H	-5.398114	2.089682	-0.757088
H	-5.106199	2.114330	1.020621
H	-1.675076	-1.605401	-1.346008
H	-1.286265	-1.588517	0.357230
H	-0.060135	-1.065186	-0.823249
H	3.194253	0.715984	1.243883
H	4.516769	1.449254	0.369373
H	2.939418	0.863044	-1.803967
H	3.099128	-1.454509	-1.950663
H	4.011901	-3.986220	-0.113907
H	2.952857	-2.958714	1.903565
H	1.668382	-2.356898	0.837210
H	2.624782	-1.224775	1.825700
H	5.397588	-2.608403	1.282455
H	5.181564	-0.858432	1.144655
H	5.816254	-1.780008	-0.235668
Na	-6.000547	-2.083884	0.301770

JH-III 2Z-6E-9E and sodium $[M+Na]^+$ located on carboxyl end

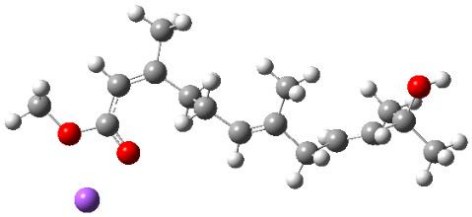

1 1

C	1.850395	1.077185	1.953298
C	1.429453	-0.204271	1.276926
C	0.182683	-0.490692	0.859495
C	-1.050301	0.367332	0.957231
C	-1.583386	0.760057	-0.459696
C	-2.812767	1.618740	-0.372252
C	-4.098717	1.163634	-0.273668
C	-4.490805	-0.225529	-0.278503
O	-3.751371	-1.217189	-0.290043
O	-5.834004	-0.549496	-0.265001
C	-6.887639	0.447992	-0.280102
C	-2.571878	3.101098	-0.369531
C	2.547071	-1.223593	1.090187
C	3.579606	-0.786197	0.074394
C	4.857333	-0.522552	0.362819
C	5.950510	-0.088759	-0.592057
O	6.483139	1.109136	0.021265
C	5.453630	0.238993	-2.005662
C	7.046030	-1.171399	-0.635975
H	2.193284	0.870891	2.976847
H	1.053940	1.823188	2.014143
H	2.700606	1.528227	1.427796
H	0.017582	-1.462595	0.389272
H	-0.860949	1.274535	1.538802
H	-1.843853	-0.185322	1.476822

H	-1.782633	-0.156973	-1.018796
H	-0.795860	1.317311	-0.978759
H	-4.889705	1.900179	-0.197949
H	-7.819425	-0.117083	-0.298355
H	-6.812413	1.066436	-1.177318
H	-6.844953	1.059034	0.624453
H	-3.477384	3.684706	-0.183664
H	-2.149896	3.407010	-1.336810
H	-1.819948	3.362842	0.386148
H	2.110047	-2.182138	0.778392
H	3.044139	-1.396358	2.055193
H	3.213344	-0.680633	-0.947037
H	5.201968	-0.619712	1.393783
H	7.305001	1.351796	-0.436256
H	6.289955	0.591653	-2.621451
H	4.698259	1.030663	-1.976227
H	5.029137	-0.641650	-2.501485
H	7.890385	-0.839639	-1.255428
H	6.661897	-2.104054	-1.064028
H	7.421942	-1.379612	0.371440
Na	-5.211261	-2.874048	-0.273702

JH-III 2Z-6E-9Z and sodium $[M+Na]^+$ located on carboxyl end

1 1

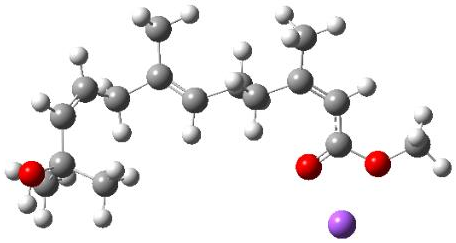

C	-1.764323	3.054493	-1.130215
C	-1.726309	1.544797	-1.116322
C	-0.613299	0.805522	-0.959862
C	0.799016	1.280261	-0.745327
C	1.302253	0.915351	0.690231
C	2.700084	1.409591	0.931485
C	3.850160	0.734618	0.628777
C	3.912607	-0.589837	0.058225
O	2.968972	-1.290401	-0.327683
O	5.142990	-1.197153	-0.105674
C	6.390845	-0.579435	0.303267
C	2.808111	2.778568	1.539528
C	-3.070511	0.854575	-1.321883
C	-4.075951	1.148136	-0.228058
C	-4.775448	0.301524	0.540657
C	-4.798179	-1.220626	0.577058
O	-5.752670	-1.509030	1.622856
C	-3.437830	-1.818986	0.983620
C	-5.311520	-1.823753	-0.743152
H	-2.302366	3.415774	-2.016691
H	-0.772443	3.513112	-1.136290
H	-2.302689	3.444558	-0.256904
H	-0.721927	-0.280747	-0.969414
H	0.887706	2.360398	-0.896792
H	1.466572	0.799087	-1.471629

H	1.239300	-0.168297	0.811791
H	0.628944	1.383214	1.416781
H	4.792670	1.223664	0.843933
H	7.163286	-1.315586	0.081278
H	6.377230	-0.368931	1.374973
H	6.571229	0.329874	-0.274696
H	3.834808	3.151714	1.582069
H	2.398682	2.761196	2.559020
H	2.193809	3.493966	0.977721
H	-2.912010	-0.219975	-1.438265
H	-3.492493	1.212306	-2.276094
H	-4.271477	2.208015	-0.066796
H	-5.466615	0.736525	1.260614
H	-5.889124	-2.469155	1.665774
H	-3.518216	-2.910415	1.079651
H	-3.123916	-1.409220	1.948688
H	-2.659583	-1.603135	0.244587
H	-5.393961	-2.916057	-0.656791
H	-4.640311	-1.606318	-1.580304
H	-6.300593	-1.420373	-0.980488
Na	4.018265	-3.103757	-1.035444

JH-III 2Z-6Z-9E and sodium $[M+Na]^+$ located on carboxyl end

1 1

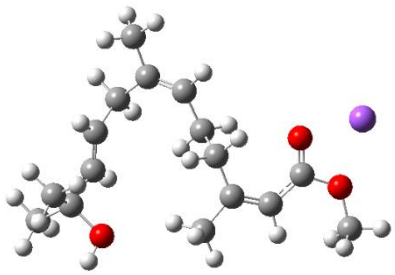

C	-1.981140	4.167011	0.397111
C	-1.505028	2.837908	-0.137374
C	-0.287921	2.359811	0.173466
C	0.314289	1.049651	-0.260609
C	0.773396	0.214316	0.975744
C	1.306436	-1.133210	0.575545
C	2.579244	-1.384890	0.136789
C	3.635895	-0.410593	0.043920
O	3.571393	0.803293	0.277594
O	4.901187	-0.819944	-0.343046
C	5.222895	-2.199570	-0.652181
C	0.337135	-2.271730	0.666989
C	-2.499287	2.095918	-1.028976
C	-3.242388	1.000460	-0.297863
C	-3.321046	-0.263495	-0.725316
C	-4.052618	-1.416737	-0.072876
O	-3.027160	-2.441763	0.066355
C	-5.150563	-1.931068	-1.021155
C	-4.632787	-1.094264	1.308543
H	-2.187380	4.868230	-0.423414
H	-1.248375	4.629293	1.066482
H	-2.923272	4.053603	0.952012
H	0.349814	2.967490	0.819071
H	1.192874	1.228900	-0.894372
H	-0.398811	0.463220	-0.846205

H	-0.090950	0.071440	1.632466
H	1.530262	0.788426	1.517410
H	2.820357	-2.403844	-0.141147
H	6.284469	-2.200529	-0.899691
H	4.643269	-2.541224	-1.512865
H	5.045591	-2.835333	0.218244
H	0.723102	-3.198177	0.232413
H	-0.625836	-2.025357	0.200975
H	0.103305	-2.455509	1.726051
H	-2.000191	1.672593	-1.908859
H	-3.225933	2.825661	-1.413515
H	-3.731077	1.296659	0.630029
H	-2.825965	-0.540859	-1.658529
H	-3.463391	-3.281911	0.285206
H	-5.635796	-2.823644	-0.603393
H	-4.727080	-2.194224	-1.996414
H	-5.923930	-1.170415	-1.172854
H	-5.095779	-1.991270	1.737235
H	-5.407525	-0.321530	1.250640
H	-3.848197	-0.757453	1.993455
Na	5.647638	1.438724	-0.117108

JH-III 2Z-6Z-9Z and sodium $[M+Na]^+$ located on carboxyl end

1 1

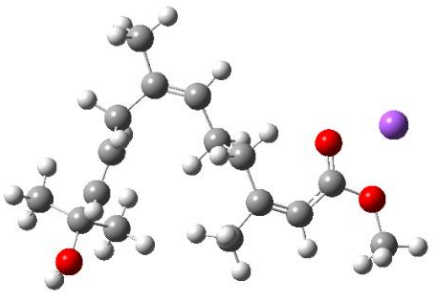

C	-2.175114	4.084629	0.213016
C	-1.730404	2.657482	0.003233
C	-0.429085	2.324567	0.057196
C	0.168601	0.956066	-0.130313
C	0.927198	0.494724	1.156650
C	1.457182	-0.903650	1.015590
C	2.664528	-1.249612	0.473371
C	3.654269	-0.320136	-0.013639
O	3.554532	0.909210	-0.110546
O	4.880049	-0.799947	-0.438390
C	5.238325	-2.204992	-0.388935
C	0.548036	-1.991926	1.506972
C	-2.852721	1.656168	-0.268587
C	-3.039350	0.633782	0.836039
C	-3.494246	-0.626178	0.765408
C	-3.981481	-1.439258	-0.428163
O	-4.340063	-2.706543	0.167312
C	-2.886798	-1.696772	-1.481238
C	-5.229764	-0.806239	-1.067826
H	-2.704290	4.463533	-0.672512
H	-1.333525	4.753665	0.419399
H	-2.882720	4.155310	1.051076
H	0.292534	3.117396	0.264030
H	0.887690	0.971938	-0.960166
H	-0.602368	0.221715	-0.379056

H	0.222157	0.520966	1.994217
H	1.732210	1.205383	1.357476
H	2.907956	-2.303932	0.419174
H	6.263658	-2.254407	-0.755315
H	4.584833	-2.786767	-1.043095
H	5.194381	-2.572440	0.638767
H	0.894927	-2.995054	1.244921
H	-0.467711	-1.846834	1.118443
H	0.462393	-1.927389	2.601069
H	-2.690737	1.165548	-1.234489
H	-3.789346	2.220647	-0.380087
H	-2.799339	1.006271	1.832689
H	-3.590017	-1.176081	1.700533
H	-4.787337	-3.251080	-0.500435
H	-3.272530	-2.358316	-2.267780
H	-2.025440	-2.189097	-1.018000
H	-2.549247	-0.775633	-1.967250
H	-5.614259	-1.447057	-1.872959
H	-5.006127	0.173342	-1.503145
H	-6.017091	-0.680980	-0.318177
Na	5.536195	1.450516	-0.928089

JH-III 2Z-6E-10R and sodium $[M+Na]^+$ located on epoxy end

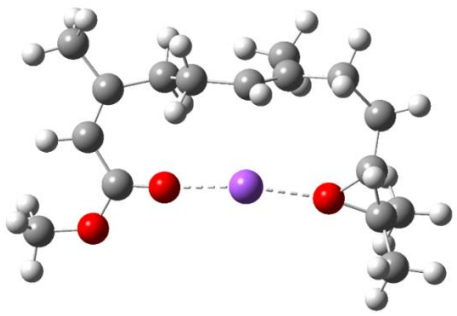

1 1

C	0.919143	-2.300563	1.4291676
C	1.123835	-2.082396	-0.0552538
C	0.162171	-1.861366	-0.9794541
C	-1.354822	-1.778772	-0.9366272
C	-2.094359	-1.539054	0.4057056
C	-3.513282	-1.063842	0.1739462
C	-3.871925	0.233639	-0.0058229
C	-2.949699	1.375090	-0.0232996
O	-1.719417	1.270771	-0.1035198
O	-3.435794	2.619433	0.0309144
C	-4.840093	2.909636	0.2001221
C	-4.565833	-2.137716	0.1563101
C	2.564000	-2.279715	-0.5203545
C	3.632668	-1.323201	0.0627696
C	3.616489	0.049468	-0.5645495
C	3.993508	1.323301	0.0871368
O	2.578071	0.988295	-0.1370229
C	4.490533	2.462161	-0.7774721
C	4.403256	1.395122	1.5416172
H	1.383429	-3.250258	1.7262446
H	-0.125729	-2.339346	1.7306724
H	1.411836	-1.521980	2.0267465
H	0.515783	-1.808701	-2.0128330
H	-1.742587	-2.702340	-1.3925595
H	-1.648832	-0.982882	-1.6330270

H	-1.560023	-0.799066	1.0050498
H	-2.131079	-2.471337	0.9795771
H	-4.925306	0.450371	-0.1439225
H	-4.888906	3.992485	0.3107054
H	-5.231763	2.427251	1.0995407
H	-5.406870	2.605775	-0.6845262
H	-5.557479	-1.754079	-0.0976924
H	-4.623154	-2.627343	1.1381390
H	-4.300830	-2.923232	-0.5642400
H	2.610430	-2.241640	-1.6159545
H	2.855646	-3.302026	-0.2400407
H	4.621957	-1.754532	-0.1434680
H	3.544668	-1.258377	1.1508436
H	3.717011	0.033454	-1.6528194
H	4.152611	3.425008	-0.3768989
H	4.134481	2.368908	-1.8079028
H	5.586655	2.473276	-0.7917447
H	4.109957	2.362017	1.9664371
H	5.493097	1.312619	1.6269389
H	3.949916	0.605547	2.1443091
Na	0.398061	0.941971	-0.2940181

JH-III 2Z-6E-10S and sodium $[M+Na]^+$ located on epoxy end

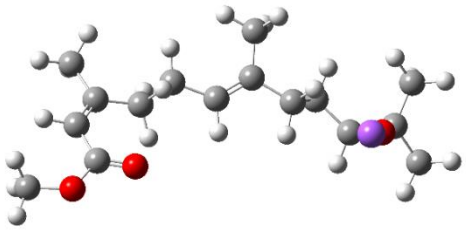

1 1

C	0.948066	2.364514	1.308629
C	0.700322	0.978019	0.763235
C	-0.507560	0.446097	0.505218
C	-1.874292	1.043491	0.682236
C	-2.663758	1.052963	-0.658206
C	-4.152498	1.223765	-0.451453
C	-5.002277	0.202895	-0.189603
C	-4.598719	-1.215946	-0.059151
O	-3.447494	-1.595165	0.090086
O	-5.569205	-2.165646	-0.088108
C	-6.943840	-1.860431	-0.365379
C	-4.672583	2.634094	-0.550573
C	1.939387	0.132020	0.531424
C	2.973173	0.720971	-0.458682
C	3.985123	-0.320438	-0.879895
C	5.460225	-0.216882	-0.827254
O	4.731981	-0.991074	0.201185
C	6.160789	1.013765	-0.298799
C	6.281304	-1.080321	-1.759137
H	1.556415	2.325829	2.224376
H	0.021551	2.887125	1.554221
H	1.496705	2.990986	0.592201
H	-0.540667	-0.576326	0.122819
H	-1.836711	2.053330	1.103795
H	-2.422297	0.410179	1.389800

H	-2.470935	0.109756	-1.175543
H	-2.286773	1.868939	-1.287914
H	-6.054317	0.439361	-0.067419
H	-7.438939	-2.828654	-0.450421
H	-7.049260	-1.313670	-1.307858
H	-7.398647	-1.295082	0.455281
H	-5.741133	2.704981	-0.327154
H	-4.502587	3.034106	-1.559621
H	-4.130741	3.295035	0.140055
H	1.625326	-0.861676	0.179198
H	2.451784	0.002323	1.508344
H	3.458353	1.598213	-0.022350
H	2.451002	1.057798	-1.363237
H	3.593700	-1.052263	-1.589825
H	7.109382	0.732263	0.172276
H	5.560605	1.556595	0.434659
H	6.392131	1.693830	-1.126898
H	7.212647	-1.393879	-1.274063
H	6.548422	-0.510375	-2.656563
H	5.730446	-1.972824	-2.070251
Na	3.885918	-1.968389	1.911011

JH-III 2Z-6Z-10R and sodium $[M+Na]^+$ located on epoxy end

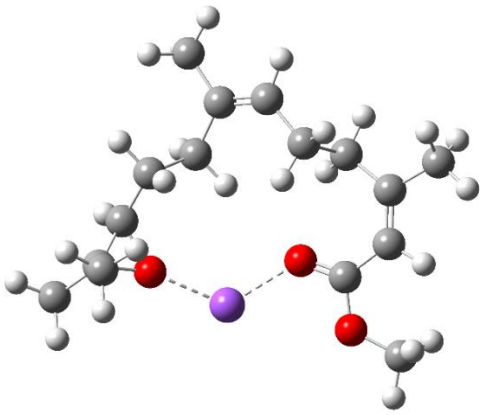

1 1

C	-1.576067	4.189914	-0.610345
C	-0.773644	2.954794	-0.270196
C	0.417471	3.052698	0.346717
C	1.346232	1.932479	0.751536
C	2.419212	1.635256	-0.341972
C	3.525189	0.741076	0.160381
C	3.499672	-0.620322	0.199691
C	2.390400	-1.461781	-0.224942
O	1.266857	-1.052778	-0.550461
O	2.541767	-2.804912	-0.253147
C	3.801534	-3.460297	0.018642
C	4.746978	1.458367	0.664195
C	-1.390655	1.634053	-0.694056
C	-2.557387	1.167097	0.208460
C	-3.252773	-0.047716	-0.357443
C	-3.835744	-1.174060	0.402646
O	-2.542508	-1.331584	-0.289981
C	-4.957892	-1.970867	-0.227411
C	-3.758416	-1.253511	1.911233
H	-1.732280	4.270997	-1.695149
H	-1.076279	5.102319	-0.271471
H	-2.573232	4.169015	-0.149957
H	0.781855	4.054889	0.575952
H	0.803444	1.006974	0.962552
H	1.852951	2.219414	1.681971

H	2.860381	2.585810	-0.664039
H	1.916650	1.189884	-1.203900
H	4.377755	-1.126439	0.583941
H	3.617105	-4.516816	-0.174592
H	4.090535	-3.322715	1.064148
H	4.580891	-3.092269	-0.653387
H	5.482550	0.786999	1.115323
H	4.463104	2.217786	1.405016
H	5.228055	2.001155	-0.160976
H	-0.626835	0.849725	-0.720027
H	-1.765830	1.742097	-1.723110
H	-3.310455	1.962396	0.289840
H	-2.186118	0.976458	1.219966
H	-3.677041	0.113156	-1.351302
H	-4.889028	-3.027441	0.057312
H	-4.934883	-1.901022	-1.319048
H	-5.927210	-1.595780	0.121341
H	-3.724538	-2.301242	2.232512
H	-4.653919	-0.802188	2.354315
H	-2.881550	-0.741367	2.312523
Na	-0.589970	-2.179153	-0.796714

JH-III 2Z-6Z-10S and sodium $[M+Na]^+$ located on epoxy end

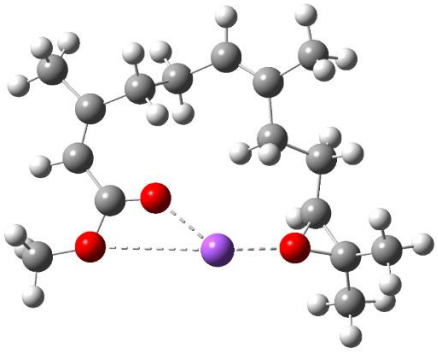

1 1

C	-1.588628	3.831508	-0.743274
C	-0.674996	2.773136	-0.170382
C	0.581709	3.072452	0.207095
C	1.634868	2.132078	0.741767
C	2.554860	1.594611	-0.399527
C	3.639696	0.683517	0.115503
C	3.563005	-0.673649	0.199822
C	2.420625	-1.496276	-0.182898
O	1.286933	-1.067121	-0.443380
O	2.559701	-2.835453	-0.249435
C	3.825768	-3.506476	-0.060053
C	4.902886	1.369178	0.559876
C	-1.231570	1.363702	-0.112086
C	-2.663471	1.228548	0.456581
C	-2.963574	-0.210186	0.824992
C	-4.051011	-1.064365	0.296992
O	-2.670721	-1.239108	-0.184861
C	-5.015219	-0.565476	-0.755587
C	-4.552546	-2.214592	1.142972
H	-1.945745	3.548037	-1.743933
H	-1.079577	4.795994	-0.829077
H	-2.480511	3.980719	-0.120556
H	0.909387	4.105072	0.080790
H	1.193488	1.276882	1.262623
H	2.249342	2.664321	1.478467

H	3.024283	2.452295	-0.897260
H	1.929092	1.080650	-1.130648
H	4.432614	-1.199713	0.577120
H	3.623961	-4.554284	-0.281207
H	4.163339	-3.408553	0.975400
H	4.576808	-3.119394	-0.753342
H	5.619929	0.684430	1.020646
H	4.674108	2.169578	1.275482
H	5.386625	1.854310	-0.298932
H	-0.554254	0.726455	0.465509
H	-1.243877	0.958473	-1.137320
H	-3.394181	1.620476	-0.256315
H	-2.761268	1.824141	1.373253
H	-2.570141	-0.503744	1.800899
H	-5.352090	-1.399545	-1.381699
H	-4.565369	0.188462	-1.405061
H	-5.900448	-0.130214	-0.277199
H	-4.829583	-3.066221	0.510748
H	-5.445775	-1.909429	1.700441
H	-3.795902	-2.543642	1.861759
Na	-0.687816	-1.897125	-0.870903

JH-III 2E-6E-10R and sodium $[M+Na]^+$ located on epoxy end

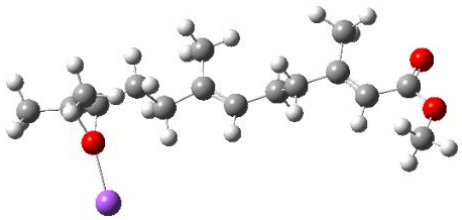

1 1

C	0.882689	-2.902962	-0.572846
C	0.971187	-1.419762	-0.850808
C	-0.083586	-0.593686	-0.973051
C	-1.549365	-0.913612	-0.854112
C	-2.237565	-0.114516	0.285116
C	-3.713835	-0.429851	0.402652
C	-4.622033	0.529468	0.113219
C	-6.089775	0.320690	0.134376
O	-6.622770	-0.771277	0.168218
O	-6.896561	1.419102	0.090394
C	-6.387317	2.753676	0.177211
C	-4.055381	-1.835773	0.829631
C	2.381040	-0.880754	-1.026145
C	3.218714	-0.871434	0.273256
C	4.648087	-0.460780	0.026785
C	5.507358	0.342638	0.921198
O	4.905458	0.957438	-0.290759
C	7.008039	0.175209	0.828321
C	4.999592	0.911477	2.226442
H	1.341276	-3.164940	0.390266
H	1.419029	-3.473615	-1.343534
H	-0.145245	-3.268829	-0.549425
H	0.127229	0.457016	-1.192680
H	-1.710574	-1.983681	-0.698295
H	-2.049516	-0.657700	-1.799480

H	-2.090137	0.959468	0.113458
H	-1.739332	-0.362069	1.233711
H	-4.254620	1.512301	-0.166535
H	-7.268309	3.392563	0.257024
H	-5.827674	3.028406	-0.724707
H	-5.761484	2.888287	1.066262
H	-4.938935	-1.864806	1.470334
H	-3.209022	-2.298666	1.350240
H	-4.300184	-2.456803	-0.041830
H	2.327001	0.145607	-1.419115
H	2.908426	-1.484240	-1.781787
H	3.250608	-1.881040	0.703920
H	2.739686	-0.224014	1.013836
H	5.180865	-1.114239	-0.667444
H	7.518827	1.127178	1.015699
H	7.312086	-0.202228	-0.152758
H	7.350590	-0.536489	1.588517
H	5.517093	1.849825	2.458041
H	5.212223	0.210617	3.042159
H	3.924963	1.102788	2.210941
Na	4.619003	2.527002	-1.706101

JH-III 2E-6E-10S and sodium $[M+Na]^+$ located on epoxy end

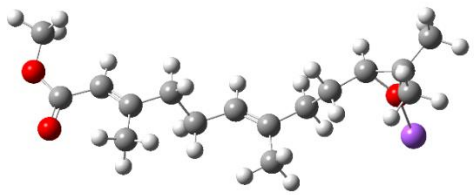

1 1

C	1.033257	-2.187961	0.447031
C	0.917329	-0.923618	-0.373444
C	-0.239599	-0.372758	-0.783828
C	-1.647455	-0.836736	-0.526941
C	-2.482820	0.225210	0.237818
C	-3.907368	-0.225081	0.483419
C	-4.923233	0.431233	-0.120729
C	-6.351156	0.047970	-0.002865
O	-6.735696	-1.036160	0.390816
O	-7.292713	0.957462	-0.381259
C	-6.963082	2.308769	-0.721787
C	-4.075671	-1.412229	1.398896
C	2.234671	-0.273340	-0.758314
C	3.043283	0.279032	0.437489
C	4.303539	0.978782	-0.004954
C	5.602171	0.993798	0.701154
O	5.408797	0.133033	-0.494353
C	5.827423	0.234167	1.988569
C	6.545039	2.152054	0.461054
H	1.701994	-2.910184	-0.044178
H	0.073593	-2.685474	0.598437
H	1.456526	-1.991029	1.441615
H	-0.172521	0.538201	-1.383714
H	-1.663652	-1.781491	0.023577
H	-2.141179	-1.027689	-1.490843

H	-2.472679	1.166427	-0.325850
H	-1.994792	0.422406	1.203365
H	-4.680147	1.286649	-0.744174
H	-7.920834	2.823002	-0.815778
H	-6.433526	2.361801	-1.680163
H	-6.370280	2.788061	0.064729
H	-4.993136	-1.349390	1.986863
H	-3.214201	-1.507330	2.070432
H	-4.156537	-2.340382	0.817891
H	2.047933	0.540017	-1.471450
H	2.859351	-1.019066	-1.284595
H	3.276267	-0.520285	1.146123
H	2.428961	1.014908	0.974634
H	4.131177	1.819300	-0.680557
H	6.874561	-0.081288	2.063947
H	5.192468	-0.650035	2.071634
H	5.619862	0.887666	2.843936
H	7.588694	1.817713	0.494042
H	6.415954	2.905478	1.246896
H	6.358375	2.631204	-0.504773
Na	5.967881	-1.280874	-1.992645

JH-III 2E-6Z-10R and sodium $[M+Na]^+$ located on epoxy end

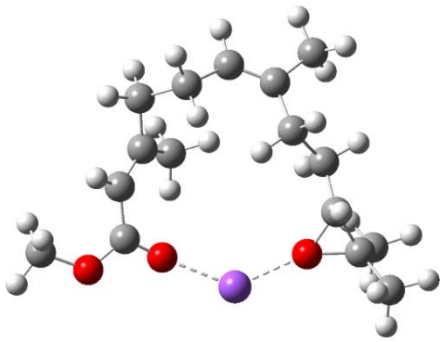

1 1

C	-2.034986	3.808788	0.526258
C	-0.987925	2.976493	-0.182278
C	0.295126	3.384872	-0.202874
C	1.474925	2.809652	-0.942685
C	2.668195	2.331890	-0.048810
C	2.460562	0.931803	0.479540
C	3.071675	-0.100073	-0.156445
C	2.829686	-1.527677	0.082126
O	1.744464	-1.991162	0.459790
O	3.795784	-2.411565	-0.181277
C	5.146586	-2.000193	-0.490138
C	1.582733	0.799188	1.691632
C	-1.494486	1.730819	-0.890613
C	-2.467115	0.880298	-0.040963
C	-2.833110	-0.428834	-0.708745
C	-3.603776	-1.521703	-0.081314
O	-2.141927	-1.642323	-0.257767
C	-4.396655	-2.460604	-0.964361
C	-4.065351	-1.439283	1.357335
H	-2.857918	4.066946	-0.155288
H	-1.611550	4.743343	0.905492
H	-2.484059	3.279245	1.376994
H	0.526265	4.303716	0.339634
H	1.874760	3.606430	-1.585364
H	1.187118	1.996411	-1.617601

H	2.801572	3.039609	0.778893
H	3.579901	2.363883	-0.654756
H	3.782545	0.132347	-0.945107
H	5.741947	-2.909464	-0.412384
H	5.500162	-1.256901	0.228485
H	5.202461	-1.610131	-1.510580
H	1.513742	-0.222630	2.064637
H	0.575781	1.177006	1.474081
H	1.976046	1.443438	2.488875
H	-0.654257	1.104733	-1.211267
H	-2.021473	2.031356	-1.810157
H	-3.393569	1.442688	0.132541
H	-2.034949	0.676554	0.945240
H	-2.883260	-0.383904	-1.798716
H	-4.400967	-3.474942	-0.547512
H	-3.984129	-2.500636	-1.976881
H	-5.438583	-2.126047	-1.029696
H	-4.084124	-2.438071	1.809780
H	-5.087447	-1.044627	1.396550
H	-3.427307	-0.794134	1.965383
Na	-0.269253	-2.667130	0.237888

JH-III 2E-6Z-10S and sodium $[M+Na]^+$ located on epoxy end

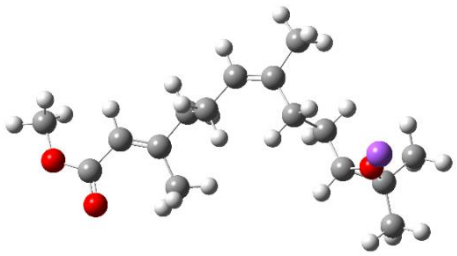

1 1

C	1.819578	3.488467	-0.468469
C	1.039350	2.279727	0.000802
C	-0.305974	2.284745	0.000397
C	-1.261515	1.201898	0.425920
C	-2.276459	0.843302	-0.692788
C	-3.204300	-0.281503	-0.286918
C	-4.516105	-0.025149	-0.085645
C	-5.498107	-1.036928	0.374705
O	-5.190338	-2.109901	0.859104
O	-6.822429	-0.742512	0.271098
C	-7.300763	0.431973	-0.396482
C	-2.562215	-1.637304	-0.116091
C	1.877138	1.107829	0.478808
C	2.588804	0.343352	-0.661969
C	3.347872	-0.856141	-0.153216
C	4.624357	-1.385504	-0.677294
O	4.598803	-0.604632	0.587229
C	5.368082	-0.716311	-1.810432
C	4.939809	-2.850786	-0.472257
H	2.466789	3.878568	0.331179
H	1.154606	4.298848	-0.781250
H	2.473582	3.254620	-1.320042
H	-0.793145	3.194357	-0.356345
H	-1.833378	1.547764	1.299693
H	-0.733782	0.295826	0.740722

H	-1.718124	0.544585	-1.591811
H	-2.850847	1.739511	-0.955925
H	-4.871342	0.986387	-0.257430
H	-8.384458	0.314544	-0.440965
H	-6.902052	0.505214	-1.413866
H	-7.061956	1.338797	0.170787
H	-3.210641	-2.442785	-0.467454
H	-2.375786	-1.849943	0.944458
H	-1.605460	-1.680463	-0.650595
H	1.267471	0.402174	1.053053
H	2.645513	1.490937	1.172964
H	3.248555	1.014269	-1.218742
H	1.834960	-0.023700	-1.371762
H	2.725647	-1.582092	0.374587
H	6.446231	-0.887366	-1.710142
H	5.190851	0.360079	-1.851311
H	5.054672	-1.152847	-2.765967
H	6.015129	-3.000076	-0.318619
H	4.652895	-3.421098	-1.363414
H	4.399612	-3.263985	0.384912
Na	5.454441	0.240385	2.351765

JH-III 2E-6E-9E and sodium $[M+Na]^+$ located on epoxy end

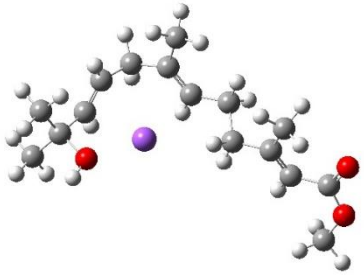

1 1

C	-1.491384	3.243170	0.260967
C	-1.491470	2.095405	-0.719420
C	-0.409801	1.354622	-1.050275
C	1.008547	1.484183	-0.552414
C	1.552025	0.164197	0.054835
C	2.994398	0.266687	0.511831
C	3.939886	-0.440859	-0.144007
C	5.391713	-0.372941	0.173591
O	5.878290	0.469800	0.900810
O	6.218585	-1.290067	-0.389933
C	5.744681	-2.380916	-1.189451
C	3.250896	1.194578	1.673260
C	-2.839754	1.811964	-1.391229
C	-3.692852	0.946364	-0.492610
C	-3.951223	-0.348137	-0.729882
C	-4.583103	-1.335987	0.235932
O	-3.383612	-1.928533	0.890119
C	-5.323779	-2.438749	-0.523336
C	-5.464962	-0.708662	1.316184
H	-2.340110	3.183204	0.954558
H	-1.607617	4.190022	-0.283816
H	-0.575931	3.313855	0.852060
H	-0.541878	0.612410	-1.845986
H	1.104190	2.292106	0.177751
H	1.653683	1.753648	-1.400050

H	1.444863	-0.646174	-0.679505
H	0.939277	-0.097281	0.940357
H	3.627330	-1.084808	-0.960743
H	6.627808	-2.985536	-1.399321
H	5.320526	-2.027173	-2.136000
H	5.012983	-2.987844	-0.645105
H	4.006485	0.794997	2.352772
H	2.326757	1.389638	2.230735
H	3.648005	2.156299	1.324447
H	-2.686980	1.312159	-2.353859
H	-3.350154	2.763089	-1.591875
H	-4.053048	1.412520	0.424901
H	-3.610836	-0.788700	-1.670669
H	-3.644703	-2.729445	1.376881
H	-5.703288	-3.202613	0.165972
H	-4.668268	-2.923683	-1.254462
H	-6.184242	-2.020208	-1.056412
H	-5.844086	-1.484846	1.990242
H	-6.328264	-0.206164	0.867644
H	-4.915582	0.017019	1.923739
Na	-1.560540	-0.656874	0.534903

JH-III 2E-6E-9Z and sodium $[M+Na]^+$ located on epoxy end

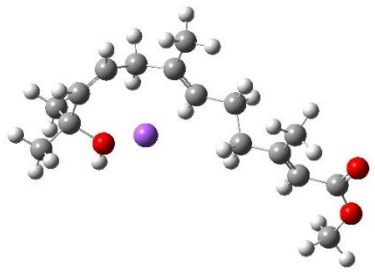

1 1

C	-1.453527	3.197239	-0.142087
C	-1.549638	1.783828	-0.666514
C	-0.491613	0.968921	-0.884883
C	0.973580	1.236636	-0.652672
C	1.645135	0.140867	0.215505
C	3.125613	0.383628	0.433986
C	4.017918	-0.477141	-0.102289
C	5.492305	-0.305872	-0.008798
O	6.026824	0.734048	0.320879
O	6.284366	-1.361828	-0.328337
C	5.762815	-2.664234	-0.619329
C	3.479502	1.611093	1.236192
C	-2.954008	1.313604	-1.060299
C	-3.923113	1.238215	0.103324
C	-4.599920	0.178890	0.587572
C	-4.600975	-1.270779	0.115886
O	-3.181335	-1.668483	0.010330
C	-5.274051	-1.432377	-1.254335
C	-5.271304	-2.167018	1.163465
H	-1.761103	3.901216	-0.927318
H	-0.444549	3.472982	0.169193
H	-2.125162	3.369608	0.707613
H	-0.699694	0.006617	-1.366241
H	1.134772	2.217599	-0.198593
H	1.482699	1.256567	-1.626603

H	1.487531	-0.840426	-0.251746
H	1.150085	0.121427	1.204007
H	3.640966	-1.336069	-0.649958
H	6.637399	-3.311231	-0.698418
H	5.223900	-2.674173	-1.573674
H	5.117026	-3.026918	0.187774
H	4.357251	1.448254	1.864330
H	2.635580	1.925073	1.862548
H	3.740366	2.446680	0.573964
H	-2.888488	0.356533	-1.582330
H	-3.364096	2.042861	-1.776488
H	-4.121406	2.190037	0.595757
H	-5.287166	0.376152	1.409712
H	-3.139943	-2.571277	-0.348434
H	-5.267909	-2.484802	-1.565304
H	-4.774309	-0.836443	-2.022147
H	-6.319118	-1.110854	-1.201109
H	-4.781297	-2.071160	2.138992
H	-5.230945	-3.218854	0.858098
H	-6.326275	-1.897744	1.283730
Na	-1.762480	-0.344960	1.101939

JH-III 2E-6Z-9E and sodium $[M+Na]^+$ located on epoxy end

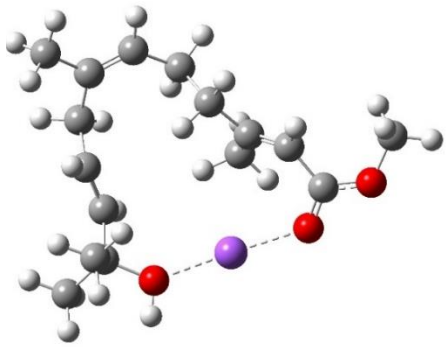

1 1

C	-3.858677	3.186764	0.804507
C	-2.673286	2.652504	0.036355
C	-1.480821	3.273734	0.069498
C	-0.215505	2.807443	-0.609498
C	0.586289	1.868803	0.323405
C	1.662075	0.992901	-0.287074
C	2.749292	0.661900	0.447324
C	3.680385	-0.446161	0.122777
O	3.275571	-1.540460	-0.287687
O	4.982161	-0.310118	0.340657
C	5.554345	0.959616	0.733008
C	1.413637	0.475393	-1.684014
C	-2.943200	1.384982	-0.769083
C	-2.770193	0.100939	0.016546
C	-2.280233	-1.042997	-0.482808
C	-2.275570	-2.391875	0.201788
O	-0.916598	-2.961872	-0.031968
C	-3.279688	-3.324652	-0.493183
C	-2.507747	-2.347879	1.712777
H	-4.670917	3.471310	0.121383
H	-3.595086	4.063707	1.403310
H	-4.274512	2.428626	1.483542
H	-1.393652	4.175889	0.675054
H	0.403367	3.668239	-0.892048
H	-0.464267	2.284458	-1.538405

H	-0.139261	1.165857	0.762058
H	0.995808	2.434932	1.168209
H	2.927161	1.174342	1.391266
H	6.626243	0.845864	0.575451
H	5.355090	1.150214	1.791379
H	5.165468	1.770473	0.112426
H	2.174613	-0.229423	-2.024750
H	1.411355	1.315821	-2.388902
H	0.415914	0.021176	-1.775233
H	-2.332787	1.343973	-1.678566
H	-3.988836	1.421653	-1.111800
H	-3.134113	0.126242	1.043496
H	-1.959599	-1.074534	-1.527342
H	-0.996517	-3.923781	0.087703
H	-3.238233	-4.336405	-0.066977
H	-3.078496	-3.388630	-1.567645
H	-4.299055	-2.950923	-0.357612
H	-2.411112	-3.352974	2.138450
H	-3.516241	-1.991920	1.946304
H	-1.784570	-1.692979	2.209282
Na	1.173322	-2.208190	-0.272909

JH-III 2E-6Z-9Z and sodium $[M+Na]^+$ located on epoxy end

1 1

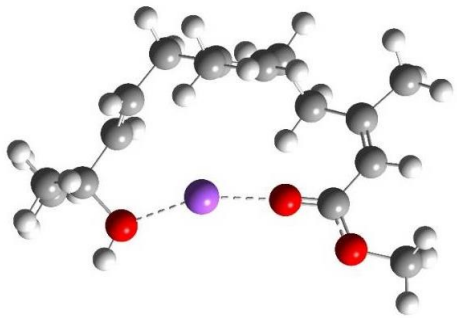

C	2.190326	4.012135	-0.021619
C	1.449756	2.729474	0.275120
C	0.110151	2.654186	0.204082
C	-0.775659	1.463665	0.460055
C	-1.844978	1.284867	-0.649700
C	-2.672511	0.033388	-0.453167
C	-3.974035	0.137643	-0.104843
C	-4.850894	-1.026335	0.173826
O	-4.435943	-2.155343	0.360445
O	-6.192250	-0.821018	0.246064
C	-6.799093	0.438234	-0.072600
C	-1.945460	-1.275545	-0.651689
C	2.331660	1.548840	0.672885
C	2.847301	0.810542	-0.546571
C	3.130981	-0.492190	-0.764164
C	3.126655	-1.724339	0.130344
O	4.571462	-2.090046	0.158921
C	2.359770	-2.859856	-0.558546
C	2.668211	-1.546500	1.577072
H	2.724922	4.374327	0.868246
H	1.512703	4.804244	-0.353043
H	2.947336	3.875613	-0.808815
H	-0.422820	3.567494	-0.066766
H	-1.301427	1.594583	1.417682
H	-0.187185	0.544308	0.550351

H	-1.337420	1.232834	-1.623743
H	-2.488416	2.172407	-0.670473
H	-4.400018	1.131783	-0.009806
H	-7.873323	0.249114	-0.059882
H	-6.503812	0.784697	-1.068590
H	-6.560116	1.197444	0.680580
H	-2.568199	-2.012656	-1.163846
H	-1.687541	-1.729572	0.313640
H	-1.023488	-1.118146	-1.224799
H	1.804243	0.875538	1.347406
H	3.186363	1.942471	1.246374
H	2.947940	1.449023	-1.426843
H	3.391654	-0.753019	-1.794866
H	4.670076	-2.995605	0.499703
H	2.438668	-3.788587	0.020028
H	2.744682	-3.043766	-1.566778
H	1.296818	-2.609966	-0.636036
H	2.802991	-2.488681	2.120556
H	1.604389	-1.295462	1.626751
H	3.240185	-0.773485	2.098114
Na	5.761960	-0.344086	-0.405590

JH-III 2Z-6E-9E and sodium $[M+Na]^+$ located on epoxy end

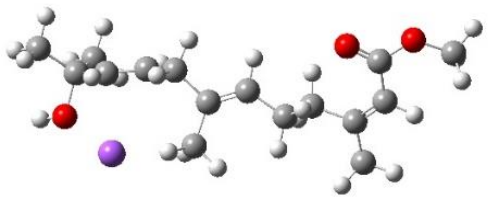

1 1

C	-1.197749	1.511648	-1.264386
C	-0.691611	0.104841	-1.020527
C	0.596732	-0.199808	-0.788898
C	1.798834	0.698620	-0.727521
C	2.475692	0.641665	0.672529
C	3.887109	1.188930	0.655582
C	4.976489	0.459345	0.321718
C	4.939832	-0.966526	-0.082535
O	3.923830	-1.558958	-0.408708
O	6.105995	-1.658317	-0.110219
C	7.348863	-1.103696	0.345355
C	4.035877	2.638176	1.040748
C	-1.741608	-0.997884	-1.090567
C	-2.850761	-0.845059	-0.077976
C	-4.159114	-0.789528	-0.377896
C	-5.320645	-0.625430	0.587188
O	-5.739959	0.784499	0.355269
C	-4.958159	-0.781590	2.063883
C	-6.476587	-1.547648	0.188832
H	-1.924011	1.528963	-2.095170
H	-0.403084	2.210461	-1.534119
H	-1.670068	1.934453	-0.356699
H	0.842028	-1.251604	-0.634241
H	1.562311	1.736633	-0.986924
H	2.521314	0.329169	-1.463998

H	2.488253	-0.399761	1.002551
H	1.870819	1.217239	1.385586z
H	5.943613	0.950946	0.351702
H	8.058214	-1.931561	0.313222
H	7.268205	-0.733444	1.372432
H	7.696150	-0.306869	-0.321214
H	5.065250	2.994670	0.941599
H	3.715344	2.793536	2.080247
H	3.390709	3.273224	0.417582
H	-1.248802	-1.963442	-0.918425
H	-2.177609	-1.042889	-2.100460
H	-2.529137	-0.803310	0.963847
H	-4.458817	-0.880196	-1.426692
H	-6.617514	0.932771	0.747042
H	-5.839824	-0.599994	2.688482
H	-4.181513	-0.073514	2.370326
H	-4.606466	-1.797036	2.273379
H	-7.352786	-1.373610	0.825576
H	-6.184755	-2.596153	0.309036
H	-6.767138	-1.388683	-0.854917
Na	-4.068979	1.853262	-0.610332

JH-III 2Z-6E-9Z and sodium [M+Na]$^+$ located on epoxy end

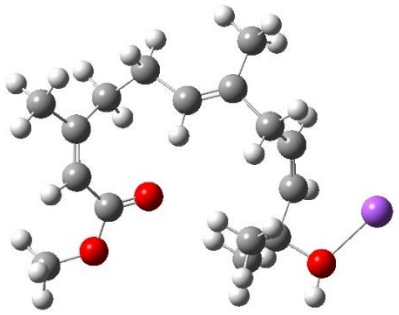

1 1

C	0.819834	3.953473	-0.469639
C	0.534296	2.614198	0.166362
C	-0.678797	2.049791	0.286941
C	-1.993705	2.564119	-0.237190
C	-2.870989	1.442007	-0.866216
C	-3.594193	0.566910	0.135369
C	-3.315297	-0.732195	0.394214
C	-2.199818	-1.518216	-0.175395
O	-1.129472	-1.052056	-0.539338
O	-2.349442	-2.864615	-0.255383
C	-3.614540	-3.509375	-0.023358
C	-4.772033	1.213571	0.823149
C	1.753145	1.872187	0.722593
C	2.548193	1.252555	-0.403974
C	2.872321	-0.024004	-0.704889
C	2.640879	-1.364103	-0.019975
O	4.039576	-1.804896	0.273818
C	2.023038	-2.345359	-1.021506
C	1.866956	-1.371039	1.295479
H	1.208619	4.658146	0.279544
H	-0.067883	4.408790	-0.913744
H	1.579728	3.884567	-1.260084
H	-0.739055	1.087277	0.791366
H	-1.835317	3.332369	-1.000496
H	-2.554796	3.054928	0.571416

H	-2.251588	0.840782	-1.535181
H	-3.641698	1.934247	-1.475370
H	-3.970345	-1.260772	1.081315
H	-3.484821	-4.531012	-0.382474
H	-4.416906	-3.021704	-0.584425
H	-3.855108	-3.529258	1.044780
H	-5.238738	0.552393	1.558778
H	-5.533275	1.501007	0.085275
H	-4.473286	2.136853	1.335532
H	1.435036	1.131100	1.453770
H	2.399721	2.593456	1.249045
H	2.853081	1.979574	-1.159689
H	3.369132	-0.164026	-1.670219
H	4.042439	-2.760672	0.449840
H	1.989621	-3.355828	-0.593473
H	2.600374	-2.380117	-1.951523
H	0.992808	-2.049554	-1.243678
H	1.830767	-2.393905	1.688397
H	0.835847	-1.047020	1.131284
H	2.338319	-0.739247	2.054875
Na	5.271481	-0.006997	0.340962

JH-III 2Z-6Z-9E and sodium $[M+Na]^+$ located on epoxy end

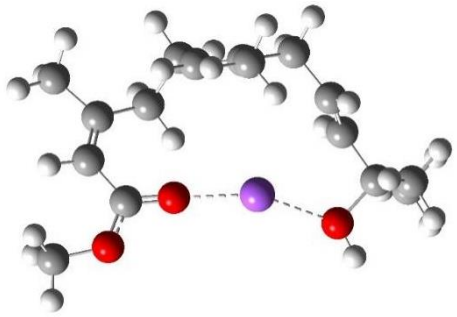

1 1

C	0.601416	-2.133836	2.536350
C	0.447568	-2.181004	1.030630
C	-0.771278	-2.088214	0.464597
C	-1.170847	-2.244066	-0.980197
C	-1.971948	-1.050217	-1.581445
C	-3.267059	-0.732560	-0.870954
C	-3.504400	0.368869	-0.112704
C	-2.544516	1.430326	0.214610
O	-1.317993	1.332049	0.096788
O	-2.998132	2.591424	0.705369
C	-4.403051	2.907505	0.812117
C	-4.384763	-1.719331	-1.090124
C	1.741602	-2.387456	0.248922
C	2.688234	-1.217692	0.405236
C	2.980154	-0.344601	-0.569575
C	3.855549	0.891408	-0.451370
O	2.862162	1.983365	-0.330750
C	4.659032	1.099059	-1.739419
C	4.762307	0.922315	0.780530
H	1.037959	-3.071122	2.908384
H	-0.361657	-1.992967	3.036072
H	1.272109	-1.329742	2.869401
H	-1.611303	-1.948141	1.147183
H	-1.781405	-3.154291	-1.067782
H	-0.304455	-2.407253	-1.628401

H	-2.224270	-1.324885	-2.614848
H	-1.332449	-0.168314	-1.620234
H	-4.505560	0.491232	0.286227
H	-4.430936	3.955363	1.109802
H	-4.879716	2.295273	1.583062
H	-4.905164	2.781890	-0.150661
H	-5.293360	-1.450898	-0.544735
H	-4.083751	-2.727650	-0.778226
H	-4.628331	-1.786371	-2.158870
H	1.542705	-2.554722	-0.812851
H	2.239157	-3.293458	0.626214
H	3.147667	-1.098332	1.385620
H	2.539660	-0.490394	-1.559432
H	3.299459	2.838905	-0.479683
H	5.229622	2.035137	-1.697494
H	3.999487	1.132850	-2.613111
H	5.375147	0.282233	-1.879065
H	5.326238	1.861564	0.806621
H	5.485275	0.100386	0.754008
H	4.189156	0.854571	1.710511
Na	0.816584	1.253765	0.275256

JH-III 2Z-6Z-9Z and sodium $[M+Na]^+$ located on epoxy end

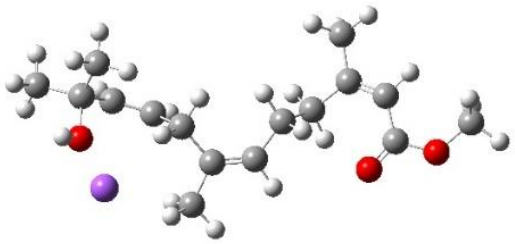

1 1

C	-1.447854	-2.547338	-0.402868
C	-0.806484	-1.217691	-0.063946
C	0.533015	-1.109632	-0.043237
C	1.401541	0.069609	0.290646
C	2.334976	0.438196	-0.897413
C	3.481036	1.333938	-0.477069
C	4.644769	0.879829	0.042393
C	4.955519	-0.549565	0.283698
O	4.119642	-1.438944	0.294087
O	6.243895	-0.896285	0.526312
C	7.328628	0.039693	0.438950
C	3.263646	2.812585	-0.669454
C	-1.767187	-0.088233	0.275651
C	-2.659073	0.319760	-0.882419
C	-3.946677	0.721427	-0.882826
C	-4.908401	0.867357	0.295279
O	-4.962751	-0.465710	0.936611
C	-6.313996	1.211750	-0.207924
C	-4.426506	1.898708	1.323243
H	-2.084594	-2.912691	0.425247
H	-0.703920	-3.330063	-0.574125
H	-2.043486	-2.495835	-1.333945
H	1.109286	-2.004116	-0.284714
H	2.034807	-0.222489	1.136174
H	0.823111	0.947383	0.600484

H	1.744181	0.943527	-1.672501
H	2.727085	-0.488901	-1.322626
H	5.403755	1.611538	0.300245
H	8.231908	-0.560315	0.555618
H	7.281026	0.778519	1.246270
H	7.346964	0.539686	-0.534712
H	4.096590	3.411957	-0.290598
H	2.345914	3.138758	-0.160160
H	3.127615	3.044609	-1.734769
H	-1.194036	0.800777	0.566088
H	-2.369245	-0.355755	1.154989
H	-2.150215	0.339026	-1.848072
H	-4.358185	1.045668	-1.838706
H	-5.502553	-0.406830	1.743148
H	-7.023649	1.264624	0.625426
H	-6.674663	0.462027	-0.921440
H	-6.315967	2.186559	-0.707809
H	-5.143141	1.981834	2.150303
H	-4.346580	2.886018	0.856935
H	-3.449356	1.633630	1.733734
Na	-4.192786	-2.028545	-0.405708

Appendix Table 5.5. Geometry coordinates of JH-III $[M+H]^+$ *m/z* 267 structures and optimized structures.

JH-III 2Z-6E-10R and proton $[M+H]^+$ located on carboxyl end

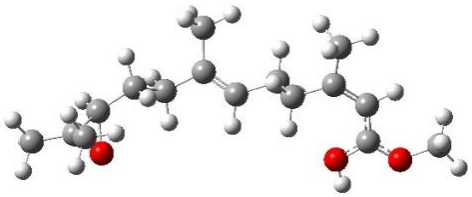

1 1

C	-1.121908	2.763652	-0.840989
C	-1.097071	1.262605	-0.997992
C	0.008921	0.496971	-0.917646
C	1.425205	0.932633	-0.671040
C	1.930315	0.415718	0.732654
C	3.347174	0.816566	0.973114
C	4.472053	0.136402	0.544638
C	4.515129	-1.098260	-0.143385
O	3.420177	-1.722200	-0.511307
O	5.607453	-1.727714	-0.480036
C	6.943887	-1.235838	-0.156880
C	3.548215	2.101438	1.714558
C	-2.434134	0.609565	-1.286688
C	-3.462778	0.727844	-0.137253
C	-4.707751	-0.070441	-0.456159
C	-5.517113	-0.855603	0.502852
O	-4.587940	-1.506811	-0.403081
C	-6.976839	-1.110360	0.180365
C	-5.167000	-0.957975	1.973767
H	-1.595212	3.229966	-1.715158
H	-0.131330	3.210690	-0.722844
H	-1.722599	3.056083	0.029875
H	-0.112801	-0.579395	-1.049403
H	1.532062	2.020538	-0.709960

H	2.082719	0.515920	-1.444138
H	1.799590	-0.667566	0.764427
H	1.294057	0.862069	1.502728
H	5.439135	0.572972	0.763857
H	7.611888	-1.997188	-0.554138
H	7.051530	-1.155807	0.926373
H	7.111111	-0.279538	-0.656058
H	4.586194	2.441933	1.727322
H	3.207164	1.973056	2.752236
H	2.914399	2.888902	1.286827
H	-2.285414	-0.453784	-1.504820
H	-2.865105	1.062417	-2.192518
H	-3.750305	1.776731	0.017730
H	-3.009112	0.370059	0.792680
H	-5.231410	0.278018	-1.352073
H	-7.273139	-2.110116	0.520268
H	-7.158101	-1.049452	-0.897022
H	-7.619888	-0.378590	0.684827
H	-5.457743	-1.944410	2.355045
H	-5.711835	-0.202669	2.553724
H	-4.096928	-0.832240	2.154440
H	3.635720	-2.564308	-0.962325

JH-III 2Z-6E-10S and proton $[M+H]^+$ located on carboxyl end

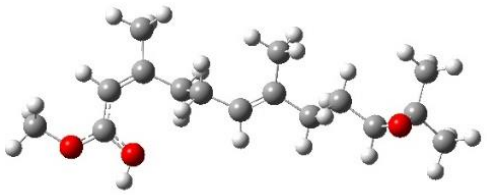

1 1

C	1.230287	1.802911	1.352932
C	1.059994	0.372523	0.899455
C	-0.123656	-0.210207	0.622912
C	-1.495875	0.394889	0.709256
C	-2.156325	0.497385	-0.721265
C	-3.509988	1.119267	-0.639510
C	-4.693847	0.466030	-0.350202
C	-4.878406	-0.920739	-0.146316
O	-3.870210	-1.762028	-0.164553
O	-6.027970	-1.496476	0.076646
C	-7.291511	-0.765484	0.123416
C	-3.564530	2.600157	-0.852053
C	2.337661	-0.436292	0.798187
C	3.353666	0.091703	-0.240930
C	4.581974	-0.791583	-0.279243
C	5.986502	-0.340716	-0.410080
O	5.445841	-0.750146	0.872944
C	6.369123	1.121759	-0.514234
C	7.005602	-1.304011	-0.987572
H	1.848186	1.842862	2.259162
H	0.286841	2.309299	1.572558
H	1.755035	2.396581	0.593404
H	-0.111835	-1.254963	0.307469
H	-1.473861	1.389928	1.162661
H	-2.142811	-0.231183	1.336354

H	-2.190359	-0.503933	-1.155046
H	-1.510353	1.122297	-1.345057
H	-5.595577	1.062956	-0.284595
H	-8.038596	-1.535231	0.305206
H	-7.466914	-0.277450	-0.837061
H	-7.268674	-0.049988	0.947501
H	-4.538387	3.039481	-0.623966
H	-3.315930	2.819878	-1.900648
H	-2.792973	3.098631	-0.251273
H	2.093232	-1.479823	0.562607
H	2.835263	-0.442501	1.778221
H	3.637938	1.119869	-0.000558
H	2.892212	0.102508	-1.239257
H	4.373422	-1.812682	-0.615309
H	7.344629	1.282788	-0.039811
H	5.647920	1.775945	-0.018821
H	6.455354	1.425220	-1.565086
H	7.972961	-1.179435	-0.486172
H	7.154749	-1.116810	-2.058243
H	6.685444	-2.342143	-0.855927
H	-4.182229	-2.678443	-0.017127

JH-III 2Z-6Z-10R and proton $[M+H]^+$ located on carboxyl end

1 1

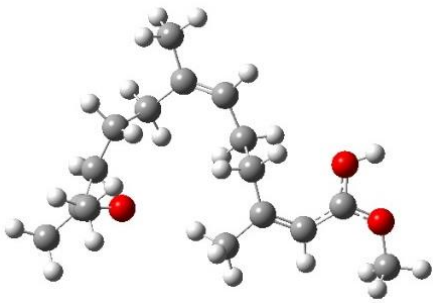

C	-2.048933	3.970593	0.257945
C	-1.356966	2.720651	-0.229272
C	-0.043295	2.526788	0.002626
C	0.787821	1.346165	-0.418643
C	1.133808	0.418833	0.811117
C	1.758838	-0.851646	0.337624
C	3.091535	-1.032826	0.007025
C	4.140552	-0.099474	0.141552
O	3.933744	1.118828	0.590139
O	5.392896	-0.332899	-0.149830
C	5.862810	-1.617270	-0.658336
C	0.832137	-2.011052	0.173213
C	-2.235716	1.725773	-0.957336
C	-3.156079	0.910041	-0.004706
C	-3.504031	-0.425290	-0.620680
C	-3.727394	-1.694770	0.103237
O	-2.461375	-1.434824	-0.577137
C	-4.568468	-2.768288	-0.558314
C	-3.647512	-1.796358	1.612664
H	-2.481865	4.527701	-0.583916
H	-1.365851	4.637485	0.793087
H	-2.881105	3.726207	0.932144
H	0.495198	3.292438	0.563277
H	1.731229	1.687429	-0.860690
H	0.275903	0.746629	-1.175759

H	0.200030	0.181037	1.327327
H	1.780253	0.972533	1.495383
H	3.384821	-2.002429	-0.377537
H	6.933868	-1.477928	-0.789262
H	5.382867	-1.828969	-1.615676
H	5.663564	-2.397786	0.078436
H	1.269614	-2.843242	-0.383934
H	-0.117875	-1.705142	-0.286555
H	0.556989	-2.372585	1.176785
H	-1.626408	1.021299	-1.530394
H	-2.858887	2.257364	-1.688834
H	-4.078088	1.466386	0.208329
H	-2.647799	0.752625	0.951525
H	-3.971775	-0.351058	-1.606516
H	-4.183773	-3.764459	-0.308083
H	-4.560136	-2.661316	-1.647102
H	-5.607224	-2.712976	-0.210817
H	-3.257200	-2.780342	1.900536
H	-4.646471	-1.696338	2.053964
H	-3.001947	-1.031811	2.051254
H	4.775312	1.617200	0.629351

JH-III 2Z-6Z-10S and proton $[M+H]^+$ located on carboxyl end

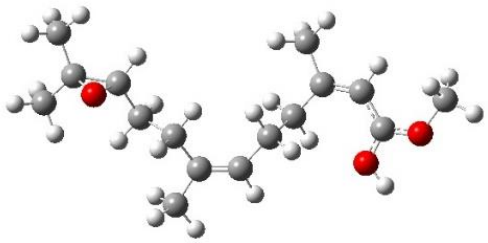

1 1

C	-1.729649	3.193911	0.237822
C	-1.051551	1.883640	-0.092808
C	0.288965	1.784107	0.014319
C	1.166365	0.608375	-0.310468
C	1.909076	0.087381	0.981002
C	2.773218	-1.086316	0.660993
C	4.063641	-1.041398	0.166747
C	4.852047	0.109480	-0.063496
O	4.386342	1.319274	0.145297
O	6.083871	0.097123	-0.493449
C	6.812855	-1.132112	-0.794268
C	2.148256	-2.432361	0.858508
C	-1.964310	0.778221	-0.578790
C	-3.096939	0.403304	0.406288
C	-3.908766	-0.756561	-0.127520
C	-5.383915	-0.887321	-0.097236
O	-4.686565	-0.514648	-1.314847
C	-6.286451	0.181760	0.483972
C	-5.988871	-2.277512	-0.131308
H	-2.354298	3.530808	-0.600097
H	-1.004526	3.982148	0.462179
H	-2.394735	3.093669	1.104965
H	0.833853	2.664804	0.359224
H	1.928309	0.904146	-1.042777
H	0.599864	-0.215041	-0.754020

H	1.149144	-0.213507	1.708168
H	2.481178	0.915356	1.404325
H	4.549275	-1.982816	-0.060955
H	7.794090	-0.788763	-1.115159
H	6.309139	-1.666239	-1.602057
H	6.893902	-1.739189	0.109249
H	2.746991	-3.255758	0.462263
H	1.150735	-2.457524	0.401370
H	1.989894	-2.598266	1.934157
H	-1.395660	-0.126504	-0.821377
H	-2.436726	1.101192	-1.517476
H	-3.741269	1.268829	0.579048
H	-2.669798	0.117235	1.378792
H	-3.347075	-1.696138	-0.176117
H	-7.233872	0.204307	-0.067644
H	-5.843359	1.178301	0.421770
H	-6.516870	-0.035562	1.534336
H	-6.915670	-2.274676	-0.717390
H	-6.232919	-2.619886	0.882012
H	-5.300770	-2.996482	-0.586894
H	5.068160	1.991979	-0.058449

JH-III 2E-6E-10R and proton $[M+H]^+$ located on carboxyl end

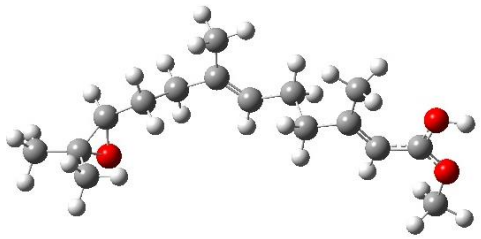

1 1

C	-1.325834	2.794197	-0.219027
C	-1.357315	1.394816	-0.784285
C	-0.271956	0.627156	-1.003968
C	1.171166	0.968189	-0.758467
C	1.754383	0.110051	0.431119
C	3.210023	0.374768	0.617901
C	4.108357	-0.560392	0.137596
C	5.516683	-0.466081	0.173835
O	6.114362	0.586031	0.686156
O	6.345352	-1.370577	-0.270633
C	5.902329	-2.624131	-0.874981
C	3.590571	1.669810	1.269322
C	-2.730562	0.859931	-1.138082
C	-3.678020	0.686795	0.072411
C	-4.969678	0.026080	-0.356168
C	-5.749436	-0.966051	0.417253
O	-4.902538	-1.375661	-0.688549
C	-7.234704	-1.095810	0.139726
C	-5.316096	-1.460032	1.782781
H	-1.864880	3.484382	-0.881311
H	-0.316527	3.190263	-0.079319
H	-1.835316	2.834860	0.752364
H	-0.434765	-0.368747	-1.418534
H	1.311268	2.030546	-0.540074
H	1.762120	0.742232	-1.656107

H	1.563974	-0.948051	0.225278
H	1.209175	0.388030	1.340344
H	3.709901	-1.464595	-0.307102
H	6.826089	-3.140954	-1.126400
H	5.323533	-2.410777	-1.775595
H	5.326605	-3.197327	-0.145902
H	4.211395	1.493286	2.156201
H	2.704011	2.230861	1.570175
H	4.193279	2.293742	0.598113
H	-2.630898	-0.109875	-1.637981
H	-3.203487	1.542592	-1.860412
H	-3.915333	1.661936	0.519548
H	-3.178107	0.086243	0.839443
H	-5.532760	0.609086	-1.092029
H	-7.547298	-2.143639	0.224841
H	-7.478572	-0.748172	-0.868791
H	-7.817726	-0.510523	0.861562
H	-5.622501	-2.505153	1.912028
H	-5.794703	-0.871984	2.575768
H	-4.232863	-1.411100	1.916848
H	7.087496	0.488723	0.639455

JH-III 2E-6E-10S and proton $[M+H]^+$ located on carboxyl end

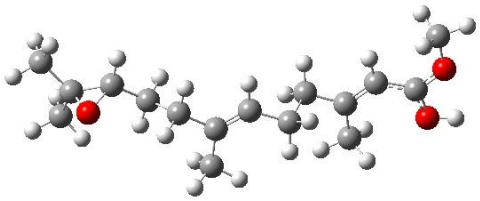

1 1

C	-1.392996	-1.970442	0.913727
C	-1.296597	-0.463220	0.921918
C	-0.141702	0.231591	0.908283
C	1.260754	-0.308825	0.892626
C	1.957734	-0.030658	-0.496839
C	3.364676	-0.524591	-0.494268
C	4.379775	0.397971	-0.317489
C	5.761616	0.118629	-0.239572
O	6.211900	-1.112388	-0.331825
O	6.704145	1.007282	-0.082419
C	6.432243	2.435575	0.053359
C	3.569185	-2.002988	-0.632286
C	-2.618118	0.275834	0.984498
C	-3.533569	0.058643	-0.242885
C	-4.821958	0.837812	-0.092073
C	-6.176402	0.380629	-0.478893
O	-5.748441	0.371336	0.907681
C	-6.435518	-0.983251	-1.086349
C	-7.231012	1.424153	-0.793405
H	-2.052270	-2.313334	1.721313
H	-0.429670	-2.472683	1.035601
H	-1.836873	-2.331323	-0.023108
H	-0.205553	1.320762	0.920235
H	1.286931	-1.382260	1.099586
H	1.858372	0.185080	1.670241

H	1.910708	1.043438	-0.702665
H	1.383741	-0.556119	-1.268241
H	4.106624	1.443645	-0.238102
H	7.415678	2.884894	0.174319
H	5.818688	2.607617	0.939625
H	5.950429	2.803129	-0.854565
H	4.201250	-2.227519	-1.500437
H	2.615655	-2.519872	-0.753660
H	4.091295	-2.420335	0.237055
H	-2.432087	1.350255	1.107509
H	-3.170067	-0.053041	1.876216
H	-3.751456	-1.005823	-0.365873
H	-3.018148	0.396722	-1.153865
H	-4.673424	1.922137	-0.058483
H	-7.422723	-1.345118	-0.774745
H	-5.696669	-1.724322	-0.772719
H	-6.432224	-0.925066	-2.181983
H	-8.213893	1.089427	-0.440441
H	-7.301302	1.592773	-1.875215
H	-7.000803	2.376507	-0.305930
H	7.188291	-1.130588	-0.261279

JH-III 2E-6Z-10R and proton $[M+H]^+$ located on carboxyl end

1 1

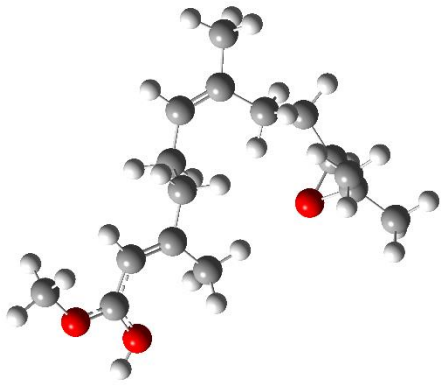

C	-2.998711	3.718626	0.367660
C	-2.070820	2.680606	-0.214483
C	-0.733758	2.807098	-0.102473
C	0.313057	1.868537	-0.644663
C	0.735029	0.786930	0.426237
C	1.788969	-0.113594	-0.122609
C	3.098118	0.096725	0.277702
C	4.237326	-0.594581	-0.181798
O	4.148785	-1.519623	-1.111549
O	5.459408	-0.400964	0.240294
C	5.789987	0.564727	1.282099
C	1.348235	-1.148373	-1.110877
C	-2.739043	1.504726	-0.891535
C	-3.380057	0.506267	0.119514
C	-3.308694	-0.906163	-0.411387
C	-3.123150	-2.137002	0.386452
O	-2.004448	-1.543008	-0.342961
C	-3.602818	-3.453079	-0.192563
C	-2.997386	-2.118584	1.895682
H	-3.625237	4.161624	-0.418409
H	-2.452276	4.526716	0.863566
H	-3.685136	3.272979	1.100453
H	-0.345730	3.669866	0.439696
H	1.206816	2.439279	-0.924904
H	-0.032731	1.352633	-1.545289

H	-0.154989	0.194149	0.663244
H	1.075607	1.302267	1.330099
H	3.284355	0.866955	1.016779
H	6.865267	0.461623	1.412592
H	5.263973	0.305338	2.202862
H	5.539837	1.571139	0.940803
H	1.788464	-2.126306	-0.890538
H	1.695662	-0.883859	-2.120024
H	0.260180	-1.241657	-1.120923
H	-2.016063	0.958739	-1.504897
H	-3.514251	1.867767	-1.579350
H	-4.427881	0.771493	0.309461
H	-2.856465	0.565149	1.078487
H	-3.786137	-1.038751	-1.386378
H	-2.932369	-4.269294	0.102796
H	-3.637129	-3.415152	-1.285535
H	-4.606577	-3.692989	0.178370
H	-2.320829	-2.917375	2.223373
H	-3.973875	-2.300950	2.360221
H	-2.609991	-1.169430	2.272861
H	5.029845	-1.900406	-1.303423

JH-III 2E-6Z-10S and proton $[M+H]^+$ located on carboxyl end

1 1

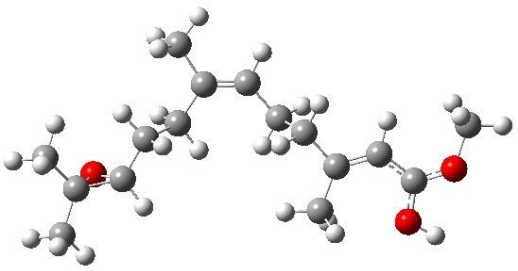

C	-2.157924	3.361900	0.061881
C	-1.357796	2.120449	-0.261808
C	-0.011045	2.166323	-0.216709
C	0.968490	1.073077	-0.541878
C	1.754874	0.617663	0.748335
C	2.761171	-0.431534	0.415534
C	4.086763	-0.053357	0.306103
C	5.169200	-0.888195	-0.048173
O	4.985283	-2.160737	-0.318927
O	6.415436	-0.512302	-0.136662
C	6.851643	0.857455	0.119977
C	2.246478	-1.817770	0.170855
C	-2.167797	0.907092	-0.665597
C	-3.169374	0.421248	0.408935
C	-3.885936	-0.828833	-0.053195
C	-5.327084	-1.129768	0.109628
O	-4.790210	-0.686799	-1.164359
C	-6.291120	-0.169327	0.775789
C	-5.767365	-2.580890	0.122856
H	-2.853799	3.599207	-0.753632
H	-1.513375	4.230906	0.225306
H	-2.767163	3.222415	0.964107
H	0.452541	3.111109	0.071932
H	1.705652	1.440575	-1.268452
H	0.480133	0.204935	-0.992344

H	1.024393	0.214949	1.459042
H	2.226817	1.496365	1.199553
H	4.339129	0.979447	0.515388
H	7.927096	0.830514	-0.042376
H	6.625159	1.124812	1.153827
H	6.372030	1.532651	-0.591109
H	2.483295	-2.161497	-0.843264
H	1.165758	-1.865178	0.315994
H	2.722443	-2.534599	0.851347
H	-1.516826	0.070085	-0.942430
H	-2.745131	1.155068	-1.567494
H	-3.891275	1.211486	0.629236
H	-2.636573	0.198074	1.345159
H	-3.225176	-1.697022	-0.156076
H	-7.283767	-0.267607	0.320383
H	-5.979785	0.872238	0.669005
H	-6.389867	-0.399297	1.843961
H	-6.734139	-2.688661	-0.383252
H	-5.884160	-2.942748	1.151950
H	-5.041489	-3.218268	-0.391755
H	5.834934	-2.594449	-0.539634

JH-III 2E-6E-9E and proton $[M+H]^+$ located on carboxyl end

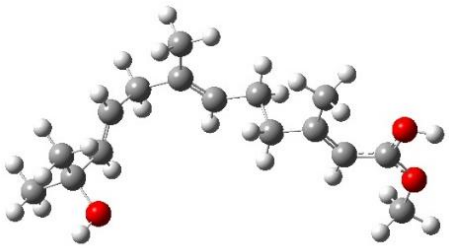

1 1

C	-1.483914	3.018013	0.206948
C	-1.475560	1.910172	-0.816209
C	-0.384722	1.231641	-1.217468
C	1.029368	1.391175	-0.734559
C	1.434235	0.173886	0.187027
C	2.857373	0.274066	0.618006
C	3.786601	-0.538808	-0.005800
C	5.177715	-0.557158	0.231622
O	5.730464	0.258102	1.101802
O	6.033287	-1.350589	-0.353346
C	5.640903	-2.342020	-1.350695
C	3.183011	1.290362	1.670419
C	-2.833831	1.558589	-1.410026
C	-3.721543	0.824610	-0.426248
C	-4.052475	-0.463900	-0.551183
C	-4.927871	-1.287236	0.371016
O	-4.112440	-2.448777	0.665978
C	-6.192295	-1.731126	-0.388775
C	-5.299682	-0.579097	1.679161
H	-2.139720	2.764377	1.049845
H	-1.885961	3.939752	-0.234562
H	-0.496199	3.249132	0.614675
H	-0.521798	0.447997	-1.963774
H	1.172303	2.325457	-0.184418
H	1.717132	1.411435	-1.589993

H	1.245517	-0.755927	-0.358558
H	0.780450	0.193523	1.066556
H	3.427154	-1.244997	-0.744827
H	6.574397	-2.827966	-1.626635
H	5.200257	-1.837972	-2.212888
H	4.951631	-3.059439	-0.901400
H	3.684739	0.821130	2.525228
H	2.279016	1.787806	2.026237
H	3.878335	2.049490	1.291329
H	-2.696439	0.941382	-2.304619
H	-3.332291	2.485585	-1.731629
H	-4.087491	1.401599	0.421853
H	-3.677805	-1.030825	-1.405333
H	-4.671214	-3.112525	1.103019
H	-6.799155	-2.402750	0.233494
H	-5.923341	-2.264357	-1.306911
H	-6.814030	-0.869709	-0.656356
H	-5.888189	-1.252852	2.313538
H	-5.908329	0.314281	1.498363
H	-4.400321	-0.292087	2.233286
H	6.696973	0.109548	1.149597

JH-III 2E-6E-9Z and proton $[M+H]^+$ located on carboxyl end

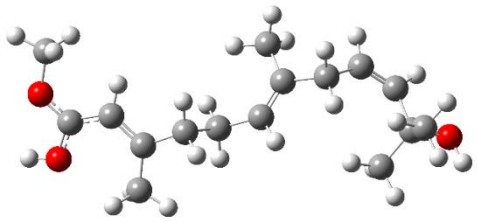

1 1

C	0.848366	2.254124	-0.712724
C	1.336285	1.070504	0.086772
C	0.641003	-0.066446	0.277401
C	-0.715758	-0.419180	-0.266121
C	-1.771730	-0.538164	0.897488
C	-3.103259	-0.968318	0.381196
C	-4.114735	-0.027620	0.317712
C	-5.421545	-0.234559	-0.176063
O	-5.789051	-1.400097	-0.658376
O	-6.368366	0.662854	-0.204952
C	-6.182034	2.028228	0.278160
C	-3.231200	-2.391363	-0.071729
C	2.720910	1.220310	0.706082
C	3.809707	1.542934	-0.296381
C	4.908719	0.845578	-0.615673
C	5.427910	-0.488354	-0.096970
O	6.619764	-0.700646	-0.884541
C	4.450440	-1.647192	-0.367820
C	5.822027	-0.413387	1.390094
H	0.994714	3.183799	-0.147303
H	-0.208945	2.190353	-0.983426
H	1.421377	2.359397	-1.642539
H	1.099128	-0.849529	0.883526
H	-0.662955	-1.381747	-0.791113
H	-1.072070	0.319045	-0.990418

H	-1.832336	0.422758	1.416658
H	-1.402057	-1.289127	1.607919
H	-3.904565	0.969215	0.686620
H	-7.146814	2.503896	0.114947
H	-5.405786	2.520679	-0.310497
H	-5.937408	2.008846	1.341791
H	-4.053400	-2.895646	0.449802
H	-2.309045	-2.945780	0.111470
H	-3.470209	-2.449529	-1.140909
H	2.960259	0.323458	1.281798
H	2.674263	2.051936	1.429485
H	3.684439	2.497138	-0.807740
H	5.576121	1.281516	-1.357210
H	7.052277	-1.516283	-0.584503
H	4.900387	-2.600397	-0.059630
H	4.221598	-1.702348	-1.436567
H	3.511676	-1.528339	0.182609
H	6.276102	-1.360698	1.710996
H	4.956686	-0.225806	2.034614
H	6.549680	0.388629	1.546991
H	-6.722520	-1.374896	-0.952952

JH-III 2E-6Z-9E and proton $[M+H]^+$ located on carboxyl end

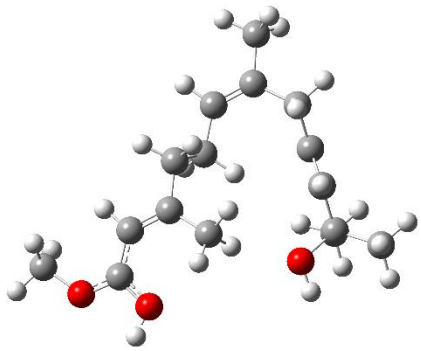

1 1

C	-3.197801	3.967388	0.176115
C	-2.390761	2.695493	0.063214
C	-1.093934	2.687106	0.428966
C	-0.126997	1.536467	0.384011
C	0.950668	1.723765	-0.751471
C	1.803157	0.498299	-0.834405
C	3.027301	0.525263	-0.186968
C	3.933725	-0.544693	-0.040347
O	3.651161	-1.754060	-0.469844
O	5.107905	-0.462195	0.529164
C	5.646675	0.788378	1.051369
C	1.223851	-0.680504	-1.543640
C	-3.168502	1.508069	-0.511693
C	-3.023965	0.189714	0.210487
C	-2.699643	-0.961844	-0.385846
C	-2.523116	-2.318413	0.260901
O	-1.125328	-2.651188	-0.016468
C	-3.429277	-3.347236	-0.435098
C	-2.745029	-2.329992	1.776771
H	-4.045124	3.832390	0.862330
H	-3.627028	4.242846	-0.797412
H	-2.597857	4.809138	0.534958
H	-0.674186	3.623969	0.799288
H	-0.646718	0.591106	0.229338
H	0.410637	1.462277	1.339060

H	1.546724	2.617017	-0.536341
H	0.425904	1.878609	-1.699247
H	3.335234	1.458927	0.268997
H	6.640978	0.525012	1.406203
H	5.024851	1.137047	1.878259
H	5.706793	1.525838	0.248743
H	1.978261	-1.313327	-2.013191
H	0.498294	-0.353708	-2.293030
H	0.667880	-1.315863	-0.831613
H	-2.904996	1.377184	-1.571663
H	-4.232526	1.782924	-0.509687
H	-3.214071	0.217984	1.283096
H	-2.509070	-0.965615	-1.461306
H	-0.997052	-3.594481	0.179630
H	-3.252141	-4.354730	-0.035443
H	-3.238705	-3.365559	-1.513522
H	-4.485670	-3.106674	-0.274537
H	-2.554234	-3.334261	2.173497
H	-3.776444	-2.065026	2.033959
H	-2.065607	-1.634302	2.279336
H	4.397842	-2.362736	-0.296716

JH-III 2E-6Z-9Z and proton $[M+H]^+$ located on carboxyl end

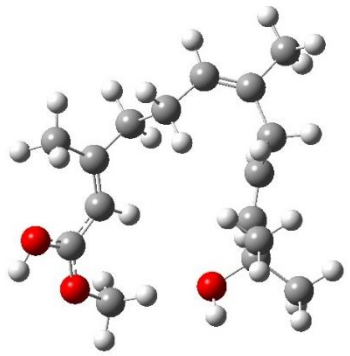

1 1

C	-4.587214	-1.899462	-0.658054
C	-3.232858	-1.535661	-0.103596
C	-2.276338	-2.466163	0.064293
C	-0.886047	-2.233565	0.588085
C	0.166759	-2.346080	-0.573648
C	1.541843	-2.021709	-0.086794
C	2.070637	-0.797610	-0.435992
C	3.326963	-0.281533	-0.041797
O	4.098790	-0.941251	0.795074
O	3.835667	0.844136	-0.447022
C	3.160566	1.711898	-1.420509
C	2.219320	-3.038065	0.783545
C	-3.032328	-0.059982	0.234535
C	-2.236150	0.670021	-0.831120
C	-1.391657	1.711635	-0.757729
C	-0.948326	2.616174	0.377009
O	0.509033	2.677825	0.229260
C	-1.259778	2.159626	1.805544
C	-1.524939	4.022446	0.126584
H	-5.378351	-1.676899	0.071088
H	-4.654537	-2.959099	-0.922405
H	-4.816643	-1.307660	-1.555594
H	-2.502458	-3.495316	-0.217449
H	-0.642934	-2.973702	1.361121
H	-0.793590	-1.243243	1.043470

H	-0.134933	-1.671075	-1.378514
H	0.146433	-3.374093	-0.957639
H	1.475041	-0.144775	-1.062308
H	3.849337	2.544830	-1.546825
H	2.204406	2.043603	-1.008532
H	3.046260	1.165001	-2.358615
H	3.219497	-3.281343	0.407859
H	1.632716	-3.957099	0.841845
H	2.363074	-2.651429	1.800568
H	-2.572168	0.043006	1.218189
H	-4.022617	0.411347	0.314104
H	-2.411881	0.286743	-1.837791
H	-0.976152	2.054308	-1.706972
H	0.826489	3.416083	0.776601
H	-0.831247	2.875749	2.517552
H	-0.821452	1.179208	2.014924
H	-2.336607	2.120976	1.995627
H	-1.142948	4.735445	0.869844
H	-2.617128	4.013547	0.203871
H	-1.252886	4.383129	-0.870676
H	4.934642	-0.454752	0.946019

JH-III 2Z-6E-9E and proton $[M+H]^+$ located on carboxyl end

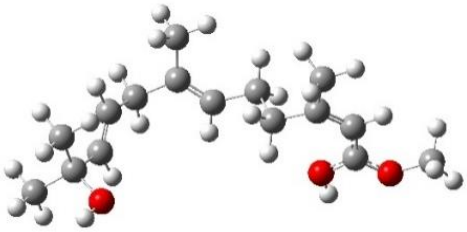

1 1

C	-1.274436	3.037415	-0.079133
C	-1.172996	1.792681	-0.924702
C	-0.055141	1.065057	-1.105947
C	1.302266	1.290577	-0.504574
C	1.595659	0.201909	0.603213
C	2.946215	0.397483	1.204022
C	4.140367	-0.093300	0.707809
C	4.319285	-0.925938	-0.420044
O	3.311648	-1.284152	-1.182230
O	5.464777	-1.409517	-0.817883
C	6.720563	-1.163691	-0.115092
C	2.997845	1.240297	2.440163
C	-2.465828	1.354863	-1.601317
C	-3.472921	0.795011	-0.617843
C	-3.813019	-0.496108	-0.566257
C	-4.802597	-1.154956	0.372419
O	-4.048554	-2.253460	0.942986
C	-5.983506	-1.715580	-0.442502
C	-5.303398	-0.240366	1.496538
H	-1.642858	3.877664	-0.682580
H	-0.326129	3.343457	0.370562
H	-1.997547	2.896909	0.734718
H	-0.125632	0.179648	-1.739541
H	1.393159	2.285517	-0.059310
H	2.075512	1.210387	-1.278058

H	1.486325	-0.784336	0.148753
H	0.834714	0.306505	1.382149
H	5.050104	0.163000	1.237504
H	7.460479	-1.719115	-0.687589
H	6.651498	-1.550610	0.903256
H	6.944661	-0.095441	-0.131772
H	4.012601	1.495406	2.754387
H	2.499823	0.702279	3.260020
H	2.421236	2.162720	2.294413
H	-2.244853	0.599291	-2.363184
H	-2.905283	2.218983	-2.122417
H	-3.920380	1.505072	0.076288
H	-3.355466	-1.196787	-1.267097
H	-4.664747	-2.832758	1.421030
H	-6.669640	-2.273466	0.209112
H	-5.625294	-2.394409	-1.223826
H	-6.553328	-0.908901	-0.916520
H	-5.974262	-0.798824	2.160388
H	-5.868022	0.612952	1.103874
H	-4.466192	0.131137	2.095991
H	3.616389	-1.871386	-1.904059

JH-III 2Z-6E-9Z and proton $[M+H]^+$ located on carboxyl end

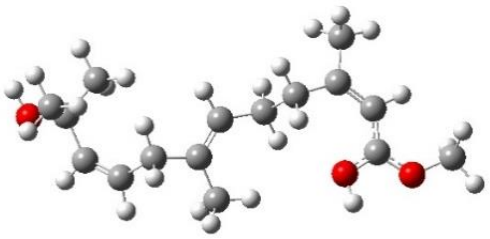

1 1

C	-0.473009	-2.155392	-0.403723
C	-1.039803	-0.899165	0.212448
C	-0.413563	0.292067	0.236633
C	0.926890	0.641067	-0.347458
C	1.941724	1.058124	0.786171
C	3.223013	1.556722	0.205076
C	4.336033	0.796481	-0.101761
C	4.510277	-0.591392	0.105956
O	3.539377	-1.348046	0.563039
O	5.609602	-1.250689	-0.136610
C	6.830066	-0.615314	-0.626814
C	3.275345	3.021838	-0.098254
C	-2.420915	-1.041080	0.840728
C	-3.474606	-1.569588	-0.110422
C	-4.615181	-0.999683	-0.523376
C	-5.233696	0.351118	-0.190130
O	-6.421820	0.374360	-1.010421
C	-4.334417	1.532206	-0.600106
C	-5.649481	0.440754	1.290205
H	-0.590243	-3.004777	0.282101
H	0.587144	-2.071784	-0.657864
H	-1.012960	-2.417769	-1.322254
H	-0.926254	1.128174	0.714402
H	0.815546	1.487324	-1.038660
H	1.353101	-0.185380	-0.921741

H	2.088624	0.202352	1.445420
H	1.481078	1.865673	1.365745
H	5.186766	1.304153	-0.540536
H	7.549463	-1.429330	-0.686106
H	7.160781	0.140703	0.087617
H	6.647447	-0.191170	-1.615952
H	4.156383	3.318645	-0.671893
H	3.264647	3.584377	0.846694
H	2.371490	3.329358	-0.639970
H	-2.720635	-0.087174	1.280397
H	-2.334372	-1.755928	1.676634
H	-3.279754	-2.573352	-0.487559
H	-5.242246	-1.577958	-1.199943
H	-6.916762	1.188244	-0.823162
H	-4.857157	2.482141	-0.425831
H	-4.087345	1.463796	-1.663993
H	-3.402023	1.555808	-0.027282
H	-6.167355	1.390100	1.483037
H	-4.785955	0.391208	1.961874
H	-6.328698	-0.379922	1.540335
H	3.839949	-2.275089	0.659408

JH-III 2Z-6Z-9E and proton $[M+H]^+$ located on carboxyl end

1 1

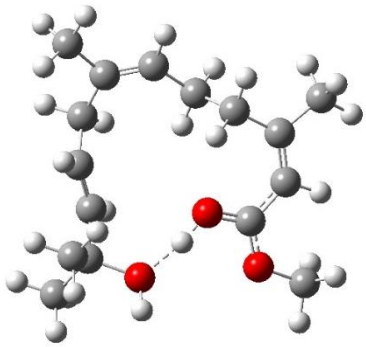

C	-2.835316	3.743037	0.328070
C	-1.766926	2.841646	-0.243008
C	-0.464835	3.080815	-0.009683
C	0.723800	2.290647	-0.490998
C	1.632732	1.878773	0.714902
C	2.905549	1.217186	0.267525
C	3.083262	-0.120533	0.017985
C	2.094830	-1.149159	0.141133
O	0.892968	-0.886925	0.506911
O	2.336769	-2.413681	-0.116182
C	3.637372	-2.897360	-0.550911
C	4.073049	2.136596	0.064789
C	-2.287495	1.678656	-1.082977
C	-2.508669	0.427459	-0.264489
C	-2.130435	-0.796634	-0.647144
C	-2.320008	-2.085456	0.117798
O	-0.930476	-2.618981	0.239027
C	-3.117322	-3.098665	-0.711816
C	-2.896195	-1.926100	1.524178
H	-3.403047	4.231834	-0.475482
H	-2.416355	4.522060	0.972200
H	-3.563901	3.170558	0.919414
H	-0.214252	3.954760	0.594283
H	1.319135	2.903068	-1.183880
H	0.417622	1.392059	-1.032850

H	1.055629	1.233361	1.378158
H	1.895433	2.788246	1.267598
H	4.063071	-0.445618	-0.310399
H	3.500525	-3.970262	-0.672494
H	4.386741	-2.695207	0.217214
H	3.905863	-2.439524	-1.505215
H	4.940718	1.644722	-0.381688
H	4.371257	2.565584	1.031799
H	3.780481	2.986705	-0.565517
H	-1.620730	1.455975	-1.923286
H	-3.246058	1.983902	-1.527399
H	-3.013723	0.569261	0.690400
H	-1.640021	-0.925849	-1.614036
H	-0.939323	-3.477658	0.695545
H	-3.168130	-4.071091	-0.205540
H	-2.660742	-3.241920	-1.696140
H	-4.142378	-2.742015	-0.855127
H	-2.929459	-2.896961	2.032956
H	-3.922868	-1.548159	1.482476
H	-2.295581	-1.240429	2.129740
H	0.205655	-1.676164	0.447107

JH-III 2Z-6Z-9Z and proton $[M+H]^+$ located on carboxyl end

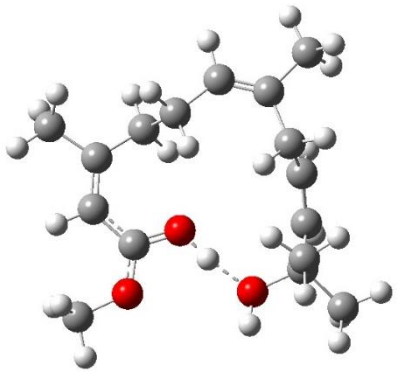

1 1

C	2.591486	3.845947	-0.179330
C	1.563183	2.814882	0.220793
C	0.255849	3.127619	0.268591
C	-0.899620	2.243257	0.657963
C	-1.734241	1.815687	-0.597237
C	-2.976896	1.058907	-0.222423
C	-3.065340	-0.292156	0.002853
C	-1.990521	-1.235156	-0.071764
O	-0.777804	-0.858459	-0.244141
O	-2.161375	-2.533206	0.051411
C	-3.474049	-3.142799	0.197221
C	-4.219525	1.885686	-0.078090
C	2.125754	1.440319	0.554273
C	2.441340	0.648313	-0.702701
C	2.559285	-0.670631	-0.923430
C	2.466230	-1.871528	-0.003039
O	1.138526	-2.479527	-0.337111
C	2.506384	-1.608462	1.504037
C	3.533858	-2.898182	-0.399718
H	3.278271	4.050272	0.653775
H	2.128924	4.791466	-0.477531
H	3.212977	3.495799	-1.014919
H	-0.025940	4.144363	-0.008905
H	-1.555383	2.791829	1.347242
H	-0.565946	1.344073	1.181392

H	-1.088893	1.225652	-1.250367
H	-2.029790	2.721799	-1.138117
H	-4.036193	-0.699829	0.257726
H	-3.277409	-4.213306	0.204665
H	-4.105201	-2.878952	-0.653725
H	-3.924788	-2.834704	1.143058
H	-5.071961	1.324109	0.311987
H	-4.493305	2.308810	-1.054760
H	-4.026460	2.743794	0.579276
H	1.442783	0.889898	1.202606
H	3.051944	1.577775	1.133599
H	2.596131	1.269677	-1.585026
H	2.769753	-0.962985	-1.951947
H	1.063827	-3.358205	0.074862
H	2.528242	-2.558944	2.050656
H	1.637280	-1.043318	1.847695
H	3.409367	-1.051992	1.774724
H	3.429288	-3.821881	0.183700
H	4.532695	-2.494415	-0.203595
H	3.465167	-3.145487	-1.463465
H	-0.039215	-1.615983	-0.273863

JH-III 2Z-6E-10R and proton $[M+H]^+$ located on epoxy end

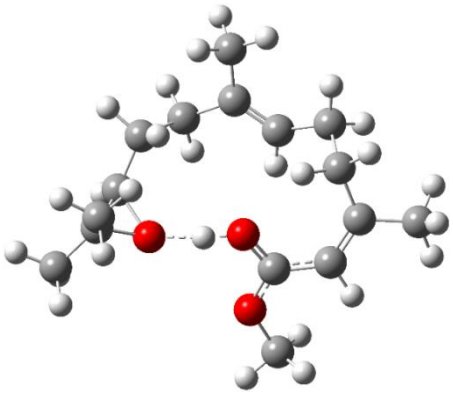

1 1

C	-0.012262	3.884472	0.113262
C	0.092497	2.587939	-0.653186
C	1.195919	1.824542	-0.746869
C	2.500852	1.993178	-0.020417
C	2.737403	0.874750	1.062863
C	3.250276	-0.414378	0.483497
C	2.517101	-1.505179	0.090421
C	1.093273	-1.667840	0.127026
O	0.314781	-0.802491	0.671643
O	0.487278	-2.703449	-0.399870
C	1.185130	-3.767288	-1.102410
C	4.742026	-0.482311	0.321443
C	-1.190463	2.136430	-1.326804
C	-2.270830	1.688664	-0.286677
C	-2.852321	0.328726	-0.585684
C	-3.380976	-0.632337	0.408145
O	-2.062246	-0.861461	-0.229765
C	-4.424073	-1.634821	-0.033801
C	-3.340244	-0.362605	1.896153
H	-0.263737	4.704619	-0.573110
H	0.906699	4.161973	0.634105
H	-0.817474	3.847501	0.858974
H	1.134815	0.939767	-1.382363
H	2.540389	2.949059	0.507521
H	3.342127	1.995563	-0.726618

H	1.814522	0.729345	1.624697
H	3.503783	1.245815	1.753620
H	3.063774	-2.343809	-0.324040
H	0.391500	-4.426564	-1.448979
H	1.844410	-4.299168	-0.413123
H	1.736938	-3.357581	-1.950977
H	5.076646	-1.351477	-0.250035
H	5.211273	-0.517684	1.314983
H	5.118963	0.428869	-0.159574
H	-0.969193	1.307290	-2.009554
H	-1.599627	2.946111	-1.944556
H	-3.106467	2.400578	-0.272611
H	-1.844876	1.694034	0.720744
H	-3.250477	0.226428	-1.596719
H	-4.298210	-2.582942	0.501168
H	-4.358739	-1.829729	-1.107947
H	-5.427403	-1.253606	0.190062
H	-3.221379	-1.303858	2.445047
H	-4.287538	0.087370	2.215415
H	-2.529470	0.309155	2.186242
H	-0.689607	-0.879506	0.389788

JH-III 2Z-6E-10S and proton $[M+H]^+$ located on epoxy end

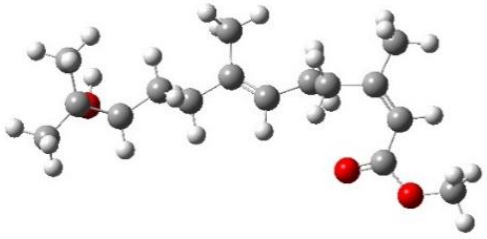

1 1

C	-1.220872	2.538302	-1.052662
C	-0.940399	1.055975	-0.964890
C	0.273007	0.501948	-0.795498
C	1.613166	1.164428	-0.648676
C	2.248020	0.859621	0.740350
C	3.746345	1.069063	0.748969
C	4.642445	0.135998	0.350015
C	4.286254	-1.213009	-0.147360
O	3.157711	-1.553930	-0.465397
O	5.274882	-2.134964	-0.273697
C	6.626608	-1.887400	0.139331
C	4.220216	2.415044	1.232077
C	-2.147709	0.146606	-1.125685
C	-3.059114	0.125465	0.127355
C	-4.198842	-0.841381	-0.002292
C	-5.539022	-0.739196	0.612876
O	-5.347900	-0.449614	-0.970435
C	-5.978043	0.469004	1.390301
C	-6.356128	-1.988112	0.773317
H	-1.655768	2.797376	-2.028796
H	-0.320004	3.141943	-0.925947
H	-1.937769	2.869970	-0.287127
H	0.336681	-0.587808	-0.773325
H	1.563597	2.246251	-0.809993
H	2.269705	0.747525	-1.420790

H	2.021752	-0.177177	1.000572
H	1.783897	1.509792	1.493275
H	5.695285	0.393538	0.400347
H	7.143573	-2.838400	0.004825
H	6.675148	-1.593132	1.192735
H	7.101882	-1.127816	-0.490686
H	5.304707	2.532824	1.150343
H	3.934057	2.566713	2.282047
H	3.741436	3.222001	0.660207
H	-1.814506	-0.877287	-1.332861
H	-2.740304	0.467729	-1.996883
H	-3.410426	1.131319	0.382228
H	-2.471644	-0.224223	0.989477
H	-3.907777	-1.845963	-0.305026
H	-7.044301	0.661045	1.236068
H	-5.407169	1.373093	1.167333
H	-5.836918	0.245666	2.455752
H	-7.424756	-1.776905	0.674814
H	-6.180712	-2.377314	1.784911
H	-6.071131	-2.761976	0.056302
H	-5.321678	0.515137	-1.148740

JH-III 2Z-6Z-10R and proton $[M+H]^+$ located on epoxy end

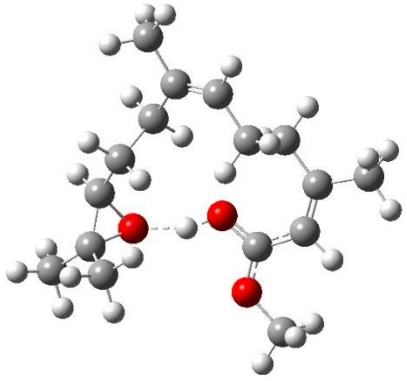

1 1

C	-0.971275	4.551718	-0.138607
C	-0.344913	3.181936	-0.034695
C	0.839211	3.004658	0.580790
C	1.561466	1.694310	0.809132
C	2.416009	1.227309	-0.418166
C	3.206828	-0.020046	-0.123730
C	2.718907	-1.303781	-0.074371
C	1.361028	-1.702555	-0.293880
O	0.462603	-0.834167	-0.582566
O	0.941199	-2.940891	-0.201575
C	1.829961	-4.053518	0.095784
C	4.661747	0.194839	0.166070
C	-1.133330	2.049488	-0.676802
C	-2.054036	1.279840	0.301991
C	-2.789449	0.148780	-0.381895
C	-3.132554	-1.162938	0.213296
O	-2.024314	-1.054107	-0.762733
C	-4.317563	-1.924127	-0.338660
C	-2.724012	-1.542579	1.619312
H	-1.074561	4.857064	-1.188958
H	-0.382947	5.313305	0.381814
H	-1.983561	4.556941	0.289367
H	1.336920	3.886546	0.983163
H	0.855640	0.899004	1.060378
H	2.227679	1.806487	1.672839

H	3.111344	2.029912	-0.684031
H	1.749976	1.068282	-1.269318
H	3.414223	-2.099185	0.165526
H	1.182293	-4.928091	0.082554
H	2.273162	-3.923230	1.085356
H	2.594297	-4.136585	-0.679596
H	5.184474	-0.714492	0.472685
H	4.778802	0.956594	0.948814
H	5.155839	0.602875	-0.726897
H	-0.451847	1.336553	-1.147986
H	-1.750828	2.461148	-1.485776
H	-2.811938	1.960625	0.713495
H	-1.472861	0.912735	1.152882
H	-3.419247	0.468869	-1.213426
H	-4.135081	-3.003879	-0.297366
H	-4.519613	-1.646437	-1.376832
H	-5.210861	-1.710320	0.259943
H	-2.536289	-2.620864	1.676851
H	-3.538919	-1.311975	2.315284
H	-1.829691	-1.015714	1.959508
H	-0.550446	-1.112844	-0.608693

JH-III 2Z-6Z-10S and proton $[M+H]^+$ located on epoxy end

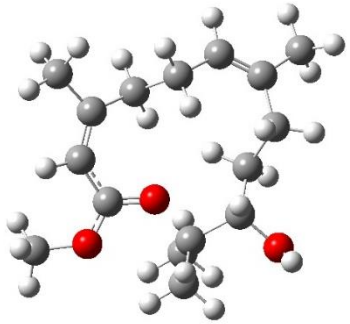

1 1

C	-4.788934	0.353647	0.715669
C	-3.441790	0.525631	0.059449
C	-2.826466	1.722803	0.022710
C	-1.486659	2.029162	-0.601031
C	-0.380193	2.234705	0.487875
C	0.964812	2.598131	-0.075711
C	2.022551	1.745261	-0.242728
C	2.059648	0.320453	-0.031226
O	0.993988	-0.387200	-0.161409
O	3.172108	-0.313000	0.238151
C	4.422931	0.385520	0.507951
C	1.159082	4.046982	-0.418760
C	-2.818856	-0.724829	-0.544621
C	-1.665969	-1.297880	0.320381
C	-0.632616	-2.094812	-0.489367
C	0.840953	-1.921075	0.001425
O	-0.961769	-3.481907	-0.425031
C	1.040101	-2.282718	1.464668
C	1.807407	-2.625589	-0.943261
H	-5.536919	0.017355	-0.015240
H	-5.149382	1.283033	1.167327
H	-4.751157	-0.416079	1.499048
H	-3.324265	2.572418	0.491560
H	-1.564196	2.946155	-1.199524
H	-1.168829	1.232727	-1.280599

H	-0.317078	1.334469	1.100345
H	-0.701787	3.052857	1.144455
H	2.970455	2.173427	-0.553480
H	5.085585	-0.385602	0.896783
H	4.262278	1.168027	1.251468
H	4.822544	0.792155	-0.423451
H	2.115164	4.248740	-0.908059
H	1.092194	4.658915	0.491094
H	0.349128	4.389254	-1.075561
H	-2.429726	-0.487920	-1.543600
H	-3.586694	-1.491820	-0.694155
H	-2.063410	-1.952772	1.103670
H	-1.173835	-0.467551	0.826997
H	-0.647637	-1.754175	-1.533650
H	2.085004	-2.183885	1.769491
H	0.744198	-3.329233	1.590067
H	0.412983	-1.676100	2.123490
H	1.542812	-3.687329	-0.956059
H	2.844940	-2.548145	-0.616981
H	1.720844	-2.238844	-1.964997
H	-0.923845	-3.885572	-1.304666

JH-III 2E-6E-10R and proton $[M+H]^+$ located on epoxy end

1 1

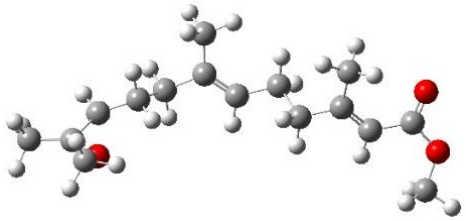

C	-1.329318	2.774634	-0.077272
C	-1.315873	1.391578	-0.686026
C	-0.213222	0.658630	-0.925283
C	1.224367	1.002063	-0.646226
C	1.923065	-0.072420	0.228815
C	3.375154	0.259206	0.502169
C	4.343227	-0.519146	-0.031879
C	5.796013	-0.260104	0.119119
O	6.261430	0.791004	0.514878
O	6.665686	-1.250535	-0.225132
C	6.232961	-2.566852	-0.585447
C	3.624871	1.475488	1.359022
C	-2.674944	0.843982	-1.088195
C	-3.587679	0.537520	0.125269
C	-4.948650	0.069284	-0.283409
C	-5.837473	-0.853614	0.453957
O	-4.971678	-1.401667	-0.798014
C	-7.312988	-0.829731	0.165954
C	-5.396314	-1.545416	1.709819
H	-1.824102	3.489627	-0.749529
H	-0.326892	3.155910	0.123817
H	-1.878591	2.801927	0.874579
H	-0.355144	-0.316860	-1.397364
H	1.317206	1.982127	-0.170346
H	1.764833	1.066238	-1.601933

H	1.841815	-1.048262	-0.266252
H	1.384858	-0.148423	1.185047
H	4.039924	-1.380061	-0.620058
H	7.146851	-3.157720	-0.663906
H	5.722285	-2.568695	-1.555444
H	5.586055	-3.001714	0.184204
H	4.485658	1.340678	2.016979
H	2.738993	1.715905	1.958511
H	3.862386	2.347469	0.735889
H	-2.543846	-0.075350	-1.671102
H	-3.187465	1.570820	-1.737908
H	-3.760467	1.453209	0.710428
H	-3.102974	-0.180710	0.792667
H	-5.449832	0.705070	-1.014239
H	-7.742411	-1.835516	0.210130
H	-7.555081	-0.364550	-0.795418
H	-7.797951	-0.233036	0.949407
H	-5.908171	-2.505477	1.821294
H	-5.681498	-0.911563	2.559727
H	-4.318606	-1.706365	1.750105
H	-5.520525	-1.495706	-1.605470

JH-III 2E-6E-10S and proton $[M+H]^+$ located on epoxy end

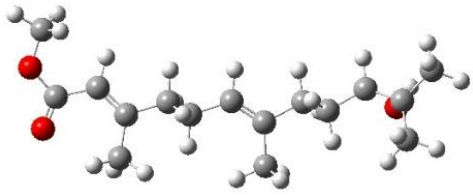

1 1

C	1.397890	-2.364416	-0.419817
C	1.280603	-0.917311	-0.840607
C	0.125566	-0.245762	-0.998804
C	-1.282146	-0.731165	-0.785378
C	-2.052235	0.142626	0.240355
C	-3.478786	-0.322842	0.444312
C	-4.497449	0.474884	0.052104
C	-5.930480	0.104764	0.151087
O	-6.328665	-1.027625	0.343679
O	-6.860722	1.087813	-0.003788
C	-6.510543	2.472180	-0.108742
C	-3.645575	-1.682897	1.075434
C	2.596291	-0.218546	-1.143063
C	3.458560	0.028522	0.119122
C	4.724222	0.767962	-0.187359
C	6.001838	0.700857	0.553509
O	5.823658	-0.120587	-0.832508
C	6.214573	-0.262031	1.683794
C	6.978158	1.836778	0.425314
H	1.951608	-2.943189	-1.172189
H	0.426910	-2.844534	-0.288017
H	1.942013	-2.475166	0.528736
H	0.192530	0.791637	-1.336604
H	-1.300584	-1.776606	-0.465825
H	-1.820527	-0.686915	-1.743252

H	-2.037379	1.187757	-0.093210
H	-1.520256	0.102122	1.202272
H	-4.253119	1.443486	-0.373854
H	-7.458741	3.011026	-0.076462
H	-6.009693	2.687391	-1.059822
H	-5.883571	2.792676	0.730431
H	-4.516067	-1.723880	1.733042
H	-2.747024	-1.961653	1.638514
H	-3.817483	-2.448702	0.307859
H	2.398229	0.743765	-1.632147
H	3.181025	-0.826674	-1.849449
H	3.672925	-0.907188	0.641379
H	2.901766	0.667565	0.821613
H	4.592840	1.663926	-0.795383
H	7.270546	-0.534629	1.765246
H	5.616335	-1.168812	1.588539
H	5.925049	0.244364	2.614060
H	8.010685	1.473780	0.415651
H	6.865750	2.476487	1.310377
H	6.794942	2.461770	-0.454945
H	6.264201	0.331773	-1.583183

JH-III 2E-6Z-10R and proton $[M+H]^+$ located on epoxy end

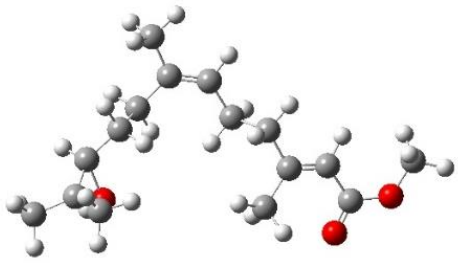

1 1

C	-2.264517	3.844963	0.253881
C	-1.517569	2.608334	-0.195357
C	-0.180096	2.521803	-0.081885
C	0.738026	1.396645	-0.479054
C	1.689391	0.983325	0.675595
C	2.555020	-0.203116	0.310268
C	3.884597	-0.032568	0.137872
C	4.810431	-1.115395	-0.276815
O	4.440926	-2.188879	-0.715586
O	6.147629	-0.893881	-0.179938
C	6.695266	0.286612	0.421668
C	1.834347	-1.519895	0.144608
C	-2.378172	1.517438	-0.808597
C	-3.199306	0.741884	0.251274
C	-4.113817	-0.274172	-0.359697
C	-4.572319	-1.542492	0.246303
O	-3.376584	-1.555970	-0.845052
C	-5.829014	-2.184719	-0.272068
C	-4.051630	-2.025052	1.567882
H	-2.801084	4.310398	-0.584878
H	-1.584567	4.592745	0.671867
H	-3.015657	3.622327	1.025476
H	0.330887	3.383887	0.350758
H	1.359303	1.719197	-1.327573
H	0.179647	0.519254	-0.822411

H	1.084159	0.729812	1.558415
H	2.311306	1.843071	0.951437
H	4.297779	0.958020	0.300840
H	7.771299	0.112694	0.463732
H	6.312129	0.433314	1.437056
H	6.499668	1.173882	-0.190928
H	2.404987	-2.350870	0.565641
H	1.700406	-1.763443	-0.916900
H	0.846313	-1.480107	0.620096
H	-1.766100	0.805026	-1.369387
H	-3.074084	1.974746	-1.528016
H	-3.854799	1.433257	0.801428
H	-2.534661	0.281804	0.987540
H	-4.739207	0.101761	-1.170344
H	-5.746285	-3.276096	-0.271537
H	-6.108881	-1.833852	-1.270896
H	-6.647521	-1.918663	0.409413
H	-4.069607	-3.117593	1.613115
H	-4.720662	-1.644892	2.351072
H	-3.041805	-1.673514	1.780988
H	-3.692561	-1.847886	-1.726670

JH-III 2E-6Z-10S and proton $[M+H]^+$ located on epoxy end

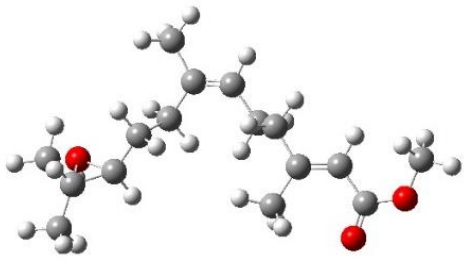

1 1

C	-2.253077	3.634462	0.165262
C	-1.434869	2.439237	-0.269508
C	-0.096235	2.420900	-0.144875
C	0.870367	1.331112	-0.525317
C	1.807404	0.942843	0.649908
C	2.702298	-0.229246	0.309140
C	4.031287	-0.035787	0.159233
C	4.983726	-1.104923	-0.230834
O	4.641140	-2.185499	-0.673944
O	6.314442	-0.861359	-0.104786
C	6.828562	0.329021	0.507067
C	2.008999	-1.560510	0.140676
C	-2.233510	1.292842	-0.870003
C	-2.821289	0.357430	0.214839
C	-3.620806	-0.769853	-0.364007
C	-4.743245	-1.490122	0.273626
O	-5.036249	-0.347237	-0.841121
C	-5.314443	-1.062326	1.592724
C	-5.094018	-2.868435	-0.213118
H	-2.770014	4.091726	-0.689943
H	-1.627972	4.402783	0.629341
H	-3.030905	3.360088	0.892775
H	0.370942	3.308094	0.286275
H	1.500085	1.676892	-1.358137
H	0.348683	0.437555	-0.885453

H	1.190482	0.682691	1.522664
H	2.406584	1.816289	0.932620
H	4.423758	0.963289	0.321620
H	7.905756	0.171935	0.576478
H	6.417760	0.472173	1.512081
H	6.634551	1.211562	-0.112805
H	2.590302	-2.379274	0.570703
H	1.890510	-1.810183	-0.921306
H	1.015695	-1.537877	0.606930
H	-1.618633	0.701158	-1.557063
H	-3.060937	1.707882	-1.461769
H	-3.411185	0.924465	0.939848
H	-2.000145	-0.115670	0.773778
H	-3.124008	-1.314327	-1.167990
H	-6.372687	-1.329958	1.660131
H	-5.201546	0.006050	1.779310
H	-4.779038	-1.607299	2.381433
H	-6.176580	-3.029479	-0.203443
H	-4.650347	-3.591993	0.483285
H	-4.693823	-3.087040	-1.208801
H	-5.258850	-0.738634	-1.712637

JH-III 2E-6E-9E and proton $[M+H]^+$ located on epoxy end

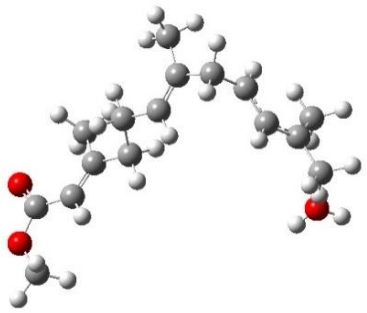

1 1

C	1.503619	-3.543609	0.780135
C	1.593674	-2.534773	-0.333301
C	0.604835	-1.719228	-0.762545
C	-0.818877	-1.667587	-0.293483
C	-1.257788	-0.223434	0.076580
C	-2.691417	-0.169742	0.562719
C	-3.625680	0.428664	-0.210258
C	-5.065419	0.505983	0.143736
O	-5.561417	-0.085916	1.082437
O	-5.881695	1.271247	-0.629692
C	-5.403053	2.063126	-1.722582
C	-2.962212	-0.820457	1.897011
C	2.963680	-2.450777	-1.037575
C	3.592862	-1.314140	-0.337060
C	3.937985	-0.110694	-0.933130
C	4.531150	0.969211	-0.267402
O	3.564392	4.178141	1.216838
C	4.970471	2.151387	-1.055923
C	4.753569	1.043783	1.202232
H	2.339500	-3.441630	1.485385
H	1.565046	-4.561802	0.371513
H	0.577674	-3.463546	1.352331
H	0.838920	-1.034638	-1.580944
H	-0.986636	-2.340086	0.551875
H	-1.468039	-2.020712	-1.108172

H	-1.123759	0.427226	-0.796454
H	-0.594601	0.151691	0.869504
H	-3.305665	0.872252	-1.148066
H	-6.276028	2.608236	-2.084165
H	-5.013666	1.434894	-2.531819
H	-4.641027	2.779338	-1.395808
H	-3.608856	-0.200210	2.522662
H	-2.026699	-1.021277	2.431679
H	-3.501529	-1.767367	1.771654
H	2.873735	-2.275985	-2.112803
H	3.521762	-3.381472	-0.876117
H	3.759003	-1.447202	0.729815
H	3.795079	-0.018170	-2.008005
H	4.116798	4.877639	1.601603
H	4.457152	3.045936	-0.668797
H	4.786899	2.047417	-2.127261
H	6.041626	2.337190	-0.890476
H	4.251962	1.949225	1.576779
H	5.823038	1.194784	1.404796
H	4.407136	0.178532	1.767378
H	2.656552	4.515662	1.280332

JH-III 2E-6E-9Z and proton $[M+H]^+$ located on epoxy end

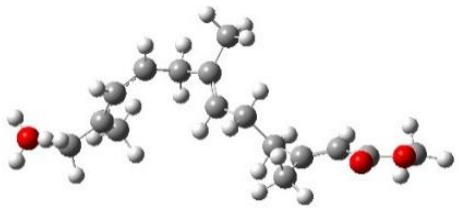

1 1

C	0.517217	3.042314	-0.672476
C	1.081357	1.724378	-0.216391
C	0.477494	0.516972	-0.300340
C	-0.909333	0.206090	-0.775593
C	-1.774130	-0.456104	0.333935
C	-3.152452	-0.834198	-0.168852
C	-4.234227	-0.218166	0.355722
C	-5.630074	-0.456687	-0.095684
O	-5.917188	-0.954601	-1.166389
O	-6.643027	-0.069510	0.723802
C	-6.418321	0.390114	2.062563
C	-3.196518	-1.886723	-1.248011
C	2.509421	1.784488	0.363826
C	3.297758	1.394564	-0.826706
C	4.124430	0.300793	-1.078747
C	4.742825	-0.574902	-0.178435
O	8.074013	-1.198952	1.307841
C	5.517472	-1.720681	-0.723805
C	4.766390	-0.433759	1.307367
H	0.379261	3.712084	0.187514
H	-0.440254	2.940028	-1.185594
H	1.204681	3.556516	-1.358400
H	1.040298	-0.350432	0.052965
H	-0.832403	-0.490792	-1.622672
H	-1.420789	1.099133	-1.145533

H	-1.850835	0.229538	1.185570
H	-1.258698	-1.360642	0.690007
H	-4.078373	0.509618	1.147029
H	-7.409633	0.455570	2.513105
H	-5.955900	1.383895	2.070218
H	-5.807075	-0.317745	2.632358
H	-4.107158	-2.485744	-1.198233
H	-2.321455	-2.545119	-1.183504
H	-3.198062	-1.423567	-2.243749
H	2.624398	1.118755	1.216922
H	2.741354	2.810393	0.677889
H	3.108691	2.024108	-1.696578
H	4.349371	0.125254	-2.129094
H	8.492056	-1.984430	1.695931
H	6.581780	-1.578517	-0.473644
H	5.399932	-1.854013	-1.800934
H	5.230680	-2.645691	-0.202731
H	5.752962	-0.736629	1.679555
H	4.039167	-1.132919	1.750436
H	4.545796	0.571218	1.664229
H	8.763967	-0.516322	1.324677

JH-III 2E-6Z-9E and proton $[M+H]^+$ located on epoxy end

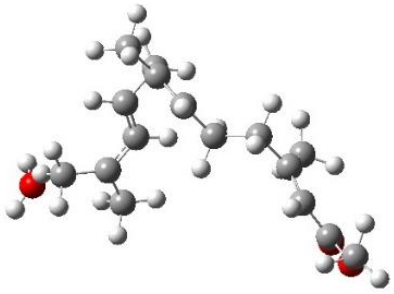

1 1

C	2.206122	4.127622	-0.561159
C	1.525670	2.893967	-0.024885
C	0.335930	2.456338	-0.493766
C	-0.460825	1.256551	-0.072979
C	-1.954294	1.595615	0.181237
C	-2.737241	0.369474	0.602747
C	-3.664646	-0.146901	-0.231348
C	-4.411732	-1.403852	0.037437
O	-4.010318	-2.274818	0.785501
O	-5.584516	-1.604535	-0.614550
C	-6.218401	-0.572129	-1.383742
C	-2.387587	-0.204146	1.955005
C	2.293740	2.146470	1.080113
C	2.981982	1.085536	0.313496
C	2.741105	-0.271714	0.443644
C	3.363561	-1.273327	-0.315566
O	6.397876	-3.193238	0.056646
C	4.323742	-1.025537	-1.424230
C	3.096560	-2.697507	0.014035
H	3.220670	3.914070	-0.925335
H	2.310554	4.882136	0.230460
H	1.643244	4.570853	-1.387294
H	-0.134818	3.071746	-1.262670
H	-0.034657	0.786628	0.819040
H	-0.419615	0.500777	-0.873016

H	-2.381711	2.032292	-0.729141
H	-2.014220	2.361196	0.967209
H	-3.864234	0.366652	-1.168100
H	-7.217270	-0.951045	-1.603614
H	-5.686444	-0.396271	-2.325625
H	-6.299597	0.358873	-0.813555
H	-3.247626	-0.671383	2.437974
H	-1.983868	0.576057	2.611652
H	-1.633804	-0.997264	1.862139
H	1.645945	1.740755	1.860777
H	3.016103	2.830513	1.542710
H	3.698859	1.430079	-0.428812
H	2.046459	-0.593897	1.216279
H	6.771034	-3.936819	-0.443625
H	5.278194	-1.508596	-1.163315
H	4.496571	0.023959	-1.662075
H	3.971220	-1.536734	-2.330586
H	4.047489	-3.165690	0.317925
H	2.778983	-3.244420	-0.884830
H	2.351284	-2.827603	0.801163
H	7.014809	-3.054904	0.793269

JH-III 2E-6Z-9Z and proton $[M+H]^+$ located on epoxy end

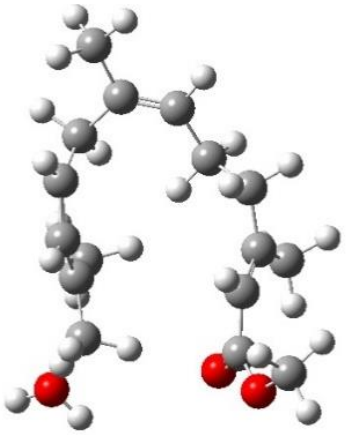

1 1

C	-4.891959	-1.499048	-0.728581
C	-3.610937	-1.051857	-0.073071
C	-2.738921	-1.913443	0.485675
C	-1.435712	-1.587300	1.158113
C	-0.254414	-2.481628	0.675484
C	1.065803	-1.763109	0.860614
C	1.824093	-1.479990	-0.217845
C	3.019044	-0.591687	-0.207935
O	3.024198	0.500572	0.340974
O	4.111516	-0.971429	-0.895121
C	4.224285	-2.298032	-1.447187
C	1.438645	-1.397441	2.274673
C	-3.364753	0.470028	-0.073296
C	-2.556419	0.754920	-1.288030
C	-1.334365	1.372678	-1.482122
C	-0.532369	2.111202	-0.580988
O	1.169336	5.161850	0.909745
C	0.824819	2.495945	-1.006106
C	-0.946588	2.539455	0.786512
H	-5.763084	-1.098807	-0.191643
H	-4.973883	-2.589283	-0.750655
H	-4.970621	-1.138710	-1.764234
H	-3.014861	-2.969111	0.483223
H	-1.552420	-1.704092	2.244919
H	-1.173348	-0.539087	0.985894

H	-0.391718	-2.732261	-0.382351
H	-0.266031	-3.426925	1.234730
H	1.533756	-1.876224	-1.190354
H	5.278552	-2.414062	-1.698962
H	3.620310	-2.390527	-2.355705
H	3.930674	-3.056396	-0.716335
H	2.416788	-0.920091	2.343191
H	1.439783	-2.300441	2.900062
H	0.703613	-0.714267	2.719496
H	-2.905478	0.811698	0.851727
H	-4.336928	0.977272	-0.169089
H	-2.981160	0.319281	-2.193312
H	-0.922833	1.276601	-2.484715
H	2.031724	5.125271	1.354296
H	1.036171	3.543948	-0.751947
H	1.032690	2.286628	-2.057436
H	1.544898	1.914388	-0.389536
H	-0.700149	1.734754	1.498597
H	-2.016089	2.741860	0.867194
H	-0.376454	3.419906	1.098856
H	0.954182	6.106564	0.853835

JH-III 2Z-6E-9E and proton $[M+H]^+$ located on epoxy end

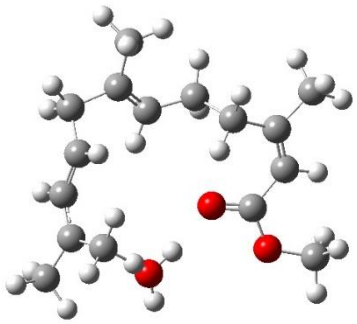

1 1

C	-1.425299	3.993717	0.201750
C	-1.550121	2.624361	-0.410267
C	-0.526279	1.822199	-0.768309
C	0.947718	2.112419	-0.687616
C	1.579637	1.554635	0.634227
C	3.016507	1.128672	0.442087
C	3.392788	-0.112587	0.044393
C	2.465429	-1.215928	-0.252129
O	1.251200	-1.074460	-0.402082
O	2.950785	-2.467230	-0.379753
C	4.337985	-2.792946	-0.165185
C	4.058483	2.180731	0.709794
C	-2.988791	2.111171	-0.611124
C	-3.104719	0.855616	0.166517
C	-3.391437	-0.375311	-0.384176
C	-3.484090	-1.578266	0.339227
O	-0.862855	-2.879932	-0.204924
C	-4.045454	-2.777921	-0.335072
C	-3.066292	-1.745579	1.750497
H	-1.962528	4.737667	-0.402319
H	-0.386529	4.317248	0.297772
H	-1.875217	4.020221	1.204123
H	-0.759081	0.835870	-1.168803
H	1.154390	3.184336	-0.770452
H	1.429071	1.626634	-1.542269

H	0.985542	0.705199	0.973171
H	1.530038	2.333511	1.404510
H	4.453965	-0.312754	-0.055013
H	4.388148	-3.878765	-0.246534
H	4.664910	-2.483059	0.831451
H	4.968246	-2.341187	-0.937075
H	5.072671	1.835529	0.490574
H	4.018408	2.496839	1.761057
H	3.861052	3.079007	0.108870
H	-3.229430	1.957829	-1.668285
H	-3.694636	2.853685	-0.214275
H	-2.928528	0.942179	1.236587
H	-3.606478	-0.418741	-1.450016
H	-0.589786	-3.751974	-0.528262
H	-3.550325	-3.690663	0.008079
H	-4.002482	-2.711940	-1.424235
H	-5.105473	-2.861010	-0.039893
H	-2.106454	-2.288391	1.696143
H	-3.763463	-2.393792	2.293569
H	-2.910550	-0.818675	2.303509
H	-0.064921	-2.311728	-0.315597

JH-III 2Z-6E-9Z and proton $[M+H]^+$ located on epoxy end

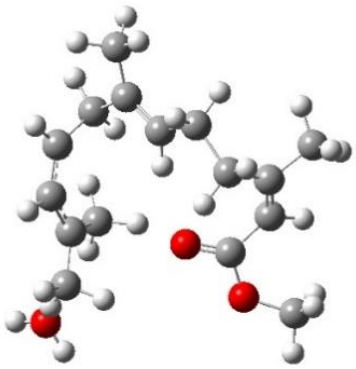

1 1

C	0.945755	4.318275	-0.403992
C	0.395390	2.918975	-0.435743
C	1.020141	1.813861	0.020758
C	2.400796	1.734436	0.623203
C	2.771946	0.300821	1.081526
C	3.093522	-0.660266	-0.045480
C	2.325650	-1.707130	-0.426275
C	0.987781	-2.062320	0.098241
O	0.151829	-1.255435	0.490834
O	0.631133	-3.364498	0.092598
C	1.574307	-4.417724	-0.189023
C	4.428270	-0.444611	-0.715049
C	-1.032998	2.748694	-1.000444
C	-1.796856	2.647674	0.265162
C	-2.423600	1.580077	0.897475
C	-2.739612	0.302926	0.408862
O	-5.472718	-2.071008	-0.691708
C	-3.170179	-0.735784	1.377178
C	-2.685264	-0.126475	-1.016342
H	1.089247	4.698312	-1.425026
H	1.904078	4.374042	0.118631
H	0.255503	5.013913	0.092844
H	0.488394	0.865334	-0.026155
H	2.454537	2.394491	1.500781
H	3.154227	2.119935	-0.076973

H	1.965382	-0.089657	1.707202
H	3.668352	0.375772	1.711380
H	2.719886	-2.368552	-1.193463
H	1.074176	-5.336550	0.117999
H	2.494418	-4.287106	0.386914
H	1.796078	-4.464795	-1.259869
H	4.596763	-1.142173	-1.540075
H	5.243869	-0.564881	0.010657
H	4.512541	0.575700	-1.110360
H	-1.104351	1.878449	-1.648060
H	-1.323423	3.642104	-1.565615
H	-1.747098	3.555597	0.867288
H	-2.673957	1.750262	1.942608
H	-5.500873	-3.037291	-0.776786
H	-4.103180	-1.211154	1.044840
H	-3.264423	-0.364162	2.399662
H	-2.402071	-1.527626	1.357029
H	-3.495889	-0.836364	-1.216675
H	-1.741527	-0.674942	-1.163956
H	-2.739665	0.694562	-1.730380
H	-6.373230	-1.774267	-0.898580

JH-III 2Z-6Z-9E and proton $[M+H]^+$ located on epoxy end

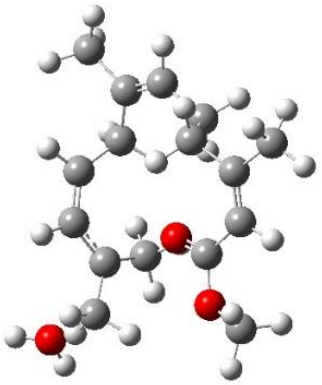

1 1

C	0.553943	4.678120	-0.316033
C	0.083291	3.316118	0.132209
C	-1.223050	3.009284	0.228652
C	-1.861626	1.721536	0.677644
C	-2.472595	0.929148	-0.513207
C	-3.249470	-0.285811	-0.057331
C	-2.717821	-1.515330	0.154192
C	-1.296595	-1.864663	0.003023
O	-0.377722	-1.048835	-0.036109
O	-0.950789	-3.170757	-0.072087
C	-1.926846	-4.228548	-0.149785
C	-4.723670	-0.066718	0.154824
C	1.195680	2.324471	0.471022
C	1.721742	1.704950	-0.782288
C	2.174047	0.434726	-1.051752
C	2.387428	-0.640278	-0.156102
O	5.785489	-1.529277	0.374496
C	2.735665	-1.961766	-0.714695
C	2.393098	-0.514420	1.324822
H	1.099445	5.186378	0.491723
H	-0.282544	5.316242	-0.614207
H	1.246262	4.619536	-1.168540
H	-1.927955	3.796068	-0.045069
H	-2.657784	1.963272	1.394801
H	-1.153653	1.068913	1.193143

H	-1.660678	0.637817	-1.183903
H	-3.149695	1.589967	-1.069241
H	-3.391185	-2.310106	0.457198
H	-1.350182	-5.132555	-0.346908
H	-2.630260	-4.055128	-0.968966
H	-2.460490	-4.338079	0.799264
H	-5.225902	-0.944305	0.571246
H	-5.208661	0.192694	-0.796136
H	-4.893636	0.783337	0.829256
H	0.865289	1.568424	1.182714
H	2.027956	2.870426	0.951804
H	1.685312	2.362852	-1.651227
H	2.365626	0.210295	-2.099075
H	6.230227	-2.096195	1.024666
H	3.823022	-2.092140	-0.552432
H	2.511764	-2.057948	-1.778762
H	2.241093	-2.758700	-0.147742
H	2.949068	-1.336836	1.781325
H	1.348535	-0.592355	1.662398
H	2.799613	0.437493	1.672384
H	6.504266	-1.143328	-0.151300

JH-III 2Z-6Z-9Z and proton $[M+H]^+$ located on epoxy end

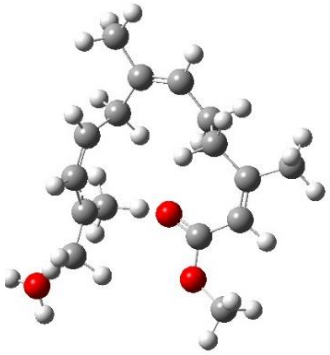

1 1

C	1.032471	4.683925	0.229693
C	1.001857	3.233769	-0.186779
C	2.126641	2.512311	-0.342777
C	2.279169	1.078350	-0.776015
C	2.668593	0.150955	0.410361
C	2.968616	-1.261483	-0.039516
C	2.046962	-2.246523	-0.178495
C	0.602065	-2.096618	0.054299
O	0.009831	-1.021415	0.107464
O	-0.154593	-3.211613	0.193764
C	0.417114	-4.532566	0.266276
C	4.416052	-1.550325	-0.336036
C	-0.393370	2.656721	-0.423301
C	-1.023915	2.297129	0.882125
C	-1.869481	1.270324	1.236707
C	-2.493187	0.310529	0.406101
O	-5.833340	-0.739452	-0.947806
C	-3.186621	-0.831390	1.040117
C	-2.566645	0.393443	-1.075419
H	0.633267	5.326100	-0.568196
H	2.048852	5.017361	0.456822
H	0.414745	4.875204	1.119184
H	3.066118	3.028894	-0.139481
H	3.065397	1.031095	-1.541670
H	1.366392	0.685368	-1.228991

H	1.850419	0.159664	1.134513
H	3.560285	0.559128	0.902726
H	2.398600	-3.225583	-0.486606
H	-0.413527	-5.187715	0.529971
H	1.187297	-4.585823	1.040751
H	0.824382	-4.835557	-0.703189
H	4.571786	-2.552325	-0.745314
H	5.017535	-1.450339	0.577728
H	4.816264	-0.817829	-1.050003
H	-0.374027	1.805760	-1.104003
H	-1.024407	3.429906	-0.899316
H	-0.709751	2.926215	1.715759
H	-2.057207	1.157217	2.302342
H	-6.190537	-1.584571	-1.264185
H	-4.249498	-0.814885	0.749255
H	-3.081109	-0.858942	2.125996
H	-2.780625	-1.758888	0.609939
H	-3.457341	-0.125542	-1.442204
H	-1.684037	-0.133536	-1.471564
H	-2.554559	1.417073	-1.453119
H	-6.577806	-0.118914	-0.998564

Appendix Table 5.6. Geometry coordinates of JH-III [M-H2O+H]$^+$ *m/z* 249 structures and optimized structures.

JH-III 2E-6E-8E JH-III [M-H2O+H]$^+$ *m/z* 249

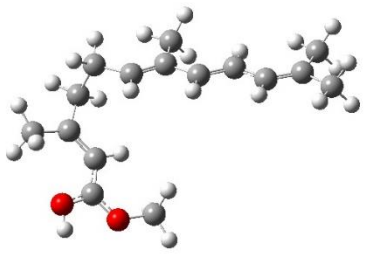

1 1

C	1.195216	-2.504337	1.050934
C	0.807694	-1.591503	-0.090946
C	-0.409582	-1.636556	-0.699953
C	-1.545650	-2.562310	-0.395834
C	-2.602948	-1.996263	0.650260
C	-3.353475	-0.830225	0.113041
C	-2.909380	0.434761	0.455237
C	-3.457256	1.661508	0.029453
O	-4.534841	1.704601	-0.724362
O	-2.989594	2.843279	0.333851
C	-1.791374	3.028690	1.145912
C	-4.499550	-1.116881	-0.809213
C	1.793694	-0.630727	-0.571142
C	3.050125	-0.453271	-0.082976
C	3.986595	0.506493	-0.624660
C	5.257071	0.740737	-0.206158
C	6.108798	1.774755	-0.895787
C	5.934576	0.024225	0.932709
H	2.060986	-3.120561	0.779377
H	0.390234	-3.180405	1.346815
H	1.482018	-1.924288	1.936922
H	-0.580470	-0.931823	-1.514819
H	-1.197625	-3.504349	0.037461
H	-2.080566	-2.822146	-1.316774

H	-2.065273	-1.739439	1.567016
H	-3.304590	-2.809674	0.868837
H	-2.051563	0.506173	1.112485
H	-1.652828	4.107423	1.176900
H	-0.941294	2.543129	0.663079
H	-1.967175	2.635387	2.149094
H	-4.433591	-0.549917	-1.743555
H	-5.446877	-0.819283	-0.338769
H	-4.558071	-2.182920	-1.039359
H	1.482225	-0.016509	-1.417794
H	3.380866	-1.064431	0.752927
H	3.621049	1.092432	-1.469143
H	6.439862	2.546279	-0.186284
H	5.578717	2.268013	-1.716425
H	7.022128	1.318933	-1.303324
H	6.278681	0.745713	1.686440
H	6.832259	-0.497248	0.572903
H	5.300332	-0.709498	1.434974
H	-4.781288	2.631387	-0.920153

JH-III 2E-6E-8Z JH-III $[M-H2O+H]^+$ *m/z* 249

1 1

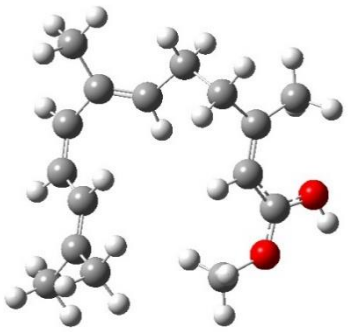

C	-2.093822	3.813391	0.108911
C	-1.561929	2.488142	-0.389466
C	-0.287721	2.064016	-0.247247
C	0.841501	2.771092	0.451055
C	1.712774	1.804976	1.333237
C	2.513715	0.854072	0.502354
C	2.087030	-0.455319	0.410261
C	2.687320	-1.481420	-0.355061
O	3.803270	-1.272098	-1.015669
O	2.225321	-2.693159	-0.479333
C	0.979965	-3.132933	0.150423
C	3.713686	1.414846	-0.199591
C	-2.540569	1.682483	-1.152605
C	-2.902978	0.392625	-0.951348
C	-2.485887	-0.473229	0.142172
C	-2.874549	-1.755003	0.355275
C	-2.478991	-2.476130	1.621533
C	-3.753930	-2.557348	-0.571064
H	-2.493620	4.396304	-0.731468
H	-1.340567	4.428652	0.606971
H	-2.928399	3.657553	0.803953
H	-0.027918	1.125601	-0.736554
H	0.475618	3.554510	1.119946
H	1.502442	3.267995	-0.273916
H	1.058020	1.272794	2.029789

H	2.407598	2.423634	1.915781
H	1.194581	-0.739128	0.954277
H	0.858994	-4.158782	-0.191086
H	0.152906	-2.507568	-0.191271
H	1.095192	-3.099892	1.235297
H	3.691536	1.212488	-1.275860
H	4.630150	0.944156	0.180102
H	3.792079	2.492076	-0.041064
H	-3.064825	2.227010	-1.939337
H	-3.645880	-0.006812	-1.637820
H	-1.860539	-0.005513	0.902502
H	-3.368364	-2.739825	2.211099
H	-1.828786	-1.868331	2.260906
H	-1.973006	-3.429650	1.405616
H	-4.700595	-2.812587	-0.074588
H	-3.276444	-3.513213	-0.828850
H	-3.992673	-2.043870	-1.504458
H	4.080075	-2.081101	-1.492977

JH-III 2E-6Z-8E JH-III [M-H2O+H]$^+$ *m/z* 249

1 1

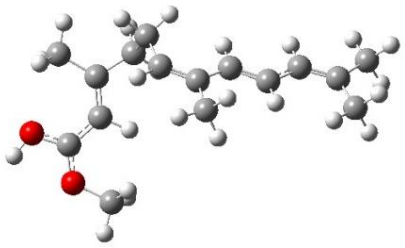

C	-1.049948	0.789916	2.448985
C	-0.834731	-0.326906	1.448988
C	0.335846	-1.023910	1.477066
C	0.706753	-2.189416	0.609765
C	1.382088	-1.803463	-0.776472
C	2.739375	-1.223037	-0.596479
C	2.857774	0.155494	-0.603326
C	4.042726	0.897075	-0.422831
O	5.206718	0.302040	-0.275933
O	4.120818	2.201389	-0.398476
C	2.948853	3.060583	-0.526092
C	3.868576	-2.180739	-0.364326
C	-1.901799	-0.625366	0.504537
H	-1.249465	1.747532	1.951251
H	-0.176249	0.916771	3.095246
H	-1.912282	0.579321	3.093300
H	1.078717	-0.726674	2.216481
H	-0.169735	-2.786232	0.339848
H	1.383360	-2.861714	1.149575
H	0.713574	-1.110835	-1.295298
H	1.460732	-2.726008	-1.363754
H	1.957909	0.736891	-0.761873
H	3.344130	4.069793	-0.430767
H	2.245641	2.842760	0.279920
H	2.496233	2.916288	-1.509056

H	4.466429	-1.914969	0.513444
H	4.559008	-2.165685	-1.219057
H	3.496580	-3.201234	-0.250097
H	-1.740702	-1.453841	-0.183703
C	-3.091013	0.031138	0.415365
C	-4.123183	-0.318590	-0.533394
C	-5.338200	0.270903	-0.679185
H	5.920640	0.963008	-0.168753
C	-6.306878	-0.229837	-1.718613
H	-7.244491	-0.560256	-1.249907
H	-5.899580	-1.066257	-2.294687
H	-6.578166	0.572205	-2.419398
H	-6.767207	1.155063	0.660468
H	-6.088547	2.278559	-0.509233
H	-5.127896	1.781587	0.893980
C	-5.838256	1.430036	0.142403
H	-3.286442	0.858598	1.092287
H	-3.890377	-1.155391	-1.193302

JH-III 2E-6Z-8Z JH-III $[M-H2O+H]^+$ *m/z* 249

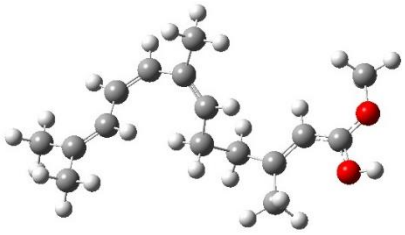

1 1

C	-0.727554	3.007140	1.161246
C	-1.065070	1.785455	0.332619
C	-0.299200	0.673309	0.403291
C	-0.460406	-0.575082	-0.412068
C	0.781200	-0.882327	-1.334837
C	2.009547	-1.227923	-0.564872
C	3.025119	-0.291267	-0.499118
C	4.251970	-0.431676	0.183480
O	4.546422	-1.533743	0.837043
O	5.194626	0.470278	0.235011
C	5.081331	1.769490	-0.420888
C	2.042020	-2.569565	0.102802
C	-2.238118	1.948980	-0.551361
H	-0.598687	3.888301	0.518249
H	0.189385	2.868137	1.744508
H	-1.544539	3.244545	1.854053
H	0.534363	0.684457	1.108594
H	-1.318696	-0.488403	-1.082372
H	-0.645037	-1.448950	0.227500
H	0.949100	-0.022409	-1.989555
H	0.510551	-1.745894	-1.957053
H	2.881814	0.646711	-1.021499
H	6.015208	2.273265	-0.180430
H	4.231162	2.315043	-0.007148
H	4.987557	1.626749	-1.499082

H	2.230136	-2.484069	1.178961
H	2.860943	-3.179106	-0.300631
H	1.104836	-3.107204	-0.052491
H	-2.217206	2.846344	-1.171750
C	-3.366415	1.196053	-0.593564
C	-3.688686	0.063467	0.255824
C	-4.808928	-0.699044	0.198788
H	5.434175	-1.467194	1.244372
C	-5.028079	-1.807635	1.197265
H	-5.947220	-1.634876	1.774574
H	-4.196151	-1.897909	1.903115
H	-5.159735	-2.774318	0.690972
H	-6.869640	-0.334479	-0.297038
H	-6.061700	-1.466852	-1.372225
H	-5.748081	0.267968	-1.528870
C	-5.918084	-0.534769	-0.808385
H	-4.127222	1.516081	-1.301843
H	-2.967583	-0.165840	1.039333

JH-III 2Z-6E-8E JH-III [M-H2O+H]$^+$ *m/z* 249

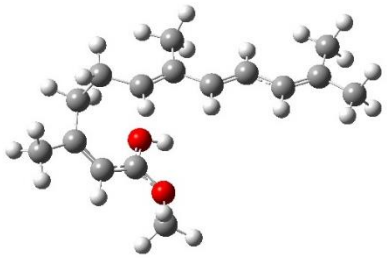

1 1

C	0.491533	-2.392885	0.956241
C	0.264043	-1.470359	-0.220173
C	-0.926386	-1.387602	-0.878446
C	-2.172323	-2.171519	-0.605871
C	-3.215803	-1.489773	0.385917
C	-3.745482	-0.222242	-0.186117
C	-3.161221	1.020032	-0.051915
C	-2.086637	1.384634	0.795986
O	-1.694319	0.632915	1.797750
O	-1.443249	2.520370	0.724202
C	-1.668526	3.488753	-0.341612
C	-4.949021	-0.347054	-1.070040
C	1.375689	-0.645314	-0.674121
C	2.626841	-0.614464	-0.139367
C	3.696211	0.206295	-0.660112
C	4.972694	0.279907	-0.200660
C	5.974355	1.179770	-0.875766
C	5.512819	-0.498301	0.970303
H	1.267958	-3.132224	0.724433
H	-0.407349	-2.939239	1.248427
H	0.839154	-1.835325	1.835092
H	-0.974843	-0.702163	-1.725283
H	-1.949376	-3.141384	-0.152146
H	-2.690997	-2.382959	-1.548166
H	-2.727531	-1.344140	1.348091

H	-4.039411	-2.199855	0.515391
H	-3.554466	1.830516	-0.655627
H	-0.895661	4.239782	-0.190918
H	-2.659215	3.933417	-0.226708
H	-1.552517	3.002666	-1.311936
H	-5.180697	0.569137	-1.618682
H	-5.820157	-0.610454	-0.452788
H	-4.824441	-1.171909	-1.783405
H	1.176171	-0.016975	-1.544008
H	2.847519	-1.247279	0.716547
H	3.439265	0.818459	-1.525646
H	6.384773	1.911303	-0.165532
H	5.539320	1.725598	-1.718575
H	6.829765	0.599136	-1.248659
H	5.920665	0.185562	1.727301
H	6.348491	-1.135293	0.649398
H	4.774059	-1.138098	1.458134
H	-0.922647	1.036186	2.244176

JH-III 2Z-6E-8Z JH-III [M-H2O+H]$^+$ *m/z* 249

1 1

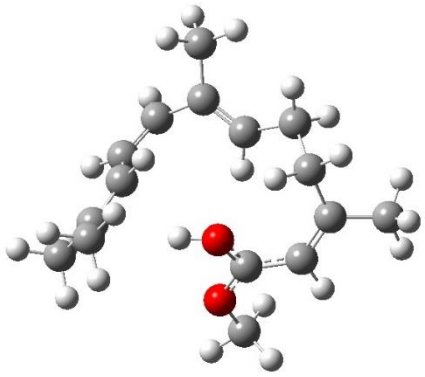

C	-0.343984	3.989068	-0.161846
C	-0.262979	2.565126	-0.661093
C	0.790129	1.736708	-0.512087
C	2.067354	1.965915	0.247031
C	2.432999	0.778666	1.212875
C	2.961186	-0.427743	0.485948
C	2.235459	-1.487822	-0.005642
C	0.825580	-1.682881	0.090712
O	0.106530	-1.010993	0.932793
O	0.157695	-2.540376	-0.634048
C	0.774371	-3.331610	-1.691975
C	4.442404	-0.427785	0.248889
C	-1.436781	2.089587	-1.439551
C	-2.297216	1.117368	-1.060710
C	-2.334090	0.495177	0.263793
C	-3.075271	-0.580491	0.650133
C	-3.175005	-0.968095	2.107163
C	-3.914271	-1.409203	-0.290189
H	-0.535289	4.670211	-1.001704
H	0.569602	4.324970	0.335216
H	-1.183336	4.111984	0.534392
H	0.724138	0.780277	-1.028662
H	2.003315	2.861797	0.870529
H	2.906750	2.129062	-0.444428
H	1.563931	0.539153	1.824996

H	3.227897	1.135971	1.877156
H	2.770265	-2.245451	-0.566890
H	-0.060396	-3.843179	-2.166912
H	1.462806	-4.056310	-1.252571
H	1.277899	-2.674057	-2.403039
H	4.776422	-1.227755	-0.416058
H	4.958066	-0.538344	1.213720
H	4.767986	0.537947	-0.158393
H	-1.622145	2.595512	-2.388551
H	-3.084607	0.845779	-1.760552
H	-1.789394	1.032072	1.041639
H	-4.209666	-0.844416	2.456066
H	-2.534378	-0.354492	2.749057
H	-2.925151	-2.026088	2.266805
H	-4.981540	-1.249024	-0.082959
H	-3.729366	-2.480133	-0.134317
H	-3.737600	-1.184280	-1.344405
H	-0.869324	-0.962171	0.689211

JH-III 2Z-6Z-8E JH-III $[M-H2O+H]^+$ *m/z* 249

1 1

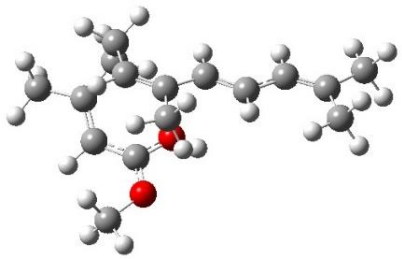

C	-0.305118	0.978290	2.470390
C	-0.021859	-0.232213	1.604486
C	1.204748	-0.823949	1.667873
C	1.661523	-2.080051	0.977861
C	2.154769	-1.954757	-0.526838
C	3.231818	-0.932884	-0.684370
C	3.007324	0.418223	-0.808088
C	1.743793	1.050620	-0.972144
O	0.723342	0.408264	-1.479127
O	1.509903	2.315186	-0.737981
C	2.497442	3.182868	-0.108958
C	4.642861	-1.422833	-0.568921
C	-1.075180	-0.723420	0.728946
C	-2.307245	-0.158200	0.569155
C	-3.325053	-0.695324	-0.303328
C	-4.581097	-0.209471	-0.492191
C	-5.532062	-0.905657	-1.429120
C	-5.144245	1.009789	0.188471
H	-0.581333	1.857957	1.873352
H	0.564687	1.241503	3.079359
H	-1.141000	0.784612	3.153450
H	1.933198	-0.373233	2.340723
H	0.862538	-2.829035	0.948186
H	2.476180	-2.523032	1.560860
H	1.293492	-1.732184	-1.153986

H	2.540592	-2.938313	-0.813745
H	3.856302	1.090765	-0.744669
H	1.955523	4.102507	0.102639
H	3.311023	3.375573	-0.811340
H	2.860094	2.723800	0.812516
H	5.379524	-0.616203	-0.538704
H	4.872246	-2.071943	-1.425844
H	4.761044	-2.049726	0.324980
H	-0.864376	-1.629701	0.162615
H	-2.550017	0.735443	1.139232
H	-3.048518	-1.597190	-0.850881
H	-6.438486	-1.223707	-0.895516
H	-5.083945	-1.786948	-1.897594
H	-5.866117	-0.223968	-2.223768
H	-6.025286	0.735827	0.784663
H	-5.492666	1.735775	-0.558603
H	-4.438867	1.517445	0.849982
H	-0.116298	0.900201	-1.360384

JH-III 2Z-6Z-8Z JH-III $[M-H2O+H]^+$ *m/z* 249

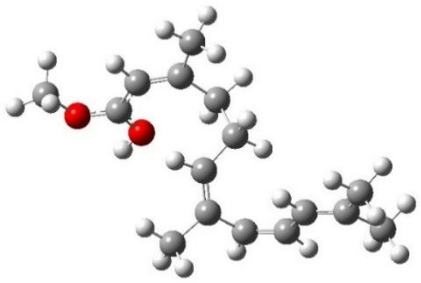

1 1

C	0.258088	-2.773156	1.291166
C	0.684896	-1.579580	0.462508
C	0.066097	-0.385688	0.605054
C	0.335190	0.858954	-0.185429
C	-0.891817	1.376876	-1.039234
C	-2.052457	1.766595	-0.189336
C	-3.176530	1.005001	0.067425
C	-3.533145	-0.241419	-0.501020
O	-2.825419	-0.812618	-1.445289
O	-4.599201	-0.923568	-0.175543
C	-5.538238	-0.497411	0.856559
C	-1.958981	3.108724	0.471857
C	1.768461	-1.859924	-0.502633
C	2.977621	-1.252150	-0.605848
C	3.497262	-0.196019	0.244195
C	4.700356	0.419410	0.126917
C	5.126954	1.460205	1.130985
C	5.710581	0.145707	-0.957417
H	-0.018672	-3.617126	0.644514
H	-0.593148	-2.540998	1.940771
H	1.085254	-3.124606	1.920510
H	-0.708564	-0.312915	1.371164
H	1.139693	0.689307	-0.904573
H	0.663402	1.676257	0.471182
H	-1.147244	0.615235	-1.773076

H	-0.542378	2.270078	-1.571215
H	-3.898148	1.401709	0.771950
H	-6.269837	-1.301575	0.900818
H	-6.014273	0.437166	0.553682
H	-5.016081	-0.398678	1.810016
H	-2.725775	3.272619	1.232676
H	-2.061445	3.889569	-0.295971
H	-0.968872	3.254410	0.920190
H	1.595981	-2.729497	-1.139054
H	3.642963	-1.643350	-1.372374
H	2.865481	0.098374	1.081345
H	6.059635	1.160322	1.628991
H	4.368942	1.627166	1.903048
H	5.336242	2.420159	0.638167
H	6.656176	-0.199180	-0.517014
H	5.944045	1.070461	-1.502845
H	5.387778	-0.599663	-1.687046
H	-3.230221	-1.662504	-1.713693

VITA

ALAN ALEXANDER McKENZIE-COE

	Born, Miami, Florida
2006-2012	B.S.c, Chemistry Florida International University Miami, Florida
2013	McKnight Fellowship Florida International University Miami, Florida
2014	Second Place Oral Presentation Graduate Student Appreciation Week Scholarly Forum Miami, Florida
2016	M.S., Chemistry Florida International University Miami, Florida
2016	Doctoral Candidate Florida International University Miami, Florida
2017	Second Place Oral Presentation Graduate Student Appreciation Week Scholarly Forum Miami, Florida
2017-2018	Teaching Assistant Florida International University Miami, Florida
2018	First Place Oral Presentation Graduate Student Appreciation Week Scholarly Forum Miami, Florida

SELECTED PUBLICATIONS AND PRESENTATIONS

McKenzie-Coe, Alan; Ramirez, Cesar E., Nouzova, Marcela, Noriega, Fernando G., and Fernandez-Lima, Francisco. Rapid screening of labile juvenile hormone III using liquid chromatography – trapped ion mobility spectrometry – mass spectrometry. Talanta (under revision).

McKenzie-Coe, Alan; Fernandez-Lima, Francisco. The influence of bath gas on mobility separation and stability of explosives. *International Journal of Ion Mobility Spectrometry*. 2019. doi:10.1007/s12127-019-00246-y

McKenzie-Coe, A.; Bell, S.; Fernandez-Lima, F., Detection of firearm discharge residue from skin swabs using Trapped Ion Mobility Spectrometry coupled to Mass Spectrometry. *Analytical Methods*. doi:10.1039/C8AY00658J

McKenzie-Coe, A., DeBord, J. D., Ridgeway, M., Park, M., Eiceman, G., & Fernandez-Lima, F. (2015). Lifetimes and stabilities of familiar explosive molecular adduct complexes during ion mobility measurements. *Analyst*, 140(16), 5692-5699. doi:10.1039/C5AN00527B

"Liquid chromatography-trapped ion mobility-mass spectrometry (HPLC-TIMS-MS) for the analysis of Juvenile Hormone III from insects" Alan McKenzie Coe; Cesar E. Ramirez, Marcela Nouzova, Fernando G. Noriega, and Francisco Fernandez-Lima. American Society of Mass Spectrometry Annual Conference, San Diego CA. June 3-7, 2018 (Poster)

"Implementing trapped ion mobility-mass spectrometry (TIMS-MS) for the analysis of juvenile hormone III" Alan McKenzie Coe; Cesar E. Ramirez, Marcela Nouzova, Fernando G. Noriega, and Francisco Fernandez-Lima. Florida Statewide Graduate Research Symposium. Tallahassee, Fl. April 20, 2018. Invited. (Poster)

"Decomposition Pathways during Explosive Analysis using TIMS-MS and molecular dynamics" Alan McKenzie-Coe; Mark E. Ridgeway, Melvin A. Park; and Francisco Fernandez-Lima. American Society of Mass Spectrometry Annual Conference, San Antonio TX. June 5-9, 2016 (Poster)

"Adduct Formation of Explosives and Separation from Complex Mixtures Using Trapped Ion Mobility Spectrometry- Mass Spectrometry" Alan McKenzie-Coe, Gary Eiceman, John Daniel DeBord, Mark Ridgeway, Melvin Park, and Francisco Fernandez-Lima. International Society for Ion Mobility Spectrometry. Asheville, North Carolina. July – 1st August 2014. (Oral)